UNIVERSITAT DE BARCELONA

High-throughput phenotyping in cereals and implications in plant ecophysiology

Fenotipat de camp d'alt rendiment i implicacions en l'ecofisiologia vegetal

Omar Vergara Díaz

High-throughput phenotyping in cereals and implications in plant ecophysiology

Omar Vergara Díaz

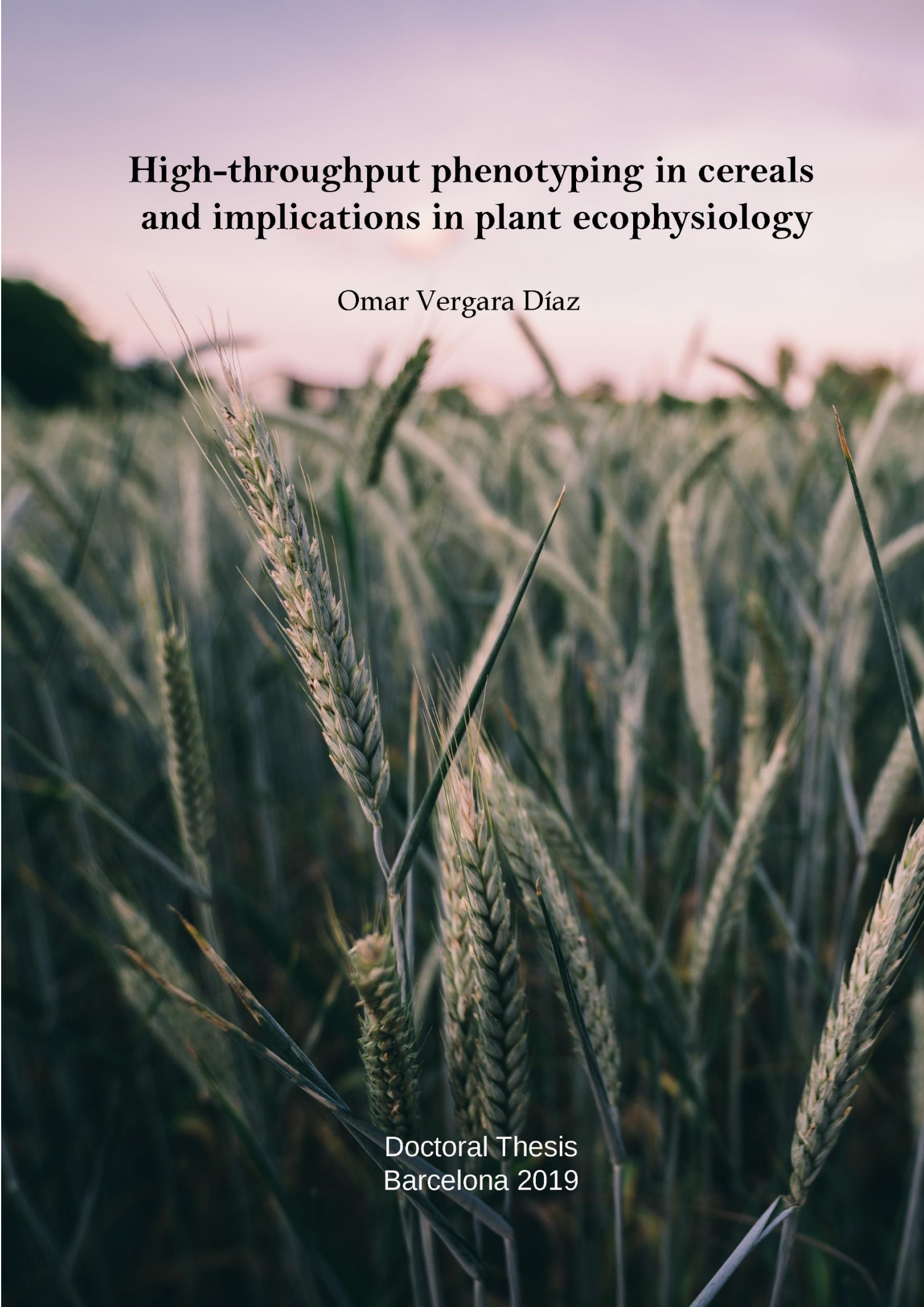

Doctoral Thesis
Barcelona 2019

Programa de doctorat d'Ecologia, Ciències Ambientals i Fisiologia Vegetal, adscrit al departament de Biologia Evolutiva, Ecologia i Ciències Ambientals.

High-throughput field phenotyping in cereals and implications in plant ecophysiology

Fenotipat de camp d'alt rendiment i implicacions en l'ecofisiologia vegetal

Memòria presentada per n'Omar Vergara Diaz per optar al grau de doctor per la Universitat de Barcelona

Omar Vergara Diaz

Josep Lluís Araus Ortega

UNIVERSITAT DE BARCELONA

B:KC Barcelona Knowledge Campus

Campus of Internacional Excellence

ABSTRACT

Global climate change effects on agroecosystems together with increasing world population is already threatening food security and endangering ecosystem stability. Meet global food demand with crops production under climate change scenario is the core challenge in plant research nowadays. Thus, there is an urgent need to better understand the underpinning mechanisms of plant acclimation to stress conditions contributing to obtain resilient crops. Also, it is essential to develop new methods in plant research that permit to better characterize non-destructively plant traits of interest. In this sense, the advance in plant phenotyping research by high throughput systems is key to overcome these challenges, while its verification in the field may clear doubts on its feasibility. To this aim, this thesis focused on wheat and secondarily on maize as study species as they make up the major staple crops worldwide. A large panoply of phenotyping methods was employed in these works, ranging from RGB and hyperspectral sensing to metabolomic characterization, besides of other more conventional traits. All research was performed with trials grown in the field and diverse stressor conditions representative of major constrains for plant growth and production were studied: water stress, nitrogen deficiency and disease stress. Our results demonstrated the great potential of leave-to-canopy color traits captured by RGB sensors for in-field phenotyping, as they were accurate and robust indicators of grain yield in wheat and maize under disease and nitrogen deficiency conditions and of leaf nitrogen concentration in maize. On the other hand, the characterization of the metabolome of wheat tissues contributed to elucidate the metabolic mechanisms triggered by water stress and their relationship with high yielding performance, providing some potential biomarkers for higher yields and stress adaptation. Spectroscopic studies in wheat highlighted that leaf dorsoventrality may affect more than water stress on the reflected spectrum and consequently the performance of the multispectral/hyperspectral approaches to assess yield or any other relevant phenotypic trait. Anatomy, pigments and water changes were responsible of reflectance differences and the existence of leaf-side-specific responses were discussed. Finally, the use of spectroscopy for the estimation of the metabolite profiles of wheat organs showed promising for many metabolites which could pave the way for a new generation phenotyping. We concluded that future phenotyping may benefit from these findings in both the low-cost and straightforward methods and the more complex and frontier technologies.

Acknowledgements

The culmination of this thesis has been possible thanks to the help and contribution of a great research team and an extensive network of collaborators. First, I thank my thesis director, prof. Josep Lluís Araus for his valuable dedication and guidance in the development of the thesis. Also, I thank prof. Maria Dolors Serret and prof. Jordi Bort for their great contribution in the functioning of the research team. I want to thank past doctoral students Rut Sánchez, Abdelhalim Elazab and Bangwei Zhou who kindly welcomed me when I joined the group, and gave me great lessons on statistics, isotopes, image processing, sensors and organizational skills in the field. In addition, I sincerely thank the very nice trainings, assistance and confidence from the post-doctorates Rubén Vicente and Thomas Vatter and the associate professor Shawn C. Kefauver. Lastly but not least, I want to thank all predoctoral mates Fadia Chairi, José Armando Fernández, Adrián Gracia, Samuel Kamphorst and Susan Medina, and new doctoral students Fatima Zahra, Maria Luisa Buchaillot, Melissa Chang, Joel Segarra and Ludovico Caracciolo, with whom it was a real pleasure to collaborate, discuss and travel, and made a nice work environment possible.

In addition, I thank the technicians of the department and of the experimental field facilities Carmen Cañueto, Josep Matas and Marta Pintó for their undoubtedly contribution for the development and materialization of some projects in which I was involved. Also, I thank the collaborators Nieves Aparicio from ITACyL-Valladolid, Maria Teresa Nieto, José Novo, Antonio Escolano and Jesús Vega from INIA-Colmenar de Oreja and Jesús Merida and Natalia Marín from INIA-Coria del Río for their involvement in field trials design and management, and Pablo Zarco and Alberto Hornero from IAS-Córdoba for their training and assistance in image processing. Finally, I want to specially thank to the international collaborators that kindly hosted and guided me in diverse research stays: Benhildah Masuka, Mainassara Zaman-Allah and Jill Cairns from CIMMYT-Harare (Zimbabwe), Toshihiro Obata and Alisdair Fernie from MPI-Golm (Germany) and Pedro Injante from EEA-Chiclayo (Perú).

Table of Contents

INTRODUCTION

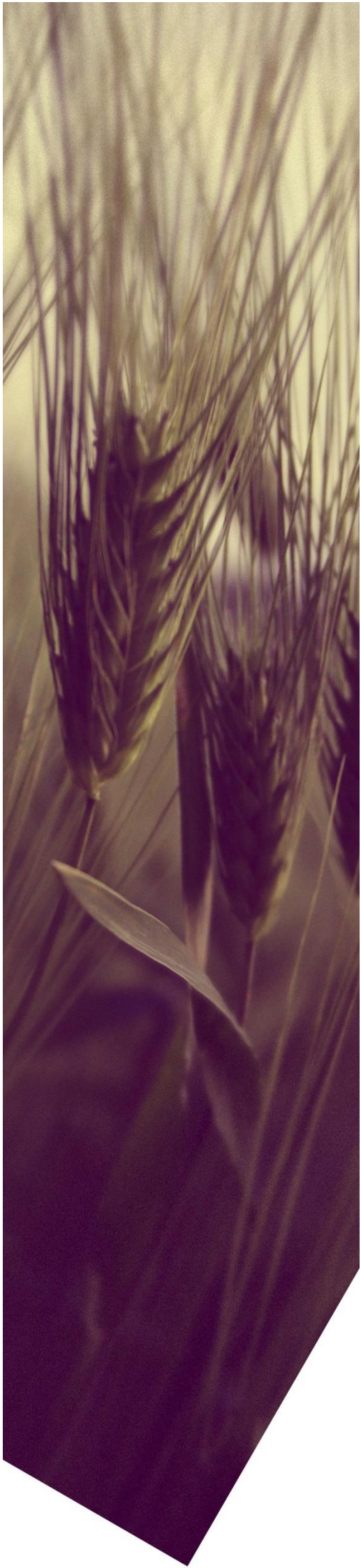

INTRODUCTION

Climate change and global warming: global and regional aspects

The Fourth Assessment Report of the Intergovernmental Panel on Climate Change (IPCC) did evidence that physical and biological systems on all continents and in most oceans are already affected by recent climate changes (Rosenzweig *et al.*, 2017). According to the last IPCC report (Allen *et al.*, 2018) human-induced global warming reached approximately 1°C above pre-industrial levels in 2017, currently increasing at 0.2°C per decade. However, warming greater than the global average has already been experienced in many regions and seasons, with higher average warming over land than over the ocean. Between 20–40% of the global human population is living in regions that, by the decade 2006–2015, had already experienced warming of more than 1.5°C above pre-industrial values. Past emissions alone are unlikely to raise global-mean temperature to 1.5°C above pre-industrial levels, but past emissions do commit to other climate processes and drivers that exacerbate the effects of global warming, even if all anthropogenic emissions were reduced to zero immediately. In global terms, there is evidence that the number and intensity of hot days have increased markedly in the last three decades and the occurrence of heat waves has doubled; and these increases will continue through the 21st century (Fig. 1). In addition, extreme phenomena such as heavy rainfalls may become more frequent during the 21st century in many parts of the world which may lead to more intense soil erosion even if the total rainfall does not increase (IPCC, 2014a).

That said, global change has a strong regional component. In Europe, average temperature has continued to increase, with regionally and seasonally different rates of warming, being the strongest over Scandinavia, especially in winter, whereas the Iberian Peninsula warmed mostly in summer (IPCC, 2014b). In agreement, for all emission scenarios the strongest warming is projected in Southern Europe in summer, and in Northern Europe in winter (Goodess *et al.*, 2009; Kjellström *et al.*, 2011). Even under an average global temperature increase limited to 2°C compared to preindustrial times, the climate of Europe is simulated to depart significantly in the next decades from today's conditions (Van der Linden and Mitchell, 2009; Jacob and Podzun, 2010).

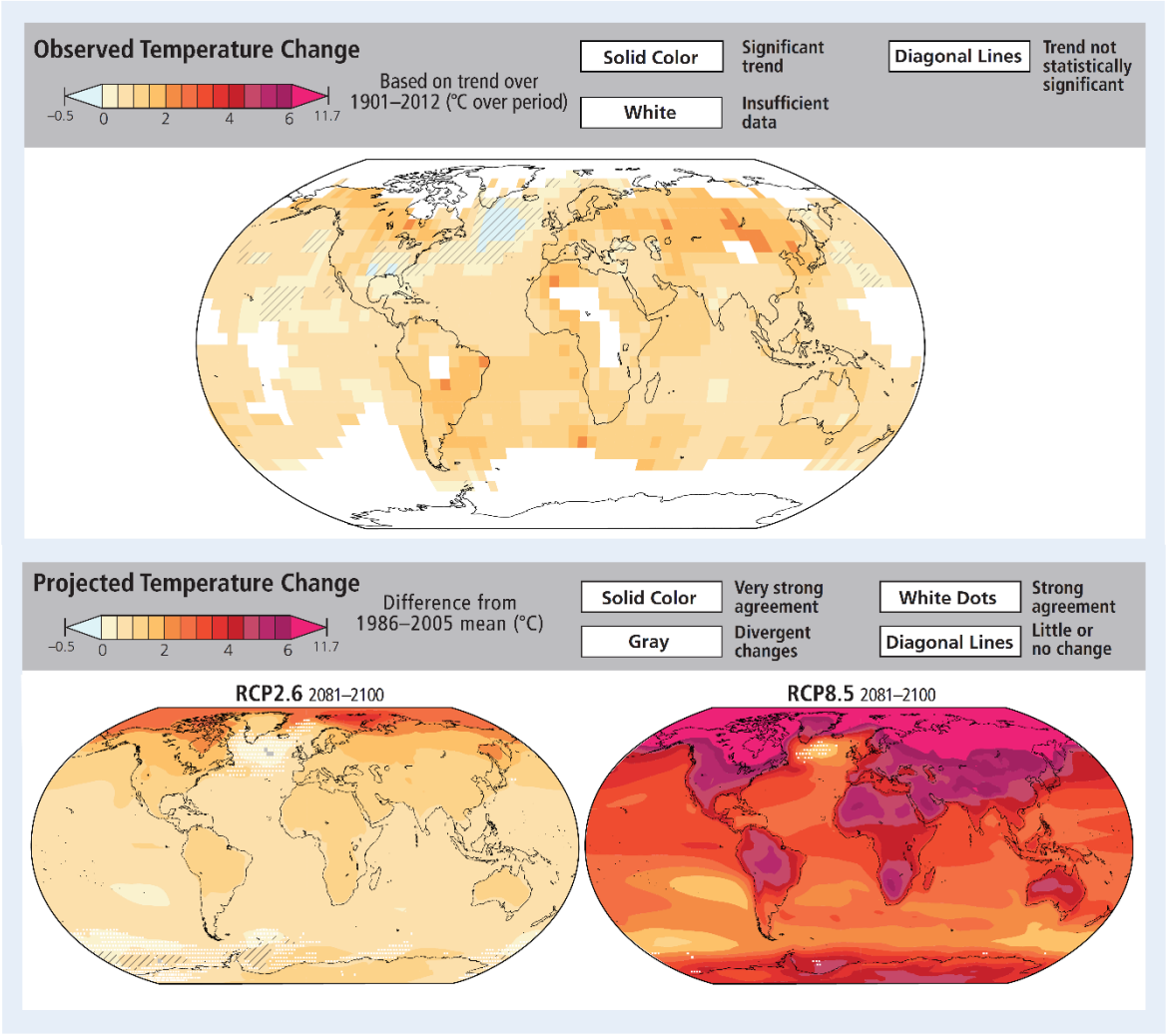

FIGURE 1. OBSERVED AND PROJECTED CHANGES IN ANNUAL AVERAGE SURFACE TEMPERATURE. IT ILLUSTRATES TEMPERATURE CHANGE OBSERVED TO DATE (TOP) AND PROJECTED WARMING (BOTTOM) UNDER AMBITIOUS MITIGATION (RCP 2.6) AND UNDER CONTINUED HIGH EMISSIONS (RCP 8.5) EXTRACTED FROM IPCC (2014A) REPORT

Precipitation changes associated with global warming are less clear and vary regionally and seasonally. Even so, increasing precipitation in Northern Europe and decreasing in Southern Europe are observed with a medium confidence level (Kjellström *et al.*, 2011)(Fig. 2). Consequently, dryness has increased mainly in Southern Europe and this may magnify regional differences for agriculture and forestry. Climate projections warn of a marked increase in extremes in Europe, including heat waves, droughts, and heavy precipitation events (Beniston *et al.*, 2007; Lenderink and van Meijgaard, 2008). Southern Europe may likely suffer more intense and longer meteorological droughts and their soil water content will decline. Changes in the patterns of soil saturation and drainage, snow accumulation and melting will impact by reducing groundwater recharge and/or water table level by the end of the 21st century (García-Ruiz *et al.*, 2011; Goderniaux *et al.*, 2011; Guardiola-Albert and Jackson, 2011). In addition, soil

degradation is already intense in parts of the Mediterranean and Central-Eastern Europe and, together with prolonged drought periods and fires, is already contributing to an increased risk of desertification. Projected risks for future desertification are the highest in these areas where extreme events may contribute about half of total erosion.

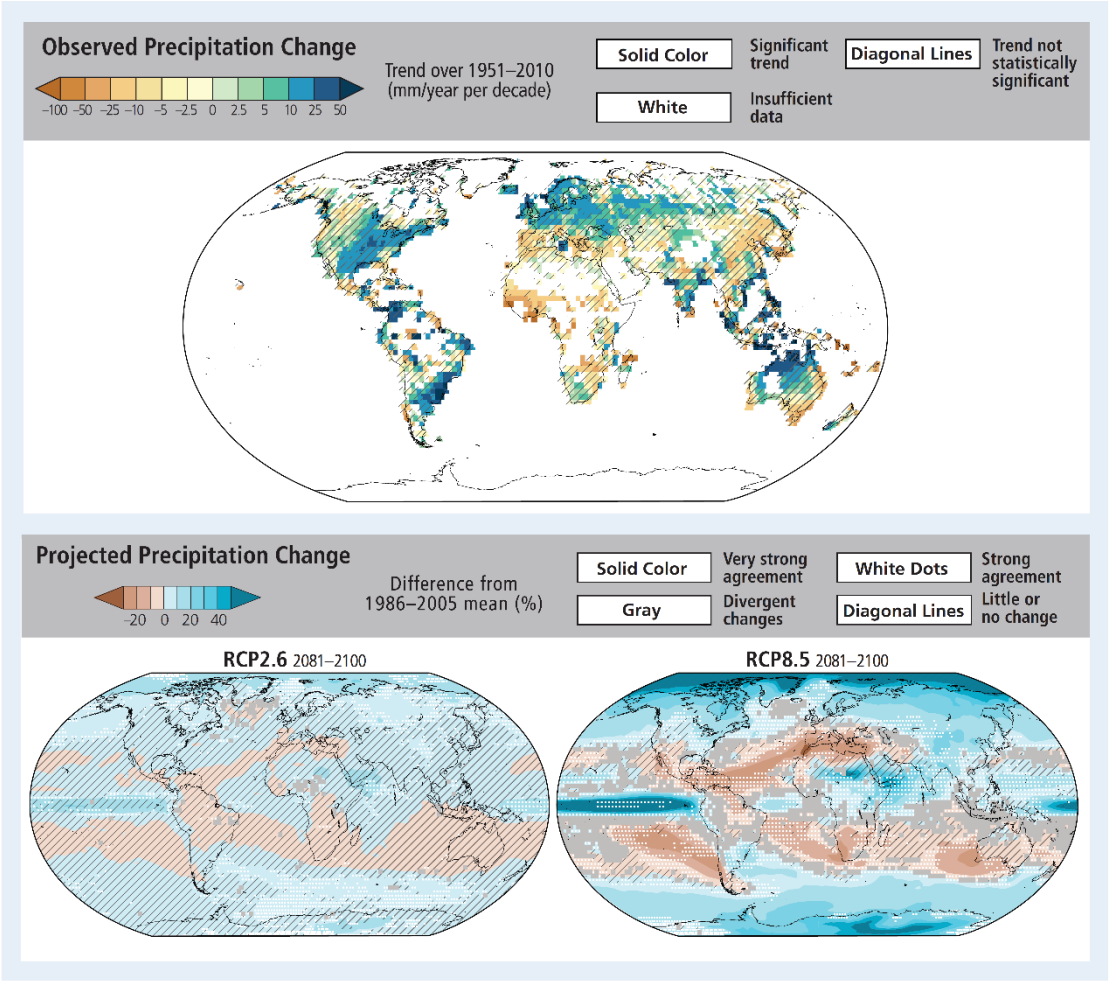

FIGURE 2. OBSERVED AND PROJECTED CHANGES IN ANNUAL AVERAGE SURFACE PRECIPITATION. IT ILLUSTRATES CHANGES OBSERVED TO DATE (TOP) AND PROJECTED CHANGES (BOTTOM) UNDER AMBITIOUS MITIGATION (RCP 2.6) AND UNDER CONTINUED HIGH EMISSIONS (RCP 8.5). EXTRACTED FROM IPCC (2014A) REPORT

Effects on agroecosystems

From early 1950s, a conjunction of advances and technology transfer initiatives in agronomy led to an unprecedented increase in agricultural productivity, particularly affecting the so called, small grain cereals. This was called Green Revolution and included the development of high yielding varieties, the massive synthesis and use of chemicals fertilizers as well as an increase in the level of mechanisation in cultivation. However, this intensification had several negative impacts on the ecological properties of agricultural systems, such as carbon sequestration, nutrient cycling, soil structure and functioning,

water eutrophication and pollination. At present, agriculture is an important land user across the world, covering about 35% of the total land area of western Europe (Rounsevell *et al.*, 2006). In terms of water use, agriculture accounts for 24% of total national freshwater abstraction in Europe and more than 80% in some Southern European countries (EEA, 2009).

On the other hand, excessive heat interacts with key physiological processes in plants leading to shortening of crop cycle, growth cessation and even early senescence and leaf defoliation (Teixeira *et al.*, 2013). At the global scale, increased frequency of unusually hot nights and extremely high daytime temperatures are damaging and occasionally lethal to crops (Schlenker and Roberts, 2009; Peng *et al.*, 2004; Porter and Gawith, 1999). In balance, local temperature increases of 2ºC or more -above late 20th century levels- will negatively impact production of major crops (wheat, rice and maize), although certain temperate regions may benefit (Fig. 3).

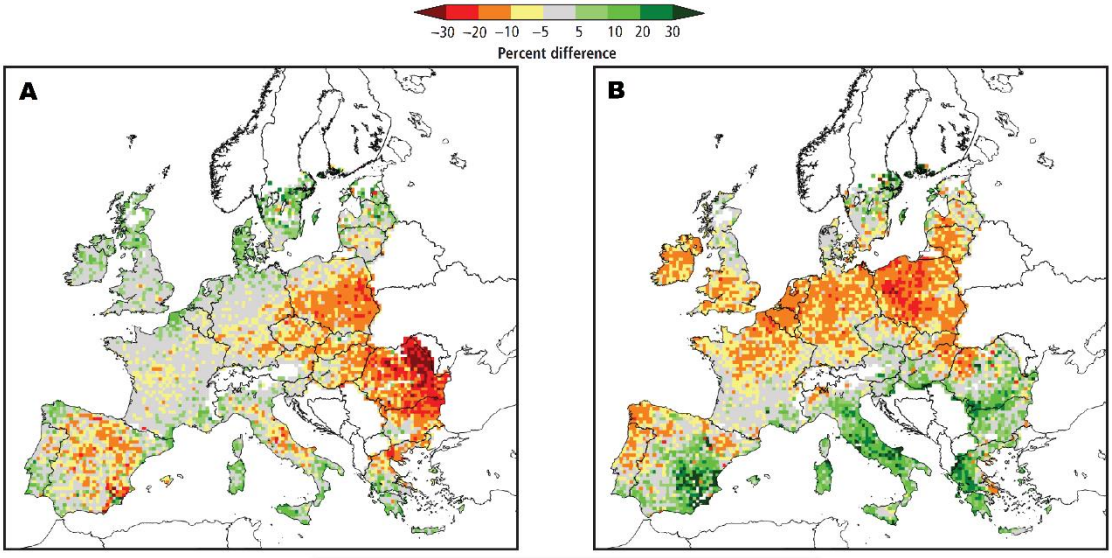

FIGURE 3. PERCENTAGE CHANGE IN SIMULATED WATER-LIMITED YIELD FOR WINTER WHEAT (WITHOUT ADAPTATION) IN 2030 WITH RESPECT TO THE 2000 BASELINE FOR THE A1B SCENARIO USING ECHAM5 (A) AND HADCM3 (B) MODELS. EXTRACTED FROM IPCC (2014B) REPORT.

Increases on global temperature together with the reduction in precipitation in many regions will affect global water demand of crops, with projected increases between 7 to 21% (Wada *et al.*, 2013) with a pronounced regional pattern. As consequence, agriculture production will be threatened (Trnka *et al.*, 2011; Daccache and Lamaddalena, 2010), particularly in those regions, such as the Mediterranean area, where irrigation might not be a viable option due to the projected declines in total surface water streams and groundwater resources (Olesen *et al.*, 2011).

In terms of crop production, there is already evidence of negative effect of climate changes on the production of major crops such as wheat and maize in many regions, and medium confidence for

negative impacts on global production (Lobell *et al.*, 2011). For instance, heat waves and droughts events in 2003 and 2010 summers caused grain losses of up to 20-30% in some growing regions of Europe and Russia, whereas in the Iberian Peninsula cereal production fell by 40% at 2004/2005 drought (Barriopedro *et al.*, 2011; Ciais *et al.*, 2005). Therefore, crop suitability is likely to change, particularly in regions like Southern Europe where yield losses may reach 25% by 2080 (Ciscar *et al.*, 2011), with increased risks of rainfed-crops failure (Ferrara *et al.*, 2010; Bindi and Olesen, 2011). At the world level, projections also identified South Asia and Southern Africa as the most potentially affected regions, suffering the most negative impacts on wheat, maize, sorghum and millets production (Lobell *et al.*, 2008). It must also be noted that climate changes, particularly temperature increases, may result in changes in overwintering, summer survival and geographic ranges of pests and diseases, with subsequent increases in potential yield losses.

Several experimental studies in CO_2 enriched environments (growing chambers or free-air CO_2 enrichment trials) point out an initial benefit from increasing CO_2 concentration in photosynthesis, plant growth and yield. Furthermore, CO_2-induced stomatal resistance may trigger a stronger response to elevated CO_2 in water-stressed crops than in well-watered ones. Thus, in some cases, elevated atmospheric CO_2 concentration could have fertilizer effect and might partly cancel out the adverse effect of climate change, increasing water use efficiency of crops while reducing water demand (Konzmann *et al.*, 2013). Even in this optimistic case, future irrigation demand is projected to exceed local water availability in many regions such as Southern Europe (Wada *et al.*, 2013).

Agriculture challenges and adaptation strategies

In the context of the explained climate changes associated with past greenhouse gases (GHG) emissions and considering the very high likelihood of additional emissions and climate changes, and the impacts on food security and production, agricultural systems require some level of adaptation. Also, the agriculture sector will need to reduce its contribution to total anthropogenic GHG emissions, besides facing a changing and more variable climate (Lavalle *et al.*, 2009; Smith and Olesen, 2010). It is also paramount to consider that global agricultural demand is expanding because of increasing world population as well as by changes in dietary habits in emerging economies and increasing competition of crops as sources for bio-energy, fibres and other industrial purposes (Rahaman *et al.*, 2015). Indeed, the Food and Agriculture Organization (FAO) has projected that cereal production must be doubled before 2050 in order to meet crop production demand, evidencing the urgency to adopt new strategies and develop novel methods in plant biology.

Strategies to adapt agriculture are broad and include from alteration in agronomy practices and management to plant breeding. Adjusting cultivation in terms of sowing and harvest times is already

adopted by farmers in some regions and may be an effective adaptation enhancing food security and sustainable livelihoods (IPCC, 2014b). However, this strategy may not be effective in many regions such those with Mediterranean climates, where early sowing of cereals depends on adequate rains in autumn and these are projected to decrease. In these circumstances, the use of short cycle cultivars has been proposed as a mitigation option in order to reduce exposure to terminal droughts and high temperatures (Orlandini *et al.*, 2009). Another group of strategies to adapt cropping systems are those practiced in conservation agriculture: reduced tillage, addition of crop residues and manure to the soil and increase diversity in crops rotation, which contribute to increase soil carbon and nitrogen, reduce soil erosion and improve soil water holding capacity (Smith and Olesen, 2010). Other pathways would be the implementation of more efficient irrigation and drainage systems and, ultimately, the change in land allocation and in the cultivated varieties or even crop species. Considering the projected climate scenarios, a conjunction of all possible strategies will need to be applied. Even so, plant breeding is the only way to obtain more resilient cultivars to future stressor scenarios reducing risks of yield shortfall (Olesen *et al.*, 2011; Ventrella *et al.*, 2012). In this sense, breeding challenges are several: improving cultivar tolerance to high temperatures and drought while optimizing water use efficiency. Furthermore, taking in consideration that a new variety usually takes between 8 to 14 years to be delivered (Ziska *et al.*, 2012), much more efforts must be dedicated in the development of plant breeding.

Basics on cereal biology and cultivation

Cereals are a diverse group of monocots grasses typically cultivated for their edible grains (caryopsis) and forage uses and belong to the family of Poaceae. This family is characterized for its cosmopolitan distribution due to the great adaptability to diverse soil and climate environments. Cereals comprise many cultivated species sown (in temperate climates) at spring like rice, sorghum and maize and other typically sown at autumn such as wheat, barley and oats. Cereals, together with legumes (Fabaceae) were the first plant families cultivated and domesticated, beginning about 12000 years ago, in the transition between the Epipaleolithic and the Neolithic in nuclear regions (e.g. Near East and East China) and permitted the sedentarism of human populations and the development of the first Great Civilizations. Wild varieties were initially cultivated and over time, these species were probably domesticated gradually by the selection of advantageous characteristics. In the case of cereal grasses, this human selection -in different sites and from different species- converged in some traits: from small-sized, naturally dispersed and coated seeds into larger seeds and devoid of dormancy and dispersal ability (Remigereau *et al.*, 2011). In the case of wheat, domestication of diploid (*Triticum monococcum*, 2n=2x=14) and tetraploid (*Triticum turgidum*, 2n=4x=28) forms is thought to have occurred at least 9000 years ago, whereas hybridization event producing hexaploid wheat (*Triticum*

aestivum, 2n=6x=42) probably occurred 6000 years ago, although this chronology is not yet entirely sure and in fact radiocarbon calibrated evidence of domesticated wheats and barley older that these dates have been published (e.g. Araus et al. 2014). Thus, ancestral selection resulted in the obtention of cereal species with which populations were feed, typically wheat and barley in Near-Middle East and Europe, rice in Far East, maize in America and millet in Africa. At present, more than 50% of caloric intake by world population is derived directly from cereal grain consumption (Awika, 2011). From these cereals, wheat is the most widely cultivated staple cereal worldwide with over 218 Mha in cultivation whereas maize is the second one and the most commonly cultivated cereal in Africa in terms of land area and production (FAO, 2013).

Regarding growth and development, cereals are herbaceous, annual and predominantly self-pollinating plants (not for maize). Despite clear similarities, cereals encompass several subfamilies and tribes so that further explanation of cereal biology will be focused predominantly on wheat as it is the main species studied in the current thesis and secondly on maize.

Wheat plants have a principal stem from which alternate leaves emerge. The stem is composed by repeating segments -phytomers- that contain a node, an internode and a leaf. The stem is erect and hollow -fistulous- except in the node, where the other tissues converge, and terminates in the ear. The leaf is made up of the leaf blade and the leaf sheath, which is inserted in the node and wraps the inter-node below. In the junction between the blade and the sheath there is a ligule and a pair of auricles, which are characteristic structures of cereals. Cereal leaves are amphistomatous and isobilateral and basically consist in an epidermis covered with an epicuticular wax and these enclose the mesophyll that is transected by the vascular tissues. The terminal leaf in cereals is called flag leaf. Besides, wheat plants have secondary tillers, which are lateral branches originated from the main stem and have the same morphoanatomical traits as the main tiller. Wheat has two types of roots: i) seminal or primary roots are the first root type to emerge and sustain plant development during the first stages and ii) the nodal or secondary roots that develop as tillering starts. Wheat root system can grow up to 2 m deep, but most roots are concentrated in the top 30 cm of soil. The ear -or spike- of wheat is an inflorescence that has a central rachis that supports two rows of spikelets and these in turn contain the florets (flowers). Spikelets are surrounded by protective bracts called glumes, whereas florets are enclosed by other bracts, a lemma (outer position) and a palea (inner position). In some varieties, lemmas may form an awn in their top. The sexual tissues of florets are composed of the carpel, containing the ovary and the stigmas, and three stamen and anthers enclosing the pollen grains. Finally, wheat caryopsis or grain is made up of external bran coat consisting of the pericarp, the testa and the aleurone layers; enclosed is the endosperm that stores the starch and proteins and separated by the scutellum is the embryo containing the root radicle and the shoot apex surrounded by the coleoptile.

Regarding plant development, the main stages in wheat growth are germination, seedling growth, tillering, stem elongation, booting, awn emergence, flowering, grain filling (comprising milk and dough development) and ripening (Fig. 4). The vegetative shoot apex initiates variable number of leaf primordia after seed germination. Leaf appearance and extension will be mainly influenced by temperature. Nodal roots develop simultaneously and roots originating from tillers start developing after a tiller has formed three leaves. Stem elongation coincides with the growth of leaves, tillers, roots and the inflorescence. The first tillers emerge from the axils of the coleoptile; in winter wheat few of them may form in autumn or winter followed by a rapid increase in tiller number with warmer spring temperatures. Elongation of the stem begins when most florets on the developing spike have initiated stamen primordia. The peduncle is the final segment to elongate. Reproductive stage begins once the ear is formed and emerges, afterwards flowering -anthesis- occurs followed by fertilization, grain filling and ripening. Cereal development is usually quantified by decimal codes among which Zadoks' scale is the most widely used (Zadoks *et al.*, 1974).

On the other hand, maize is a typically tropical and subtropical crop but is has been adopted in many temperate regions and it is of great importance for human consumption, animal feed and for its derived products like corn ethanol. The origin of maize occurred in the Mesoamerican region, probably in the Balsas River Valley, whereas several theories have been proposed for its domestication. It is generally accepted that a small annual Teosinte species (likely *Zea mays* ssp. *parviglumis*) is the genetic background of modern maize (Matsuoka *et al.*, 2002) although the hybridization with other grasses like *Zea diploperennis* and/or *Tripsacum dactyloides* during domestication process has also been proposed (Eubanks, 1997). Maize is a tall, monoecious and annual plant that produces large, narrow, opposite leaves borne from the stem. Ears (female inflorescences) develop approximately in the midsection of the plant between the stem and the leaf sheath whereas tassels (male inflorescences) forms in the apex of the stem.

It should be mentioned that, as a C4 species, maize leaves have a typical Kranz anatomy in which carbon fixation is compartmentalized, so that small mesophyll cells surround a sheath of parenchyma cells called bundle sheath, where carbon enters the Calvin Cycle. Maize development is split into vegetative and reproductive stages, and these are listed depending on the number of fully developed leaves (with visible collar) and on the development of the forming grains, respectively (Fig. 4). After seedling (or sprouting) stage, there is an initial gradual development and extrusion of leaf blades, followed by a rapid growth (usually at V10-V17) called Grand Growth Phase, as long as stress, moisture and temperature permit. Vegetative stage terminates when tassels make visible (VT) and plants have attained their maximum height. Thereafter, the extrusion of silks (elongated stigmas) from the husks marks the first reproductive stage, silking stage (R1), that involves the maturity of female flowers. At this point, pollination phase can be initiated. After fertilization, development stages comprised in grain

filling are classified by grain maturity, from soft-dough (R2-R3, milky stage) to hard-dough grain (R4-R5, maturity stage).

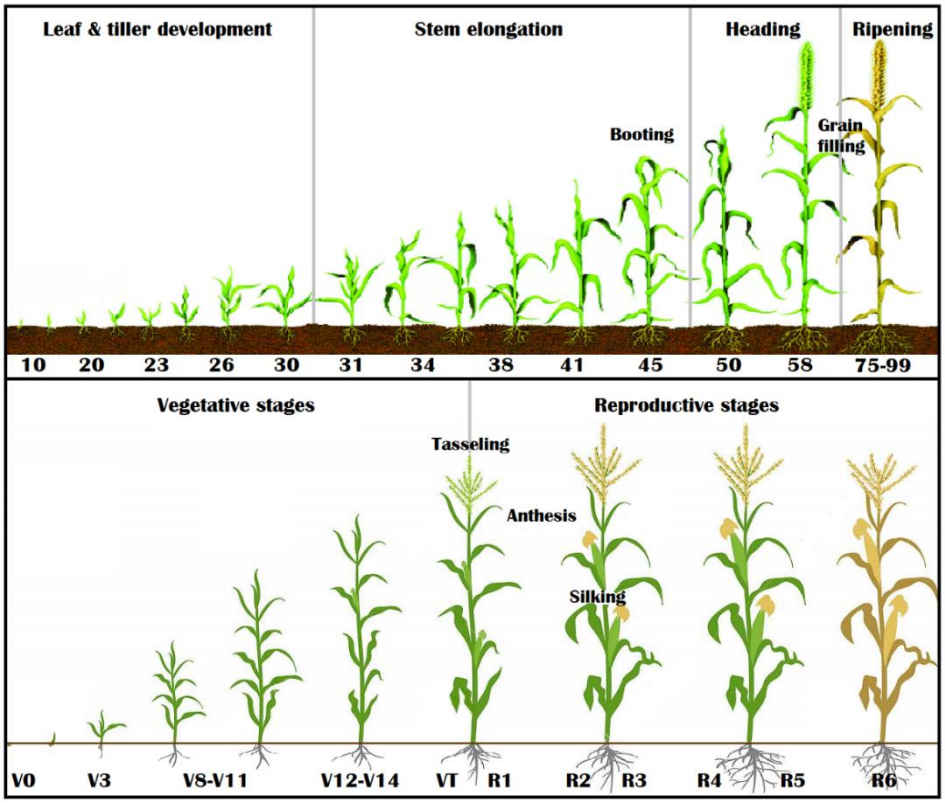

FIGURE 4. WHEAT (ABOVE) AND MAIZE (BELOW) DEVELOPMENT AND GROWTH STAGES. ZADOKS GROWTH SCALE IS SHOWN FOR WHEAT

Stresses constraining agroecosystems and crop production

In broad sense, it is considered that plant stress occurs when the genetic potential for plant growth and reproduction is constrained by any biotic or abiotic factor (Jones and Qualset, 1984). In general terms, we can distinguish two types of stress: abiotic stress, which refers to any environmental conditions or combination of them affecting plant growth like heat, drought, freezing and salinity; whereas biotic stress refers to any damage in the plant done by other organisms like fungi, bacteria, insects, viruses and herbivores. All agroecosystems are subjected to some degree of stress in their life history, but undoubtedly the severity of the stresses will exacerbate under climate change scenarios, particularly due to heat and water stresses.

Water stress occurs when water absorption by the plant -associated with root characteristics and soil properties- is lower than the evaporative demand of the atmosphere. Water stress occasioned by water scarcity may trigger several mechanisms of acclimation such as changes in genetic expression and modulation of plant metabolism, physiology and morphoanatomy leading to homeostatic

compensation (Flexas *et al.*, 2006). Furthermore, the extent of the impact of water stress on plant growth and reproduction is stage dependent as certain development stages are particularly sensitive. In the case of cereals, although water stress may occur in any stage due to environment factors, the most critical phase may occur from double ridge to anthesis, when the potential number of kernels is determined. In the beginning of crop growth, water scarcity may reduce seed germination and crop establishment, with subsequent effect on crop early vigor. After emergence, total leaf area development is the most affected trait as a result of reduced leaf expansion and tillering, whereas the number of spikelet primordia may also decrease (Peterson *et al.*, 1984; Rickman *et al.*, 1983; Oosterhuis and Cartwright, 1983). In the period comprised from booting to anthesis there is a very active plant growth, so that water-stress in this stage involves a decrease in cell growth and leaf area with a consequent decrease in photosynthetic area. This may be followed by an increase in stomatal resistance, involving a decrease in leaf internal CO_2 (Ci) which leads to reduced net photosynthesis (Acevedo *et al.*, 1991). Water stress affecting from anthesis to grain filling causes an acceleration of crop development by shortening of grain filling period and an early senescence. Consequently, grain weight is affected negatively (Kobata *et al.*, 1992). Reports indicate that more than 50% of land where wheat is grown is already affected by periodic droughts during flowering and grain filling stages (Pfeiffer *et al.*, 2005). In the case of maize, anthesis to silking interval (ASI) has been directly related to the degree of the stress so that the higher stress suffered the longer ASI.

Regarding heat stress, it causes an acceleration of plant development, a dysfunctional photosynthesis, lower fertility and poor fruit formation, having subsequent effects on crop yield. Heat stress may be mainly avoided by transpiration permitting the cooling of tissues. However, heat stress is often accompanied by water deficit; that is the case of the typical Mediterranean hot and dry summer. In such cases, non-limited transpiration as strategy may not be implemented, so that cereal breeding purposes should address heat and water stresses in combination.

Nutrient deficiency is usual in agroecosystems and may originate diverse kinds of nutrient stress. Major nutrients constraining ecosystem and crop growth are nitrogen, phosphorus and in a minor extent potassium or iron. Plant symptoms of nutrient deficiency are element-specific, in general chlorosis, necrosis, reduced growth and reduced tillering and yield in cereals are usual. At the metabolic level, nutrient deficiency may involve enzyme dysfunction or degradation like in the cases of Rubisco and Nitrate Reductase complexes. Focusing on crops, low soil fertility, together with drought and heat, is a major stress factor limiting productivity globally (Stewart *et al.*, 2005). In certain regions such as sub-Saharan Africa, agricultural productivity remains the lowest in the world partly, due to low soil fertility particularly poor in nitrogen (Cairns *et al.*, 2013; Fischer *et al.*, 2014). In developed countries the intensive use of fertilizers has enabled to increase crop production but serious environmental problems such as groundwater pollution and eutrophication have been

generated. Therefore, an optimization of nutrients use efficiency of crops is critical to ensure food security, especially in the low productive regions, while an appropriate fertilization management may prevent further degradation of the environment.

Biotic stress is an additional constraint to ecosystem and crop production that yearly causes certain percentage of losses, in the case of wheat and maize crops they have been estimated in 28% and 31% of production loss worldwide, respectively (Oerke, 2006). Biotic stress may be exerted by many organisms that cause diseases, pests and competition for resources in plants, like bacteria, fungi, arthropods and nematodes besides of herbivory and weeds. From an ecosystemic or agricultural point of view, the presence of certain organisms causing damage in plants is unavoidable and admissible as long as its incidence is not dramatic. However, weather seasonal variability and climate changes associated with global warming can aggravate the level of spread of pests and diseases and occasionally cause great impacts on ecosystems and crops production. Also, intrusion of foreign disease-causal agents, due to global market trade or to changes in their geographical ranges, entail further hazards to ecosystem stability and food security. For instance, the appearance of new races of yellow rust (*Puccinia striiformis* f.sp. *tritici*) has recently threatened durum wheat production in Mediterranean regions and temperate Europe where the losses due to this fungal disease were previously minimal (Almacellas *et al.*, 2013; Martinez-Moreno and Solís, 2019). Due to abnormally cool temperatures and high humidity this rust spread epidemically and caused widespread yield losses in Spain (Almacellas *et al.*, 2013). Development of resistant varieties is essential for effective control; however, to date no variety with resistance to the strain has been recommended in Spain (Martinez-Moreno and Solís, 2019).

Events stated above evidence the urgency to breed for new-tolerant crop varieties to face these challenges, besides other strategies that may be adopted. Furthermore, in the case of post-green revolution wheats, the genetic gain has stagnated or even declined (Chairi *et al.*, 2018) so that breeding for stress tolerance is urgent, particularly in regions that are highly sensitive to climate change such as the Mediterranean Basin (Field *et al.*, 2014). In this sense, recent investigations on the role of plant tissues other than leaves revealed that the performance of the ears could be particularly relevant under stress acclimation (Tambussi *et al.*, 2007; Sanchez-Bragado *et al.*, 2014; Merah *et al.*, 2017; Vicente *et al.*, 2018), which offers new opportunities for plant breeding.

Ecophysiology and the study of plant-crop traits and phenotypes: tools and techniques in plant biology research and phenotyping

Plant ecophysiology refers to the study of plant functioning (i.e. physiology) including the responses to environmental conditions. Unlike animals, plant cannot -literally- hide or scape from unfavorable

conditions so that they must trigger acclimation mechanisms to endure these conditions which is possible because of the great phenotypic plasticity of plants. The concept phenotype refers to the set of observable characteristics of an organism, which includes in broad sense its morphological, physiological and biochemical traits, among other. This term was first proposed by the Danish botanist Wilhelm Johannsen in 1911 in order to differentiate the genetic heredity (genotype) from the observed traits of an individual (phenotype) as a result of its interaction with the environment. Thus, the phenotype of an organism is basically the product of the expression of its genetic code over the course of development influenced by environmental factors. Likewise, phenotyping refers to the study and characterization of phenotypes and their -genetic, metabolic, physiological, morpho-anatomical, etc.- particularities. Another recently coined terms are phenome and phenomics, referring to the complete set of phenotypes of an organism and their systematic study, respectively. These require the acquisition of high-dimensional phenotypic data (i.e. different categories of phenotypic traits measured at different spatial and temporal resolutions), aiming to understand the pathways connecting genotypes to phenotypes (Houle *et al.*, 2010; Großkinsky *et al.*, 2018). The integration of multi-omics techniques (including the physiological approach) into phenomics is proposed for this understanding (Rahaman *et al.*, 2015; Großkinsky *et al.*, 2018). Indeed, plant metabolome and proteome (and enzymes activity level or activomics) constitutes the internal phenotype, which is determined by the genome by interacting with the environment (concerning the fields of epigenomics and transcriptomics) (Großkinsky *et al.*, 2018; Großkinsky *et al.*, 2015). These internal phenotypes in turn shape external phenotypes that can be determined by non-invasive techniques (e.g. imaging) (Fig. 5).

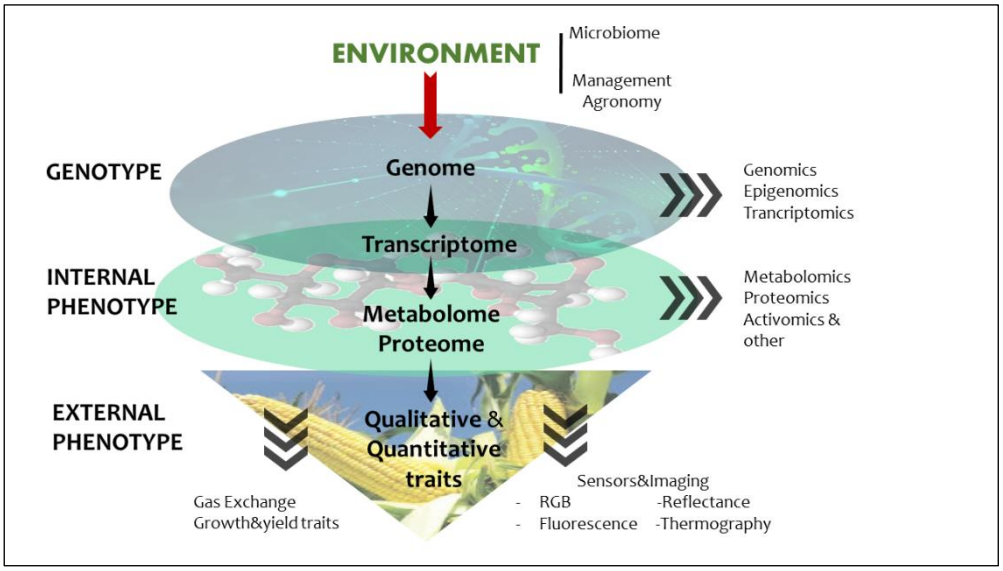

FIGURE 5. SCHEMATIC ILLUSTRATION OF VARIOUS 'OMICS' TECHNIQUES AIMED TO ANALYZE PLANTS BY DETERMINING THE INTERNAL PHENOTYPE ON THE PHYSIOLOGICAL AND BIOCHEMICAL LEVEL, AND BY NON-INVASIVE IMAGING, TO DETERMINE THE EXTERNAL PHENOTYPE. ADAPTED FROM GROßKINIKY (2015).

The development and implementation of bioinformatics and modeling is a crucial part of the phenotyping pipeline that enables to process and integrate huge amount of information and databases. With regard to the advancement of crop breeding, phenotyping is considered nowadays a major bottleneck (Araus and Cairns, 2014; Araus *et al.*, 2008; Cabrera-Bosquet *et al.*, 2012). The efforts of researchers and an adequate financing have made possible the advance in the design of new techniques, applications and experimental platforms, particularly aimed to practical phenotyping under field conditions, usually called high-throughput phenotyping (HTP) systems. The development of meaningful high throughput phenotyping (HTP) systems require an ecophysiological understanding of plant responses to new environmental conditions to connect plant genotype to phenotype to environment (Araus and Cairns, 2014). In this sense, it is fundamental that experimental set up, including the chosen methodology and phenotyping tools are appropriate for the purposes of the investigation (i.e. for the studied phenotypic traits and plant processes). Also, new generation phenotyping should reflect the different realities and needs and aspire to the acquisition of broad-use and affordable methods while exploiting the capabilities of other methods (Araus and Kefauver, 2018).

Conventional phenotyping -implemented as decision criteria in breeding programs- has been based principally on quantitative measurements of agronomic traits like grain yield and its components such as the harvest index, thousand kernel weight, ear density and the number of kernels per ear. Obviously, this kind of characterization requires to complete the whole crop cycle which implies a delay in breeding programs advance. Instead, early vigor and crop establishment measurements that are related with potential yield can be assessed at the beginning of growth, but they may be deceptive about cultivar performance in the coming conditions. Gas exchange and florescence can be directly measured in the field through infrared gas analyzer systems and fluorimeters, providing valuable information about photosynthesis, transpiration or respiration functioning. However, these measurements are considerably time-consuming when diverse experimental conditions or large number of genotypes are considered or when response curves are performed.

In plant research, compositional and morphological traits usually analyzed are the water content, the relative water content, the water potential, the specific leaf area (or leaf mass per area), leaf thickness, plant height, nitrogen concentration, nitrogen per unit leaf area or the carbon to nitrogen ratio, informing on water status, nitrogen use efficiency and leaf construction or the prevalence of supporting elements (Poorter and Evans, 1998; Feng *et al.*, 2008; Taylor *et al.*, 1989). Other morphoanatomical approaches address the quantitative measurement at the microscope of tissue or organ traits of interest, like epidermis and cuticle thickness and composition, stomatal density or leaf glaucousness. Morphoanatomical traits can be determinant of photosynthesis under stress (by influencing light distribution, delivery of CO_2 and water relations), including diseases (due to mesophyll structure), whereas their adaptation may improve water-use efficiency and drought resistance

(Djanaguiraman *et al.*, 2011; Tholen *et al.*, 2012; Rosyara *et al.*, 2007; Ennajeh *et al.*, 2015; Sagaram *et al.*, 2007). While all these traits can be used for characterizing plant stress and functioning, and for screening ecotypes and provenances for breeding, their routinely use in HTP in the field is not feasible. This is because they usually require cooling or freezing temperatures at sampling, chemical fixation (for the measurement of anatomy traits), besides of carrying samples to the lab where physiologic, compositional and anatomic analyses can be performed.

The study of stable isotope composition in plant-tissues dry matter is a reliable information for phenotyping as it constitutes an integrative indicator of plant status during growth (Masuka *et al.*, 2012). Carbon isotope composition ($\delta^{13}C$) is indicative of water use efficiency and water stress, nitrogen isotope composition ($\delta^{15}N$) may inform about nitrogen use efficiency (Serret *et al.*, 2008), whereas oxygen isotope composition ($\delta^{18}O$) provides information regarding leaf evaporative conditions throughout the crop cycle and water use (Barbour *et al.*, 2000; Cabrera-Bosquet *et al.*, 2009). Although isotope analyses are usually done from oven-dried samples (so there is no need for freezing or fixation at sampling) with subsequent grinding, they do require a precision weighing and sealing at the lab prior to detection with an isotope-ratio mass-spectrometry elemental analyzer.

Sensing methods and imaging systems

Sensing methods make use of a set of non-destructive techniques for the acquisition of information of an object or phenomenon from more or less distant sensors, without making direct contact to them. Remote and proximal sensing may be implemented in plant sciences including plant physiology, ecology and agronomy and aim to phenotype plant and crop performance in the field. In general terms, sensing technologies are based on the detection of a propagated signal (e.g. electromagnetic radiation) from an object throughout the electromagnetic spectrum. Remote sensing sensors are classified as active if they emit a signal and its reflection by the object is detected by the sensor (e.g. Radar and LiDAR); and passive if they detect the radiation emitted by the object which comes from another source, usually sunlight (e.g. radiometers and photography). Furthermore, this set of sensors can be implemented at diverse scales: remote sensing evaluation, including satellites and manned and unmanned aerial systems and at the ground level. Different categories of sensors may be deployed, including among others: spectrometers, thermal sensors and RGB imagers (Fig. 6). Logically, the choice of appropriate sensors, platforms (e.g. aerial vehicles, buggies and stationary platforms) and range of application is fundamental and directly impacts the scale of the research conducted (e.g. from ecosystem to single plant), the trait of interest (e.g. from biome primary production to leaf photosystems status) and the associated costs.

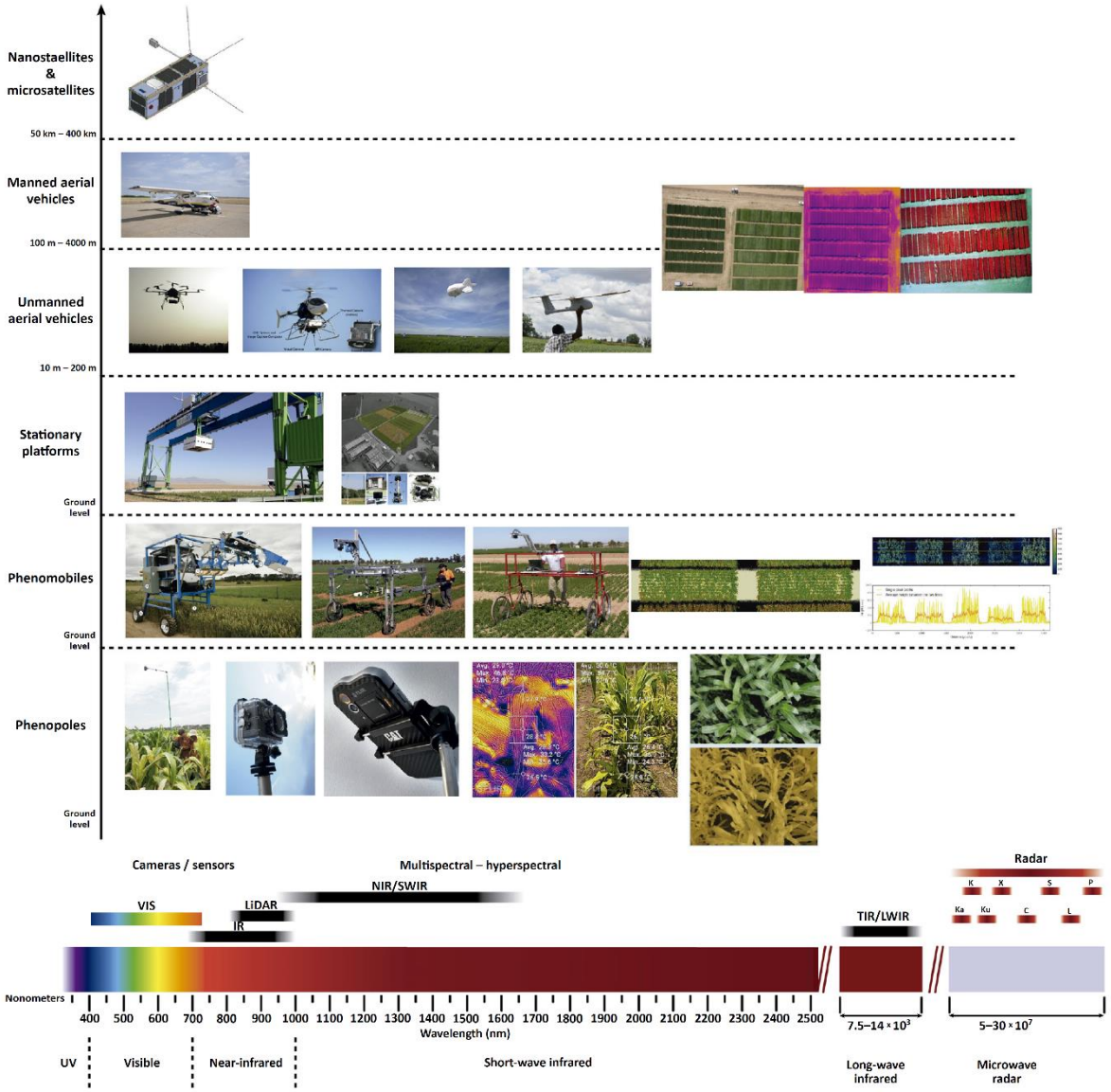

FIGURE 6. POTENTIAL AND ACTUAL GROUND AND AERIAL PHENOTYPING PLATFORMS, ALONG WITH THE SPECTRAL RANGES USED FOR DIFFERENT REMOTE SENSING TOOLS. X AXIS CORRESPONDS TO THE SPECTRAL RANGE OF SENSORS AND Y AXIS CORRESPONDS TO THE SCALE OF APPLICATIONS AND PLATFORMS EMPLOYED. VIS, VISIBLE; IR, INFRA-RED; NIR, NEAR-INFRARED; SWIR, SHORT-WAVE INFRARED; TIR, THERMAL INFRARED; LWIR, LONG WAVE-INFRARED; LIDAR, LIGHT DETECTION AND RANGING SENSORS. REDRAWN FROM ARAUS ET AL. (2018).

The spectral ranges measured through imagery systems, radiometers or other types of sensors are typically split in the ultraviolet (UV, 10-400 nm), visible (VIS, 400-700 nm), near infrared (NIR, 700-1400 nm), short wave infrared (SWIR, 1400-2500 nm) and the thermal infrared (TIR, 3 to 15 μm). Two important aspects, that must be taken in consideration, are, the spatial resolution which is the real area size corresponding to a pixel; and when spectroradiometers are considered, the spectral resolution which is the wavelength range recorded per each frequency band. In that sense, one can distinguish multispectral systems that records spectral information in multiple wavebands (usually

broadbands), and the hyperspectral systems which generates a continuous spectrum (whose range depends on the sensor) with narrow spectral bands. Earth observation systems integrated in launched satellites are commonly multispectral imagers such as those in Landsat, NOAA and Sentinel programs. On the other hand, at the proximal and field levels, both multispectral and hyperspectral systems can be employed providing higher spatial resolution, which is particularly important when investigating small land areas such as crop plots and forest trees.

Remote and proximal sensing are broadly used in plant sciences for the understanding of the functioning, structure and dynamics of agroecosystems and for the monitoring and mapping of traits of interest, like ecosystem biodiversity and its biochemical and mineral content. The basis for the spectroscopic studies of vegetation lies on the interaction of radiation with foliage which has a characteristic spectral signal. Thus, vegetation-plant spectrum is the result of combined spectral signatures of its components, mainly pigments (in the VIS), water (in the NIR-SWIR), nitrogen-protein molecules and carbon compounds (in the SWIR), besides of the effects of plant architecture and turgor on the reflected spectrum (Homolová *et al.*, 2013; Pauli *et al.*, 2016). The classical approach has involved the development of numerous vegetation spectral reflectance indices (calculated from the combination of specific wavebands) associated with vegetation traits such as above-ground biomass, vegetation coverage, water content, pigments -mainly chlorophyll- content, nitrogen and phenolic content and other structural plant compounds like lignin and cellulose (Ustin *et al.*, 2009; Kokaly and Skidmore, 2015; Kokaly *et al.*, 2009; Boegh *et al.*, 2002; Peñuelas *et al.*, 1993). Recent studies have addressed the use of hyperspectral reflectance for the evaluation of diverse physiological traits such as photosystems functioning, including maximum Rubisco activity and dark respiration (Lobos *et al.*, 2019; Coast *et al.*, 2019). Furthermore, the biophysical and structural traits of single plants and communities, such as leaf mass per area, leaf area index or plant height may potentially be estimated (Yang *et al.*, 2016; Olsoy *et al.*, 2016). Despite all these spectroscopic applications, the retrieval of biochemical compounds has not been addressed in terms of broad metabolite profiles, which might open the door of a new generation of phenotyping applications.

Although multi and hyper-spectral sensors and imagers are becoming more affordable recently, they are still expensive and complex from the operational point of view. As a low-cost and user-friendly alternative, vegetation indices derived from conventional Red Green Blue (RGB) digital imaging have demonstrated to be feasible and high-throughput indicators of plant and crop traits. The use of these technologies is currently expanding due to their versatility and affordability (Araus and Kefauver, 2018). Digital cameras operating in the field (usually taken zenithal images), integrated in RPAs or at the single leaf level have shown great capabilities for the assessment of crop growth and yield, fertilization requirements and incidence of foliar diseases (Kampmann and Hansen, 1994; Adamsen *et al.*, 1999; Casadesús *et al.*, 2007; White *et al.*, 2012; Andrade-Sanchez *et al.*, 2014; Svensgaard *et al.*,

2014). Also, these applications offer an additional interest; RGB cameras of mobile phones could be used to take field images that may be processed through specific apps and/or can be easily connected to databases and decision support systems (Araus and Kefauver, 2018; Aquino *et al.*, 2017; Confalonieri *et al.*, 2017).

Lastly, the implementation of thermal imaging systems enables rapid observations of plant-crop water status and its cooling ability (Araus and Cairns, 2014; Araus *et al.*, 2008). Temperature of vegetation covers, and single plants depends on plant transpiration, which is mainly related to water availability but also to genotypic resistance to loss water. Under water scarcity conditions, plants tend to limit stomatal conductance, preventing water loss and plant cooling, therefore increasing the temperature of the organs. Thereby, this technology can be employed for monitoring on real time plant water status at different organization scales (single organ, individual plants, plots, crop field or even larger extensions), and can be useful for irrigation scheduling or as a phenotyping trait when breeding for drought resilience.

Currently, many research institutions have developed costly and advanced plant phenotyping platforms such as IPK Gatersleben (Germany), the Plant Accelerator in Adelaide (Australia), Crop Design in Gent (Belgium), the PhenoArch in Montpellier (France) and the Maricopa Phenotyping in Arizona (USA). In addition, the International Plant Phenotyping Network (http://www.plant-phenotyping.org) was formed to provide leadership and coordinate multinational research efforts for plant phenotyping.

Molecular approaches in plant research

Metabolomics as proteomics may became a new frontier for deep plant phenotyping, even under field conditions, disentangling complex and dynamic phenotypic responses. In molecular biology, the development of analytical procedures based on big databases like metabolomics, transcriptomics or proteomics, is crucial to understand the underlying molecular mechanisms of plant responses that confer genotypic resilience to stress conditions. The fields of genetics, transcriptomics, and proteomics have been extensively used to study stress response pathways so that many key enzymes in biosynthetic and detoxification pathways and transcription factors playing essential roles in plant stress responses have been identified (Maruyama et al., 2014; Nakashima et al., 2014). Metabolomics defines the final products of gene expression and protein activities in a given moment and conditions, providing a high-throughput tool to understand physiological responses to environment while depending on phenology and genotype (Bundy et al., 2009; Saia et al., 2019). However, cereals and especially wheat metabolomics remain understudied. Metabolite profiling has been proposed as a

molecular phenotyping approach due to the large effect of genotype by environment interaction (Beleggia et al., 2013; Saia et al., 2019).

In particular, water stress is known to trigger major reprogramming of plant metabolism, including a decrease in photosynthetic carbon metabolism, an increase in photorespiration and accumulation of reactive oxygen species, a generalized inhibition of nitrogen assimilation and accumulation of certain amino acids that function as osmoprotectants and signaling molecules (Tezara *et al.*, 1999; Ergen *et al.*, 2009; Xu and Yu, 2006; Bown and Shelp, 2016; Ullah *et al.*, 2017). Initial accumulation of metabolites is produced because growth processes (carbon demand) are affected earlier than assimilation processes (carbon supply), and some of the metabolites may function as osmoprotectants, antioxidants and carbon storage (Fàbregas and Fernie, 2019; Obata *et al.*, 2015; Muller *et al.*, 2011).The metabolic profiles of leaves and roots in cereals have even been used for predicting complex agronomic traits including yield (Riedelsheimer *et al.*, 2012; Obata *et al.*, 2015; Xu *et al.*, 2016; de Abreu e Lima *et al.*, 2017). However, the metabolome of wheat organs other than leaves such as ear bracts, and their response to stress has still to be elucidated. Therefore, these techniques may contribute to link plant metabolism with plant-crop performance in the field and may enhance stress resilience by identifying key molecular mechanisms or proper biomarkers. As a drawback, sample preparation and data processing can be time consuming and requires costly laboratory equipment. For this reason, the possibility of non-destructively estimate the metabolite(s) content from proximal sensors, such as hyperspectral techniques, as done for other plant constituents (e.g. pigments, nitrogen and lignin) could offer new opportunities.

In summary, the research lines around phenotyping and ecophysiology that make up the present thesis are: low-cost approaches using RGB imagers, as compared to the performance of the more stablished approaches like spectroradiometrics in an application area such as N fertilization, where typically these sensors (e.g. canopy NDVI and chlorophyll meters) have been the canonical approach (Vergara-Díaz *et al.*, 2016; Vergara-Diaz *et al.*, 2015). We further moved to more sophisticated, and still expensive, sensing approaches which may indeed represent the future frontier of phenotyping, such is the use of hyperspectral sensors to assess biochemical and anatomy responses to drought (Vergara-Díaz *et al.*, 2018) as well as the metabolite profiles at the single organ and whole canopy levels (Vergara-Díaz *et al.*, submitted b), besides to deepening into the metabolomic response of different wheat organs to water stress (Vergara-Díaz *et al.*, submitted a).

OBJECTIVES

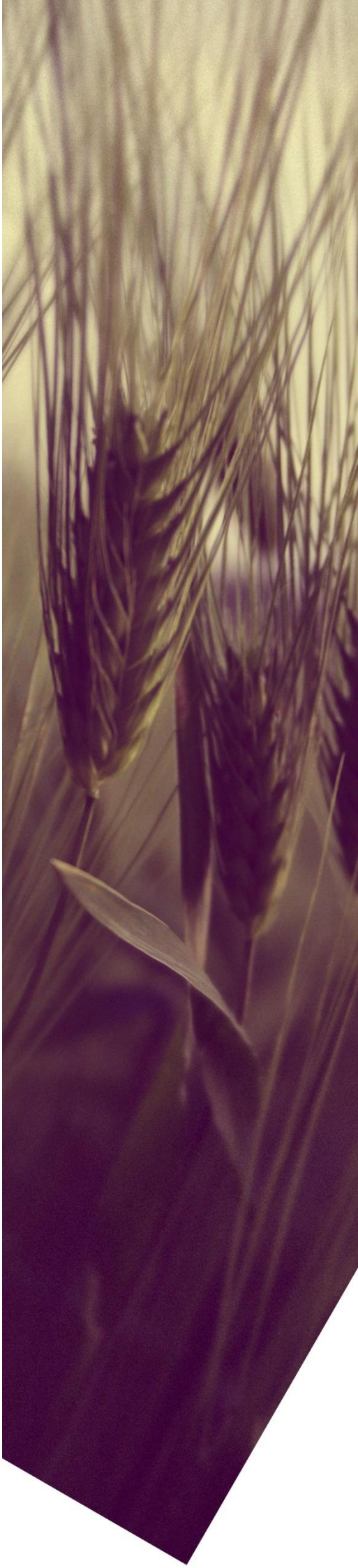

OBJECTIVES

The thesis presented has the general objective of contributing to the advancement of plant phenotyping and ecophysiology while providing new approaches and methods of broad application, including low-cost approaches together with frontier technologies. The works presented hereafter were performed under diverse environmental stress conditions with trials grown in the field where different panels of wheat and maize were studied. Thereby, we aimed to develop novel and high throughput phenotyping systems for the study of cereal performance under a broad range of conditions. These environmental conditions included biotic and abiotic stresses, since the incidence of a fungal disease (yellow rust), water stress and nitrogen deficiency were targeted. Therefore, we consider that this investigation is proper and valuable since the stressor conditions addressed are representative of some of the most important plant-crop constraints and challenges in plant breeding, particularly under the scenarios projected of global change.

A wide corpus of analytical and remote-proximal sensing methods was employed for these purposes and their performance for specific aims were evaluated such as the prediction of agronomic traits and the retrieval of plant biochemical compounds. Initially, we assessed the potential and capabilities of RGB-derived vegetation indices, particularly as compared to the most widely used spectral vegetation index, the NDVI, at both the canopy and the single leaf levels. Thus, we aimed to test and develop the applications of this low-cost and easy-to-use technique, as it may contribute to overcome the needs for plant breeding, particularly in developing countries. Also, the capabilities of spectroscopic approaches were explored with the aim of increase the knowledge and the potential utilities for the extraction of phenotyping traits of interest under water stress conditions. Furthermore, metabolomic approach was employed with the aim of deep into the metabolic processes that drives water stress as well as inter-tissue and genotypic variability associated with yield performance and their relationship with field spectroscopy.

Specific aims

i) The first chapter of the current thesis focus on biotic stress and aimed to assess the sensitivity of a panel of winter wheat (*Triticum turgidum* subsp. *durum*) modern varieties to yellow rust (*Puccinia striiformis* f. sp. *tritici*) under field conditions. For this, diverse field phenotyping methods were tested including RGB and spectral (NDVI) derived vegetation indices of canopies, canopy temperature, leaf chlorophyll content (measured with a portable device) and stomatal conductance. Although RGB image analysis techniques have previously been employed to detect the presence of pests and diseases, these were performed using organ (leaves or grains) images instead of plot canopy images, so the approach presented represents a novel and practical alternative. Thus, we aimed to relate these

phenotypic traits to grain yield and yield losses associated with the severity of yellow rust spread. In addition, the effects of yellow rust on agronomic yield components and their cross-relations were dissected. Lastly, the best remotely sensed vegetation indices and agronomic metrics in terms of their relation to grain yield were combined in stepwise multivariate regression models for the prediction of grain yield and yield losses. This work was published in The Crop Journal.

ii) The second chapter of the thesis addressed other important environmental constraint, nitrogen deficiency, in another key cereal worldwide, maize crop (*Zea mays* subsp. *mays*). We aimed to develop affordable easy-to-use phenotyping tools that increase selection efficiency for grain yield and leaf nitrogen concentration under contrasting nitrogen fertilization conditions in a set of ten maize hybrids grown in the field. For this, we compared the accuracy of RGB-derived vegetation indices and the NDVI spectral index for the assessment of maize grain yield and leaf nitrogen concentration. In this study, RGB indices were obtained at the plot level from ground-based measurements and at the leaf level whereas the spectral index NDVI was measured at the plot level from ground-based measurements and from an unmanned aerial vehicle. Firstly, we assessed the performance of these phenotypic traits when combining all fertilization levels together, and subsequently we dissected the correlations within each nitrogen level for further discussion. Secondly, simple regression models were made for grain yield prediction and these models were tested and validated against the experimental yield of another trial. Additionally, the performance of the leaf compositional and biophysical traits nitrogen per leaf area, carbon to nitrogen ratio, specific leaf area, and the $\delta^{13}C$ and $\delta^{15}N$ were related to crop performance and vegetation indices. This work was published in Frontiers in Plan Science journal.

iii) The third chapter of the thesis focused on water stress and leaf dorsoventrality effects when implementing hyperspectral measurements. Its aim was to investigate the effect of water regime as well as leaf-side-specific responses on flag leaf reflectance traits in field-grown durum wheat. Therefore, we intended to elucidate how in a species such as wheat, with isobilateral leaf blades, a basic aspect such as leaf side (adaxial versus abaxial) may affect the spectrum of the reflected radiation and the different categories of spectral indices. A wide collection of spectral reflectance indices was calculated for both the adaxial and abaxial leaf sides and diverse leaf compositional and anatomical traits were measured. Thus, we aimed to discuss the effect of water stress on leaf spectral properties and their association with diverse physiological, biochemical and anatomical traits of the leaf. Lastly, the similarity and dissimilarities between both leaf spectra and that of the spectrum of the canopy, and their implications for yield prediction were also addressed. This work was published in the Journal of Experimental Botany.

iv) The fourth chapter of the thesis aimed to characterize the metabolite profiles of wheat flag leaves and ear bracts (glumes and lemmas) in response to water stress. In addition, we explored the existence of organ-specific metabolic traits and physiological functions and identify metabolites associated with

genotypic outperformance. Finally, we modelled metabolite-grain yield association aiming to identify metabolic functions related to yield performance in each tissue as well as to identify possible biomarkers for yield improvement under water stress. This work has been submitted (2nd revision) to the Journal of Experimental Botany.

v) The fifth chapter of the thesis aimed to assess the metabolome of different plant tissues from hyperspectral information. To that aim, we tested the performance of multiple regression models for the prediction of flag leaves and ear bracts (glumes and lemmas) metabolite profiles using the reflectance spectra of the flag leaves, ears and plot canopies. Whereas the prediction of grain yield from hyperspectral data using canopy or leaf reflectance is not novel, the employment of ear spectrum has not been tested so far and was evaluated in this work. Finally, we aimed to assess which wavebands of the spectrum are related with specific metabolites. This work has been submitted to The Plant Journal.

REPORT OF THE THESIS DIRECTOR

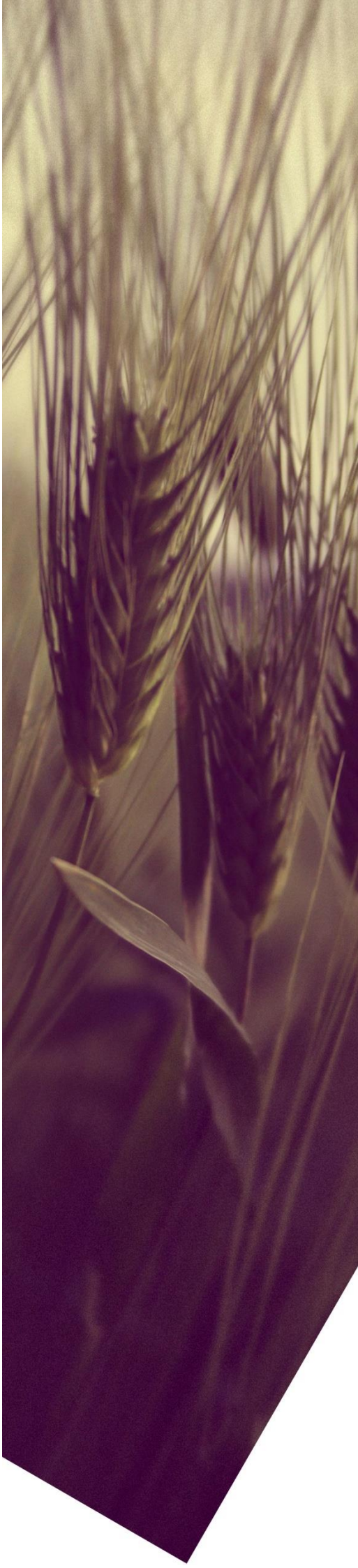

REPORT OF THE THESIS DIRECTOR

Integrative Crop Ecophysiology Group

https://integrativecropecophysiology.com

Plant Physiology Section, Department of Evolutionary Biology, Ecology and Environmental Sciences, Faculty of Biology, University of Barcelona, Diagonal 643, 08028, Barcelona, Spain. Tel. 934 021 465, Fax 934 112 842

Dr. José Luis Araus, as director of the thesis titled "High-throughput field phenotyping in cereals and implications in plant ecophysiology" which was developed by the doctoral student Omar Vergara Díaz, reports about the impact factor and the participation of the doctoral student in the articles included as chapters in the doctoral thesis.

Chapter 1: The article "Grain yield losses in yellow-rusted durum wheat estimated using digital and conventional parameters under field conditions" published in *The Crop Journal* in 2015 with an impact factor of 3.179 in 2018, is a journal placed within the first decile of the science area: Agricultural and Biological Sciences: Plant Science and Agronomy and Crop Science. To date, this work has accumulated 27 citations (Google Scholar). In this study, RGB images of field plots were processed and subsequent RGB indices were used to predict grain yield and yield losses associated with yellow rust disease in wheat. We concluded that this approach outperformed other phenotypic traits (SPAD-meter, CTD, NDVI, g_s) and enabled to accurately assess grain yield under disease conditions. To our knowledge,

this was the first work addressing disease incidence with RGB methods in the field using plot images, at the time of publication. The doctoral student was involved in field data collection, image processing, statistical analysis of data; moreover, the doctoral student drafted the manuscript.

Chapter 2: The article "A Novel Remote Sensing Approach for Prediction of Maize Yield Under Different Conditions of Nitrogen Fertilization" was published in the open access journal of *Frontiers in Plants Science* with an impact factor of 4.495 in the year of publication and of 4.106 in 2018, is a journal placed within the first decile of the science area: Agricultural and Biological Sciences: Plant Science. To date, this work has accumulated 50 citations (Google Scholar). In this study, RGB images of field plots and of leaves were processed and subsequent RGB indices were used to predict grain yield and leaf nitrogen concentration in maize leaves. The results demonstrated the high success of RGB methods for capturing high-throughput phenotypic information and were particularly accurate for characterizing genotypes within nitrogen application levels. The doctoral student was involved in field data collection and sampling, laboratory processing, image processing and statistical analysis of data; moreover, the doctoral student drafted the manuscript. All field data and samples were collected by the doctoral student during his stay in the International Maize and Wheat Improvement Center (CIMMYT) in Harare (Zimbabwe).

Chapter 3: The article "Leaf dorsoventrality as a paramount factor determining spectral performance in field-grown wheat under contrasting water regimes" submitted to the *Journal of Experimental Botany* with an impact factor of 5.36 in 2018, therefore placed in the first decile of the science areas: Agricultural and Biological Sciences: Plant Science - Biochemistry, Genetics and Molecular Biology: Physiology. In this work, we addressed the importance of leaf dorsoventrality and the effect of water stress by analyzing the spectral performance of wheat leaves in the field. We concluded that the spectral traits studied were more affected by the leaf side than by the water regime, and compositional changes could also be inferred, showing that the importance of dorsoventrality in spectral traits is paramount, even in isobilateral leaves. This work was the first addressing dorsoventrality in wheat leaves from a spectroscopic approach. The doctoral student was involved in

field data collection and sampling, laboratory processing, spectroscopic data microscope images processing, and statistical analysis of data; moreover, the doctoral student drafted the manuscript.

Chapter 4: The article "Metabolome profiling supports the key role of the spike in wheat yield performance" has been submitted to the *Journal of Experimental Botany* (2nd revision). In this work, we characterized the metabolome of wheat leaves and spike bracts, its responsiveness to water stress and its relationship with crop yield. Thus, we provided information on the metabolic response to water stress in each organ and identified possible biomarkers for higher yields. To our knowledge, this is the first work analyzing the metabolome of spike bracts. The doctoral student was involved in field data collection and sampling, sample preparation, metabolite profiling and statistical analysis of data; moreover, the doctoral student drafted the manuscript. Metabolite profiling analyses included in this work were performed by the doctoral student during his stay in the Max Planck Institute of Molecular Plant Physiology (Potsdam, Germany).

Chapter 5: The article "Assessing durum wheat ear and leaf metabolomes in the field through hyperspectral data" has been submitted and is, to date, under review in *The Plant Journal*, with and impact factor of 5.726. In this study, we have developed a new technical approach to estimate the metabolite content of leaves and ears under field conditions from hyperspectral information, employing novel multivariate regression models. The results show the capabilities of field spectroscopy for the retrieval of several metabolites fundamental in diverse metabolic processes. Previous works addressing the retrieval of biochemicals focused on pigments or structural elements in leaves. However, to the knowledge of the authors, this approach has not been reported to date in the terms of current work. The doctoral student was involved in field data collection and sampling, spectroscopic data processing, sample preparation, metabolite profiling and statistical analysis of data; moreover, the doctoral student drafted the manuscript. Metabolite profiling analyses included in this work were performed by the doctoral student during his stay in the Max Planck Institute of Molecular Plant Physiology (Potsdam, Germany).

The skills acquired during this Thesis by the doctoral student have contributed to other research activities of the team. As a result, He is coauthor in the following publications:

Proceedings papers in conference that include oral presentation:

- Conference SPIE Remote Sensing 2018.

Kefauver, S. C., El-Haddad, G., Vergara-Diaz, O., & Araus, J. L. (2015, October). RGB Picture vegetation indexes for high-throughput phenotyping platforms (HTPPs). In Remote Sensing for Agriculture, Ecosystems, and Hydrology XVII (Vol. 9637, p. 96370J). International Society for Optics and Photonics.

Other articles where the doctoral student participated as a co-author:

- Plant Methods. Impact factor of 3.449 in 2015. Cited 119 times (Google Scholar), to date.

Zaman-Allah, M., Vergara, O., Araus, J. L., Tarekegne, A., Magorokosho, C., Zarco-Tejada, P. J., Hornero, A., Hernández-Albà, A., Das, B., Craufurd, P., Olsen, M., Prasanna, B.M. & Cairns, J. (2015). Unmanned aerial platform-based multi-spectral imaging for field phenotyping of maize. Plant methods, 11(1), 35.

- Computers and Electronics in Agriculture. Impact factor of 1.892 in 2015. Cited 25 times (Google Scholar), to date.

Zhou, B., Elazab, A., Bort, J., Vergara, O., Serret, M. D., & Araus, J. L. (2015). Low-cost assessment of wheat resistance to yellow rust through conventional RGB images. Computers and Electronics in Agriculture, 116, 20-29.

- Agricultural Water Management. Impact factor of 2.603 in 2016. Cited 18 times (Google Scholar), to date.

Yousfi, S., Kellas, N., Saidi, L., Benlakehal, Z., Chaou, L., Siad, D., Herda, F., Karrou, M., Vergara-Diaz, O., Gracia-Romero, A., Araus, J. L. & Serret, M.D. (2016). Comparative performance of remote sensing methods in assessing wheat performance under Mediterranean conditions. Agricultural Water Management, 164, 137-147.

- Frontiers in Plant Science. Impact factor of 4.298 in 2017. Cited 25 times (Google Scholar), to date

Kefauver, S.C., Vicente, R., Vergara-Díaz, O., Fernandez-Gallego, J.A., Kerfal, S., Lopez, A., Melichar, J.P.E., Serret Molins, M.D., Araus, J.L., 2017. Comparative UAV and Field Phenotyping to Assess Yield and Nitrogen Use Efficiency in Hybrid and Conventional Barley. *Front. Plant Sci.* 8, 1–15. doi:10.3389/fpls.2017.01733

- Frontiers in Plant Science. Impact factor of 4.298 in 2017. Cited 28 times (Google Scholar), to date

Gracia-Romero, A., Kefauver, S. C., Vergara-Díaz, O., Zaman-Allah, M. A., Prasanna, B. M., Cairns, J. E., & Araus, J. L. (2017). Comparative performance of ground vs. aerially assessed RGB and multispectral indices for early-growth evaluation of maize performance under phosphorus fertilization. *Front. Plant Sci.*, 8, 2004.

- Remote Sensing. Impact factor of 4.118 in 2018. Cited 9 times (Google Scholar), to date.

Gracia-Romero, A., Vergara-Díaz, O., Thierfelder, C., Cairns, J., Kefauver, S., & Araus, J. (2018). Phenotyping conservation agriculture management effects on ground and aerial remote sensing assessments of maize hybrids performance in Zimbabwe. Remote Sensing, 10(2), 349.

- Environmental and Experimental Botany. Impact factor of 3.712 in 2018. Cited 5 times (Google Scholar), to date.

Vicente, R., Vergara-Díaz, O., Medina, S., Chairi, F., Kefauver, S. C., Bort, J., Serret, M.D., Aparicio, N. & Araus, J. L. (2018). Durum wheat ears perform better than the flag leaves under water stress: Gene expression and physiological evidence. Environmental and Experimental Botany, 153, 271-285.

- Frontiers in Plant Science. Impact factor of 4.106 in 2018. Cited 2 times (Google Scholar), to date.

Medina, S., Vicente, R., Nieto-Taladriz, M. T., Aparicio, N., Chairi, F., Vergara-Diaz, O., & Araus, J. L. (2018). The plant-transpiration response to vapor pressure deficit (VPD) in Durum Wheat is associated with differential yield performance and specific expression of genes involved in primary metabolism and water transport. Frontiers in plant science, 9.

- Field Crops Research. Impact factor of 3.868 in 2018. Cited 6 times (Google Scholar), to date

Chairi, F., Vergara-Diaz, O., Vatter, T., Aparicio, N., Nieto-Taladriz, M. T., Kefauver, S. C., Bort, J., Serret, M.D. & Araus, J.L. (2018). Post-green revolution genetic advance in durum wheat: The case of Spain. Field crops research, 228, 158-169.

- Remote Sensing. Impact factor of 4.12 in 2019. Cited 1 time (Google Scholar), to date.

Gracia-Romero, A., Kefauver, S.C., Fernandez-Gallego, J.A., Vergara-Díaz, O., Nieto-Taladriz, M.T. & Araus, J.L., 2019. UAV and Ground Image-Based Phenotyping: A Proof of Concept with Durum Wheat. *Remote Sens.* 11, 1244. doi:10.3390/rs11101244.

- Sensors. Impact factor of 2.475 in 2018. Cited 3 times (Google Scholar), to date.

Buchaillot, M., Gracia-Romero, A., Vergara-Diaz, O., Zaman-Allah, M. A., Tarekegne, A., Cairns, J. E., Prasanna, B.M., Araus, J.L. & Kefauver, S. C. (2019). Evaluating Maize Genotype Performance under Low Nitrogen Conditions Using RGB UAV Phenotyping Techniques. Sensors, 19(8), 1815.

- Journal of Visualized Experiments. Impact factor of 1.184 in 2018.

Fernandez-Gallego, J. A., Buchaillot, M. L., Gracia-Romero, A., Vatter, T., Vergara-Diaz, O., Aparicio, N., Nieto-Taladriz, M.T., Kerfal, S., Serret, M.D., Araus, J.L. & Kefauver, S. C. (2019). Cereal Crop Ear Counting in Field Conditions Using Zenithal RGB Images. JoVE (Journal of Visualized Experiments), (144), e58695.

- Plant Science. Impact factor of 3.785 in 2018.

Vicente, R., Vergara-Díaz, O., Kerfal, S., López, A., Melichar, J., Bort, J., Serret, M.D., Araus, J.L. & Kefauver, S. C. (2019). Identification of traits associated with barley yield performance using contrasting nitrogen fertilizations and genotypes. Plant Science, 282, 83-94.

To certify this for corresponding purposes,

Dr. Jose Luis Araus Ortega

Barcelona, 10th September 2019

CHAPTER 1

Grain yield losses in yellow-rusted durum wheat estimated using digital and conventional parameters under field conditions

Omar Vergara-Diaz, Shawn C. Kefauver, Abdelhalim Elazab,
Maria Teresa Nieto-Taladriz, José Luis Araus

Published in:
The Crop Journal (2015) Vol. 3, 200-210.

ABSTRACT

The biotrophic fungus *Puccinia striiformis* f. sp. *tritici* is the causal agent of the yellow rust in wheat. Between the years 2010–2013 a new strain of this pathogen (Warrior/Ambition), against which the present cultivated wheat varieties have no resistance, appeared and spread rapidly. It threatens cereal production in most of Europe. The search for sources of resistance to this strain is proposed as the most efficient and safe solution to ensure high grain production. This will be helped by the development of high performance and low-cost techniques for field phenotyping. In this study we analyzed vegetation indices in the Red, Green, Blue (RGB) images of crop canopies under field conditions. We evaluated their accuracy in predicting grain yield and assessing disease severity in comparison to other field measurements including the Normalized Difference Vegetation Index (NDVI), leaf chlorophyll content, stomatal conductance, and canopy temperature. We also discuss yield components and agronomic parameters in relation to grain yield and disease severity. RGB-based indices proved to be accurate predictors of grain yield and grain yield losses associated with yellow rust (R^2=0.581 and R^2=0.536, respectively), far surpassing the predictive ability of NDVI (R^2=0.118 and R^2=0.128, respectively). In comparison to potential yield, we found the presence of disease to be correlated with reductions in the number of grains per spike, grains per square meter, kernel weight and harvest index. Grain yield losses in the presence of yellow rust were also greater in later heading varieties. The combination of RGB-based indices and days to heading together explained 70.9% of the variability in grain yield and 62.7% of the yield losses.

THE CROP JOURNAL 3 (2015) 200–210

HOSTED BY

ELSEVIER

Available online at www.sciencedirect.com

ScienceDirect

Grain yield losses in yellow-rusted durum wheat estimated using digital and conventional parameters under field conditions

Omar Vergara-Diaz[a], *Shawn C. Kefauver*[a,*], *Abdelhalim Elazab*[a], *Maria Teresa Nieto-Taladriz*[b], *José Luis Araus*[a]

[a]*Unit of Plant Physiology, Department of Plant Biology, Faculty of Biology, University of Barcelona, Diagonal 645, 08028 Barcelona, Spain*
[b]*National Institute for Agricultural and Food Research and Technology (INIA), Ctra de la Coruña 7.5, 28040, Madrid Spain*

ARTICLE INFO

Article history:
Received 17 December 2014
Received in revised form
25 February 2015
Accepted 3 March 2015
Available online 11 April 2015

Keywords:
Wheat yellow rust
Field phenotyping
NDVI
Phenology, *Puccinia striiformis*
RGB-based indices
Triticum durum

ABSTRACT

The biotrophic fungus *Puccinia striiformis* f. sp. *tritici* is the causal agent of the yellow rust in wheat. Between the years 2010–2013 a new strain of this pathogen (Warrior/Ambition), against which the present cultivated wheat varieties have no resistance, appeared and spread rapidly. It threatens cereal production in most of Europe. The search for sources of resistance to this strain is proposed as the most efficient and safe solution to ensure high grain production. This will be helped by the development of high performance and low cost techniques for field phenotyping. In this study we analyzed vegetation indices in the Red, Green, Blue (RGB) images of crop canopies under field conditions. We evaluated their accuracy in predicting grain yield and assessing disease severity in comparison to other field measurements including the Normalized Difference Vegetation Index (NDVI), leaf chlorophyll content, stomatal conductance, and canopy temperature. We also discuss yield components and agronomic parameters in relation to grain yield and disease severity. RGB-based indices proved to be accurate predictors of grain yield and grain yield losses associated with yellow rust ($R^2 = 0.581$ and $R^2 = 0.536$, respectively), far surpassing the predictive ability of NDVI ($R^2 = 0.118$ and $R^2 = 0.128$, respectively). In comparison to potential yield, we found the presence of disease to be correlated with reductions in the number of grains per spike, grains per square meter, kernel weight and harvest index. Grain yield losses in the presence of yellow rust were also greater in later heading varieties. The combination of RGB-based indices and days to heading together explained 70.9% of the variability in grain yield and 62.7% of the yield losses.

* *Corresponding author.*
E-mail address: sckefauver@ub.edu (S.C. Kefauver).
Peer review under responsibility of Crop Science Society of China and Institute of Crop Science, CAAS.

http://dx.doi.org/10.1016/j.cj.2015.03.003

1. Introduction

Wheat is the second most cultivated cereal in Spain [1] and the most widely cultivated cereal worldwide, with over 218 Mha in cultivation [2]. *Puccinia striiformis* is the causal agent of yellow rust in grasses and has been described as infecting a wide variety of cultivated cereals, including wheat, rye, barley and triticale. The *forma specialis* (f. sp.) *tritici* primarily infects wheat. The presence and severity of this fungal disease in Mediterranean and temperate cultivars has not been of importance until recently. The use of wheat varieties resistant to this pathogen had previously ensured that losses were minimal in the Mediterranean region [3]; however, the presence of a new *Pst* race called the Warrior/Ambition race, first described during 2009/2010 in the United Kingdom, Germany, Denmark, France and Scandinavia, has severely affected winter wheat production in recent years [4]. One year after it was first discovered in Europe, its presence was also detected in Spain [4] and the disease spread extensively during the 2012/2013 winter wheat season. Several epidemic events resulting in serious crop damage and widespread yield losses in Spain [3] have since been recorded. The rapid spread of this strain was favored by the climatic conditions of the 2012/2013 season: cool temperatures during spring, high humidity and prolonged rainy conditions [5].

P. striiformis f. sp. *tritici* has a great capacity for dispersal and for variation [6]. The new Warrior/Ambition strain is virulent for most of the currently deployed resistance genes [3] and can therefore parasitize most of the wheat varieties presently grown around the world. In addition, this fungus spreads by wind over hundreds of kilometers, germinates quickly at low temperatures (7–10 °C) [6,7], and infects wheat crops at a relatively early growth stage. The most apparent visible sign of infection is the orange-yellowish mass of urediniospores being produced by uredinia arranged in long, narrow stripes along the leaf veins. Development of resistant varieties is essential for effective control; however, to date no variety with resistance to the strain has been recommended in Spain [8]. There is an urgent need to develop improved high throughput field phenotyping approaches for breeding for yellow rust resistance in wheat.

The diversity of existing wheat varieties provides a source of genetic variability from which we can select a high number of features of interest, such as drought and salinity tolerance, improvements in nutrient use efficiency or, in our case, disease resistance. Phenomics arises as a complex and integrative discipline that tries to characterize plant functional traits related to specific conditions from the cell to community level. However, it is considered a major bottleneck with regard to the advancement of crop breeding [9–13]. Thus, high-performance phenotyping systems are required to understand the relationships between genotype, phenotype and environment. Phenotyping requires that the studied trait and the chosen methodology for its measurement are appropriate for the purpose of the investigation.

There are currently several criteria for field phenotyping by monitoring and analyzing different plant traits as a response to stress conditions. However, most of these techniques are time-consuming, unrepresentative of the whole plot and/or require sampling, laboratory processing and costly equipment. Visible and near infrared (VNIR) spectral measurements have high performance in characterizing physiological and biochemical processes as well as agronomic traits at both crop and leaf levels [14–20], whereas, thermal imaging enables rapid observations of plant water status and their cooling ability [9,10]. Both approaches can be integrated as part of field-monitoring platforms, but their implementation is expensive. As an alternative, vegetation indices based on conventional digital Red, Green, Blue (RGB) digital imaging are high-performance, low-cost techniques for predicting plant and crop traits, and can be based on processing pictures of either crop canopies or single leaves [21]. The use of these technologies is currently expanding due to their versatility and affordability. Some of their proven applications are: the development of predictive models for crop yield under specific growing conditions [22], crop growth assessment under water stress conditions [23], fertilization monitoring and nitrogen requirements [24], LAI (leaf area index) for lodging risk evaluation in winter wheat [25], and quantification of pollen release [26].

The efficacy of RGB digital methods for the evaluation of a pest or disease at the leaf level has also been reported, including powdery mildew on cucumber leaves [27], assessment of foliar disease symptom severities in corn, wheat and soybean [28], determination of the impact of disease severity of specific grain diseases [29], and of different types of fungal diseases in wheat [30,31]. In all these cases image analysis techniques were employed to detect the presence of the pest or disease and the infected, necrotic and/or dry areas using scans or photographic images of leaves or other plant parts. This approach has proven highly accurate in its predictions, but is cumbersome and time consuming in practice because it requires manually intensive and destructive harvesting and photographing the plant organs of interest. Studies on sensitivity of crops to biotic stress using hyperspectral crop canopy data have been conducted previously [32–35], but no previous studies using digital RGB cameras at the canopy level are known to the authors. Thus, the development of prediction models of grain yield (GY) and crop pathogen sensitivity using digital RGB photography of crop canopies represents a novel and practical alternative to other remote sensing approaches, such as VNIR-derived vegetation indices, for wheat phenotyping under field conditions.

The objective of this study was to assess the sensitivity of autumn sown wheat varieties to yellow rust under field conditions using different methodologies. First, we assessed the performance and accuracy of RGB indices in comparison to the Normalized Difference Vegetation Index (NDVI) for prediction of grain yield losses associated with yellow rust. Second, we evaluated the performance of other agronomic metrics commonly used in field phenotyping (leaf chlorophyll content, stomatal conductance and canopy temperature) and their relationships with GY and disease severity. Third, we investigated the effects of yellow rust on the relationships between common agronomic parameters, GY and the grain yield loss index (GYLI). Finally, we combined the best remotely-sensed vegetation indices and agronomic metrics in stepwise multivariate predictive models of GY and GYLI.

2. Materials and methods

2.1. Experimental field, plant material and growing conditions

Field trials were carried out at the experimental station of Colmenar de Oreja (40° 04′ N, 3° 31′ W) belonging to the Instituto Nacional de Investigación y Tecnología Agraria y Alimentaria (INIA) of Spain during the 2012/2013 crop season. The average annual precipitation corresponding to this region is about 425 mm and the average annual temperature is 13.7 °C. The region has an altitude of 590 m in the middle of the Tajo River basin. The ground has a slightly alkaline soil (pH 8.1) and corresponds to a xerofluvent soil [36]. It is a kind of alluvial entisol with a xeric moisture regime [37]. Before planting, the field was fertilized with 400 kg ha^{-1} of a 15:15:15 N:P:K (15% N, 15% P_2O_5, 15% K_2O) fertilizer. A second application of 150 kg ha^{-1} of urea 46% dilution was applied before stem elongation.

Sixteen durum wheat varieties (*Triticum turgidum* L. subsp. *durum* (Desf) Husn.) were grown, 13 of Spanish registration (Vitrón, Regallo, Gallareta, Bolo, Don Pedro, Sula, Bólido, Dorondón, Murgos, Pelayo, Don Sebastian, Don Ricardo and Kiko Nick) and three European (Simeto, Claudio and Iride from Italy). The experimental design was established in randomized blocks with three replicates and a total of 48 plots. The planting took place on December 5, 2012, with a planting density of 250 seeds per square meter. The plots had an area of 7 × 1.5 m^2 and a distance of 0.2 m between rows. Rainfall during the 2012/2013 crop season was 278 mm and the average temperature was 11.4 °C. This amount of precipitation was considerably higher than the same period in previous years (200–230 mm). Furthermore, rainfall was focused in the spring months: March (106 mm), April (44 mm) and May (53 mm). The average humidity during the period was 10–15% higher than normal according to historical records [38]. This trial was not irrigated.

Field measurements and plot canopy pictures were taken five times throughout the trial: February 27–28, April 8–10, April 29–30, May 22–23 and May 30–31, 2013, corresponding with the development stages of tillering, stem elongation or jointing, heading, anthesis and post-anthesis (first half of grain filling), respectively. Plant height (PH) was measured during the last field visit. Field operators measured the number of days to heading (DH) (when approximately 50% of stems have showed half-emerged spikes). Harvesting was carried out on July 10, 2013, and grains were dried in an oven at 60 °C for 48 h. The measured traits included GY, spikes per square meter, grains per spike, thousand kernel weight (TKW) and harvest index (HI).

2.2. Disease identification of fungus

Disease was identified by station staff as yellow rust. Detailed photographs show its presence (Fig. 1) and characteristic symptoms. A camera (Pixera 150ES, USA) coupled to a zoom microscope (Olympus SZ 60, USA) was used to observe and photograph a selection of flag leaf samples from post-anthesis stage samples. These pictures show the characteristically linear lesions on the wheat leaf surface (Fig. 2). The correct identification of yellow rust was confirmed by the numerous outbreaks reported all around Spain during the same period by the Group for the Evaluation of New Varieties of Extensive Crops in Spain (GENVCE) [39] state network.

2.3. Assessment of yield losses attributed to yellow rust

As previously described, environmental conditions especially favored the development of yellow rust 2012/2013. Furthermore, continuous rains made it impossible to apply fungicides to contain the disease. Damage was evident in late April (heading stage) and worsened during the following months. In order to evaluate grain yield losses associated with the disease, grain yields of the same genotypes were measured in the following season (2013/2014) and potential yield was used as a reference. Materials in the second season were planted in the same experimental station and using a similar design and agricultural practices; the presence of rust was negligible. The average temperature during the 2013/2014 growing season

Fig. 1 – Wheat leaves damaged by yellow rust during 2012–2013.

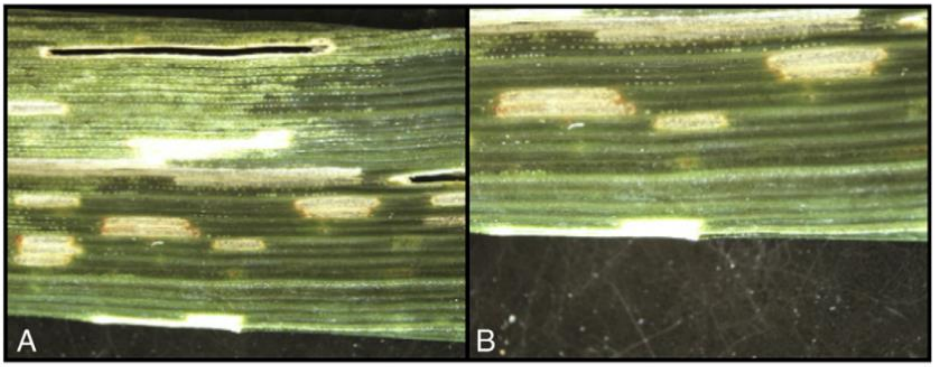

Fig. 2 – Zoomed photographs of damaged leaves.

was 13.6 °C, rainfall was 213 mm and concentrated in the cooler months: December (32 mm), January (51 mm), February (47 mm) and March (29 mm). Irrigation was also used to achieve optimal growth. Sprinkler irrigation was applied seven times, providing 355 mm of irrigation water and thus a total of 568 mm for the season. GYLI was calculated as: GYLY = (GY 2013/2014 – GY 2012/2013) / (GY 2013/2014) × 100, where GY 2013/2014 represents the potential grain yield obtained in the 2013/14 season when the yellow rust was not present, and GY 2012/2013 corresponds to grain yield in the presence of yellow rust. Finally, in order to confirm the causal relationship between the presence of the disease and the grain yield losses — ignoring possible water stress effects — grain yields from the 2013/2014 growing season (not affected by wheat rust) in rainfed conditions only, hereafter considered as sub-optimal yield conditions, were compared to grain yields of the 2012/2013 season (affected by rust).

2.4. Vegetation indices

NDVI was determined with a portable spectroradiometer (GreenSeeker handheld crop sensor, Trimble, USA) on three dates: February 27, April 10 and May 22, 2013, coincident with the development stages of tillering, jointing and anthesis, respectively. NDVI was calculated using the equation: NDVI = (NIR – R) / (NIR + R), where R is the reflectance in the red band (660 nm) and NIR is the reflectance in the near-infrared band (760 nm). The distance between the sensor and the plot canopy was 0.5–0.6 m above and perpendicular to the canopy.

One digital RGB picture was taken per plot, holding the camera at 0.8–1.0 m above the plant canopy, in a zenithal plane and focusing near the center of each plot. Photographs were taken with a Nikon D40 camera on four dates: February 27, April 8, May 23 and May 30, 2013, coincident with tillering, jointing, anthesis and post-anthesis, respectively. The D40 had a focal length of 18 mm, shutter speed of 1/125 and horizontal and vertical fields of view (FOV) of 66° 43′ and 46° 51′, respectively. No flash was used and the aperture of remained in automatic. Photographs were saved in JPEG format with a size of 1920 × 1280 pixels.

Pictures were subsequently analyzed with open source Breedpix 0.2 software designed for digital photograph processing [21]. This software enabled determination of RGB vegetation indices from the different properties of color. RGB indices were previously proven to be good indicators of plant growth and crop senescence [23]. The following five digital indices were used in this study: a*, u*, hue, green area (GA) and greener area (GAA). The last two indices analyze the number of green pixels in the image, but differ in that GAA excludes yellowish-green tones and therefore more accurately describes the amount of photosynthetically active biomass and leaf senescence. The a* and u* indices require the use of Java Advanced Imaging for calculation, and the use of formulae described by O'Gorman et al. [40] and Vrhel et al. [41], respectively, in order to analyze specific features and color components.

2.5. Leaf chlorophyll content, canopy temperature and leaf stomatal conductance

A handheld Minolta SPAD-502 sensor (Spectrum Technologies Inc., Plainfield, IL, USA) was used to measure relative leaf chlorophyll content (LCC). Five flag leaves per plot were measured at each sampling date: April 10, April 30, and May 30, 2013, corresponding to jointing, heading and post-anthesis stages, respectively. A portable thermal infra-red MIDAS 320L camera (DIAS Infrared Systems, Germany) was used to measure canopy temperatures. Photographs of whole plot were taken at midday from a distance of approximately one meter in direct sunlight. These pictures were processed using PYROSOFT Professional (DIAS Infrared Systems, Germany) for DIAS infrared cameras selecting a representative area of each plot from two dates, May 22 and May 30, 2013, corresponding to the anthesis and post-anthesis stages. Air temperature and humidity were simultaneously recorded with a thermo-hygrometer (Testo 177-H1 Logger, Germany) at the same time as each thermal picture. Air temperature was used to calculate the canopy temperature depression (CTD), the difference between plant canopy temperature and air temperature. Finally, stomatal conductance (g_s) was measured with a Decagon Leaf Porometer SC-1 (Decagon Device Inc., Pullman, WA, USA). One flag leaf was measured for each plot on April 10, April 29, May 23 and May 30, 2013, corresponding to the development stages of jointing, heading, anthesis and post-anthesis, respectively.

2.6. Statistical analysis

All data was analyzed with SPSS 21 (IBM SPSS Statistics 21, Inc., Chicago, IL, USA). Several simple and multiple variance analyses were run to investigate genotypic and the experimental condition

Table 1 – Means and deviations of grain yield (t ha^{-1}) in disease conditions and potential conditions and grain yield loss index (GYLI) of sixteen durum varieties.

Genotype	GY disease conditions	GY potential conditions	GYLI (%)
Iride	6.66 ± 0.58c	6.98 ± 0.61abcd	4 ± 13.29a
Dorondón	6.65 ± 0.51c	6.82 ± 0.58abcd	1.7 ± 13.7a
Pelayo	6.64 ± 0.59c	7.82 ± 0.3de	15 ± 9.54ab
Don Ricardo	6.56 ± 0.81c	7.03 ± 0.56abcd	6.8 ± 5.29a
Simeto	6.48 ± 0.84c	6.72 ± 0.36abc	2.9 ± 18.55a
Kiko Nick	6.48 ± 0.94c	7.61 ± 0.4cde	14.8 ± 9.88ab
Bolo	6.33 ± 0.26c	7.3 ± 0.04abcde	13.2 ± 3.46ab
Regallo	6.33 ± 0.84c	7.51 ± 0.17bcde	15.9 ± 9.62ab
Claudio	6.26 ± 0.37c	7.16 ± 0.63abcde	12.2 ± 6.45ab
Bólido	6.22 ± 0.19c	6.8 ± 0.8abcd	7.6 ± 13.04a
Gallareta	6.14 ± 0.62c	6.84 ± 0.48abcd	10.4 ± 5.89a
Vitrón	5.97 ± 0.16bc	7.09 ± 0.56abcde	15.5 ± 5.55ab
Burgos	5.57 ± 0.68bc	8.08 ± 0.77e	30.3 14.04b
Don Sebastián	5.03 ± 0.13b	6.34 ± 0.8a	19.8 ± 11.8ab
Sula	3.33 ± 0.11a	7.79 ± 0.16de	57.2 ± 1.63c
Don Pedro	2.81 ± 0.1a	6.51 ± 0.33ab	56.8 ± 0.74c
Mean	5.84 ± 1.23	7.15 ± 0.65	17.8 ± 18.5
ANOVA			
Genotype	<0.001	0.009	<0.001

Different letters indicate significant differences within columns according to Duncan's multiple range test ($P < 0.05$).

effects. Duncan post-hoc tests were performed to make multiple correlation comparisons. Pearson correlation coefficient matrices were calculated to look at the multiple bivariate correlations between parameters. Finally, multiple regression analysis with stepwise parameter selection was used in order to develop prediction models for grain yield and grain yield losses.

3. Results

3.1. Grain yield and grain yield loss index

Genotypic differences were found in grain yield in the presence of yellow rust, in potential yield conditions and also in GYLI (Table 1). In the season affected by the yellow rust, there was a difference of 3.85 t ha^{-1} between the most productive genotype and the less productive one. However, in potential conditions, the difference was of 1.74 t ha^{-1} (Table 1). Mean grain losses of all genotypes exceeded 1.3 t ha^{-1}, or on average about 18% of the losses in grain yield. The degree of measured negative effects as measured by GYLI was varied widely between genotypes, ranging between 1.7% (Dorondon) and 57.2% (Sula).

For further description of the parameter relationships a correlation matrix was made between grain yields of in disease-affected season (2012/2013), potential yield conditions (2013/2014 well watered), sub-optimal conditions (2013/2014 rainfed) and GYLI. Grain yield in the disease-affected season did not correlate significantly with potential yield or with sub-optimal yield conditions ($r = 0.065$, $P = 0.662$ and $r = 0.241$, $P = 0.098$, respectively). GYLI was strongly correlated with GY from the disease-affected season ($r = -0.914$; $P < 0.001$) and moderately correlated with potential yield ($r = 0.334$; $P = 0.020$). Potential and sub-optimal yields were marginally correlated ($r = 0.307$; $P = 0.034$).

3.2. Vegetation indices and their relationships with grain yield

The best correlations were clearly found at anthesis (Table 2), whereas the coefficients were lower at the jointing and post-anthesis stages, but GA and GAA were always highly correlated. Significant genotypic differences in GA, GAA and u* were identified at tillering, jointing, anthesis and post-anthesis, whereas significant differences were not detected in hue and a* at the jointing and post-anthesis stages, respectively. We also found genotypic differences in NDVI at tillering and jointing, but not at anthesis.

In general terms, all the measured parameters, especially the RGB indices, fit considerably well to GY and GYLI (Table 3). The parameters that were most strongly correlated to GY and GYLI were GA, GAA and u*, whereas hue, a* and NDVI demonstrated a more variable and less reliable performance. GA proved to be the most reliable RGB index as a predictor of GY and GYLI with the highest coefficients of correlation at all stages. However, the rest of the RGB indices were also very good indicators of GY and GYLI, especially at anthesis, but also at jointing and post-anthesis. NDVI was a good predictor of GY and GYLI at jointing, when disease had not spread, but its effectiveness was considerably lower at anthesis.

Table 2 – P-values from multivariate analysis of variance for genotypes depending on five RGB-based indices, Normalized Difference Vegetation Index (NDVI) as a spectral index and leaf chlorophyll content (LCC), stomatal conductance (g_s) and canopy temperature depression (CTD) as a field measures at five wheat development stages.

	Tillering	Jointing	Heading	Anthesis	Post-anthesis
RGB-indices					
hue	<0.001	0.478	–	<0.001	<0.001
a*	0.004	<0.001	–	<0.001	0.478
u*	0.003	<0.001	–	<0.001	<0.001
GA	<0.001	<0.001	–	<0.001	<0.001
GAA	<0.001	<0.001	–	<0.001	<0.001
Spectral index					
NDVI	0.002	<0.001	–	0.157	–
Field-measures					
LCC	–	0.078	0.002	–	0.116
g_s	–	0.802	0.740	0.616	0.068
CTD	–	–	–	0.885	0.063

Table 3 – Correlations coefficients between RGB-based indices, Normalized Difference Vegetation Index (NDVI), leaf chlorophyll content (LCC), stomatal conductance (g_s), canopy temperature depression (CTD) and grain yield in disease conditions and grain yield loss index (GYLI).

	GY 2012/13 (disease conditions)					GYLI				
	Tillering	Jointing	Heading	Anthesis	Post-anthesis	Tillering	Jointing	Heading	Anthesis	Post-anthesis
RGB-indices										
hue	0.362 *	0.117	–	0.744 **	0.585 **	−0.400 **	−0.069	–	−0.705 **	−0.613 **
a*	−0.345 *	−0.499 **	–	−0.620 **	0.113	0.362 *	0.487 **	–	0.561 **	−0.177
u*	−0.331 *	−0.514 **	–	−0.749 **	−0.601 **	0.356 *	0.507 **	–	0.687 **	0.570 **
GA	0.430 **	0.493 **	–	0.762 **	0.698 **	−0.471 **	−0.521 **	–	−0.732 **	−0.673 **
GAA	0.404 **	0.511 **	–	0.737 **	0.628 **	−0.430 **	−0.523 **	–	−0.681 **	−0.619 **
Spectral index										
NDVI	0.212	0.511 **	–	0.343 *	–	−0.171	−0.526 **	–	−0.357 *	–
Field-measures										
LCC	–	0.079	−0.022	–	0.171	–	−0.001	−0.018	–	−0.200
g_s	–	−0.124	0.095	0.011	0.194	–	0.164	−0.103	−0.109	−0.200
CTD	–	–	–	0.073	0.101	–	–	–	0.001	−0.127

** $P < 0.01$.
* $P < 0.05$.

3.3. Conventional field-phenotyping parameters and their relationship with grain yield

Significant genotypic differences in LCC were found only at the heading stage (Table 2). No significant differences g_s were found at any sampling date. Finally, no genotypic differences were found in CTD values at any developmental stage. Despite significant differences in LCC at one growth stage, no significant correlation was found between LCC, g_s, CTD and GY or GYLI at any developmental stage (Table 3).

3.4. Agronomic parameters and their effect on yield

Except for the number of spikes per square meter and PH all measured agronomic parameters differed significantly between potential and disease-affected conditions ($P \leq 0.01$) (Table 4). The numbers of grains per square meter, grains per spike, TKW and HI were significantly reduced in disease-affected compared to potent yield conditions. Finally, DH was significantly higher under disease-affected than potential yield conditions.

A Pearson correlation matrix was calculated in order to compare the agronomic parameters with the GY value under biotic-stress (2012/2013 cultivars) and non-biotic-stress conditions (2013/2014 cultivars), and with grain yield losses associated to the presence of rust (Table 5). The GY of disease-affected crops was highly correlated with the number of grains per square meter, spikes per square meter and with HI, moderately correlated with DH and TKW, but not significantly related with number of grains per spike or PH. GYLI showed a strong negative relationship with the number of grains per square meter, spikes per square meter, and with HI, and positively correlated with DH. GYLI showed a trend towards negative relationships with number of grains per spike, TKW and PH, but these are not significant. Regarding potential yield conditions, GY was highly positively related to the number of grains per square meter and moderately correlated with the number of spikes per square meter. However, potential GY was not significantly correlated with the number of grains per spike, TKW, HI, DH or PH.

Finally, the interrelationships between the agronomic parameters themselves in both growing conditions were studied in order to ascribe alteration in these relationships with the presence of disease. Results are shown in Table S1. Relationships between the number of spikes per square meter, grains per spike and HI were maintained in both conditions. DH was negatively related to HI only in disease conditions whereas in potential conditions phenology was only related with PH. For its part, PH was closely correlated in potential conditions with DH, spikes per square meter, grains per spike and with HI; whereas in disease conditions PH was unrelated to the other parameters. Another difference was for TKW which was unrelated to the rest of parameters under disease conditions, but in potential

Table 4 – Mean grains per square meter, grains per spike, spikes per square meter, thousand kernel weight (TKW), harvest index (HI), plant height (PH) and the number of days to heading (DH) under the presence of disease and potential yield conditions. P-values are from multivariate analysis of variance for each agronomic parameter.

	Disease-affected conditions	Potential-yielding conditions	Difference P-value
Grain number (m^{-2})	11,909.40	13,498.90	0.001
Grain number ($spike^{-1}$)	33.35	39.93	<0.001
Spike number (m^{-2})	372.79	348.46	0.204
TKW (g)	44.34	48.07	<0.001
HI (%)	36.04	47.37	<0.001
PH (cm)	101.25	103.23	0.091
DH	154.27	147.10	<0.001

Table 5 – Correlations coefficients between grain yields for potential yielding conditions, disease-affected conditions and grain yield loss index (GYLI) with the number of grains per square meter, grains per spike, spikes per square meter, thousand kernel weight (TKW), harvest index (HI), plant height (PH) and number of days to heading (DH).

	GY disease-affected conditions	GYLI	GY potential-yielding conditions
Spike number (m^{-2})	0.495**	−0.441**	0.302*
Grain number ($spike^{-1}$)	0.203	−0.229	0.082
Grain number (m^{-2})	0.899**	−0.852**	0.653**
TKW	0.298*	−0.213	0.122
HI	0.513**	−0.446**	0.076
DH	−0.345*	0.333*	0.086
PH	0.101	−0.156	−0.100

** $P < 0.01$.
* $P < 0.05$.

conditions TKW was highly negatively associated with the number of grains per square meter and the grains per spike.

3.5. Predictive models

With the aim of obtaining a predictive model for grain yield and grain yield losses, we performed a multivariate regression analysis using RGB indices, g_s, NDVI, LCC, CTD, DH and PH as independent variables (Table 6). The best correlated measuring dates with GY and GYLI were chosen for this purpose. For the prediction of GY, the first model selected the RGB-indices GA, GAA, hue and/or u*, always together with DH and was able to explain 69–71% of yield variability in disease conditions ($P < 0.001$). Moreover, the second model explained 60–63% of the variability of grain yield losses by using the RGB-indices GA or hue with DH ($P < 0.001$).

4. Discussion

4.1. Effect of disease on grain yield

The genotypic differences in GY in disease conditions may be largely attributed to the crop sensitivity to yellow rust, as confirmed by the lack of correlations between the GY of the disease-affected field season and the GY of the disease-free field season under both potential and sub-optimal yield conditions. Moreover, as a decrease in PH is usually related to increased water stress [42], the lack of differences in PH between potential and disease conditions suggests that water stress effects under disease conditions were negligible. Potential GY can be considered to scarcely affect the GYLI, since the genotypic variability of potential yield was not related to the observed varietal sensitivity to the disease.

4.2. Performance of vegetation indices

RGB-indices were demonstrated to be the best predictors of grain yield in the presence of yellow rust. The wide range of genotypic differences in most of the RGB-indices at all the growth stages was strongly related with yield variability. NDVI has been used with satisfactory results in many prediction models of yield in wheat at the field level [43], even at regional or state levels [44] using satellite imagery. According to those reports, grain yield could effectively be predicted using NDVI at an early growth stage (jointing), but its accuracy decreased considerably at anthesis (afterwards no data were available). These results were possibly due to a saturation of NDVI in conditions of high biomass [45], as suggested by the narrower confidence interval of NDVI at anthesis (CI = [0.6837, 0.7625]) in comparison to the RGB-index GA (CI = [0.8476, 1.0162]). Moreover, this loss of accuracy may also be attributed to a rapid deterioration of the relationship between NDVI and GY as wheat ripens [46]. In fact, both vegetation index approaches were previously reported to lose accuracy at the late developmental stages [23], but this deterioration in prediction appears to be less pronounced for the RGB indices (from BreedPix software). Therefore, when the ground is totally covered, the information that NDVI provides is more limited, whereas RGB-indices have proved to be even better predictors with dense canopies.

NDVI was previously employed to successfully distinguish between infected, non-infected and N-deficient wheat plots [47]. However, it was mostly used in combined multi-spectral methods with other spectral indices where NDVI acted as a first level biomass sensor in order to discard non-plant spectra [31,32,48] and subsequently the analysis proceeded with the use of other indices. Moreover, these studies based on multi-spectral methods [31,32,48] and previous studies based on digital image analysis [27,29,30] focused on disease detection, leaf classification with regard to infection status and disease level, but its association with yield loss was not described. In this study, the effectiveness of NDVI with regard to GY prediction decreased with disease spread, suggesting

Table 6 – Multivariate regression models explaining grain yield (GY) variation in disease conditions and the grain yield loss index (GYLI) from vegetation indices at anthesis and agronomic traits.

Predicted parameter	Multivariate model	R^2	SEP	F	P-value
GY disease conditions	GY = 27.79 + 0.148 × hue − 0.22 × DH	0.694	0.696	51.13	<0.001
	GY = 26.203 + 3.755 × GAA − 0.179 × DH + 5.113 × GA	0.698	0.700	33.94	<0.001
	GY = 32.021 − 0.291 × u* + 3.355 × GAA − 0.198 × DH	0.709	0.687	35.66	<0.001
GYLI	GYLI = − 302.077 − 2.106 × hue + 3.178 × DH	0.627	11.555	37.78	<0.001
	GYLI = − 173.154 − 154.226 × GA + 2.169 × DH	0.596	12.018	33.22	<0.001

R^2: determination coefficient; SEP: standard error of prediction. RGB-based indices used in these models: GA, GGA, hue and u*. DH: days to heading.

that color changes at the canopy level associated disease spread were missed or omitted by NDVI. Therefore, NDVI may be useful for GY prediction in disease-free conditions and as part of combined methods for disease-detection, but is not an appropriate index of GY assessment in disease-affected conditions. In agreement with previous reports that used digital indices from BreedPix software [23,49] and other image processors [50,51], GY was accurately predicted by RGB indices. As a further contribution, our study demonstrated that RGB indices are also able to predict GY and yield losses in yellow rust infected cultivars at the canopy level. Canopy color characteristics are indicative of the degree of yellow rust infection, thus it was possible to quantify disease severity empirically, and therefore to accurately evaluate grain yield losses in field conditions. Although traditional observational techniques for evaluating crop disease under field conditions have proven to be powerful tools for wheat genotypic selection [52,53], these methodologies are often tedious and difficult to quantify objectively. In this sense, the proposed alternative in this study is particularly interesting for the use in field conditions due to its low cost, precision, rapidity and repeatability.

4.3. Performance of LCC, g_s and CTD

LCC is usually related to nitrogen content, photosynthetic capacity and production [54,55]. Previous studies reported a reduction in chlorophyll content in wheat associated with the presence of wheat yellow rust [56]. In our study we note a widespread decrease in LCC of flag leaves at the post-anthesis stage, but this decrease was not correlated with GYLI or GY. Unlike some of the RGB indices, LCC could not describe (according to our methodology) the entire greenness of the plot canopy. In contrast, the water status parameters (g_s and CTD) were insensitive to variation in grain yield. Smith et al. [57] reported the following progression during yellow rust infection: increased transpiration, causing a reduction in temperature due to rupture of the epidermis, followed by overheating of tissues associated with leaf necrosis. On the other hand, recent studies detected leaf temperature changes induced by powdery mildew in wheat under greenhouse conditions by using thermal imaging [58]. Instead, our results suggest that tissue temperature at the canopy level and stomatal conductance were not affected by the amount of disease. Moreover, g_s measurements were time-consuming and surely unrepresentative of the whole plot as only one replicate was measured and weather conditions could oscillate. Thus, these may not be reliable parameters for the selection of varieties resistant to yellow rust under field conditions.

4.4. Effect of disease on agronomic traits

Anthesis has widely been reported to be a critical period in determining the number of kernels per spike and the number of kernels per square meter [59], whereas the grain filling period is critical in determining TKW and HI [60]. In our study, disease was detected approximately one month before anthesis, so our results are consistent with previous reports since grain yield losses were mainly associated with reductions in the number of grains per spike, TKW, HI and grains per square meter (Table 4). Contrary to previous reports [61] wherein infection began at a very early growth stage, the number of spikes per square meter was not significantly decreased in our study. The favorable growing conditions during tillering and before disease spread enabled good establishment of tillers, which could explain the high number of spikes per square meter [62–64] as it is comparable to potential yielding conditions. In summary, our results suggest that the reduction in grain yield in disease conditions was probably due to: (i) increased grain abortion (or reduction in fertility) shown by a reduction of grains per spike and grains per square meter and (ii) a reduction in the amount of photoassimilates [65] intended for grain filling, explaining the reductions in TKW and HI.

The contribution of each agronomic parameter to variation in grain yield showed clear differences depending on the experimental conditions (Table 5). The main difference lies in the correlation of DH, TKW and HI with GY, which occurred only in the disease presence. Moreover, in the disease-affected trial we noted a significant negative relationship between HI and DH (Table S1), which suggested that early heading enabled a degree of disease escape, and made it possible for the plants to achieve a greater HI and thereby achieve higher yields in these conditions. This highlights the importance of wheat phenology for avoiding stress conditions [57], whereas in good agronomic conditions, the phenological characteristics were not good determinants of yield. In contrast, the rest of the agronomic parameters showed similar trends in relation to grain yield in all conditions. The yield component compensation principle [66] explains that the strong cross-correlation between spikes per square meter, grains per spike and HI remained robust even in the presence of disease.

4.5. Predictive model assessment

Finally, the multivariate regression models revealed the most appropriate parameters for field phenotyping in the presence of yellow rust. Yield was ignored in this model because the main interest was to assess GY and GYLI using independent traits measured before maturity. The development of yellow rust involves gradual changes in the color characteristics of crop canopies as epidemics' progress, and this information is obtained by the RGB-indices. According to the results of multivariate models, information contained in the RGB-indices, together with phenology, are closely related to GY and GYLI as the predictions are robust (R^2 = 0.6 and R^2 =0.7; respectively) and reliable ($P < 0.001$). Both models demonstrated the potential of digital vegetation indices to characterize biotic stress produced by yellow rust, its utility for grain yield losses assessment and, therefore, selection of resistant varieties. Although the correlations of DH with GY and GYLI were mild, all regression models chose DH as a predictive parameter; so, our study suggests that this phenological trait provides a: (i) different information compared to the rest of the included parameters, (ii) useful data and (iii) information related to grain yield in biotic stress conditions.

5. Conclusions

The Warrior/Ambition strain of *P. striiformis* f. sp. *tritici* seriously affected most of the genotypes of our collection. For some

genotypes it resulted in losses greater than 50% of the potential yield. This highlights the need to find genotypically resistant varieties by using high throughput phenotyping tools such as those used in the present study. For the first time, RGB-indices demonstrated the potential of using digital images of crop canopies instead of pictures and scans of isolated leaves or conventional observational evaluations for GY assessment in infected disease nurseries. This represents a marked advantage as this procedure has also been shown to be: (i) considerably faster, (ii) more representative of the whole plot, and (iii) more objective than those mentioned above. Unlike NDVI, which is much less efficient by itself, digital indices provide accurate and useful information for wheat breeding with dense canopy coverage. Moreover, LCC, g_s and CTD proved to be inappropriate for grain yield loss assessments in the presence of yellow rust. We also demonstrated the association of the presence of the wheat yellow rust disease to changes in the interrelationships between agronomic traits themselves and their contribution to grain yield compared to potential conditions. To the best of our knowledge this is the first report showing that phenology can play a significant role with regard to biotic stress conditions in wheat. Finally, the optimal yield predictive models include DH always together with RGB indices and they set robust and reliable predictions. The versatility, low cost, and high throughput of digital RGB techniques show promise as potentially useful tools in many agronomic areas, and should be considered in future phenotyping strategies.

Acknowledgments

This study was supported by the Spanish project AGL2013-44147-R. We thank Jesús Vega, head of INIA Station at Aranjuez, José Novo and our partners, Dr. Salima Yousfi, Rut Sánchez-Bragado, Dr. Jordi Bort and Bangwei Zhou, for their assistance with the collection of phenotic data during the study. We also thank Dr. Isabel Trillas and Dr. Néstor Hladun for their help in fungus verification. Finally we thank Dr. Jaume Casadesús for providing the BreedPix software.

Supplementary material

Supplementary material to this article can be found online at http://dx.doi.org/10.1016/j.cj.2015.03.003.

REFERENCES

[1] Survey about surfaces and crop yields in Spain (ESYRCE), Framework Survey of Areas in Spain, Publication prepared by the Technical Secretariat, General Statistics Branch, Madrid 2013Ministry of Agriculture, Food and Environment, Government of Spain, 2013.
[2] FAO, Statistical yearbook 2013, World Food and Agriculture, FAO, Rome, 2013.
[3] J. Almacellas, A. López, F. Álvaro, J. Serra, G. Capellades, J. Marín, Yellow rust of wheat, an emerging problem (La roya amarilla de los trigos, un problema emergente; Vida Rural), Rural Life publication, by Agronline, Winter wheat Dossier, num., 370, November 2013.
[4] J.G. Hansen, P. Lassen, M. Hovmoller, D. Hodson, ICT framework for global wheat rust surveillance and monitoring, 10th Conference of European Foundation for Plant Pathology, Wageningen, The Netherlands, 2012.
[5] E. Sanchez-Monge, Evolution of wheat yellow rust virulence in Spain: 2010–2013 (Evolución de la virulencia a la roya amarilla del Trigo en España: 2010–2013), Limagrain, Ibérica, 2013.
[6] M.S. Hovmøller, A.F. Justesen, J.K.M. Brown, Clonality and long-distance migration of *Puccinia striiformis* f. sp. *tritici* in north-west Europe, Plant Pathol. 51 (2002) 24–32.
[7] W. Chen, C. Wellings, X. Chen, Z. Kang, T. Liu, Wheat stripe (yellow) rust caused by *Puccinia striiformis* f. sp. *tritici*, Mol. Plant Pathol. 15 (2014) 433–446.
[8] N. Aparicio Gutierrez, C. Carnicero Saldaña, F.J. Puertas Jorde, Yellow rust development on the wheats of Castilla y León (El desarrollo de la roya amarilla en los trigos de Castilla y León), Agricultural Technology Institute (ITA), Government of Castilla y León, Ministry of Agriculture and Livestock, Valladolid, May 2014.
[9] J.L. Araus, J. Cairns, Field high-throughput phenotyping—the new crop breeding frontier, Trends Plant Sci. 19 (2014) 52–61.
[10] J.L. Araus, G.A. Slafer, C. Royo, M.D. Serret, Breeding for yield potential and stress adaptation in cereals, Crit. Rev. Plant Sci. 27 (2008) 1–36.
[11] L. Cabrera-Bosquet, J. Crossa, J. von Zitzewitz, M.D. Serret, J.L. Araus, High-throughput phenotyping and genomic selection: the frontiers of crop breeding converge, J. Integr. Plant Biol. 54 (2012) 312–320.
[12] J.N. Cobb, G. DeClerck, A. Greenberg, R. Clark, S. McCouch, Next-generation phenotyping: requirements and strategies for enhancing our understanding of genotype–phenotype relationships and its relevance to crop improvement, Theor. Appl. Genet. 126 (2013) 867–887.
[13] R.T. Furbank, M. Tester, Phenomics — technologies to relieve the phenotyping bottleneck, Trends Plant Sci. 16 (2011) 635–644.
[14] G.A. Carter, Reflectance wavebands and indices for remote estimation of photosynthesis and stomatal conductance in pine canopies, Remote Sens. Environ. 63 (1998) 61–72.
[15] A.R. Huete, A soil adjusted vegetation index (SAVI), Remote Sens. Environ. 25 (1988) 295–309.
[16] J.A. Gamon, J. Peñuelas, C.B. Field, A narrow waveband spectral index that tracks diurnal changes in photosynthetic efficiency, Remote Sens. Environ. 41 (1992) 35–44.
[17] W. Huang, D.W. Lamb, N. Zheng, Y. Zhang, L. Liu, J. Wang, Identification of yellow rust in wheat using in-situ spectral reflectance measurements and airborne hyperspectral imaging, Precis. Agric. 8 (2007) 187–197.
[18] J. Peñuelas, J.A. Gamon, K.L. Griffin, C.B. Field, Assessing type, biomass, pigment composition and photosynthetic efficiency of aquatic vegetation from spectral reflectance, Remote Sens. Environ. 46 (1993) 110–118.
[19] J. Peñuelas, I. Filella, J.A. Gamon, Assessment of photosynthetic radiation — use efficiency with spectral reflectance, New Phytol. 131 (1995) 291–296.
[20] E.W. Chappelle, M.S. Kim, J.E. McMurtrey III, Ratio analysis of reflectance spectra (RARS): an algorithm for the remote estimation of the concentrations of chlorophyll A, chlorophyll B, and carotenoids in soybean leaves, Remote Sens. Environ. 39 (1992) 239–247.
[21] J. Casadesús, C. Biel, R. Savé, Turf color measurement with conventional digital cameras, in: J. Boaventura (Ed.), EFITA/WCCA Joint Congress on IT in Agriculture, Vila Real, Portugal, 2005.
[22] USDA, Foreign Agricultural Service, Ethiopia 2008 Crop Assessment Travel Report, 2008.

[23] J. Casadesus, Y. Kaya, J. Bort, M.M. Nachit, J.L. Araus, S. Amor, G. Ferrazzano, F. Maalouf, M. Maccaferri, V. Martos, H. Ouabbou, D. Villegas, Using vegetation indices derived from conventional digital cameras as selection criteria for wheat breeding in water-limited environments, Ann. Appl. Biol. 150 (2007) 227–236.
[24] F.J. Adamsen, P.J. Pinter, E.M. Barnes, R.L. LaMorte, G.W. Wall, S.W. Leavitt, B.A. Kimball, Measuring wheat senescence with a digital camera, Crop Sci. 39 (1999) 719–724.
[25] Managing Lodging Risk in Winter Wheat, Featuring the new Canopy Assessment Tool, Developed by BASF plc Crop Protection in collaboration with ADAS, http://www.pgrplus.basf.com/.
[26] M. Gils, K. Kempe, A. Boudichevskaia, R. Jerchel, D. Pescianschi, R. Schmidt, M. Kirchhoff, R. Schachschneider, Quantitative assessment of wheat pollen shed by digital image analysis of trapped airborne pollen grains, Adv. Crop Sci. Tech. 2, (2013)http://dx.doi.org/10.4172/2329-8863.1000119.
[27] H. Kampmann, O.B. Hansen, Using colour image analysis for quantitative assessment of powdery mildew on cucumber, Euphytica 79 (1994) 19–27.
[28] P. Vincelli, D.E. Hershman, Assessing Foliar Diseases of Corn, Soybeans and Wheat, Plant Pathology Fact Sheet, University of Kentucky, College of Agriculture, November 2011.
[29] V. Maloney, S. Petersen, R.A. Navarro, D. Marshall, A.L. McKendry, J.M. Costa, J.P. Murphy, Digital image analysis method for estimation of Fusarium-damaged kernels in wheat, Crop Sci. 54 (2014) 2077–2083.
[30] E.L. Stewart, B.A. McDonald, Measuring quantitative virulence in the wheat pathogen *Zymoseptoria tritici* using high-throughput automated image analysis, Phytopathology 104 (2014) 985–992.
[31] D.M. Ashourloo, R. Mobasheri, A. Huete, Evaluating the effect of different wheat rust disease symptoms on vegetation indices using hyperspectral measurements, Remote Sens. Environ. 6 (2014) 5107–5123.
[32] D. Moshou, C. Bravo, R. Oberti, J. West, L. Bodria, A. McCartney, H. Ramon, Plant disease detection based on data fusion of hyper-spectral and multi-spectral fluorescence imaging using Kohonen maps, Real-Time Imaging 11 (2005) 75–83.
[33] T. Mahmood, D. Marshall, Remote assessment of leaf rust of wheat in cultivars mixture and component purelines, Pak. J. Agric. Sci. 40 (2003) 63–66.
[34] M. Mirik, G.J. Michels, S. Kassymzhanova-Mirik, D. Jones, N.C. Elliott, V. Catana, R. Bowling, Hyperspectral field spectrometry for estimating greenbug (Homompeta: Aphidae) damage in wheat. in: 20th Biennial Workshop on Aerial Photography, Videography, and High Resolution Digital Imagery for Resource Assessment October 4–6, 2005, Weslaco, Texas.
[35] C.H. Bock, G.H. Poole, P.E. Parker, T.R. Gottwald, Plant disease severity estimated visually, by digital photography and image analysis, and by hyperspectral imaging, Crit. Rev. Plant Sci. 29 (2010) 59–107.
[36] C. Trueba, R. Millán, T. Schmid, C. Roquero, M. Magister, Database of Pedology Properties of Spanish soils (Base de Datos de Propiedades Edafológicas de los Suelos Españoles), Volume V. Madrid, Department of Environmental Impact of Energy, December, 1998.
[37] United States Department of Agriculture, Natural Resources Conservation Service, Keys to Soil Taxonomy, 10th edition, 2006.
[38] Agro-climatic Information System for Irrigation (Sistema de Información Agroclimática para el Regadío, SIAR) (http://eportal.magrama.gob.es/websiar/). Ministry of Agriculture, Food and Environment, Government of Spain and the European Agricultural Fund for Rural Development (Last consulted on August 2014).
[39] Group for the Evaluation of New Varieties of Extensive Crops in Spain (Grupo para la Evaluación de Nuevas Variedades de Cultivos Extensivos en España — GENVCE), http://www.genvce.org/.
[40] L. O'Gorman, M.J. Sammon, M. Seul, Practical Algorithms for Image Analysis: Description, Examples and Code, Second edition Cambridge University Press, Cambridge, 2000.
[41] M.J. Vrhel, E. Saber, H.J. Trussell, Color image generation and display technologies, IEEE Signal Process. Mag. (January 2005) 23–33.
[42] N.K. Gupta, S. Gupta, A. Kumar, Effect of water stress on physiological attributes and their relationship with growth and yield of wheat cultivars at different stages, J. Agron. Crop Sci. 186 (2001) 55–62.
[43] N. Aparicio, D. Villegas, J. Casadesus, J.L. Araus, C. Royo, Spectral vegetation indices as nondestructive tools for determining durum wheat yield, Agron. J. 92 (2000) 83–91.
[44] M. Moriondo, F. Maselli, M. Bindi, A simple model of regional wheat yield based on NDVI data, Eur. J. Agron. 26 (2007) 266–274.
[45] T. Hobbs, The use of NOAA-AVHRR NDVI data to assess herbage production in the arid rangelands of Central Australia, Int. J. Remote Sens. 16 (1995) 1289–1302.
[46] J.K. Aase, F.H. Siddoway, Assessing winter wheat dry matter production via spectral reflectance measurements, Remote Sens. Environ. 11 (1981) 267–277.
[47] J. Jacobi, W. Kühbauch, Site-specific identification of fungal infection and nitrogen deficiency in wheat crop using remote sensing, in: J.V. Stafford (Ed.), Proceedings of the 5th European Conference on Precision Agriculture, Wageningen Academic Publishers, The Netherlands 2005, pp. 73–80.
[48] J. Franke, G. Menz, Multi-temporal wheat disease detection by multi-spectral remote sensing, Precis. Agric. 8 (2007) 161–172.
[49] A. Morgounov, N. Gummadov, S. Belen, Y. Kaya, M. Keser, J. Mursalova, Association of digital photo parameters and NDVI with winter wheat grain yield in variable environments, Turk. J. Agric. For. 38 (2014) 624–632.
[50] T. Jensen, A. Apan, F. Young, L. Zeller, Detecting the attributes of a wheat crop using digital imagery acquired from a low-altitude platform, Comput. Electron. Agric. 59 (2007) 66–77.
[51] G. Pan, F.M. Li, G.J. Sun, Digital camera based measurement of crop cover for wheat yield prediction, Geoscience and Remote Sensing Symposium, 2007. IGARSS 2007IEEE International 23–28 July 2007, pp. 797–800, http://dx.doi.org/10.1109/IGARSS.2007.4422917.
[52] S. Ali, S.J.A. Shah, K. Maqbool, Field-based assessment of partial resistance to yellow rust in wheat germplasm, J. Agric. Rural. Dev. 6 (2008) 99–106.
[53] F.M. Nzuve, S. Bhavani, G. Tusiime, P. Njau, Field screening of bread wheat for partial sources of resistance to stem rust, Research Application Summary, Third Ruforum Biennal Meeting, 24–28 September 2012, Entebbe, Uganda.
[54] J.R. Evans, Nitrogen and photosynthesis in the flag leaf of wheat, Plant Physiol. 72 (1983) 297–302.
[55] J.R. Seemann, T.D. Sharkey, J. Wang, C.B. Osmond, Environmental effects on photosynthesis, nitrogen-use efficiency, and metabolite pools in leaves of sun and shade plants, Plant Physiol. 84 (1987) 796–802.
[56] M.T. McGrath, S.P. Pennypacker, Alteration of physiological processes in wheat flag leaves caused by stem rust and leaf rust, Phytopathology 80 (1989) 677–686.
[57] R.C.G. Smith, A.D. Heritage, M. Stapper, H.D. Barrs, Effect of stripe rust (*Puccinia striiformis* West.) and irrigation on the yield and foliage temperature of wheat, Field Crop Res. 14 (1986) 39–51.

[58] Y.M. Awad, A.A. Abdullah, T.Y. Bayoumi, K. Abd-Elsalam, A.E. Hassanien, Early detection of powdery mildew disease in wheat (*Triticum aestivum* L.) using thermal imaging techniques, Intelligent Systems' 2014, Advances in Intelligent Systems and ComputingSpringer International Publishing, Cham, Switzerland 2015, pp. 755–765.
[59] S.A. Herrera-Foessel, R.P. Singh, J. Huerta-Espino, J. Crossa, J. Yuen, A. Djurle, Effect of leaf rust on grain yield and yield traits of durum wheats with race-specific and slow-rusting resistance to leaf rust, Plant Dis. 90 (2006) 1065–1072.
[60] R.A. Fischer, Selection traits for improving yield potential, in: M.P. Reynolds, J.I. Ortiz-Monasterio, A. McNab (Eds.), Application of Physiology in Wheat Breeding, CIMMYT, Mexico, 2001.
[61] R.P. Singh, J. Huerta-Espino, Effect of leaf rust gene *Lr34* on grain yield and agronomic traits of spring wheat, Crop Sci. 37 (1994) 390–395.
[62] S. Elhani, V. Martos, Y. Rharrabti, C. Royo, L.F. García del Moral, Contribution of main stem and tillers to durum wheat (*Triticum turgidum* L. var. *Durum*) grain yield and its components grown in Mediterranean environments, Field Crop Res. 103 (2007) 25–35.
[63] R.A. Richards, A.G. Condon, G.J. Rebetzke, Traits to improve yield in dry environments, in: M.P. Reynolds, J.I. Ortiz-Monasterio, A. McNab (Eds.), Application of Physiology in Wheat Breeding, CIMMYT, Mexico 2001, pp. 88–100.
[64] B.L. Duggan, R.A. Richards, A.F. van Herwaarden, N.A. Fettell, Agronomic evaluation of a tiller inhibition gene (Tin) in wheat: I. Effect on yield, yield components, and grain protein, Aust. J. Agric. Res. 56 (2005) 169–178.
[65] R.E. Gaunt, The relationship between plant disease severity and yield, Annu. Rev. Phytopathol. 33 (1995) 119–144.
[66] M.W. Adams, Basis of yield component compensation in crop plants with special reference to field bean, *Phaseolus vulgaris*, Crop Sci. 7 (1967) 505–510.

Supplementary material

Table S1 – Correlation matrix between all agronomic traits in the three growing conditions.

Parameter	GY	PH	DH	Spike number (m^{-2})	Grain number ($spike^{-1}$)	TKW	HI	Grain number (m^{-2})
GY	1	–0.126	–0.092	0.304*	0.076	0.135	0.063	0.650**
PH	0.101	1	–0.521**	0.341*	–0.452**	0.207	–0.336*	–0.281
DH	–0.345*	0.154	1	0.111	–0.142	0.247	–0.179	–0.105
Spike number (m^{-2})	0.495**	0.176	–0.160	1	–0.808**	0.136	–0.519**	0.116
Grain number ($spike^{-1}$)	0.194	–0.185	–0.068	–0.613	1	–0.509**	0.555**	0.459**
TKW	0.299*	–0.086	0.013	–0.119	–0.021	1	–0.227	–0.662**
HI	0.512**	–0.240	–0.362*	–0.311*	0.777**	0.171	1	0.214
Grain number (m^{-2})	0.899**	–0.182	–0.041	0.577**	0.206	–0.141	0.446**	1

Above the diagonal: potential yielding conditions; under the diagonal: disease-affected conditions. Parameters are: grain yield (GY), plant height (PH), days to heading (DH), spike number (m^{-2}), grain number ($spike^{-1}$), thousand-kernel weight (TKW), harvest index (HI) and grain number (m^{-2}).
** $P < 0.01$; * $P < 0.05$.

CHAPTER 2

A Novel Remote Sensing Approach for Prediction of Maize Yield Under Different Conditions of Nitrogen Fertilization

Omar Vergara-Díaz, Mainassara A. Zaman-Allah, Benhildah Masuka, Alberto Hornero, Pablo Zarco-Tejada, Boddupalli M. Prasanna, Jill E. Cairns and José L. Araus

Published on:
Frontiers in Plant Science (2016) Vol. 7, No 666

ABSTRACT

Maize crop production is constrained worldwide by nitrogen (N) availability and particularly in poor tropical and subtropical soils. The development of affordable high-throughput crop monitoring and phenotyping techniques is key to improving maize cultivation under low-N fertilization. In this study several vegetation indices (VIs) derived from Red-Green-Blue (RGB) digital images at the leaf and canopy levels are proposed as low-cost tools for plant breeding and fertilization management. They were compared with the performance of the normalized difference vegetation index (NDVI) measured at ground level and from an aerial platform, as well as with leaf chlorophyll content (LCC) and other leaf composition and structural parameters. A set of ten hybrids grown under five different nitrogen regimes were tested at the CIMMYT station of Harare (Zimbabwe). Grain yield and leaf N concentration across N fertilization levels were strongly predicted by most of these RGB indices (with R^2 ~ 0.7), outperforming the prediction power of the NDVI and LCC. RGB indices also outperformed the NDVI when assessing genotypic differences in grain yield and leaf N concentration within a given level of N fertilization. The best predictor of leaf N concentration across the five N regimes was LCC but its performance within treatments was inefficient. The leaf traits evaluated also seemed inefficient as phenotyping parameters. It is concluded that the adoption of RGB-based phenotyping techniques may significantly contribute to the progress of plant breeding and the appropriate management of fertilization

.

frontiers in Plant Science

ORIGINAL RESEARCH
published: 18 May 2016
doi: 10.3389/fpls.2016.00666

A Novel Remote Sensing Approach for Prediction of Maize Yield Under Different Conditions of Nitrogen Fertilization

*Omar Vergara-Díaz[1], Mainassara A. Zaman-Allah[2], Benhildah Masuka[2], Alberto Hornero[3], Pablo Zarco-Tejada[3], Boddupalli M. Prasanna[2], Jill E. Cairns[2] and José L. Araus[1]**

[1] Integrative Crop Ecophysiology Group, Plant Physiology Section, Faculty of Biology, University of Barcelona, Barcelona, Spain, [2] International Maize and Wheat Improvement Center, CIMMYT Southern Africa Regional Office, Harare, Zimbabwe, [3] Laboratory for Research Methods in Quantitative Remote Sensing, QuantaLab, Institute for Sustainable Agriculture, National Research Council, Cordoba, Spain

Maize crop production is constrained worldwide by nitrogen (N) availability and particularly in poor tropical and subtropical soils. The development of affordable high-throughput crop monitoring and phenotyping techniques is key to improving maize cultivation under low-N fertilization. In this study several vegetation indices (VIs) derived from Red-Green-Blue (RGB) digital images at the leaf and canopy levels are proposed as low-cost tools for plant breeding and fertilization management. They were compared with the performance of the normalized difference vegetation index (NDVI) measured at ground level and from an aerial platform, as well as with leaf chlorophyll content (LCC) and other leaf composition and structural parameters at flowering stage. A set of 10 hybrids grown under five different nitrogen regimes and adequate water conditions were tested at the CIMMYT station of Harare (Zimbabwe). Grain yield and leaf N concentration across N fertilization levels were strongly predicted by most of these RGB indices (with $R^2 \sim 0.7$), outperforming the prediction power of the NDVI and LCC. RGB indices also outperformed the NDVI when assessing genotypic differences in grain yield and leaf N concentration within a given level of N fertilization. The best predictor of leaf N concentration across the five N regimes was LCC but its performance within N treatments was inefficient. The leaf traits evaluated also seemed inefficient as phenotyping parameters. It is concluded that the adoption of RGB-based phenotyping techniques may significantly contribute to the progress of plant breeding and the appropriate management of fertilization.

Keywords: breeding, crop management, field phenotyping, maize, nitrogen fertilization, NDVI, RGB indices

OPEN ACCESS

Edited by:
Susana Araújo, ITQB-Universidade Nova de Lisboa, Portugal

Reviewed by:
Cristina Cruz, University of Lisbon, Portugal
Jan F. Humplík, Palacký University Olomouc, Czech Republic
Jean-Luc Regnard, Montpellier SupAgro, France

****Correspondence:***
José L. Araus
jaraus@ub.edu

Specialty section:
This article was submitted to Crop Science and Horticulture, a section of the journal Frontiers in Plant Science

Received: *18 November 2015*
Accepted: *01 May 2016*
Published: *18 May 2016*

Citation:
Vergara-Díaz O, Zaman-Allah MA, Masuka B, Hornero A, Zarco-Tejada P, Prasanna BM, Cairns JE and Araus JL (2016) A Novel Remote Sensing Approach for Prediction of Maize Yield Under Different Conditions of Nitrogen Fertilization. Front. Plant Sci. 7:666. doi: 10.3389/fpls.2016.00666

INTRODUCTION

Low soil fertility, alongside drought and heat, is a major stress factor limiting crop productivity on a world scale (Stewart et al., 2005). In the case of sub-Saharan Africa, the lack of nitrogen (N) is the main constraint on cereal yields in areas with more than 400 mm average annual rainfall (Buerkert et al., 2001). Therefore, an optimization of N use is critical for increased grain production, especially in the low productive regions. On the other hand, on the basis of environmental and economic

sustainability, a more restricted and reasonable use of fertilizers is necessary. Plant scientists, especially breeders and agronomists, face the challenge of solving these limitations while taking into account the additional implications of climate change on food security (Cairns et al., 2012, 2013).

Maize is the second most cultivated cereal worldwide and the most commonly cultivated cereal in Africa in terms of land area and production (FAO, 2013). In particular, agricultural productivity of sub-Saharan Africa remains the lowest in the world partly due to low soil fertility (Cairns et al., 2013; Fischer et al., 2014). Therefore, improving tolerance of maize to low N will increase yields and impact positively on livelihoods and food security (Masuka et al., 2012).

In this sense, two strategies are considered paramount for crop scientists: (i) breeding to improve varieties toward higher nutrient use efficiency and tolerance to nutrient-deficiency (ii) and appropriate fertilization management (Wezel et al., 2014), including precision agriculture (PA; Hatfield, 2000; Chen et al., 2014). Thereby, the implementation of such improvements may increase farmers' profits by maintaining crop yield and reducing the use of resources while preventing further degradation to the environment (Hergert et al., 1996; Delgado et al., 2001; Roberts et al., 2001; Wang et al., 2003). In that sense, technologies for crop monitoring and breeding must be high performing, broad-use and affordable, particularly (but not only) when national agricultural systems, seed companies, or small farmers from developing countries are the targets. Moreover, in the case of breeding, improvements are needed to overcome the field phenotyping bottleneck that limits breeding and advances in PA (Araus et al., 2008; Furbank and Tester, 2011; Araus and Cairns, 2014).

Remote proximal sensing technologies are being used currently for precise management of crops, whereas its potential application for field high throughput phenotyping has gathered increasing interest in recent years (Araus and Cairns, 2014; Liebisch et al., 2015). The classical approach has involved the use of multispectral sensors and the development of numerous vegetation indices associated with vegetation parameters such as above-ground biomass, water and nutrient-deficiency and crop yield (Petropoulos and Kalaitzidisz, 2012). Among the indices, the Normalized Difference Vegetation Index (NDVI) is the most widely used. Concerning crop N performance, several studies have shown that it is possible to quantify it satisfactorily using multispectral data at both the aerial and ground levels (Barnes et al., 2000; Boegh et al., 2002). However, multi and hyper-spectral imagers are relatively expensive and complex from the operational point of view.

As a low-cost alternative, vegetation indices derived from Red-Green-Blue (RGB) cameras have been employed for remote sensing assessment in field conditions, providing a wide-range of phenomic data about genotypic performance under different stress conditions and species, including water stress and foliar diseases in bread wheat, durum wheat and tritordeum and triticale (Casadesus et al., 2007; Casadesús and Villegas, 2014; Vergara-Diaz et al., 2015; Zhou et al., 2015). Moreover, digital sensors have been successfully integrated on board unmanned aerial vehicles (UAV) to assess crop vigor, vegetation coverage, and greenness (White et al., 2012; Andrade-Sanchez et al., 2014; Svensgaard et al., 2014). For example, digital indices derived from RGB images have been proposed for grain yield (GY) assessment in water limiting conditions (Casadesus et al., 2007) and for quantifying leaf N concentration (Rorie et al., 2011). However, the use of RGB images to assess genotypic performance in terms of yield and crop N accumulation in response to different levels of soil fertility has not yet been assessed. RGB images may represent a proper alternative to spectroradiometric approaches at different levels: at the whole trial level from aerial platforms, at the plot level from ground-based measurements or even at the single leaf level replacing leaf chlorophyll meters.

Information derived from plant samples may also be relevant for crop monitoring and phenotyping (Araus and Cairns, 2014). For example the stable isotope composition in plant matter constitutes an integrative selection criterion because it can describe the behavior of the crop under stress (Masuka et al., 2012). Nitrogen isotope composition ($\delta^{15}N$) can be employed to characterize the efficiency in using N fertilizers (Evans, 2001; Serret et al., 2008). For its part, implementing carbon isotope composition ($\delta^{13}C$) in maize is not clear for assessing genotypic differences due to the C_4-photosynthetic metabolism of this species, but still appears responsive to differences in growing conditions (Monneveux et al., 2007; Araus et al., 2010). Finally, some other morphological and compositional traits such as the specific leaf area (SLA), N concentration, N per unit leaf area (N/LA), and carbon to nitrogen ratio (C/N), which are in turn related to nitrogen use efficiency, leaf construction, and primary metabolism (Poorter and Evans, 1998; Feng et al., 2008), have the potential to be useful for breeding, but knowledge about their association with crop yield is scarce.

The main goal of this study is to develop affordable easy-to-use new phenotyping tools that increase selection efficiency for grain yield and leaf N concentration under different N fertilization conditions in maize. To accomplish this objective, we compared the accuracy of field-spectroradiometer data vs. RGB-derived vegetation indices assessing GY and leaf N concentration in a set of ten maize hybrids grown in the field under five N-fertilizer levels. Firstly, we assessed the performance of these parameters for all the N-treatments together, and subsequently we dissected the correlations within each N-level for further discussion of phenotyping. Additionally, simple regression models were made for GY prediction and these models were tested and validated against the experimental yield of another trial. The performance of the leaf parameters N/LA, C/N, SLA, and $\delta^{13}C$ and $\delta^{15}N$ were also studied with the aim of relating these structural and compositional leaf properties with crop performance and phenotyping data. All RGB and UAV imagery were obtained at flowering stage in order to integrate the differences in crop performance from plant emergence to flowering stage, when the number of kernels per ear is determined.

MATERIALS AND METHODS

Experimental Design and Growing Conditions

Field trials were carried out at the Southern Africa regional station of CIMMYT (International Maize and Wheat

Improvement Center) located in Harare (17°43′32″S, 31°00′59″E) where two field experiments were studied. Before sowing, soil pH, total soluble salts (TSS), nitrogen as nitrate (NO_3^-) and phosphorus (P_2O_5) were analyzed in three soil depth ranges (0–30, 30–60, and 60–90 cm) and six replicates for each depth range were produced. Mean values for the full soil profile were pH = 5.8, TSS = 240.9 ppm, NO_3^- = 4.12 ppm, and P_2O_5 = 18.93 ppm.

Ten maize hybrids were sown, three of them were commercial hybrids (PAN7M-81, SC635, SC537) and the other seven were maize hybrids developed at CIMMYT (TH11894, TH127591, TH127053, TH127618, TH13466, CZHH1155, TH127004). These maize hybrids cover a big range of agronomical sensitivity to low nitrogen conditions. A split-plot arrangement in a randomized block design was set up and five nitrogen fertilization levels (0, 10, 20, 80, and 160 kg·ha^{-1} NH_4NO_3) were applied in both trials. Two and three replicates were set for the first and second trials, with 100 and 150 being the respective number of plots in each trial (trials S and P, respectively). A two-row border was sown between fertilization treatments and on the edges of the trial to prevent spatial variability.

Seeds were sown during the wet season, on December 23th 2013, in two rows per plot; rows were 4 m long and 75 cm apart (6 m^2/plot), with 17 planting points per row and 25 cm between plants within a row. All trials were homogeneously fertilized with 400 kg·ha^{-1} of super-phosphate and potassium oxide fertilizer (P_2O_5 14% and K_2O 7%). Weather conditions throughout growing season were recorded with a weather station. The mean temperature was 18.9°C, mean humidity 81.2 and total rainfall during the crop period was 563.1 mm, therefore, preventing the water deficit in these rainfed conditions.

The trials were harvested on May 20th 2014. The central 3.5 m of each row was harvested discarding 2 plants at each end, thus the collected weight corresponded to 5.25 m^2 (0.75 m apart × 2 rows × 3.5 m long). The cobs were threshed and the grains dried until they reached around 12% moisture, and then the grain from each plot was weighed. Grain yield (GY, Mg·ha^{-1}) was calculated as follows: (X kg plot^{-1} × 10)/5.25 where X is the grain weight per plot.

NDVI Calculation

The normalized difference vegetation index (NDVI) was calculated using the equation:

$$NDVI = (NIR - R)/(NIR + R)$$

where R is the reflectance in the red band and NIR is the reflectance in the near-infrared band. NDVI was obtained around the flowering stage by using two different approaches: using ground measurements and from aerial multispectral images (**Figure 1**).

The NDVI of individual plots at ground level ($NDVI_{ground}$) was determined with a ground-based portable spectroradiometer with an active sensor (GreenSeeker handheld crop sensor, Trimble, USA). This equipment uses the spectral wavelengths 650–670 nm as the red band and 765–795 nm as the near infrared. The distance between the sensor and the plots was kept constant using a ladder, around 0.5–0.6 m above and perpendicular to the canopy. The whole areas of the two trials were measured from 12 to 14 h on March 3rd and 4th, 2014.

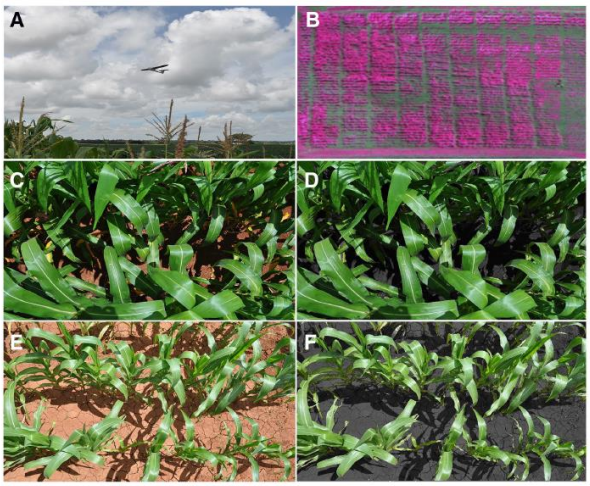

FIGURE 1 | (A) The unmanned aerial vehicle flying over the maize crops; **(B)** Multispectral false-color image at the aerial level showing near infrared (800 nm) as red, green (550 nm) as blue and red (670 nm) as green, spatial resolution of 10 cm/px; **(C)** RGB digital image from the high-nitrogen fertilization treatment at the canopy level; **(D)** and its resulting processed image with BreedPix; **(E)** RGB image from the low-nitrogen treatment and **(F)** its respective processed image.

The aerial NDVI index ($NDVI_{aerial}$) was obtained using a UAV-based remote sensing platform developed by Airelectronics (Montegancedo campus, Spain) in collaboration with the Crop Breeding Institute-Zimbabwe, CIMMYT, QuantaLab at the Institute for Sustainable Agriculture (IAS-CSIC, Spain) and the University of Barcelona. This aerial platform was equipped with a multispectral camera (ADC-Lite, Tetracam, Inc., Chatsworth, CA, US), which provides spectral images on the green, the red and the near-infrared bands, with a final ground resolution of 10 cm per pixel when flying at an object distance of 150 m. These bands are approximately equal to the Landsat Thematic Mapper (TM) bands TM2, TM3, and TM4, respectively, so that the spectral wavelengths from 630 to 690 nm represent the red band and 760 to 920 nm the near infrared band. The flight was conducted at an altitude of 150 m at midday on a sunny day when crops were around the flowering stage. The collected images covered 220 out of the total 250 plots, completely covering the block S trial (100 plots) and partially covering block P (120 of the total of 150 plots). Aerial images were subsequently corrected and calibrated with ImapQ (QuantaLab-IAS-CSIC, Cordoba, Spain) which converts images to radiance. Mosaicking and rectifying processes were applied with Autopano (Kolor SARL, Francin, France) by applying the image stitching technique (SIFT algorithm) in addition to a manual orthorectification from several checkpoints selected. NDVI values were finally extracted from the images using ENVI software (Exelis Visual Information Solutions, Boulder, Colorado, USA).

RGB Indices

Vegetation indices derived from red-green-blue (RGB) images were evaluated at the plot and the single leaf level (RGB_{canopy} and RGB_{leaf} indices, respectively; **Figure 1**). In the case of RGB_{canopy}, one digital RGB picture was taken per plot by holding the camera about 0.8–1.0 m above the canopy, in a zenithal plane and focusing near the center of each plot. Plot images were taken on the same days as the measurements with the ground spectroradiometer using a Nikon COOLPIX S8000 digital compact camera without flash and with a focal length of 54 mm and were saved in a 4288 × 2848 pixel JPEG format. Later, six leaves per plot were taken from the S trial (100 plots) and were subsequently scanned with a Dell 2155 cdn multifunction color printer (Round Rock, TX, USA). Finally, scanned images were saved in the same format with a resolution of 2338 × 1653 pixels and RGB_{leaf} indices calculated as below.

Subsequently, images were analyzed with the open source Breedpix 0.2 software (Casadesus et al., 2007) designed to process digital images. This software enables calculation of several RGB vegetation indices based on the different properties of color inherent in RGB images. RGB VIs were obtained either from the average color of the whole image or from the hue histogram in each image. BreedPix produces several automatic conversions of the original RGB image to other color spaces (i.e., each model that numerically represents the color in terms of different coordinates). Four VIs (a*, b*, u*, and v*) belonging to CIE (from the French abbreviation of International Commission on Illumination) color spaces were calculated and used in this study. The software require the use of Java Advanced Imaging (JAI) for the conversion of RGB color space to CIE-XYZ color space and the resulting coordinates are subsequently converted to other color spaces. First, the VIs a* and b* belong to CIE-Lab color space, being L* the lightness dimension and a* and b* the color-opponent coordinates. Red/green opponent-colors are represented along a* axis, whereas b* axis represent the yellow/blue opponent colors. Similarly, u* and v* indices represent the axis in the chromaticity diagram of CIE-Luv color space. Thereby the software obtains the average values of these components of color for each one of the processed images. Hue component is calculated using the JAI functions which employ the formulae described in Seul et al. (2000) whereas the components of CIE-Lab and CIE-Luv color spaces are calculated as described in Trussell et al. (2005). The relative green area (GA) and the relative "greener area" (GGA) are based on the sum of frequencies of the histogram classes included in a certain range of hue in the image. GA is the percentage of pixels in the image in the hue range from 60 to 180°, that is, from yellow to bluish green. On the other hand GGA is somewhat more restrictive since the range of hue considered by this index is from 80 to 180°, excluding yellowish-green tones and therefore, it more accurately describes the amount of photosynthetically active biomass and leaf senescence.

Analysis of Leaf Parameters

The leaf portions in the RGB_{leaf} indices were also used the subsequent measures. Firstly, immediately before being scanned, a handheld spectroradiometer developed for leaf chlorophyll measurements (Minolta SPAD-502, Spectrum Technologies Inc, Plainfield, IL, USA) was used to measure the index related to leaf chlorophyll content (LCC). Four measurements were made for each leaf segment. Secondly, the leaves were oven dried at 70°C for 24 h and the dry weight was measured. Then the specific leaf area (SLA) was calculated using the equation

$$SLA = LA \,/\, DW$$

where LA is the total leaf area (m^2) measured previously from the scanned images using the open-source Java-based software ImageJ (http://rsb.info.nih.gov.sire.ub.edu/ij/) and DW is the corresponding dry weight (kg).

Finally, dry leaves were ground to a fine powder and 0.7–0.9 mg of leaf dry matter from each plot was weighed and sealed into tin capsules. Stable carbon ($^{13}C/^{12}C$) and nitrogen ($^{15}N/^{14}N$) isotope ratios as well as the leaf N and C concentrations (%) were measured using an elemental analyser (Flash 1112 EA; Thermo Finnigan, Bremen, Germany) coupled with an isotope ratio mass spectrometer (Delta C IRMS, Thermo Finnigan) operating in a continuous flow mode. Samples were loaded into a sampler and analyzed. Measurements were conducted at the Scientific Facilities of the University of Barcelona. Isotopic values were expressed as a composition notation (δ) as follow:

$$\delta\ (‰) = (^{13}C/^{12}C)_{sample}/\ (^{13}C/^{12}C)_{\ standard} - 1$$

where "sample" refers to plant material and "standard" to international secondary standards of known $^{13}C/^{12}C$ ratios (IAEA CH7 polyethylene foil, IAEA CH6 sucrose and USGS 40 L-glutamic acid) calibrated against Vienna Pee Dee Belemnite calcium carbonate with an analytical precision (standard deviation) of 0.15‰. The same δ notation was used for the $^{15}N/^{14}N$ ratio expression but with the standard referring to air. For nitrogen, international isotope secondary standards IAEA N1, IAEA N2, IAEA NO3, and USGS 40 were used with a precision of 0.3‰. Further, the C/N ratio was obtained from these analyses and total nitrogen concentration per unit leaf area (N/LA) was calculated with the formula:

$$N\,/LA = \left(\frac{DW}{LA}\right) x\, N$$

where LA is the total leaf area (m^2), DW is the corresponding dry weight (g) and N is its nitrogen concentration (in % dry matter).

Statistical Analysis

Statistical analyses were conducted using SPSS 21 (IBM SPSS Statistics 21, Inc., Chicago, IL, USA). Multiple variance analyses, the multiple comparison Duncan *post-hoc* test and bivariate correlations were performed. The presented leaf parameters (LCC, N, $\delta^{15}N$, N/LA, SLA, $\delta^{13}C$, C/N) and RGB_{leaf} indices from scanned leaves were only analyzed for the S trial, whereas the $NDVI_{ground}$, $NDVI_{aerial}$, and RGB_{canopy} indices were studied for both trials. The determination coefficients of the linear relationships of GY and leaf N concentration with the vegetation indices NDVI and RGB were calculated for the entire trials and within each N fertilization treatment. All graphs were

performed with SigmaPlot 10.0 (Systat Software Inc., San Jose, California, US).

RESULTS

Significant differences in GY between genotypes and nitrogen-fertilization levels were observed in this study (**Table 1**) with GY increasing in response to N fertilization (**Table 2**). Differences within nitrogen-input levels were also detected with both (ground and aerial) NDVI approaches and with all RGB_{canopy} indices except by a*. Genotypic differences were detected by the RGB_{canopy} indices GGA, GA, a*, u*, and hue, whereas among the spectroradiometric indices only the NDVI at the ground level detected genotypic differences.

Leaf N concentration varied significantly between genotypes and the effect of N-fertilization levels was highly significant (**Table 1**) with values increasing as N fertilization increased (**Table 2**). All the RGB_{leaf} indices detected very significant differences between nitrogen treatments and genotypic differences were also found with GA (**Table 1**). At the same time, LCC also indicated highly significant differences between N fertilization levels but not genotypic differences.

All the analyzed leaf parameters (N, N/LA, SLA, $\delta^{15}N$, $\delta^{13}C$, C/N) were highly sensitive to variations in N fertilizer levels (**Table 1**). In contrast, apart from leaf N concentration, genotypic differences were only detected for $\delta^{13}C$. Increasing N fertilization caused significant increases in leaf N, N/LA and SLA while $\delta^{15}N$ and the C/N ratio decreased (**Table 2**). Additionally, differences among N fertilization levels were also found in $\delta^{13}C$ but its trend was somewhat different: in the low-N levels $\delta^{13}C$ was quite steady and then it decreased at 80–160N, whereas leaf-N concentration increased.

Additionally, the effect of changing light in outdoor conditions was evaluated in RGB indices obtained from canopy images (Table S1). For this purpose, 57 plots were photographed twice in nearly consecutive days, firstly in a sunny day and secondly in a partly cloudy day. All indices were strongly correlated between replicates ($p < 0.001$), particularly the indices GA, GGA, u*, a* ($R^2 > 0.72$).

TABLE 1 | *P*-values from multivariate analysis of variance with two fixed factors: genotype and nitrogen level and its interaction (GxN).

	Genotype	Nitrogen level	G x N
GY	< 0.001	< 0.001	0.884
SPECTRAL INDICES			
$NDVI_{aerial}$	0.509	< 0.001	0.745
$NDVI_{ground}$	< 0.001	< 0.001	0.500
RGB_{canopy} INDICES			
hue	0.032	< 0.001	0.997
a*	0.006	0.125	0.727
b*	0.590	< 0.001	0.997
u*	0.012	< 0.001	0.801
v*	0.567	< 0.001	0.993
GA	0.002	< 0.001	0.708
GGA	< 0.001	< 0.001	0.564
RGB_{leaf} INDICES			
hue	0.412	< 0.001	0.817
a*	0.364	< 0.001	0.882
b*	0.580	< 0.001	0.999
u*	0.310	< 0.001	0.687
v*	0.787	< 0.001	0.999
GA	0.042	< 0.001	0.604
GGA	0.289	< 0.001	0.225
LCC	0.939	< 0.001	0.973
ANALYZED PARAMETERS			
Leaf %N	0.026	< 0.001	0.999
N/LA	0.347	< 0.001	0.972
C/N	0.120	< 0.001	1.000
$\delta^{15}N$	0.375	< 0.001	1.000
$\delta^{13}C$	< 0.001	< 0.001	0.937
SLA	0.822	0.004	0.89

As dependent variables, grain yield (GY), leaf nitrogen concentration (%N), NDVI at aerial and ground levels, RGB indices from canopy images and scanned leaves, leaf chlorophyll content (LCC), nitrogen per unit area (N/area), the stable carbon ($\delta^{13}C$), and nitrogen ($\delta^{15}N$) isotope composition, carbon nitrogen ratio (C/N) and specific leaf area (SLA).

Grain Yield Assessment across Nitrogen Regimes and Genotypes

All vegetation indices (either ground and aerial NDVI, RGB_{canopy}, or LCC) were strongly correlated with GY variation across the whole set of plots of the two trials. The best results were obtained by using the RGB-indices GA and GGA at the canopy level, which showed an exponential regression model and explained 70–72% of GY variability (**Figure 2**). Meanwhile, the RGB_{canopy} indices u* and a* evolved inversely with increasing GY and demonstrated lower accuracy ($R^2 = 0.326$ and $R^2 = 0.302$, respectively, data not shown). In contrast, LCC evolved linearly with increases in GY and explained 69% of GY variation (**Figure 2**). Finally, both NDVI approaches followed a power regression model and their determination coefficients were moderate and similar ($NDVI_{ground}$ at **Figure 2**; $NDVI_{aerial}$ $R^2 = 0.293$, data not shown).

Additionally, simple regression models from the P trial that explained GY across the different N fertilization levels were obtained by using the different VIs and validated for their accuracy in estimating the GY of the S trial (**Table 3**). The estimated GY from all VIs always fitted satisfactorily with the experimental GY for the entire trial. The determination coefficients increased further when six hybrids contrasting in their grain yield were selected, with three of them being high-yielding and the remaining ones low-yielding. Genotypic differences were found in the estimated GY from GGA, $NDVI_{aerial}$ and $NDVI_{ground}$ between the six selected hybrids and the experimental GY was also significantly different. Moreover, in all models, differences between N fertilization levels were always detected by the estimated GY.

TABLE 2 | Means of grain yield (GY) (Mg·ha^{-1}) from the two trials, leaf nitrogen concentration (%N), nitrogen per unit leaf area (N/LA), specific leaf area (SLA), the stable carbon (δ^{13}C), and nitrogen (δ^{15}N) isotope composition and the leaf C/N ratio according to the ten hybrids and the five nitrogen levels.

	GY (Mg·ha^{-1})	%N	N/LA (g/m^2)	SLA (m^2·kg)	C/N ratio	δ^{15}N (‰)	δ^{13}C (‰)	LCC (u)
GENOTYPE								
PAN 7M-81	5.03b	2.203ab	111.24ab	20.23a	21.07b	4.53b	−11.7ab	41.53a
TH11894	5.12b	2.196ab	101.75a	21.48a	20.77b	3.78ab	−11.49cd	42.02a
TH127591	5.14b	2.312abc	117.87ab	20.41a	19.75ab	4.04ab	−11.79a	43.06a
TH127053	5.7bc	2.32abc	118.29ab	19.56a	19.75ab	4.18ab	−11.55bcd	41.13a
SC635	3.52a	2.506bc	125.31ab	19.98a	18.38ab	3.66ab	−11.77a	41.84a
TH127618	5.38b	2.621c	130.12ab	20.54a	17.27a	3.64ab	−11.63abc	43.56a
TH13466	5.75bc	2.4abc	117.62ab	20.91a	18.96ab	3.76ab	−11.45*d*	42.57a
CZH1155	4.63b	2.526bc	133.84b	18.9a	18.48ab	3.19a	−11.64abc	42.28a
TH127004	6.49c	2.138a	113.71ab	19.05a	21.35b	3.87ab	−11.71ab	41.76a
SC537	4.67b	2.38abc	121.71ab	20.32a	19.65ab	3.79ab	−11.7ab	42.39a
NITROGEN LEVEL								
0	3.13a	1.887a	107.62a	17.82a	23.75d	5.612*e*	−11.584bc	32.5a
10	3.9b	1.881a	92.78a	20.6b	23.43d	4.613d	−11.59bc	33.4a
20	4.61c	2.089a	107.09a	19.91ab	21.01*c*	3.877c	−11.512cd	40.4b
80	6.48d	2.739b	138.68b	20.14b	16 b	2.898b	−11.652b	50.9c
160	7.59e	3.206c	149.56b	22.22b	13.54a	2.218a	−11.869a	53.8d

Letters are significantly different according to Duncan's multiple range test ($P < 0.05$).

Grain Yield Assessment across Genotypes within Each N Regime

To further assess the accuracy of these indices, the determination coefficients for GY prediction within each N-input level across genotypic means were performed (**Table 4**). GGA, GA, u*, and a* indices were correlated significantly to GY variation within all N levels, whereas both NDVI approaches were correlated significantly to GY only for some of the studied N levels. By contrast, LCC did not correlate with GY across plots within any of the N levels.

Leaf Nitrogen Assessment across N Regimes and Genotypes

LCC was the best predictor of leaf N concentration across the entire trial, explaining more than 80% of N variability, moderately surpassing the fitting accuracy of the RGB_{leaf} indices (**Figure 3**). Thus, the RGB_{leaf} index a* explained about 69% of leaf N variation across N fertilization treatments (**Figure 3**) and u*, b*, and v* were quite similar ($R^2 = 0.682$, $R^2 = 0.643$, and $R^2 = 0.621$, respectively, data not shown). For its part, $NDVI_{aerial}$ was also a good predictor of leaf N (**Figure 3**), whereas $NDVI_{ground}$ was less accurate in its prediction ($R^2 = 0.116$, data not shown). Finally, the RGB index v* at the canopy level was more related to leaf N than it was to GY, and it was shown to be a reasonably good predictor of leaf N across the whole trial (**Figure 3**).

Leaf Nitrogen Assessment across Genotypes within Each N Regime

A table depicting the determination coefficient between the RGB_{leaf} indices, $NDVI_{aerial}$, $NDVI_{ground}$, and LCC against leaf N across genotypic means within each of the N fertilization levels is presented (**Table 5**). In the low-N treatments (0N to 20N) the best determination coefficients were provided by the RGB_{leaf} indices b*, v*, u*, and a*. In addition, most of the RGB_{leaf} indices were also sensitive to leaf N variation at the 80N level but none of them related significantly at the 160N level. For its part, LCC showed a quite similar accuracy compared with the RGB_{leaf} indices in their predictions of leaf N within the low-N levels, but it was not significantly correlated in the high-N fertilization levels (**Table 5**). Finally, $NDVI_{aerial}$ was especially sensitive to leaf N variations in the high-N and 0N treatments, whereas $NDVI_{ground}$ was generally unrelated to leaf N within each N treatment.

Leaf Parameters Performance and Relationships with VIs and Yield

Leaf N was strongly negatively correlated across N levels with δ^{15}N and the C/N ratio and to a lesser extent with δ^{13}C and SLA (Table S2). Correlations of these traits with GY were also negative but weaker, except for SLA which did not correlate.

Most of the RGB indices (both at the leaf and canopy scales), the LCC and the NDVI correlated with N/LA across N regimes, but always more moderately than they correlated with leaf N concentration (Table S2). The association of δ^{15}N with NDVI, LCC, and RGB indices (at the both scales) was highly significant and in some cases their correlation coefficients were higher than the respective coefficients between δ^{15}N and leaf N. Similarly, δ^{13}C was fairly well correlated with most of the RGB indices (especially at the leaf scale) and LCC. Regarding the C/N ratio, LCC was the best predictor but this correlation was smaller than with leaf N concentration. However, most of the RGB_{leaf} indices (a*, b* u*, v*, GA), the RGB_{canopy} indices (hue, u*, GA, GGA) as well as $NDVI_{ground}$ and $NDVI_{aerial}$ correlated more strongly with

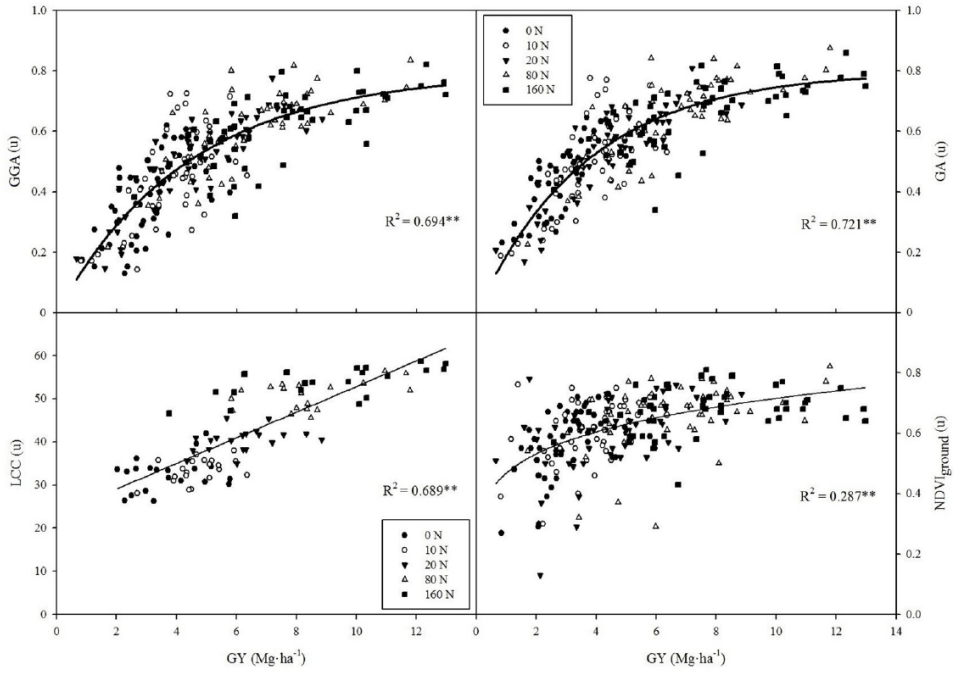

FIGURE 2 | Correlations between grain yield (GY) and leaf chlorophyll content (LCC), the RGB indices GA and GGA at the canopy level and NDVI at the ground level. R^2, determination coefficient; $^{**}P < 0.001$.

the leaf C/N ratio than they did with leaf N (Table S1). Finally, SLA correlated strongly with the RGB_{leaf} indices GA and GGA, and slightly with both NDVIs.

The relationships between leaf N, N/LA, C/N, $\delta^{13}C$, $\delta^{15}N$, and SLA with GY across genotypes within N fertilization treatments were almost all non-significant except for leaf N in the 160N treatment (**Table 4**). Regarding the genotypic correlations within each N fertilization level of these leaf traits with leaf N, only the leaf N derived parameters (C/N and N/LA) were significantly correlated (**Table 5**).

DISCUSSION

Crop Monitoring and Phenotyping Parameters for GY Estimation

As previously found in other studies in wheat grown under different stress conditions (Casadesus et al., 2007; Morgounov et al., 2014; Vergara-Diaz et al., 2015), the RGB_{canopy} indices (from BreedPix software) measured at flowering were strongly correlated with GY. RGB-based indices may perform far better than NDVI for GY prediction, which has been recently described under water and biotic stresses in wheat (Elazab et al., 2015; Vergara-Diaz et al., 2015; Zhou et al., 2015). The lower accuracy of NDVI in comparison to digital-based RGB indices can be explained in several ways. On the one hand, graphs clearly highlight (**Figure 2**) that the variability in the canopy NDVIvalues at ground level is small, with more than 90% of values being in the range 0.5–0.8 and with the NDVI values in the low N treatments being already relatively high (e.g., average of $NDVI_{ground}$ = 0.57 in the 0N treatment). Therefore, the NDVI values remained almost unchanged as GY increased from 4 to 13 Mg ha^{-1}. These results support the previously reported saturation of reflectance spectra in the red and near-infrared regions, such that increasing leaf area does not involve a parallel increase in NDVI values (Hobbs, 1995; Elazab et al., 2015). Thus, the relationship between NDVI and aerial biomass saturates as canopies become denser (i.e., LAI > 4) and as a consequence the relationship between the NDVI and GY also worsened as GY increased. Moreover near-infrared reflectance is sensitive to canopy architecture variations (Gitelson et al., 2002) which surely affected NDVI measurements in maize canopies. The use of multi-angular spectral data may solve these problems by capturing the scattering of sunlight by vegetation, which enables to assess three-dimensional vegetation structures (Hasegawa et al., 2010). Whereas this approach may improve the estimation of NDVI (and other spectral indices) for phenotyping, the increasing complexity (i.e., more time and resources needed) of the method makes it less feasible as low-cost alternative.

For its part, the range of variability in the RGB_{canopy} index, GA, was much wider (only 63% of values were in the range of 0.5–0.8) and GA values in the low N treatments were somewhat smaller (average GA = 0.46 in the 0N treatment) than those of the NDVI, and in fact GY correlated much better with GA than with the NDVI. Even so, the RGB_{canopy} indices also seemed to saturate for high GY but to a lesser extent than the NDVI because they mainly depend on changes in pigment concentration and the

TABLE 3 | Simple regression models obtained with different Vegetation Indices (the spectroradiometric indices $NDVI_{aerial}$, $NDVI_{ground}$, and the RGB_{canopy} indices GA and GGA) in the P trial, explaining Grain Yield (GY) variation across nitrogen fertilization levels, were used for GY estimation in the S trial.

			GY exp. vs. GY est.			
	Predictors	**Simple Regression models**	**R^2 for all trial**	**R^2 for 6 hybrids**	**Genotype**	**N-level**
GY est.	GA	$GY = e^{((GA - 0.195)/0.24)}$	0.674**	0.711**	0.054	< 0.001
	GGA	$GY = e^{((GGA - 0.151)/0.248)}$	0.684**	0.719**	0.040	< 0.001
	$NDVI_{aerial}$	$GY = e^{((NDVIaerial - 0.192)/0.094)}$	0.452**	0.543**	0.002	< 0.001
	$NDVI_{ground}$	$GY = e^{((NDVIground - 0.461)/0.109)}$	0.231**	0.324**	0.001	< 0.001
GY exp.		GY 3-3 hybrids	–	–	0.044	< 0.001

*The fit of the estimated Grain Yield (GY est.) to the experimental Grain Yield (GY exp.) was tested with the determination coefficient (R^2) for the entire trial and for six yield-contrasting hybrids. P-values were analyzed for all estimated GYs and for the experimental GY using the six selected hybrids. **P < 0.001.*

TABLE 4 | Determination coefficients (R^2) of RGB-indices from canopy images (RGB_{canopy}), aerial NDVI, ground NDVI, leaf chlorophyll content (LCC), the leaf nitrogen concentration on a dry matter basis (Leaf %N), the nitrogen concentration on a leaf area basis (N/LA), the ratio of carbon to nitrogen concentration (C/N), the stable carbon ($\delta^{13}C$) and nitrogen ($\delta^{15}N$) isotope composition and the specific leaf area (SLA) predicting grain yield in the five N levels separately (0, 10, 20, 80, and 160 kg·ha^{-1} NH_4NO_3) following linear regression models.

	0N	**10N**	**20N**	**80N**	**160N**
SPECTRAL INDICES					
$NDVI_{aerial}$	0.019 ns	0.415*	0.092 ns	0.074 ns	0.621**
$NDVI_{ground}$	0.741**	0.381 ns	0.421*	0.212 ns	0.289 ns
RGB_{canopy} INDICES					
hue	0.632**	0.653**	0.717**	0.364 ns	0.729**
a*	0.706**	0.634**	0.627**	0.524*	0.464*
b*	0.040 ns	0.160 ns	0.046 ns	0.056 ns	0.889**
u*	0.709**	0.608**	0.666**	0.491*	0.569*
v*	0.079 ns	0.239 ns	0.001 ns	0.120 ns	0.798 **
GA	0.771**	0.659**	0.704**	0.501**	0.764**
GGA	0.872**	0.664**	0.774**	0.555*	0.748**
LCC	0.148 ns	0.163 ns	0.076 ns	0.021 ns	0.004 ns
Leaf %N	0.059 ns	0.100 ns	0.014 ns	0.001 ns	0.504*
N/LA	0.037 ns	0.046 ns	0.006 ns	0.014 ns	0.189 ns
C/N	0.085 ns	0.069 ns	0.006 ns	0.009 ns	0.365 ns
$\delta^{13}C$	0.002 ns	0.353 ns	0.019 ns	0.073 ns	0.001 ns
$\delta^{15}N$	<0.001 ns	0.007 ns	0.005 ns	0.025 ns	0.065 ns
SLA	0.004 ns	0.002 ns	0.026 ns	0.008 ns	0.030 ns

**P < 0.05; **P < 0.001; ns, non-significant.*

canopy LAI is less affected in the visible region than in the NIR region (Casadesus et al., 2007; Elazab et al., 2015).

In the case of the airborne NDVI data, the correlation with GY was also much lower than with GA taken on individual plots with GY. In fact, the images from the ADC multispectral camera have around four-fold less resolution than current digital camera technology (3.2 vs. 12 MP in our study, respectively). Although many ADC images were employed to obtain mosaics of the entire field trials, the resolution obtained at the flight altitude generated pixels which were mixed between pure vegetation, shadows and soil components. Such effects were successfully separated in the imagery collected at the near-canopy level with the RGB camera due to the higher resolution obtained. Altogether, the NDVIaerial provides a much lower amount of information than the GA and other VIs derived from RGB images taken at the plot level.

In the case of the LCC, it correlated strongly and linearly with grain yield across fertilization levels (**Figure 2**). In fact the leaf chlorophyll meters calculate a spectral ratio of the leaf transmittance to the near-infrared and red bands and they were primarily developed to assess N fertilization levels (Fox et al., 1994; Markwell et al., 1995). LCC indirectly predicts GY when a wide range of N conditions are considered and this is probably due to the relationship between chlorophyll content, leaf N and yield (Argenta et al., 2004).

Concerning the applications in breeding, the determination coefficients within N levels across genotypic means (**Table 4**) support the strength of RGB_{canopy} indices as phenotyping

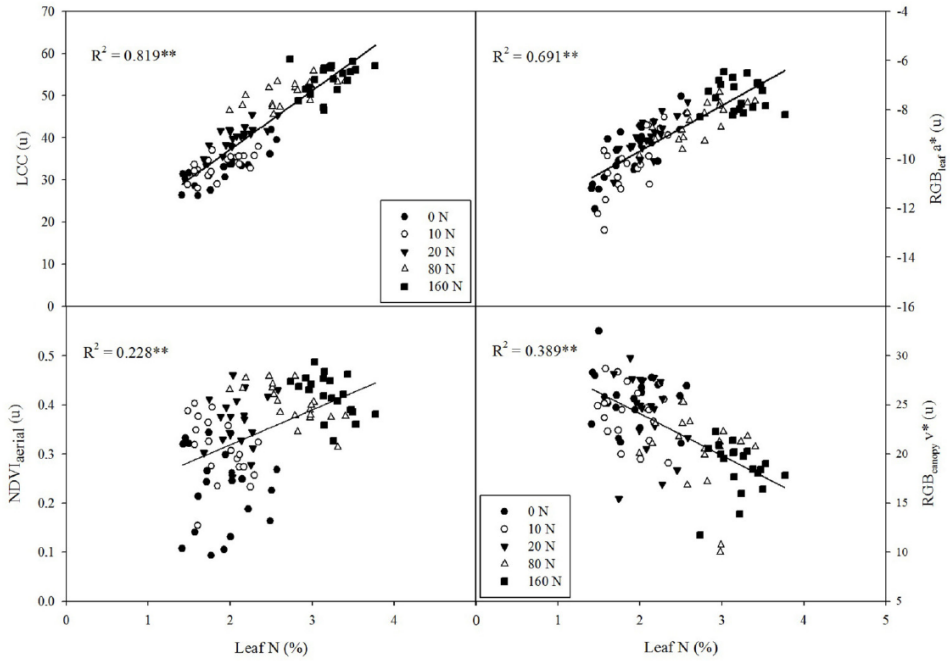

FIGURE 3 | Correlations between leaf nitrogen concentration (%N) and leaf chlorophyll content (LCC), the RGB index a* at the leaf level, the NDVI at the ground level, and the RGB index v* at the canopy level. R^2, determination coefficient; $^{**}P < 0.001$.

parameters. Thus, these indices were able to indicate the most efficient genotypes in terms of grain yield within each N fertilization level, whereas the NDVI performed much worse as a phenotyping parameter. Although genetic variability in maize hybrids in response to low N doses is high (Wang et al, 1999; Zaman-Allah et al., 2015) it has been scarcely exploited by breeding programs since they mainly focus on breeding for maize performance under favorable conditions (Machado and Fernandes, 2001). In this sense, the proposed phenotyping parameters herein, based on the use of RGB images, can significantly contribute to selection of maize hybrids resilient to low N as well as being more responsive to increases in N fertilization. For its part, LCC was unrelated to genotypic GY variation at any of the N-levels tested (**Table 4**), and this is in agreement with previous reports in maize that have noted LCC as not always being significantly correlated with genotypic differences in GY (Gallais and Coque, 2005).

Crop Monitoring and Phenotyping Parameters for Leaf N Assessment

The importance of leaf N concentration for N management and breeding lies not only in its potential contribution to grain N (Gallais and Coque, 2005) but is also due to it being a component of the nitrogen uptake efficiency (Serret et al., 2008). Moreover, leaf N is an indicator of leaf photosynthetic capacity contributing to grain yield (Richards, 2000) as well as a key fodder trait (Van der Wal et al., 2000). Therefore, the estimation of leaf N concentration within a given N fertilization treatment may provide valuable information about the genotypic efficiency for the uptake of N.

Our study highlights the potential of RGB indices for precise crop N management and for phenotyping genotypic performance under a wide-range of N conditions. As widely reported, LCC proved to be a very good indicator of leaf N concentration across nitrogen fertilization levels, therefore enabling monitoring of N application (Hirel et al., 2007). However, LCC failed to be effective as a phenotyping parameter, especially at high N-fertilization levels (**Table 5**). In contrast, the RGB_{leaf} indices demonstrated that they were the best genotypic predictors for leaf N concentration in the 0 to 80 kg·ha^{-1} N range. Thus, RGB indices at the leaf level have the potential to inform breeding programs about tolerance to N-deficiency stress in maize. This is a helpful insight because selection experiments have shown that the maximum genetic advance for low N is achieved when selecting in such N conditions (Gallais and Coque, 2005).

By contrast, in the highest N-fertilization level (160 kg ha^{-1}) the RGB_{leaf} indices and LCC were probably saturated because they did not correlate with variations in leaf N concentration. For its part, the $NDVI_{aerial}$ had an irregular trend as it was significantly correlated to changes in leaf N concentration at three of the five N fertilization levels (0, 80, and 160 kg ha^{-1}) and these correlations were especially strong in the high N levels. As discussed above, besides of some plot variability and soil exposure, the poorer performance of the $NDVI_{aerial}$ may be mainly explained by the relatively poor spectral resolution at the single plot level of the multispectral aerial images. Even

TABLE 5 | Determination coefficients (R^2) of RGB-indices from scanned leaves (RGB_{leaf}), leaf chlorophyll content (LCC), ground NDVI, aerial NDVI, the nitrogen concentration on a leaf area basis (N/LA), the ratio of carbon to nitrogen (C/N), leaf stable carbon ($\delta^{13}C$) and nitrogen ($\delta^{15}N$) isotopic composition and specific leaf area (SLA) predicting leaf nitrogen concentration on a dry matter basis separately in the five N fertilization levels (0, 10, 20, 80, and 160 kg·ha^{-1} NH_4NO_3).

	0N	10N	20N	80N	160N
SPECTRAL INDICES					
$NDVI_{aerial}$	0.545*	0.242 ns	0.352 ns	0.755**	0.650**
$NDVI_{ground}$	0.113 ns	0.223 ns	0.285 ns	0.403*	0.057 ns
RGB_{leaf} INDICES					
hue	0.081 ns	0.155 ns	0.188 ns	0.094 ns	0.012 ns
a*	0.588*	0.261 ns	0.567*	0.500*	0.149 ns
b*	0.526*	0.489*	0.566*	0.437*	0.265 ns
u*	0.607**	0.171 ns	0.534*	0.507*	0.073 ns
v*	0.581*	0.546*	0.429*	0.316 ns	0.192 ns
GA	0.097 ns	0.013 ns	0.185 ns	0.517*	0.222 ns
GGA	0.261 ns	0.026 ns	0.229 ns	0.359 ns	0.026 ns
LEAF PARAMETERS					
LCC	0.587*	0.426*	0.401*	0.168 ns	0.005 ns
N/LA	0.810**	0.127 ns	0.643**	0.496**	0.552**
C/N	0.973**	0.947**	0.918**	0.980**	0.939**
$\delta^{13}C$	0.318 ns	0.083 ns	0.069 ns	0.158 ns	0.073 ns
$\delta^{15}N$	0.006 ns	0.004 ns	0.167 ns	0.183 ns	0.295 ns
SLA	0.167 ns	0.069 ns	0.219 ns	0.022 ns	0.121 ns

*$P < 0.05$; **$P < 0.001$; ns, non-significant.*

so, according to our results this approach seems efficient for its implementation in aerial platforms.

Use of Leaf Analytical Parameters for Crop Management and Phenotyping

Besides the leaf N concentration discussed above, other leaf N parameters like the N concentration on an area basis (N/LA) and the C/N ratio were strongly associated with GY across N fertilization levels. In the case of the leaf $\delta^{15}N$, its value gradually decreased as the N application rate increased. This trend is due to the absorption of N from chemical fertilizers that are highly depleted in ^{15}N, whereas in the low N treatments plants absorb the N available in the soil, which is usually ^{15}N-enriched (Bateman et al., 2005; Masuka et al., 2012). However, the genotypic effect was not significant for $\delta^{15}N$, which does not support the use of this isotopic signature for maize phenotyping under low N stress. These results disagree with previous studies in wheat where genotypic differences were found under N stress conditions (Araus et al., 2013).

In agreement with previous studies (Dercon et al., 2006), low N induced higher $\delta^{13}C$ in maize, whereas it decreased in the high N fertilization treatments. This pattern of response appears related to the occurrence of some degree of water stress associated with a larger transpiring area due to nitrogen fertilization. In agreement with previous studies in maize, genotypic differences in leaf $\delta^{13}C$ may be attributed to differences in transpiration efficiency, but the variation in $\delta^{13}C$ was unrelated to GY within treatments (Cabrera-Bosquet et al., 2009).

Previous studies noted the relevance of SLA for the compositional and ecophysiological characterization of plants (Reich et al., 1998; Nautiyal et al., 2002). Several authors (Poorter and Evans, 1998; Meziane and Shipley, 2001) have reported a positive relationship between leaf N and SLA (**Table 2**). In turn, changes in SLA may be due to variations in leaf thickness and/or leaf density (Witkowski and Lamont, 1991). Increasing leaf density in low N conditions may be attributed to the increased synthesis of dense tissues such as sclerenchyma and vascular tissues that are rich in nitrogen-free substances (Garnier et al., 1997), whereas leaf thickness seems to have a minor role (Arendonk and Poorter, 1994). However, concerning its phenotyping use, SLA was shown to be homogeneous among the studied maize hybrids and unrelated to GY, as well as within a given N fertilization level, which excludes SLA as a phenotyping trait.

Regarding the relationship between VIs and the C/N ratio, most of the RGB indices (at the canopy and leaf levels) and both NDVI approaches were demonstrated as being even better correlated to the leaf C/N ratio than to leaf N concentration (Table S2). This finding may have considerable economic implications as the C/N ratio informs not only about the crop N status but also about the aerial biomass quality, including digestibility and nutritional quality (Van der Wal et al., 2000). Finally, all VIs and the LCC were better at capturing the differences in leaf N concentration than the amount of N concentration per unit leaf area (Table S2), thus avoiding the effect of leaf thickness or density. This evidence is enhanced by the weak relationship of the digital and spectral indices to SLA.

This finding is particularly interesting in the case of LCC (SPAD readings), which has been previously positively correlated with leaf thickness and negatively correlated with SLA in other species (Marenco et al., 2009).

Implications for Breeding and Crop Management

The tested vegetation indices based on RGB images and to a lesser extent the NDVI demonstrated a high-throughput for the accurate prediction of several traits that are highly valuable for maize breeders and agronomists such as grain yield, leaf N concentration and the ratio of carbon to nitrogen under a wide range of N fertilization levels. Proper N fertilization management may be assisted considerably by using these parameters as decision criteria controlling the expected production and the uptake of N by the above-ground biomass. Beyond this, maize breeding programs may benefit from these findings through their application during the characterization of genotypic performance within N fertilization levels. In this way the selection of the most efficient genotypes in terms of grain production and/or N uptake may respond to the needs of low N stress tolerant maize varieties.

Vegetation indices derived from RGB images proved to be broad-use because they were previously employed satisfactorily in other crops under biotic and water stress conditions (Casadesus et al., 2007; Vergara-Diaz et al., 2015). Therefore, since this technique has proven its efficiency for the evaluation of plant growth and leaf color, it may be probably applicable to a wide range of biotic and abiotic stresses and crop species. Moreover our study also supports the use of this technique to assess genotypic differences in grain yield under good agronomical conditions.

Although the performance of the RGB indices (obtained from JPEG images) worked well in this study, future research may address the possibility of further improve their accuracy by using input images saved in a lossless compression format as TIFF or PNG. Despite of storage inconvenient, their larger capability (16 bit per pixel instead of 8 bit) may maintain higher quality detail from the visible spectrum. Another important consideration is the effect of changing light conditions when making these outdoor measurements. Despite of the good strength and repeatability of the results (Table S1) fluctuating ambient lighting should be considered as a possible source of error. Further research should also be targeted toward implementation and evaluation of similar RGB phenotyping methods in remotely piloted aerial platforms (Elazab et al., 2016; Rasmussen et al., 2016).

AUTHOR CONTRIBUTIONS

BP, JC, MZ, and BM managed and directed the maize programme in the Southern Africa regional office of CIMMYT in Harare, Zimbabwe. MZ, PZ, and AH carried out the UAV flights for the obtainment of aerial measurements. On the other hand, JA, BM, JC, MZ, and OV conducted the field measurements and the collection of samples. AH and PZ processed the aerial images. OV analyzed the samples and other data and wrote the paper under the supervision of JA and with contributions from all the other authors.

ACKNOWLEDGMENTS

This article was supported by grants from the MAIZE CGIAR Research Program and the Project AGL2013-44147-R from the Ministerio de Economía y Competitividad of the Spanish Government. OV is a recipient of a research grant (APIF) sponsored by the University of Barcelona. We thank the personnel from the CIMMYT Southern Africa Regional Office at Harare for their support during the field measurements and sampling. The trials were planted under the Bill and Melinda Gates funded project Improved Maize for Africa Soils. Finally we thank Dr. Jaume Casadesús for providing the BreedPix software.

SUPPLEMENTARY MATERIAL

The Supplementary Material for this article can be found online at: http://journal.frontiersin.org/article/10.3389/fpls.2016.00666

REFERENCES

Andrade-Sanchez, P., Gore, M. A., Heun, J. T., Thorp, K. R., Carmo-Silva, A. E., French, A. N., et al. (2014). Development and evaluation of a field-based high-throughput phenotyping platform. *Funct. Plant Biol.* 41, 68–79. doi: 10.1071/FP13126

Araus, J. L., Cabrera-Bosquet, L., Serret, M. D., Bort, J., and Nieto-Taladriz, M. T. (2013). Comparative performance of δ13C, δ18O and δ15N for phenotyping durum wheat adaptation to a dryland environment. *Funct. Plant Biol.* 40, 595–608. doi: 10.1071/FP12254

Araus, J. L., and Cairns, J. E. (2014). Field high-throughput phenotyping: the new crop breeding frontier. *Trends Plant Sci.* 19, 52–61. doi: 10.1016/j.tplants.2013.09.008

Araus, J. L., Sánchez, C., and Cabrera-Bosquet, L. (2010). Is heterosis in maize mediated through better water use? *New Phytol.* 187, 392–406. doi: 10.1111/j.1469-8137.2010.03276.x

Araus, J. L., Slafer, G. A., Royo, C., and Serret, M. D. (2008). Breeding for yield potential and stress adaptation in cereals. *Crit. Rev. Plant Sci.* 27, 377–412. doi: 10.1080/07352680802467736

Arendonk, J. J. C. M., and Poorter, H. (1994). The chemical composition and anatomical structure of leaves of grass species differing in relative growth rate. *Plant Cell Environ.* 17, 963–970. doi: 10.1111/j.1365-3040.1994.tb00325.x

Argenta, G., Silva, P. R. F. D., and Sangoi, L. (2004). Leaf relative chlorophyll content as an indicator parameter to predict nitrogen fertilization in maize. *Cienc. Rural.* 34, 1379–1387. doi: 10.1590/S0103-84782004000500009

Barnes, E. M., Clarke, T. R., Richards, S. E., Colaizzi, P. D., Haberland, J., Kostrzewski, M., et al. (2000). "Coincident detection of crop water stress, nitrogen status and canopy density using ground based multispectral data," in *Proceedings of the 5th International Conference on Precision Agriculture* (Bloomington, MN), 16–19.

Bateman, A. S., Kelly, S. D., and Jickells, T. D. (2005). Nitrogen isotope relationships between crops and fertilizer: implications for using nitrogen isotope analysis as an indicator of agricultural regime. *J. Agr Food Chem.* 53, 5760–5765. doi: 10.1021/jf050374h

Boegh, E., Søgaard, H., Broge, N., Hasager, C. B., Jensen, N. O., Schelde, K., et al. (2002). Airborne multispectral data for quantifying leaf

area index, nitrogen concentration, and photosynthetic efficiency in agriculture. *Remote Sens. Environ.* 81, 179–193. doi: 10.1016/S0034-4257(01)00342-X

Buerkert, A., Bationo, A., and Piepho, H. P. (2001). Efficient phosphorus application strategies for increased crop production in sub-Saharan West Africa. *Field Crop Res.* 72, 1–15. doi: 10.1016/s0378-4290(01)00166-6

Cabrera-Bosquet, L., Sánchez, C., and Araus, J. L. (2009). How yield relates to ash content, Δ13C and Δ18O in maize grown under different water regimes. *Ann. Bot.* 104, 1207–1216. doi: 10.1093/aob/mcp229

Cairns, J. E., Hellin, J., Sonder, K., Araus, J. L., MacRobert, J. F., Thierfelder, C., et al. (2013). Adapting maize production to climate change in sub-Saharan Africa. *Food Sec.* 5, 345–360. doi: 10.1007/s12571-013-0256-x

Cairns, J. E., Sonder, K., Zaidi, P. H., Verhulst, N., Mahuku, G., Babu, R., et al. (2012). Maize production in a changing climate: impacts, adaptation and mitigation strategies. *Adv. Agron.* 144, 1–58. doi: 10.1016/B978-0-12-394275-3.00006-7

Casadesus, J., Kaya, Y., Bort, J., Nachit, M. M., Araus, J. L., Amor, S., et al. (2007). Using vegetation indices derived from conventional digital cameras as selection criteria for wheat breeding in water–limited environments. *Ann. Appl. Biol.* 150, 227–236. doi: 10.1111/j.1744-7348.2007.00116.x

Casadesús, J., and Villegas, D. (2014). Conventional digital cameras as a tool for assessing leaf area index and biomass for cereal breeding. *J. Integr. Plant Biol.* 56, 7–14. doi: 10.1111/jipb.12117

Chen, C., Pan, J., and Lam, S. K. (2014). A review of precision fertilization research. *Environ. Earth Sci.* 71, 4073–4080. doi: 10.1007/s12665-013-2792-2

Delgado, J. A., Follett, R. F., Buchleiter, G., Stuebe, A., Sparks, R. T., Dillon, M. A., et al. (2001). "Use of geospatial information for N management and conservation of underground water quality," in *Proceedings of the 3rd International Conference on Geospatial Information in Agriculture and Forestry* (Denver, CO), 5–7

Dercon, G., Clymans, E., Diels, J., Merckx, R., and Deckers, J. (2006). Differential ^{13}C isotopic discrimination in maize at varying water stress and at low to high nitrogen availability. *Plant Soil.* 282, 313–326. doi: 10.1007/s11104-006-0001-8

Elazab, A., Bort, J., Zhou, B., Serret, M. D., Nieto-Taladriz, M. T., and Araus, J. L. (2015). The combined use of vegetation indices and stable isotopes to predict durum wheat grain yield under contrasting water conditions. *Agr. Water Manage.* 158, 196–208. doi: 10.1016/j.agwat.2015.05.003

Elazab, A., Ordóñez, R. A., Savin, R., Slafer, G. A., and Araus, J. L. (2016). Detecting interactive effects of N fertilization and heat stress on maize productivity by remote sensing techniques. *Eur. J. Agron.* 73, 11–24. doi: 10.1016/j.eja.2015.11.010

Evans, R. D. (2001). Physiological mechanisms influencing plant nitrogen isotope composition. *Trends Plant Sci.* 6, 121–126. doi: 10.1016/S1360-1385(01)01889-1

FAO (2013). *Food and Agriculture Organisation of the United Nations; Statistic Division*. Available online at: http://faostat.fao.org/

Feng, Y. L., Fu, G. L., and Zheng, Y. L. (2008). Specific leaf area relates to the differences in leaf construction cost, photosynthesis, nitrogen allocation, and use efficiencies between invasive and noninvasive alien congeners. *Planta* 228, 383–390. doi: 10.1007/s00425-008-0732-2

Fischer, T., Byerlee, D., and Edmeades, G. (2014). *Crop Yields and Global Food Security*. Canberra, ACT: Australian Centre for International Agricultural Research, Monograph no. 158.

Fox, R. H., Piekielek, W. P., and Macneal, K. M. (1994). Using a chlorophyll meter to predict nitrogen fertilizer needs of winter wheat. *Commun. Soil Sci. Plan.* 25, 171–181. doi: 10.1080/00103629409369027

Furbank, R. T., and Tester, M. (2011). Phenomics–technologies to relieve the phenotyping bottleneck. *Trends Plant Sci.* 16, 635–644. doi: 10.1016/j.tplants.2011.09.005

Gallais, A., and Coque, M. (2005). Genetic variation and selection for nitrogen use efficiency in maize: a synthesis. *Maydica* 50, 531–547.

Garnier, E., Cordonnier, P., Guillerm, J. L., and Sonié, L. (1997). Specific leaf area and leaf nitrogen concentration in annual and perennial grass species growing in Mediterranean old-fields. *Oecologia* 111, 490–498. doi: 10.1007/s004420050262

Gitelson, A. A., Kaufman, Y. J., Stark, R., and Rundquist, D. (2002). Novel algorithms for remote estimation of vegetation fraction. *Remote Sens. Environ.* 80, 76–87. doi: 10.1016/S0034-4257(01)00289-9

Hasegawa, K., Matsuyama, H., Tsuzuki, H., and Sweda, T. (2010). Improving the estimation of leaf area index by using remotely sensed NDVI with BRDF signatures. *Remote Sens. Environ.* 114, 514–519. doi: 10.1016/j.rse.2009.10.005

Hatfield, J. L. (2000). *Precision Agriculture and Environmental Quality: Challenges for Research and Education*. Ames, IA: USDA National Resources Conservation Service.

Hergert, G., Ferguson, R., Gotway, C., and Peterson, T. (1996). "The Impact of VRT-N application on N use efficiency of furrow irrigated corn," in *Proceedings of the 3rd International Conference on Precision Agriculture*, eds P. C. Robert, R. H. Rust and W. E. Larson (Madison, WI), 389–397.

Hirel, B., Le Gouis, J., Ney, B., and Gallais, A. (2007). The challenge of improving nitrogen use efficiency in crop plants: towards a more central role for genetic variability and quantitative genetics within integrated approaches. *J. Exp. Bot.* 58, 2369–2387. doi: 10.1093/jxb/erm097

Hobbs, T. J. (1995). The use of NOAA-AVHRR NDVI data to assess herbage production in the arid rangelands of Central Australia. *Int. J. Remote Sens.* 16, 1289–1302. doi: 10.1080/01431169508954477

Liebisch, F., Kirchgessner, N., Schneider, D., Walter, A., and Hund, A. (2015). Remote, aerial phenotyping of maize traits with a mobile multi-sensor approach. *Plant Methods* 11, 9. doi: 10.1186/s13007-015-0048-8

Machado, A. T., and Fernandes, M. S. (2001). Participatory maize breeding for low nitrogen tolerance. *Euphytica* 122, 567–573. doi: 10.1023/A:1017543426136

Marenco, R. A., Antezana-Vera, S. A., and Nascimento, H. C. S. (2009). Relationship between specific leaf area, leaf thickness, leaf water content and SPAD-502 readings in six Amazonian tree species. *Photosynthetica* 47, 184–190. doi: 10.1007/s11099-009-0031-6

Markwell, J., Osterman, J. C., and Mitchell, J. L. (1995). Calibration of the Minolta SPAD-502 leaf chlorophyll meter. *Photosynth. Res.* 46, 467–472. doi: 10.1007/BF00032301

Masuka, B., Araus, J. L., Das, B., Sonder, K., and Cairns, J. E. (2012). Phenotyping for abiotic stress tolerance in maize. *J. Integr. Plant Biol.* 54, 238–249. doi: 10.1111/j.1744-7909.2012.01118.x

Meziane, D., and Shipley, B. (2001). Direct and indirect relationships between specific leaf area, leaf nitrogen and leaf gas exchange. Effects of irradiance and nutrient supply. *Ann. Bot.* 88, 915–927. doi: 10.1006/anbo.2001.1536

Monneveux, P., Sheshshayee, M. S., Akhter, J., and Ribaut, J. M. (2007). Using carbon isotope discrimination to select maize (*Zea mays* L.) inbred lines and hybrids for drought tolerance. *Plant Sci.* 173, 390–396. doi: 10.1016/j.plantsci.2007.06.003

Morgounov, A., Gummadov, N., Belen, S., Kaya, Y., Keser, M., and Mursalova, J. (2014). Association of digital photo parameters and NDVI with winter wheat grain yield in variable environments. *Turk. J. Agric. For.* 38, 624–632. doi: 10.3906/tar-1312-90

Nautiyal, P. C., Rachaputi, N. R., and Joshi, Y. C. (2002). Moisture-deficit-induced changes in leaf-water content, leaf carbon exchange rate and biomass production in groundnut cultivars differing in specific leaf area. *Field Crop Res.* 74, 67–79. doi: 10.1016/S0378-4290(01)00199-X

Petropoulos, G. P., and Kalaitzidisz, C. (2012). Multispectral vegetation indices in remote sensing: an overview. *Ecol. Model* 2, 15–39.

Poorter, H., and Evans, J. R. (1998). Photosynthetic nitrogen-use efficiency of species that differ inherently in specific leaf area. *Oecologia* 116, 26–37. doi: 10.1007/s004420050560

Rasmussen, J., Ntakos, G., Nielsen, J., Svensgaard, J., Poulsen, R. N., and Christensen, S. (2016). Are vegetation indices derived from consumer-grade cameras mounted on UAVs sufficiently reliable for assessing experimental plots? *Eur. J. Agron.* 74, 75–92. doi: 10.1016/j.eja.2015.11.026

Reich, P. B., Ellsworth, D. S., and Walters, M. B. (1998). Leaf structure (specific leaf area) modulates photosynthesis–nitrogen relations: evidence from within and across species and functional groups. *Funct. Ecol.* 12, 948–958. doi: 10.1046/j.1365-2435.1998.00274.x

Richards, R. A. (2000). Selectable traits to increase crop photosynthesis and yield of grain crops. *J. Exp. Bot.* 51, 447–458. doi: 10.1093/jexbot/51.suppl_1.447

Roberts, R., English, B., and Mahajanashetti, S. (2001). "Environmental and economic effects of spatial variability and weather," in *Proceedings of the 3rd*

European Conference on Precision Agriculture, eds S. Blackmore and G. Grenier (Montpellier), 545–550.

Rorie, R. L., Purcell, L. C., Karcher, D. E., and King, C. A. (2011). The assessment of leaf nitrogen in corn from digital images. *Crop Sci.* 51, 2174–2180. doi: 10.2135/cropsci2010.12.0699

Serret, M. D., Ortiz Monasterio, I., Pardo, A., and Araus, J. L. (2008). The effects of urea fertilisation and genotype on yield, nitrogen use efficiency, $\delta^{15}N$ and $\delta^{13}C$ in wheat. *Ann. App. Biol.* 153, 243–257. doi: 10.1111/j.1744-7348.2008.00259.x

Seul, M., O'Gorman, L., and Sammon, M. J. (2000). *Practical Algorithms for Image Analysis. Description, Examples, and Code.* Cambridge, UK; Cambridge University Press

Stewart, W. M., Dibb, D. W., Johnston, A. E., and Smyth, T. J. (2005). The contribution of commercial fertilizer nutrients to food production. *Agron. J.* 97, 1–6. doi: 10.2134/agronj2005.0001

Svensgaard, J., Roitsch, T., and Christensen, S. (2014). Development of a mobile multispectral imaging platform for precise field phenotyping. *Agronomy* 4, 322–336. doi: 10.3390/agronomy4030322

Trussell, H. J., Vrhel, M., and Saber, E. (2005). Color image processing. *IEEE Signal Proc. Mag.* 22, 14–22. doi: 10.1109/MSP.2005.1407711

Van der Wal, R., Madan, N., Van Lieshout, S., Dormann, C., Langvatn, R., and Albon, S. D. (2000). Trading forage quality for quantity? Plant phenology and patch choice by Svalbard reindeer. *Oecologia* 123, 108-115. doi: 10.1007/s004420050995

Vergara-Diaz, O., Kefauver, S. C., Elazab, A., Nieto-Taladriz, M. T., and Araus, J. L. (2015). Grain yield losses in yellow-rusted durum wheat estimated using digital and conventional parameters under field conditions. *Crop J.* 3, 200–210. doi: 10.1016/j.cj.2015.03.003

Wang, F., Fraisse, C. W., Kitchen, N. R., and Sudduth, K. A. (2003). Site-specific evaluation of the CROPGRO-soybean model on Missouri claypan soils. *Agr. Syst.* 76, 985–1005. doi: 10.1016/S0308-521X(02)00029-X

Wang, R. L., Stec, A., Hey, J., Lukens, L., and Doebley, J., (1999). The limits of selection during maize domestication. *Nature* 398, 236–239. doi: 10.1038/18435

Wezel, A., Casagrande, M., Celette, F., Vian, J. F., Ferrer, A., and Peigné, J. (2014). Agroecological practices for sustainable agriculture. A review. *Agron. Sustain. Dev.* 34, 1–20. doi: 10.1007/s13593-013-0180-7

White, J. W., Andrade-Sanchez, P., Gore, M. A., Bronson, K. F., Coffelt, T. A., Conley, M. M., et al. (2012). Field-based phenomics for plant genetics research. *Field Crop Res.* 133, 101–112. doi: 10.1016/j.fcr.2012.04.003

Witkowski, E. T. F., and Lamont, B. B. (1991). Leaf specific mass confounds leaf density and thickness. *Oecologia* 88, 486–493. doi: 10.1007/BF00317710

Zaman-Allah, M., Vergara, O., Araus, J. L., Tarekegne, A., Magorokosho, C., Zarco-Tejada, P. J., et al. (2015). Unmanned aerial platform-based multi-spectral imaging for field phenotyping of maize. *Plant Methods* 11:35. doi: 10.1186/s13007-015-0078-2

Zhou, B., Elazab, A., Bort, J., Vergara, O., Serret, M. D., and Araus, J. L. (2015). Low-cost assessment of wheat resistance to yellow rust through conventional RGB images. *Comput. Electron. Agr.* 116, 20–29. doi: 10.1016/j.compag.2015.05.017

Conflict of Interest Statement: The authors declare that the research was conducted in the absence of any commercial or financial relationships that could be construed as a potential conflict of interest.

Supplementary Material

A novel remote sensing approach for prediction of maize yield under different conditions of nitrogen fertilization

Omar Vergara-Díaz[1], Mainassara Zaman-Allah[2], Benhildah Masuka[2], Alberto Hornero[3], Pablo Zarco-Tejada[3], Boddupalli Prasanna[2], Jill E. Cairns[2], José Luís Araus[1*]

*** Correspondence:** Prof. José Luís Araus, Unit of Plant Physiology, Department of Plant Biology, Faculty of Biology, University of Barcelona, 643 Diagonal, Barcelona, 08028, Spain.

Supplementary Tables

Table S1. Determination coefficients (R^2) of RGB-indices from canopy RGB images explaining the variation between replicated plot images (n = 57). Indices were calculated from images taken in the same set of plots in a sunny and a cloudy days nearly consecutive.

	R^2	p-value
RGB_{canopy} indices		
hue	0.437	<0.001
a*	0.716	<0.001
b*	0.597	<0.001
u*	0.722	<0.001
v*	0.541	<0.001
GA	0.895	<0.001
GGA	0.795	<0.001

Table S2. Pearson correlation coefficients between leaf and canopy RGB indices, NDVI at ground and aerial levels, leaf chlorophyll content (LCC) and grain yield (GY) with nitrogen per unit area (N/area), the carbon to nitrogen ratio (C/N), nitrogen isotope composition ($\delta^{15}N$), carbon isotope composition ($\delta^{13}C$), specific leaf area (SLA) and leaf nitrogen concentration (%N). *, P < 0.05; **, P < 0.001; ns, non-significant.

	N/LA	C/N	$\delta^{15}N$	$\delta^{13}C$	SLA	%N
RGB_{leaf} indices						
hue	-0.451 **	0.503 **	0.464 **	0.278 *	-0.068 ns	-0.540 **
a*	0.718 **	-0.854 **	-0.505 **	-0.566 **	0.120 ns	0.831 **
b*	-0.645 **	0.826 **	0.485**	0.579 **	-0.193 ns	-0.788 **
u*	0.725 **	-0.843 **	-0.511 **	-0.542 **	0.093 ns	0.826 **
v*	-0.621 **	0.843 **	0.553 **	0.589 **	-0.259*	-0.802 **
GA	-0.005 ns	-0.243 *	-0.418 **	-0.187 ns	0.373 **	0.220 *
GAA	-0.107 ns	-0.184 ns	-0.377 **	-0.047 ns	0.450**	0.159 ns
RGB_{canopy} indices						
hue	0.362 **	-0.462 **	-0.313 *	-0.028 ns	0.098 ns	0.430 **
a*	0.000 ns	0.096 ns	0.092 ns	-0.215 *	-0.076 ns	0.032 ns
b*	-0.058 ns	0.010 ns	-0.076 ns	-0.022 ns	0.047 ns	-0.030 ns
u*	-0.174 ns	0.301 *	-0.248 *	0.101 ns	-0.124 ns	-0.245 *
v*	-0.518 **	0.604 **	0.486 **	0.361 **	-0.142 ns	-0.623 **
GA	0.397 **	-0.558 **	-0.562 **	-0.124 ns	0.181 ns	0.529 **
GAA	0.398 **	-0.574 **	-0.527 **	-0.118 ns	0.202 *	0.533 **
Spectral Indices						
$NDVI_{aerial}$	0.221 *	-0.495 **	-0.672 **	-0.190 ns	0.298 *	0.477 **
$NDVI_{ground}$	0.271 *	-0.364 **	-0.350 **	0.043 ns	0.199 *	0.341 **
LCC	0.748 **	-0.898**	-0.678 **	-0.464 **	0.195 ns	0.905 **
GY	0.608 **	-0.676 **	-0.555 **	-0.249 *	0.102 ns	0.687 **
%N	0.816 **	-0.967 **	-0.580 **	-0.590 **	0.220 *	1

CHAPTER 3

Leaf dorsoventrality as a paramount factor determining spectral performance in field-grown wheat under contrasting water regimes

Omar Vergara-Díaz, Fadia Chairi, Rubén Vicente,
Jose A. Fernandez-Gallego, Maria Teresa Nieto-Taladriz,
Nieves Aparicio, Shawn C. Kefauver and José Luis Araus

Published on:
Journal of Experimental Botany (2018) Vol. 69 No 12

ABSTRACT

The effects of leaf dorsoventrality and its interaction with environmentally induced changes in the leaf spectral response are still poorly understood, particularly for isobilateral leaves. We investigated the spectral performance of 24 genotypes of field-grown durum wheat at two locations under both rainfed and irrigated conditions. Flag leaf reflectance spectra in the VIS-NIR-SWIR (visible–near-infrared–short-wave infrared) regions were recorded in the adaxial and abaxial leaf sides and at the canopy level, while traits providing information on water status and grain yield were evaluated. Moreover, leaf anatomical parameters were measured in a subset of five genotypes. The spectral traits studied were more affected by the leaf side than by the water regime. Leaf dorsoventral differences suggested higher accessory pigment content in the abaxial leaf side, while water regime differences were related to increased chlorophyll, nitrogen, and water contents in the leaves in the irrigated treatment. These variations were associated with anatomical changes. Additionally, leaf dorsoventral differences were less in the rainfed treatment, suggesting the existence of leaf-side-specific responses at the anatomical and biochemical level. Finally, the accuracy in yield pre- diction was enhanced when abaxial leaf spectra were employed. We concluded that the importance of dorsoventrality in spectral traits is paramount, even in isobilateral leaves

.

Journal of Experimental Botany, Vol. 69, No. 12 pp. 3081–3094, 2018
doi:10.1093/jxb/ery109 Advance Access publication 31 March 2018
This paper is available online free of all access charges (see http://jxb.oxfordjournals.org/open_access.html for further details)

RESEARCH PAPER

Leaf dorsoventrality as a paramount factor determining spectral performance in field-grown wheat under contrasting water regimes

Omar Vergara-Díaz[1], Fadia Chairi[1], Rubén Vicente[1], Jose A. Fernandez-Gallego[1], Maria Teresa Nieto-Taladriz[2], Nieves Aparicio[3], Shawn C. Kefauver[1] and José Luis Araus[1,*]

[1] Integrative Crop Ecophysiology Group, Plant Physiology Section, Faculty of Biology, University of Barcelona, Diagonal 645, 08028 Barcelona, Spain
[2] National Institute for Agricultural and Food Research and Technology (INIA), Ctra de la Coruña 7.5, 28040, Madrid, Spain
[3] Technological and Agricultural Institute of Castilla y León (ITACyL), Ctra de Burgos 119, 47071, Valladolid, Spain

* Correspondence: jaraus@ub.edu

Received 20 December 2017; Editorial decision 13 March 2018; Accepted 13 March 2018

Editor: Roland Pieruschka, Forschungszentrum Jülich, Germany

Abstract

The effects of leaf dorsoventrality and its interaction with environmentally induced changes in the leaf spectral response are still poorly understood, particularly for isobilateral leaves. We investigated the spectral performance of 24 genotypes of field-grown durum wheat at two locations under both rainfed and irrigated conditions. Flag leaf reflectance spectra in the VIS-NIR-SWIR (visible–near-infrared–short-wave infrared) regions were recorded in the adaxial and abaxial leaf sides and at the canopy level, while traits providing information on water status and grain yield were evaluated. Moreover, leaf anatomical parameters were measured in a subset of five genotypes. The spectral traits studied were more affected by the leaf side than by the water regime. Leaf dorsoventral differences suggested higher accessory pigment content in the abaxial leaf side, while water regime differences were related to increased chlorophyll, nitrogen, and water contents in the leaves in the irrigated treatment. These variations were associated with anatomical changes. Additionally, leaf dorsoventral differences were less in the rainfed treatment, suggesting the existence of leaf-side-specific responses at the anatomical and biochemical level. Finally, the accuracy in yield prediction was enhanced when abaxial leaf spectra were employed. We concluded that the importance of dorsoventrality in spectral traits is paramount, even in isobilateral leaves.

Keywords: Dorsoventral effect, leaf spectroscopy, nitrogen, pigment, side-specific responses, water stress, wheat.

Introduction

Spectroradiometry is a pivotal technique in the remote sensing evaluation of plant performance, used widely for precision agriculture, high-throughput phenotyping, and ecosystem studies. Very diverse information is retrieved from the spectral signature of the light reflected by the canopy or even by single leaves (Ustin *et al.*, 2009), and to date a large corpus of spectral reflectance indices has been formulated (Xue and Su, 2017). However, this information is usually predicted in an empirical manner without a clear understanding of how a basic aspect such as leaf side (adaxial versus abaxial) may affect the spectrum of the reflected radiation and the different categories of spectroradiometrical indices. This is particularly relevant because canopy evaluations of spectroradiometrical indices, at either the ground or aerial levels,

are usually performed using the spectrum reflected from the adaxial part of the leaves (Jacquemoud and Baret, 1990; Sims and Gamon, 2002; Lu and Lu, 2015).

For its part, water stress is known to trigger mechanisms of acclimation in the leaf such as changes in gene expression and modification of plant physiology, morphology, and anatomy, leading to homeostatic compensation (Flexas *et al.*, 2006). At the leaf level, changes in morphology, anatomy, turgor status, and biochemical content can directly and/or indirectly impact the reflected radiation. In fact, this is the basis for plant status studies using a spectroscopic approach. Moreover, few studies have considered leaf-side-specific responses, and those focusing on the leaf dorsoventral effect have usually been performed on plant species with a clear bifacial leaf anatomy (Evans, 1999; Lu *et al.*, 2015).

In contrast, monocots such as wheat have typical isobilateral leaves whereby dorsoventral differences tend to be underestimated, considering the relative homogeneity in the mesophyll anatomy (lack of a clear dorsoventral gradient in terms of palisade versus spongy cells) and even on the epidermal surface of these leaves (which are amphystomatous). However, the abaxial epidermis is thinner and lacks bulliform cells and furrows, while the usually relatively erect position of the flag leaf and the fact that it is placed in the uppermost part of the canopy suggest that the light gradient through the leaf is not too strong.

Recent studies in monocots have reported side-specific anatomical and physiological responses that are usually dependent on genotypic and environmental effects (Soares *et al.*, 2008; Soares-Cordeiro *et al.*, 2011; Jafarian *et al.*, 2012). For instance, leaf side-specific responses of photosynthesis and stomatal closure to light intensity and CO_2 enrichment, as well as to chilling and water stresses, have been reported in C_3 and C_4 species (Wang *et al.*, 1998; Soares *et al.*, 2008; Soares-Cordeiro *et al.*, 2011). Even so, there is a notable lack of understanding of how and to what extent these leaf-side-specific responses to environmental stress might affect the reflected radiation at the leaf and plant canopy scales. To the best of our knowledge, this is the first study addressing side-specific responses of wheat leaves to varying water conditions using a spectroscopic approach.

The spectral signatures in the range of visible (VIS; 400–700 nm), near-infrared (NIR; 700–1400 nm), and short-wave infrared (SWIR, 1400–2500 nm) wavelengths were investigated in the flag leaves of a set of 24 wheat genotypes growing under different water regimes in the field. Leaf reflectance spectra were recorded for the two leaf sides (adaxial and abaxial) and at the canopy level. Additionally, leaf size as well as some specific morphological and anatomical traits (epidermis, mesophyll, and xylem vessel metrics) were measured, and the stable carbon ($\delta^{13}C$) isotope composition of the flag leaves and grains as well as the total carbon (%C) and nitrogen (%N) content of the flag leaves were further analysed. Although the $\delta^{13}C$ and total nitrogen content may provide information on the water and nitrogen status of the leaves (Araus *et al.*, 1997; Yousfi *et al.*, 2012), the total carbon and nitrogen and their ratio provide a broad indication of leaf chemical composition and the prevalence of structural supporting elements (Taylor *et al.*, 1989).

The aim of the present study was to investigate the effect of water regime as well as leaf-side-specific responses on leaf reflectance traits in field-grown durum wheat. Spectral reflectance indices are discussed in the context of their relationship to different physiological, biochemical, and anatomical traits of the leaf. The similarity and dissimilarities between both leaf spectra and of the spectrum of the canopy, and their implications for yield prediction were also addressed. The study was performed in the flag leaf because it has been reported to be the most isobilateral leaf in wheat (Araus *et al.*, 1986).

Materials and methods

Plant material and experimental set up

Field trials were carried out during the 2014/15 growing season at two locations: in central Spain at the experimental station of Colmenar de Oreja (Madrid), belonging to the Instituto Nacional de Investigación y Tecnología Agraria y Alimentaria (INIA) of Spain, and in northern Spain at the experimental station of Zamadueñas (Valladolid), belonging to the Instituto Tecnológico Agrario de Castilla y León (ITACyL). Geographic and agronomic information together with weather, irrigation, and soil information are all detailed in Table 1.

Twenty-four durum wheat [*Triticum turgidum* L. subsp *durum* (Desf) Husn.] varieties released during the last 40 years in Spain were grown at both experimental stations. Plots were sown in a randomized blocks design with three replicates. A total of four growing conditions were considered: rainfed and supplemental irrigated conditions for each location. At harvest, grains were dried in an oven at 60 °C for 48 h, and grain yield (GY) was determined.

Spectral data collection and index calculation

The flag leaf spectral signature was measured with a Field-Spec4 (ASD Inc. PANalytical Company, Boulder, CO, USA) full-range portable spectroradiometer, and spectra were acquired in the 350–2500 nm range. The adaxial and abaxial leaf surfaces were measured for each leaf with an ASD leaf clip accessory assembled to an ASD standard plant contact probe coupled with a fibre optic to the FieldSpec4 spectrometer. This probe is provided with a halogen bulb and has a spot size of 10 mm diameter. A total of 288 non-senescent leaves, one per plot and thus 144 from each location, were measured at the mid grain-filling stage (25–27 May; 73 in the Zadoks scale), generating a total of 576 leaf spectra. Canopy spectra were measured at midday (80 min before and after noon) with a pistol grip coupled with the fibre optic to the FieldSpec4 spectrometer. Measurements were made 1 m above the plot canopy in a zenithal plane, and the reflectance was calibrated every 15–20 min with a Spectralon white reference panel.

A collection of 85 spectral reflectance indices (SRIs) was calculated for each leaf spectrum (Supplementary Table S1 at *JXB* online). The broadband SRIs were calculated with reference to the Landsat Enhanced Thematic Mapper Plus (ETM+) sensor (Landsat 7, USGS) wavebands.

Other spectroradiometrically derived leaf traits

The leaf radiative transfer model, PROSPECT5 (Jacquemoud and Baret, 1990), was used to estimate the equivalent water thickness (EWT) and the total chlorophyll (Chl) and carotenoid (Car) contents from leaf reflectances using a numerical inversion of the PROSPECT 5 model via Matlab7.

Table 1. *Geographic, climatic, agronomic, and soil information for each study site*

	Zamadueñas experimental station	Colmenar de Oreja experimental station
Altitude (m asl)	700	590
Co-ordinates	41°42'N, 4°42'W	40°04'N, 3°31'W
Mean temp.[a] (°C)	10.73	13.01
Max. mea n temp.[a] (°C)	17.45	21.45
Min. mean temp.[a] (°C)	4.64	5.36
Precipitation[a] (mm)	258.4	206.8
Sowing date	24 November 2014	21 November 2014
Harvest date	22 July 2015	20 July 2015
Sowing density (seeds m^{-2})	250	250
Plot surface (m^2)	10.5 (7 × 1.5)	10.5 (7 × 1.5)
Irrigation provided[b] (mm)	125	180
Fertilization		
First application	300 kg ha^{-1} NPK 8:15:15	400 kg ha^{-1} NPK 15:15:15
Second application	300 kg ha^{-1} CAN 27%N	150 kg ha^{-1} Urea 46%
Soil texture	Loam	Clay-loam
Soil pH	8.44	8.1

[a] During the growing season.
[b] In the irrigated treatments.

Total leaf Chl content on an area basis was also assessed with a portable Chl meter (Minolta SPAD-502, Spectrum Technologies Inc., Plainfield, IL, USA).

Leaf morphological, anatomical, and physiological traits

The leaf lamina length and width were measured in three flag leaves from each plot. Additionally, five genotypes representative of yield variability (data not shown) were selected for the anatomical observations. Flag leaf blade segments of 10 × 5 mm were sampled and submerged in Visikol clearing solution (Visikol Inc., New Brunswick, NJ, USA). The samples were incubated with 1% osmium tetroxide and 0.8% potassium ferrocyanide, washed with MiliQ water, dehydrated with acetone at 4 °C, embedded in epoxy resin at room temperature, and blocks were left in the oven for 72 h at 80 °C. Cross-sections were obtained with an Ultracut E ultramicrotome (Reichert-Jung, Vienna, Austria) and stained with methylene blue and Van Gieson's solution. Digital images were taken with an Olympus CX41 optical microscope at ×100 and ×200 magnifications.

Images were scale-calibrated, and anatomical metrics were measured with Image J software. For the whole leaf cross-section, measurements were recorded of the leaf thickness, leaf sectional area, xylem vessel area and diameter, mesophyll cell sectional area and perimeter, epidermis cell sectional area and cell wall thickness, epidermis length, and areas of both the adaxial and the abaxial epidermis. For the cross-sections, the following ratios were calculated: total epidermis length to leaf cross-section area, the epidermis area to epidermis length ratio for the adaxial and abaxial epidermises (hereafter considered as epidermis thickness), the epidermis area to leaf area ratio for both epidermises, and the mesophyll cell area to cell perimeter ratio.

The stable carbon (^{13}C:^{12}C) isotope ratio as well as the nitrogen (N) and carbon (C) concentrations (%) were measured in leaf and grain dry matter using an elemental analyser (Flash 1112 EA; Thermo Finnigan, Bremen, Germany) coupled with an isotope ratio mass spectrometer (Delta C IRMS, Thermo Finnigan) operating in a continuous flow mode. Samples of 0.7–1 mg of leaf dry matter from each plot, together with reference materials, were weighed and sealed into tin capsules. Measurements were conducted at the Scientific Facilities of the University of Barcelona. Isotopic values were expressed in composition notation (δ) as follows: $\delta^{13}C=[(^{13}C/^{12}C)_{sample}/(^{13}C/^{12}C)_{standard}]-1$, where 'sample' refers to plant material and 'standard' to international secondary standards of known ^{13}C:^{12}C ratios (IAEA CH7 polyethylene foil, IAEA CH6 sucrose, and USGS 40 L-glutamic acid) calibrated against Vienna Pee Dee Belemnite calcium carbonate with an analytical precision (standard deviation) of 0.15‰.

In addition, a JEOL JSM-7100F scanning electron microscope (JEOL, Akishima, Japan) in the Scientific and Technological Facilities of the University of Barcelona was employed to observe the epicuticular wax structure of the adaxial and abaxial sides of the flag leaf. Lyophilized leaves were gold-coated and subsequently observed operating at 10 kV.

Finally, air (Testo 177-H1 Logger, Germany) and plot canopy temperature (PhotoTemp MXS, Raytek Corporation, CA, USA) were simultaneously recorded and the canopy temperature depression (CTD) was calculated as the difference between them.

Statistical analysis

Multivariate ANOVAs were conducted using SPSS 21 (IBM SPSS Statistics 21, Inc., Chicago, IL, USA). Principal component analysis (PCA) of reflectances was performed with CANOCO 4.5 software (Ter Braak and Smilauer, 2002). Figures were drawn with SigmaPlot 10.0 (Systat Software Inc., San Jose, CA, USA). Finally, the clustered heatmap, the LASSO, and the backward stepwise regression analyses were performed with R 3.2.2 using the GPLOTS (Warnes *et al.*, 2009), the GLMNET (Friedman *et al.*, 2010), and the MASS (Ripley *et al.*, 2013) packages, respectively.

Results

GY was significantly affected by water regime (Table 2), decreasing by 47% in Zamadueñas (from 7.17 Mg ha^{-1} to 3.77 Mg ha^{-1}) and by 10% in Aranjuez (from 5.13 Mg ha^{-1} to 4.65 Mg ha^{-1}) under rainfed compared with irrigated conditions. Yield differences in Aranjuez were lower due to severe lodging during grain filling in the irrigated treatment.

The CTD and leaf blade size (length and width) were significantly higher in irrigated conditions, whereas there was no difference in leaf Chl content assessed by a SPAD meter due to water regime. Regarding isotope composition, the $\delta^{13}C$ of leaves and grains increased significantly in rainfed compared with irrigated conditions. Total leaf nitrogen content (%N) was significantly reduced in rainfed conditions, whereas the C:N ratio was increased (Table 2).

Leaf spectrum performance

Water regime significantly affected leaf reflectance in the NIR and SWIR regions (Fig. 1a). Regardless of the leaf side, leaf reflectance was significantly higher under irrigated conditions in the NIR region (756–948 nm and 997–1000 nm), whereas in rainfed conditions it was higher in the violet (350–375 nm) and SWIR regions (1289–1886 nm and 1988–2254 nm).

This performance changed when studying each leaf side separately (Fig. 1b, c). Differences in NIR reflectance between water regimes were only detected in the abaxial leaf side (747–1000 nm), whereas leaves belonging to the irrigated treatment had higher reflectance. In contrast, in the second half of the SWIR region, reflectance differences between water regimes were detected only in the adaxial leaf side (1988–2240 nm),

and were higher in the rainfed treatment. Finally, leaf reflectance from the end of the NIR region to the SWIR region (1300–1900 nm) was quite similar in both leaf sides, with the leaf reflectance being higher in the rainfed than in the irrigated treatment.

Table 2. *Means and deviations of grain yield, leaf blade length and width, leaf SPAD readings, leaf nitrogen and carbon concentration (%N and %C), and its ratio (C:N), grain and leaf stable carbon isotope composition ($\delta^{13}C$), and the canopy temperature depression (CTD) for each water regime (R+, irrigated; R–, rainfed) along with the significance level of the respective one-way ANOVA*

	Water regime		ANOVA
	R+	R–	P_{WR}
Grain y ield (Mg ha^{-1})	6.95	4.81	<0.001
	0.097	0.097	
Leaf length (cm)	20.9	19.11	<0.001
	4.35	3.36	
Leaf width (cm)	1.679	1.547	0.038
	0.484	0.257	
SPAD reading	55.467	55.692	0.699
	5.189	4.621	
Plot CTD (°C)	4.89	0.63	<0.001
	1.199	1.92	
Leaf C (%)	40.13	40.42	0.486
	3.46	3.36	
Leaf N (%)	4.045	3.893	<0.001
	0.362	0.385	
Leaf C:N ratio	9.95	10.46	<0.001
	0.798	1.098	
Leaf $\delta^{13}C$ (‰)	–28.1	–27.83	<0.001
	0.635	0.472	
Grain $\delta^{13}C$ (‰)	–26.16	–25.34	<0.001
	0.494	1.18	

On the other hand, and regardless of the water conditions during cultivation, the reflectances of the adaxial and abaxial leaf surfaces were significantly different across several wavebands of the spectrum (Fig. 2a). In the violet region (350–425 nm), the abaxial reflectance was always significantly higher compared with the adaxial reflectance. In the red-edge region, abaxial reflectance was initially higher from 666 nm to 702 nm and then decreased significantly from 719 nm to 731 nm. Abaxial reflectance was always higher in the NIR plateau, and these differences were significant in the ranges of 752–850, 949–969, and 1035–1169 nm. Finally, in the SWIR region, adaxial reflectance was significantly higher from 1501 nm to 1739 nm and significantly lower from 1357 nm to 1437 nm, 1859 nm to 1994 nm, and 2377 nm to 2500 nm.

Additionally, differences in reflectance between leaf sides changed considerably within water regimes (Fig. 2b, c). The differences in the red-edge region between leaf sides were evident only under rainfed conditions (676–699 nm; 721–733 nm). In contrast, reflectance differences between leaf sides throughout the NIR plateau were present only under irrigated conditions (747–991 nm; 1000–1170 nm).

Additionally, four contour maps were generated of reflectance cross-correlations from across the spectrum (Fig. 3) with the aim of further investigating the intrinsic relationships of the waveband reflectances for each experimental condition. The following trends can be highlighted: cross-correlation coefficients were always higher in the adaxial side of the leaf than in the abaxial leaf side (i.e. wavebands were more closely correlated in the spectrum of the adaxial leaf side). Similarly, when water regimes were compared, higher correlation coefficients were always obtained under rainfed conditions.

Principal component analysis of reflectance ranges

To determine the most influential spectral ranges that accounted for data variability, a PCA was performed and

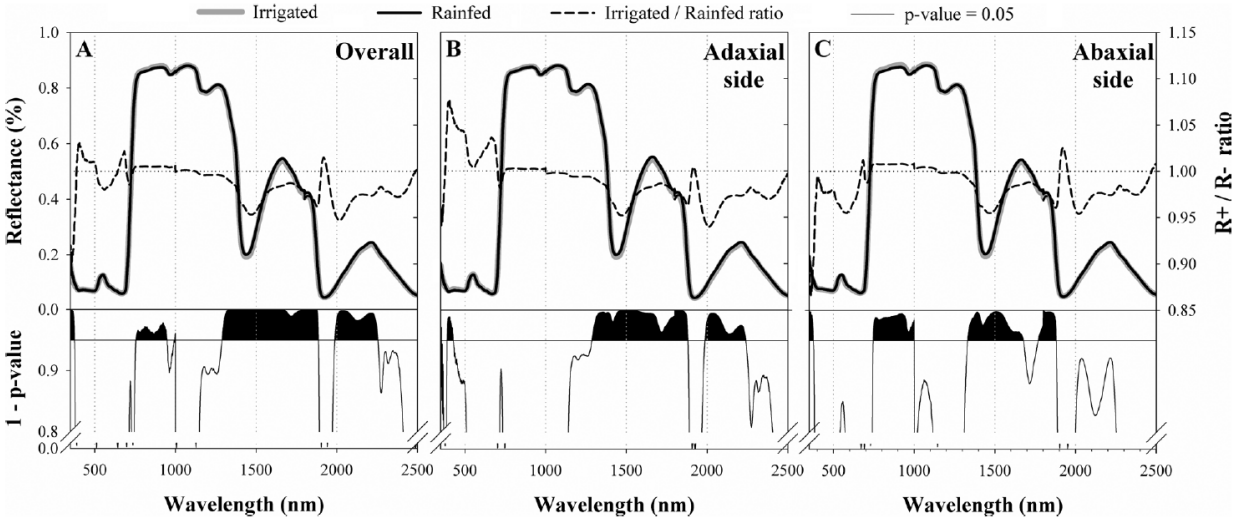

Fig. 1. Leaf reflectance spectra in irrigated (grey line) and rainfed (black line) water conditions for the entire set of records (A, *n*=576) and separated according to the leaf side measured, either in the adaxial (B, *n*=288) or in the abaxial (C) leaf side. Below: the respective *P*-value graphs for each of the one-way comparisons performed for the reflectance throughout the spectrum, where the reflectance in each wavelength is considered as a variable and the water regime as a factor. Spectral regions where differences are significant (1–*P*-value >0.95) are shaded in black.

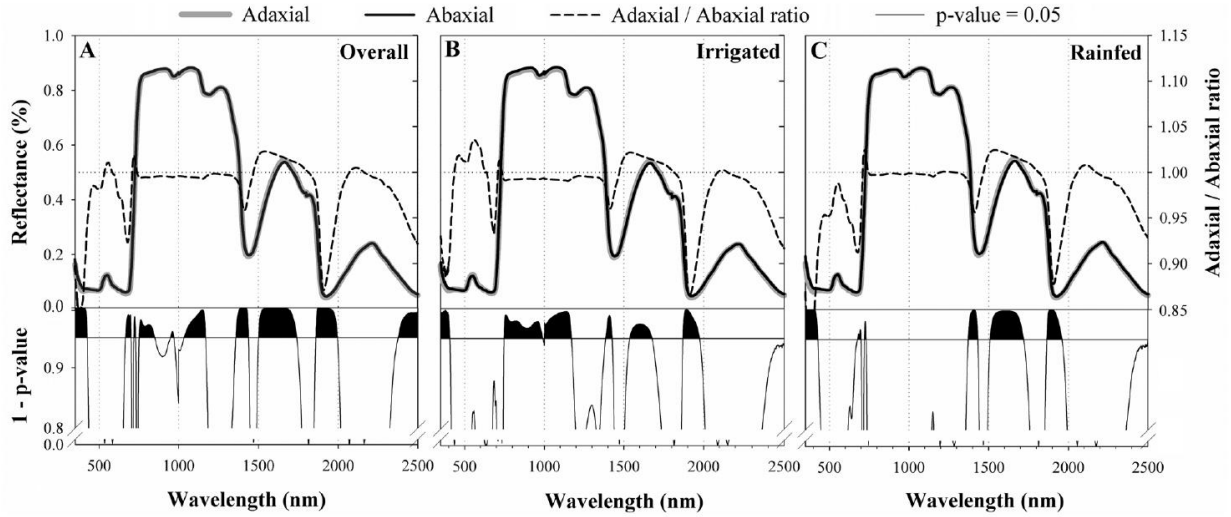

Fig. 2. Leaf reflectance spectra in adaxial (grey line) and abaxial (black line) sides of the leaf for the entire set of records (A, *n*=576) and separating into the two water conditions, under either irrigated (B, *n*=288) or rainfed (C, *n*=288) conditions. Below: the respective *P*-value graphs for each one-way comparison performed for the reflectance across the spectrum, where the reflectance in each wavelength is considered as a variable and the leaf side as a factor. Spectral regions where differences are significant (1–*P*-value >0.95) are filled in black.

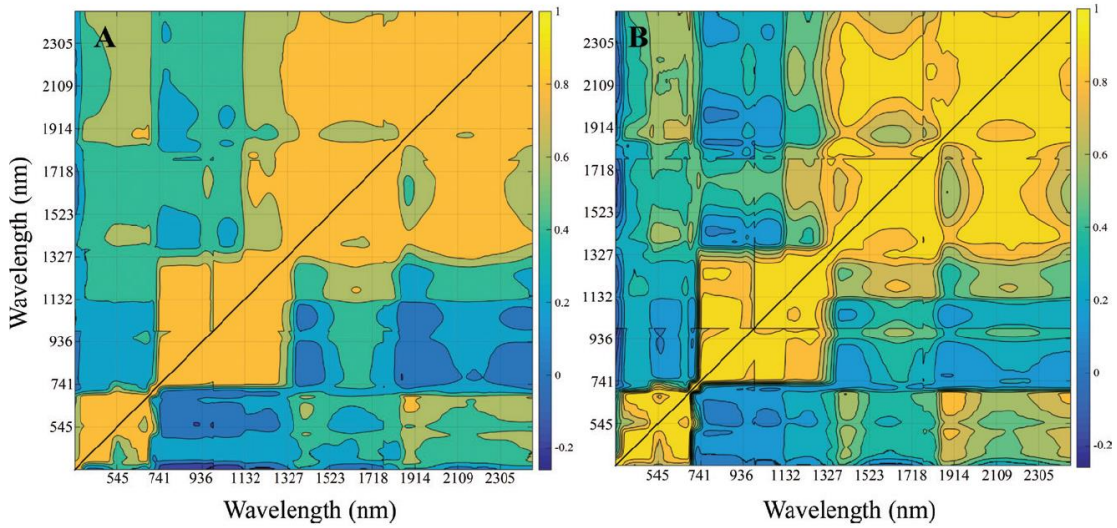

Fig. 3. Contour maps of Pearson correlation coefficients between reflectances across the spectrum depending on water conditions (A) either in the irrigated (above the diagonal) or in the rainfed treatment (below the diagonal); and depending on leaf side (B), in the adaxial (above the diagonal) or the abaxial side of the leaf (below the diagonal).

reflectances in 15 nm wavelength ranges were used as variables (Fig. 4). The resulting PCA explained almost 83% of data variability (64.6% PC1 and 18.1% PC2). Variable fitness was fixed at 57%, and 123 wavebands were selected by the analysis. First, a cluster of variables grouped the wavebands in the NIR region from 740 nm to 1309 nm. This cluster was related to the leaf-side factor, and the reflectance of this region was higher in the abaxial leaf side. Secondly, the reflectance within the SWIR region, in the 1400–1534 nm and 1850–2500 nm wavebands, was moderately related to the water regime effect, with the leaf reflectance being higher under rainfed conditions. The reflectance in the VIS region (590–664 nm and 680–694 nm) had a similar trend to that of the SWIR region, but it was a milder effect. Other wavebands in the NIR and SWIR regions were also selected by the analysis, but their relationships to the studied factors were less evident. Interaction centroids in the PCA graph were very closely related in rainfed conditions (Ad*R- and Ab*R-), but not in irrigated conditions where the interaction centroids were placed far from the principal effect.

Performance of the spectroradiometrical parameters

Factor clustering indicated that the overall differences in the spectroradiometrical parameters (including SRIs and the estimations obtained by the PROSPECT model) were greater between leaf sides than between water conditions (Fig. 5).

Water treatment differences were detected as significant by 25 of the SRIs (Supplementary Table S2), which were the most sensitive water indices, and in particular the MSI,

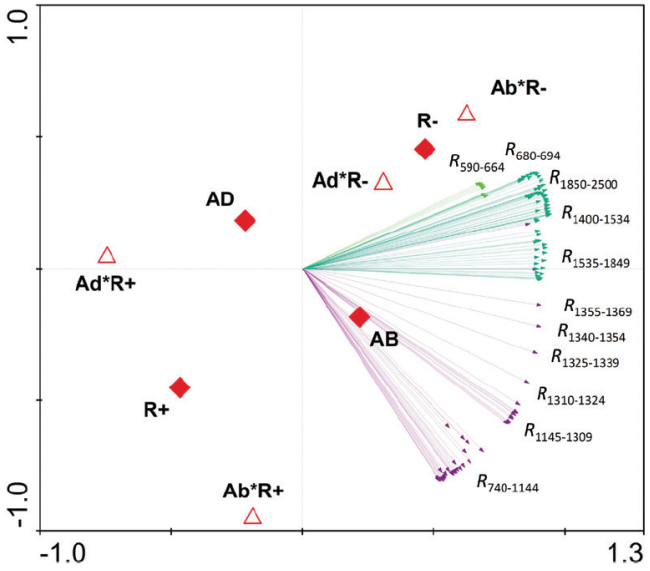

Fig. 4. Principal component analysis of reflectances introduced as variables. Light green arrows correspond to wavebands belonging to the visible region, violet arrows correspond to wavebands in the NIR region, while dark green arrows correspond to wavebands in the SWIR region. Main levels of the factors (R+, irrigated; R–, rainfed; AD, adaxial side; AB, abaxial side) are represented as filled rhomboids, and interactions (Ad*R+; Ad*R–; Ab*R+; Ab*R–) are shown as empty triangles. The variables shown in the graph were those selected by fixing the fitness at 57%. R_λ corresponds to the reflectance at λ band.

NDII, NDWI, NMDI, and SWWI (P<0.001). Many other biochemical and structurally related indices (pigment, lignin, and nitrogen) such as ARI_1, ARI_2, NDNI, mDATT, NDLI, FRI (P<0.001), $mCARI_2$, and MRCI (P<0.05) also varied significantly between water conditions. Finally, some red-edge indices including $VREI_1$, $VREI_2$ (P<0.01), and NDRE (P<0.05) were also shown to be sensitive to the water treatment factor.

Regarding the dorsoventral effect, 42 of the SRIs tested were sensitive to this factor. These SRIs mainly corresponded to biochemical, structural, and water indices, but also to some narrow and broadband greenness indices. The most robust differences between leaf sides were found by pigment-sensitive indices [Chl, Car, and anthocyanin (Anth)], and structural and water-related indices (P<0.001).

The interaction between leaf side and water regime was significant for some indices (ARI, mARI, GATB, SIPI, NPCI, SRPI, and PSRI) whose formulation included a red-edge alongside a blue or green wavelength. In such cases, the variation in these SRIs in response to water regime was clearly dependent on the side of the leaf.

Regarding the PROSPECT estimated leaf traits, only the EWT varied significantly between water regimes, and it was higher in the irrigated treatment.

Leaf anatomy

Leaf anatomy was studied in a subset of five genotypes with the aim of gaining insights into the relationship between leaf anatomy and spectral signature. The representativeness of the subset of samples used in the anatomical study was assessed by the respective performance of the SRIs. As in the main analysis presented here, water, nitrogen, and some pigment-related SRIs detected water regime differences for this subset of plots, while evidence for leaf side differences was mainly derived from pigment- and structure-related SRIs (Supplementary Table S3). Water stress induced significant decreases in xylem vessel cross-sectional area and diameter, and mesophyll cell cross-sectional area and perimeter, whereas the mesophyll cell cross-sectional area to perimeter ratio increased (Fig. 6; Table 3).

All the epidermal traits measured were significantly different between leaf sides, including the area of the epidermis cell section, the epidermis thickness, and the ratio of the epidermis sectional area to the total leaf sectional area, which were higher in the adaxial epidermis, whereas the epidermis cell wall thickness was higher in the abaxial epidermis.

Additionally, a wide range of SRIs (water-, biochemical-, and structure-related indices) significantly correlated with several anatomical traits (Fig. 7). Mesophyll cell-sectional area and the mesophyll cell area to cell perimeter ratio correlated positively with the water-related indices, NDWI and NDII, respectively (Fig. 7a, b). Meanwhile, the mesophyll cell sectional perimeter correlated positively with the N-related index, NDNI (Fig. 7c), and with the Chl-related index, RENDVI (Fig. 7d), whereas the ratio between the epidermis sectional area and the leaf sectional area correlated negatively with the Chl index, NPQI (Fig. 7e), and positively with the flavonol-related index, FRI, and with the lignin-related index, NDLI (Fig. 7f, h). Finally, the epidermis cell cross-sectional area correlated negatively with the Anth index, mARI (Fig. 6g).

Relationship between leaf and canopy spectra and their relationship to GY

The similarities between adaxial, abaxial, and canopy reflectance spectra were assessed with a PCA, setting the reflectance spectra as variables. The resulting two-component PCA (Supplementary Fig. S1) explained 94% of the variability (82.1% PC1 and 12.7% PC2). Measurements were distributed in two parallel dot clouds, where the two leaf spectra were overlapping and parallel to that of the canopy. Leaf and canopy dot clouds were mainly separated by PC1, which was mostly dependent on R_{1900}. In addition, from the collection of indices calculated, 74% of adaxial SRIs correlated significantly with the respective indices at the canopy level, whereas only 52% of abaxial SRIs correlated significantly with the respective canopy indices (data not shown).

In order to test the leaf-side effect on the ability for yield prediction, two multiple regression models were performed: a LASSO analysis using the full-range reflectance spectrum and a backward multiple regression using the SRIs (Table 4). In both analyses, the explained variability was always higher when using canopy spectral data, followed by the abaxial models and lastly the adaxial models, all of them being significant (P<0.001).

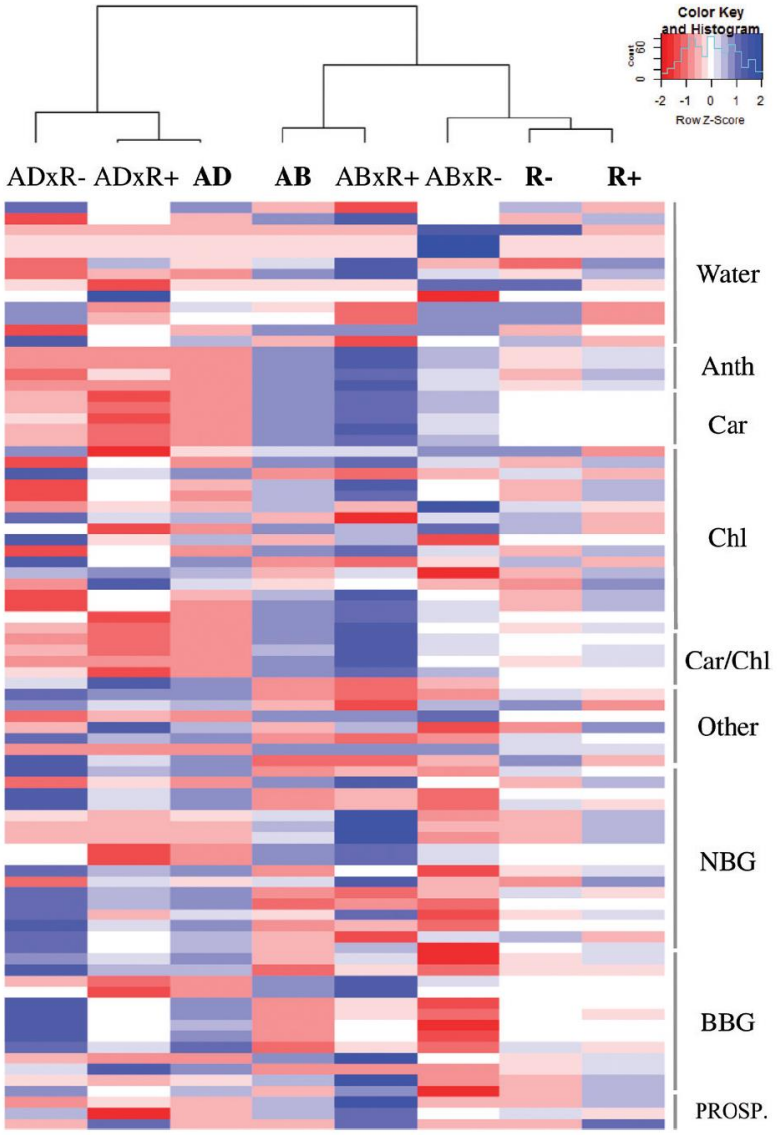

Fig. 5. Clustered heatmap of the spectroradiometer parameters (on the right) grouped by its trait targeted as water-related SRIs (Water), anthocyanin-related SRIs (Anth), carotenoid-related SRIs (Car), chlorophyll-related SRIs (Chl), carotenoid to chlorophyll ratio-related SRIs (Car/Chl), narrowband greenness indices (NBG), broadband greenness indices (BBG); other SRIs including nitrogen- and structural-related indices and estimates from the PROSPECT model (PROSPECT). At the top, a dendrogram resulting from the clustering analysis, with labels in bold indicating the main levels of the factors (R+, irrigated; R–, rainfed; AD, adaxial side; AB, abaxial side) and the interactions (Ad*R+; Ad*R–; Ab*R+; Ab*R–). The red–blue colour scale was obtained by *Z*-score transformation of the actual values.

Discussion

In this study, the decrease in GY, CTD, and leaf elongation (i.e. flag leaf blade length and width) in rainfed conditions compared with the support irrigation trial was associated with water stress as shown by the increase in leaf $\delta^{13}C$ and an even larger increase in grain $\delta^{13}C$ (Table 2) from irrigated to rainfed conditions (Araus *et al.*, 2003; Araus *et al.* 2013; Bort *et al.*, 2014).

Leaf anatomy-related spectral signal

A wide range of spectral traits was affected substantially by the leaf-side factor. In particular, clustering analysis (Fig. 5) revealed that the spectral parameters were more influenced by the side of the leaf measured than by the water regime.

Leaf reflectance was sensitive to leaf side in several wavebands of the spectrum (Fig. 2) that were beyond the expected structurally related wavebands (i.e. not only in the NIR but also in the red-edge and SWIR regions). Even so, PCA (Fig. 4) revealed the leaf-side factor to be strongly associated with leaf reflectance spectrum variability in the NIR region, and was positively related to the abaxial side of the leaf. The magnitude of reflectance in the NIR region is largely governed by structural discontinuities in the leaf (i.e. cell layers and interfaces) and leaf dry matter content (Peñuelas and Filella, 1998; Ceccato *et al.*, 2001; Homolova *et al.*, 2013). In particular, previous studies have reported that leaf NIR reflectance

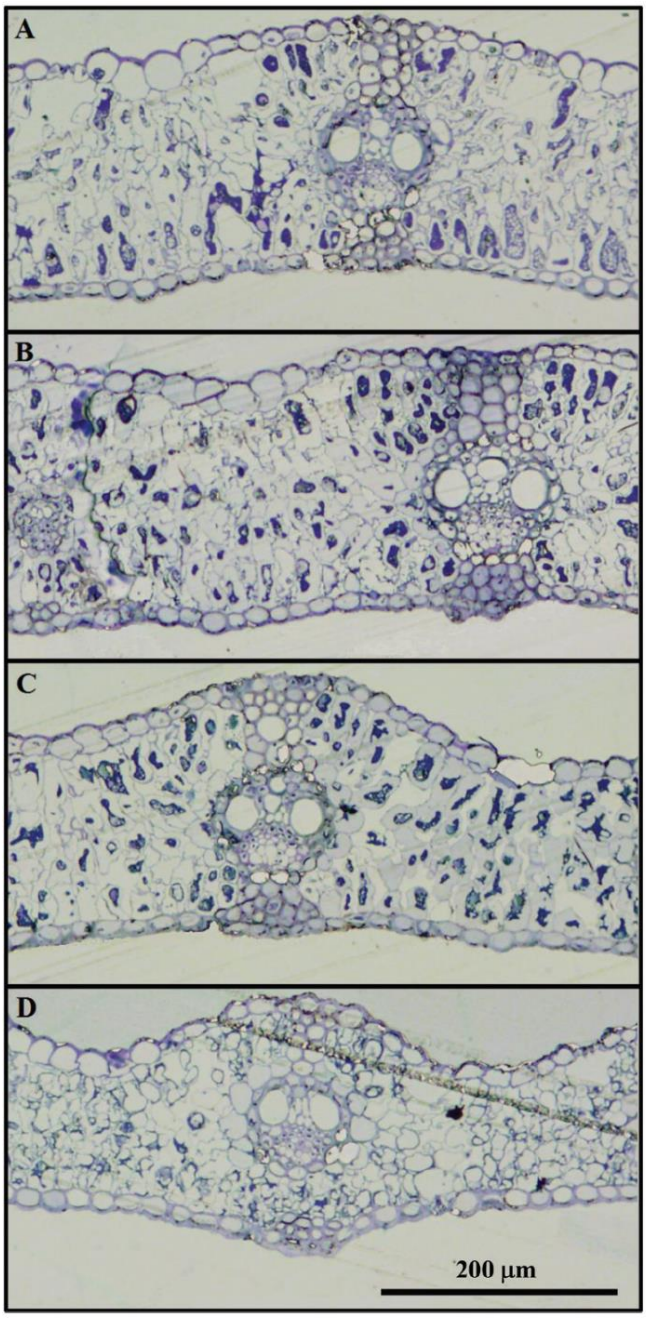

Fig. 6. Flag leaf transverse section images of two durum wheat genotypes; (A, C) var. Tussur; (B, D) var. Avispa; grown under irrigated (A, B) and rainfed (C, D) conditions.

is increased in flat and thick leaves possessing thin epidermal and epicuticular layers and long palisade cells (Knapp and Carter, 1998; Johnson *et al.*, 2005; Ollinger, 2011; Kozhoridze *et al.*, 2016). In concordance, the increased NIR reflectance in the abaxial compared with the adaxial leaf side (Fig. 2) can be consistently associated with a thinner and flatter epidermis in the abaxial surface (Table 3). Thus, the existence of anatomical differences between the adaxial and abaxial leaf sides, particularly in the epidermis, greatly impacts on leaf reflectance in the NIR region, even in an isobilateral leaf.

Similarly, the reported leaf anatomical differences between water regimes, such as the larger size of the mesophyll cell cross-sectional area and perimeter and a lower cell packing level (higher cell area to perimeter ratio) in the irrigated treatment (Table 3), led to an increase in NIR reflectance (Knapp and Carter, 1998; Johnson *et al.*, 2005; Ollinger, 2011) in irrigated compared with rainfed leaves (Fig. 1). The observed trends of increasing leaf thickness and decreasing epidermis sectional area relative to the total leaf sectional area in irrigated compared with trials might also contribute to a higher NIR reflectance of the former.

PCA (Fig. 4) revealed that adaxial and abaxial reflectance properties were closely related in rainfed conditions but were markedly differentiated in irrigated conditions. In other words, water stress caused changes in the leaf that tended to reduce dorsoventral differences in the spectrum. For instance, overall reflectance differences between leaf sides were detected in the NIR region in the irrigated treatment but not in rainfed conditions (Fig. 2b, c). This trend is further supported by the contour maps of correlations between waveband reflectance for the four main effects (rainfed and irrigated conditions, adaxial and abaxial leaf sides) (Fig. 3). In these analyses, higher correlation coefficients for the adaxial side compared with the abaxial side (Fig. 3a) can be explained by lower variation (i.e. greater similarity) of the adaxial spectral traits between water regimes. Meanwhile, reflectance differences between leaf sides were lower in rainfed conditions, which explains the higher correlation coefficients in rainfed compared with irrigated conditions (Fig. 3b).

It must be noted that leaf anatomical and biochemical characteristics can be affected by the gradient of light exposure during growth. Thus, while more erect leaves are characterized by an isobilateral anatomy, more horizontal leaves may exhibit increased dorsoventrality. In the case of wheat, an insertion gradient exists, with the flag leaf exhibiting more isobilateral characteristics than the basal (tillering) leaves (Araus *et al.*, 1986), which is probably associated with a progressive increase in verticality of the successive leaves. However, environmental conditions other than the light gradient cannot be discarded. Thus an increase in the level of atmospheric drought and the intensity of solar radiation during growth seems to affect the degree of isobilaterality of the flag wheat leaf laminas growing in the field (Araus *et al.*, 1989).

In fact, as previously mentioned in this study, the leaf dorsoventral gradient was less pronounced in rainfed conditions. Nevertheless, despite there being no clear differences among the genotypes in the angle of the laminas for given growing conditions (i.e. site and water regime) (data not shown), it should be noted that during stem elongation the laminas usually extrude vertically and the final position of each lamina is only achieved when it is fully expanded.

In agreement with previous observations in cereals, the wax cover was uniform and denser on the adaxial leaf side (Supplementary Fig. S2a, c) (Araus *et al.*, 1991). As described by Willick *et al.* (2018), the filament size of the epicuticular waxes was larger and longer in the abaxial leaf side

Table 3. *Means of the leaf section anatomical metrics for each water regime (R+, irrigated; R–, rainfed) and leaf side along with the significance levels of the respective two-way ANOVA*

	Water regime		Leaf side		Adaxial		Abaxial		Significance		
	R+	R-	Adaxial	Abaxial	R+	R-	R+	R-	P_{WR}	P_{LS}	P_{WR*LS}
Leaf											
Thickness (µm)	199.98	176.23	-	-	-	-	-	-	.065	-	-
Perimeter/area ($µm^{-1}$)	0.112	0.118	-	-	-	-	-	-	.350	-	-
Epidermis area/Leaf area	0.177	0.185	-	-	-	-	-	-	.249	-	-
Mesophyll			-	-	-	-	-	-		-	-
Cell area ($µm^2$)	577.17	407.89	-	-	-	-	-	-	.001	-	-
Cell perimeter (µm)	111.47	88.80	-	-	-	-	-	-	.000	-	-
Cell area/Cell perimeter (µm)	5.04	4.42	-	-	-	-	-	-	.006	-	-
Xylem vessels											
Major diameter (µm)	32.50	23.28	-	-	-	-	-	-	.011	-	-
Vessels area ($µm^2$)	544.34	281.69	-	-	-	-	-	-	.008	-	-
Epidermis											
Thickness (µm)	15.91	15.72	17.06	14.57	17.35	16.77	14.46	14.67	.740	.000	.477
Area/leaf area	.089	.092	.100	.081	.099	.102	.078	.083	.192	.000	.784
Cell area ($µm^2$)	220.9	237.5	294.7	163.7	278.3	311.2	163.5	163.9	.385	.000	.398
Wall thickness (µm)	3.988	4.066	3.581	4.473	3.621	3.541	4.355	4.592	.643	.000	.352

(Supplementary Fig. S2b, d), whereas water stress seemed to induce an increase in wax density (Supplementary Fig. S2c, d). Previous studies have reported that the presence of waxes (glaucousness) is important for reflecting UV–VIS light with respect to non-waxy leaves, with the UV–blue regions being particularly affected (Clark and Lister, 1975; Reicosky and Hanover, 1978; Febrero and Araus, 1994). Thus, reflectance differences between leaf sides and water regimes in the violet region could be associated with the observed structural differences in the wax cover density and size. In comparison with the waveband range of this study, changes in biochemical composition of the epicuticular waxes between leaf sides and water regimes have been reported for longer wavebands (Mid-IR) (Willick *et al.*, 2018), whereas wax determination has been addressed with shorter wavebands (UV) (Bianchi and Figini, 1986).

Leaf water- and composition-related spectral signals

Leaf reflectance in the SWIR region has been related to water and N-protein absorption as well as to other biochemical constituents such as lignin, cellulose, and starch (Peñuelas and Filella, 1998; Ustin *et al.*, 2009; Homolova *et al.*, 2013). Even so, the amount of water available in the internal leaf structure largely controls SWIR reflectance (Ceccato *et al.*, 2001; Ollinger, 2011). Thus, the increase in leaf reflectance in the SWIR region under rainfed conditions (Fig. 1) consistently indicates lower leaf water content. At wavelengths beyond 1400 nm, water absorption partially overshadows the absorption features of other biochemical compounds (Ollinger, 2011). Nevertheless, the reported relationship between SWIR reflectance and the water regime effect (Fig. 4), as well as the performance of several SRIs, suggest that the water regime may affect leaf biochemistry in addition to the direct effect on leaf water status.

In particular, the performance of several spectral traits revealed differences in leaf N-protein and lignin content in response to water stress. The moderate relationship between the water regime effect and the second half of the SWIR region (Fig. 4) was coincident with the absorption bands of these compounds (Kokaly 2001; Ustin *et al.*, 2009). Additionally, the SRIs related to N-protein and lignin content (NDNI and NDLI, respectively) varied in response to the low water regime, showing decreasing and increasing trends, respectively (Supplementary Table S2). The analytical measurements of leaf N concentration that indicated a decrease under rainfed conditions (Table 2) further confirmed this trend. Additionally, the reported positive correlation between the mesophyll cell section perimeter and the N-related index NDNI (Serrano *et al.*, 2002) (Fig. 7c) showed the relationship between composition and anatomical changes, which were both caused by water-limited conditions.

On the other hand, increasing the leaf C:N ratio (Table 2) in rainfed conditions could indicate the prevalence of supporting elements (i.e. cell wall materials) enriched in N-free compounds such as lignin. Moreover, the described epidermal leaf side differences (Table 3; Fig. 6) (i.e. greater epidermis thickness and cell section area, and the increased percentage of epidermis area relative to the total leaf sectional area in the adaxial leaf side) and their relationship to the lignin spectral signal (Fig.7h) further support this suggestion.

Regarding the leaf water signal, the water-related SRIs derived from the SWIR bands (e.g. MSI, NDII, NMDI, SWWI, and NDryMI) were the most sensitive to changing water conditions, indicating a decrease in water content conditions as well as an increase in leaf dry matter content in response to rainfed conditions (Supplementary Table S2). This superior performance of SWIR-based SRIs has been noted previously (Carter, 1991) following the high sensitivity

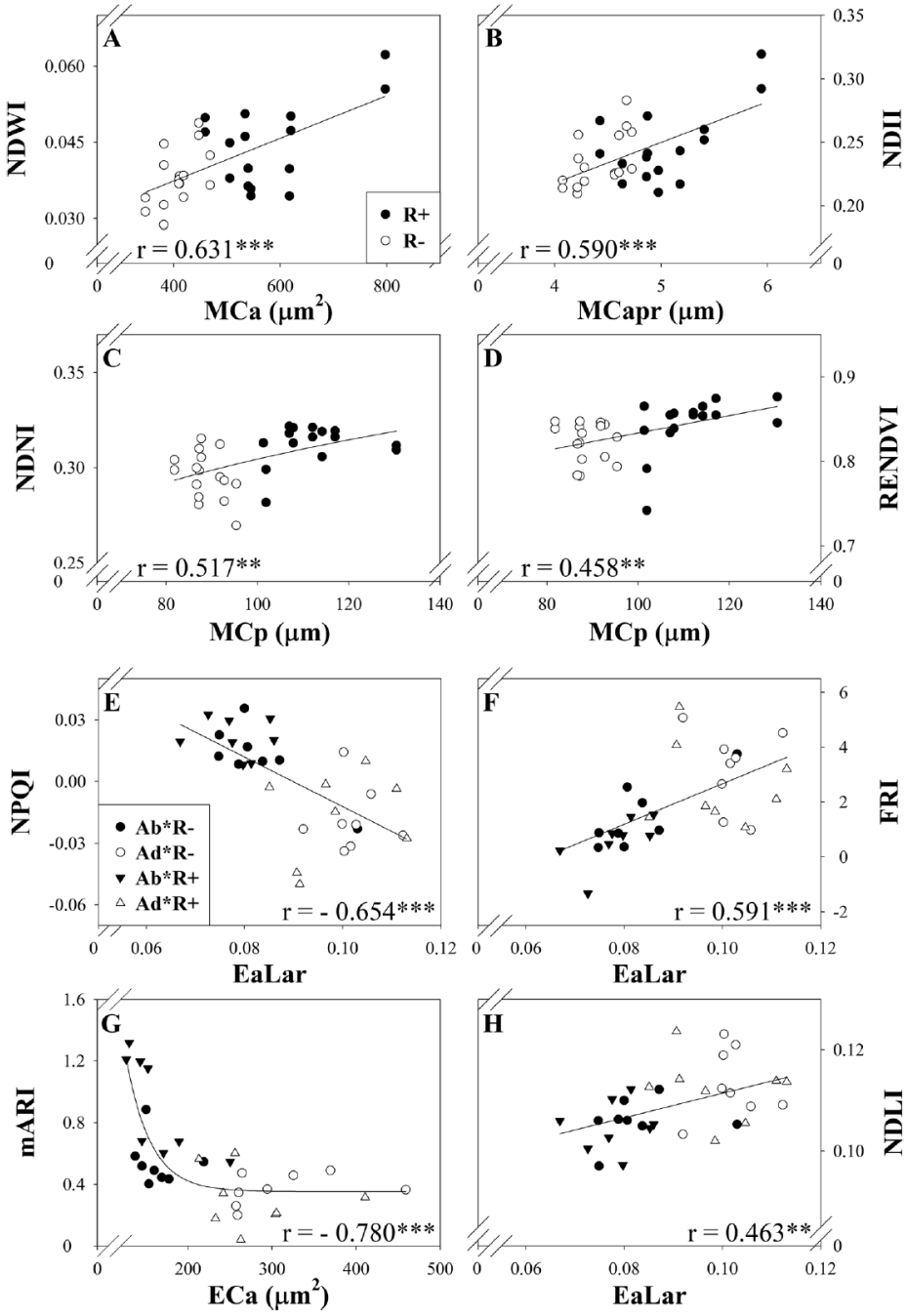

Fig. 7. Scatter plot graphs showing correlations between anatomical leaf section traits (EaLar, epidermis sectional area to leaf sectional area ratio; ECa, epidermis cell sectional area; MCa, mesophyll cell sectional area; MCp, mesophyll cell sectional perimeter; Mcapr, mesophyll cell sectional area to perimeter ratio) and spectral reflectance indices (the water-related indices NDWI and NDII; the nitrogen-related index NDNI; the chlorophyll-related indices RENDVI and NPQI; the flavonol-related index FRI; the anthocyanin-related index mARI, and the lignin-related index NDLI) for the subset of plots selected.

of reflectance to leaf water content in the water-absorbing 1300–2500 nm range. In contrast, the use of the 970 nm secondary water absorption band (which is included in indices such as WBI and NWI) was ineffective at the scale of the current work, although it has been reported as effective at the whole-plant and canopy scales (Peñuelas *et al.*, 1997; Gutierrez *et al.*, 2010). The PROSPECT EWT parameter proved to be robust, showing differences between water regimes.

In turn, for the subset of genotypes where leaf anatomy was studied, the observed variability in water-related indices, such as NDWI and NDII (Hardisky *et al.*, 1983; Gao 1996), was strongly and positively correlated with the increase in the mesophyll cell size and the decrease in the mesophyll cell packing (i.e. mesophyll cell area to perimeter ratio) from the rainfed to the irrigated treatment (Fig. 7a, b). These results show that the variation in anatomical traits (in turn caused by

Table 4. *Multiple regression analyses for grain yield prediction employing the adaxial, abaxial, or canopy reflectances*

1st Approach - Backward stepwise			
	Adaxial SRIs	**Abaxial SRIs**	**Canopy SRIs**
R^2	0.732	0.795	0.925
adjusted R^2	0.637	0.713	0.903
p-value	< 0.001	< 0.001	< 0.001
error of prediction	0.963	0.858	0.499
2nd Approach - LASSO regression			
	Adaxial spectrum	**Abaxial spectrum**	**Canopy spectrum**
R^2 actual vs estimated	0.384	0.552	0.747
p-value	< 0.001	< 0.001	< 0.001

For the first approach, the spectral reflectance indices (SRIs) calculated at the three levels (from adaxial, abaxial, and canopy measurements) were set as variables in a backward stepwise analysis. For the second approach, three LASSO regression models were performed with the whole spectrum at the three mentioned levels. Each model was obtained using a training set (75% of data), and its robustness was assessed by its respective accuracy in predicting yield (R^2) for the test set (25% of data).

the water conditions during growth) affected the leaf spectral performance.

The consistent dorsoventral differences in SWIR reflectance (centred on 1600, 1400, and 1900 nm) found under both water conditions (Fig. 2) suggest the existence of constitutive differences in biochemistry and/or water content between leaf sides that are independent of the water conditions during growth. The adaxial epidermis of wheat is characterized by the presence of bubble-shaped bulliform cells whose changes in turgidity control leaf straightening. Accordingly, we hypothesized that a higher water content signal would be expected in the adaxial epidermis. The reported decrease in adaxial reflectance (Fig. 2) in the SWIR that was coincident with strong absorption by water (centred on 1430 nm and 1950 nm) may support this hypothesis as a direct response to water changes. However, the response in the NIR region has previously been reported rather as an indirect effect via changes in leaf structure and scattering (Ollinger, 2011).

Some of the water SRIs tested, particularly those using the waveband centred on 1600 nm, detected apparently higher water content in the abaxial side of the leaf. This waveband has been reported to be indirectly sensitive to leaf and canopy water content (Ceccato *et al.*, 2001; Jackson *et al.*, 2004), but it is also related to leaf structure and biochemical characteristics (Ceccato *et al.*, 2001; Serrano *et al.*, 2002). Therefore, the possible existence of biochemical and/or structural differences between the two sides of the leaf could affect the reflectance in this waveband and thus interfere with leaf water content retrieval. Nevertheless, some other water-related SRIs ($NDMI_1$ and $NDMI_2$) combining NIR and SWIR bands as well as the EWT were insensitive to leaf side but were effective at detecting water regime differences. Thus, combining NIR and SWIR bands may remove variations induced by mesophyll structure (Ceccato *et al.*, 2001) and avoid the dorsoventral effect by improving the accuracy of water content retrieval.

Chlorophyll-related spectral signal

Regarding the dorsoventral effect on the Chl spectral signal, the observed significant changes in red-edge reflectance between leaf sides (Fig. 2) were largely related to absorption by Chl (Ustin *et al.*, 2009; Ollinger, 2011). Unlike other spectroscopic studies using species with bifacial leaves (Knapp *et al.*, 1988; Vogelmann and Evans, 2002; Johnson *et al.*, 2005), we detected an apparently higher Chl content in the abaxial side of the leaf from assessments with all of the Chl-sensitive spectral indices (Supplementary Table S2). The correlation between the Chl-related index, NPQI (Barnes *et al.*, 1992), and the ratio of the epidermis sectional area to the leaf sectional area (Fig. 7e) (which increased in the adaxial leaf side) revealed a dorsoventral gradient in the Chl spectral signal. The higher sun irradiance reaching the upper side of the leaf may involve a chloroplast acclimation process (i.e. lower Chl content) (Terashima *et al.*, 1986), which may support the existence of a leaf dorsoventral gradient in Chl.

Different responses of leaf Chl content to water stress have been reported in the literature (Loggini *et al.*, 1999; Carter and Knapp, 2001; Izanloo *et al.*, 2008; Valifard *et al.*, 2012), and can be highly dependent on genotypic variability and phenological stage. In this study, the total leaf Chl content per unit area (measured with a portable SPAD meter) was unaffected by water conditions. SPAD readings are exponentially correlated with leaf Chl content (Uddling *et al.*, 2007), so for high values of SPAD (as they occur in our study) the variation in the actual Chl content could be high, and the accuracy of the readings can also be affected by leaf water content (Martínez and Guiamet, 2004). Instead, many of the Chl-related SRIs (e.g. RECI, mSR_1, mSR_2, mDATT, $VREI_1$ MRCI, and NDRE) showed interesting trends. Indices based solely on red-edge wavebands were more sensitive to the water regime and apparently indicated a decrease in Chl content under rainfed conditions, whereas SRIs including blue or green wavebands in their formulation (e.g. ChlNDI, TCI, and TCARI) were insensitive. The interference of other pigments such as Car and Anth, which have absorption wavebands in the blue and green regions, might affect the Chl retrieval of some of the SRIs tested. As additional evidence, the reflectance in the red region was shown to be positively related to rainfed conditions in the PCA (Fig. 4). Although the estimated Chl content from the PROSPECT model did not vary significantly between water conditions, it followed the same decreasing trend in rainfed conditions. Additional evidence for this is the positive correlation between the Chl-related SRI, RENDVI (Gitelson and Merzlyak, 1994), and the mesophyll cell perimeter (Fig. 7d), whereby a higher mesophyll cell size under irrigation compared with rainfed conditions matches the increase in the Chl spectral signal. Previous studies have shown that indices using off-chlorophyll absorption wavebands (i.e. 690–730 nm) are the best Chl predictors because they have greater sensitivity to subtle changes in Chl content than the maximum absorption wavebands (i.e. 660–665 nm for Chl *a*) (Zarco-Tejada *et al.*,

2003; Main *et al.*, 2011). Altogether these results suggest a decreasing trend in leaf Chl content under rainfed conditions, with its level of significance depending on the sensitivity of the detection of the spectral parameter (i.e. SPAD meter, SRIs, PROSPECT model).

Photoprotection-related spectral signal

Besides leaf Chl, the leaf Car and Anth contents are also usually targeted because of their ecophysiological significance (Close and Beadle, 2003; Ustin *et al.*, 2009). Under stress conditions, Cars function to prevent photooxidation of the reaction centres (Ustin *et al.*, 2009), while Anths have an antioxidant and photoprotective role, besides acting as osmoregulators in plant cells (Chalker-Scott, 1999; Steyn *et al.*, 2002; Gould *et al.*, 2002).

Regarding dorsoventrality effects, all Car- and Anth-related SRIs, as well as those related to the Car:Chl ratio, indicated a higher Car and Anth content and Car:Chl ratio in the abaxial leaf side (Supplementary Table S2), suggesting a prevailing photoprotective role for the abaxial side of the leaf. The reported negative correlation between the Anth-related index, mARI (Gitelson *et al.*, 2001), and the epidermis cell sectional area (Fig. 7g) suggests the existence of an anatomy-driven dorsoventral gradient in Anth content. In agreement with this, Cartelat *et al.* (2005) reported higher leaf phenolic content, which includes Anth, in the abaxial side of wheat leaves measured with a portable device (Dualex meter). As reported by Shi *et al.* (2014), this might indicate that the upper part of wheat leaves exhibits greater light use efficiency via lower energy dissipation and photoinhibition. Although the Car estimation by PROSPECT performed similarly to the Car-related SRIs, the differences were not significant. This robust but conservative performance of the PROSPECT parameters may be explained by the large range of leaf pigment concentrations (i.e. wide range of species and conditions) used for the development of the PROSPECT model (Feret *et al.*, 2008). Finally, the results in the flavonol-related index (FRI) (Merzlyak *et al.*, 2005) suggested a possible higher flavonol content in the adaxial leaf side (Supplementary Table S2). It is worth pointing out that this index was originally developed for apple fruit, where Car and Chl contents do not interfere as much as in leaves. Flavonols are considered to have a photoprotective role as UV-absorbing compounds (Mazza *et al.*, 2000), so a possible higher concentration in the upper side of the leaf (i.e. the more exposed to sunlight) (Fig. 7f) may indicate an ecophysiological relevance for them as photoprotectors instead of Anth.

Regarding the water regime effect on photoprotective compounds, Car-related indices were unaffected, and Anth-related indices decreased under rainfed conditions, whereas the flavonol-related SRI increased (Supplementary Table S2). The performance of leaf Cars and Anths in response to water stress is quite variable according to the literature (Alexieva *et al.*, 2001; Chakraborty and Pradhan, 2012; Valifard *et al.*, 2012; Hammad and Ali, 2014). Accumulation of flavonols in the leaves has been reported in wheat in response to water stress and especially in drought-tolerant varieties (Ma *et al.*, 2014). In addition to the photoprotective function mentioned before, previous studies have suggested that flavonols act as antioxidants in plants (Hernández *et al.*, 2009), accumulating in different compartments such as the leaf epidermis (Tevini *et al.*, 1991). In this context, the increase in the ratio of the epidermis section area to the leaf section area (in the adaxial compared with the abaxial leaf side and in rainfed compared with irrigation conditions), which correlated positively with FRI (Fig. 7f), suggested an anatomy-mediated increase in leaf flavonols in response to water stress and to high sunlight levels. These results support the implementation of SRIs related to drought tolerance metabolites for plant stress studies and breeding purposes.

Main ideas and some insights into the scaling effect and yield prediction

Overall, the detailed study of leaf reflectance and several spectral-derived parameters revealed significant differences between the two sides of the leaf, which in turn are highly dependent on water regime, particularly under irrigated conditions. For instance, the significant interactions between dorsoventral and water regime effects in some of the Car:Chl- and Anth-related indices (Fig. 5; Supplementary Table S2) suggest possible side-specific photochemical changes in response to water regime. Previous studies in monocots (Soares *et al.*, 2008; Soares-Cordeiro *et al.*, 2011) have reported that side-specific physiological responses are involved in leaf acclimation to environmental stresses. In our study, the following tentative trend is hypothesized: in well-watered conditions, the two sides of the leaf are more differentiated, with the adaxial part of the leaf being photosynthetically more efficient (having a lower Car:Chl and Anth), larger epidermal and mesophyll cells, and a thicker epidermis. However, water stress induces alterations in structural, pigment, and photoprotective compounds that tend to reduce dorsoventral differences (functioning) of both leaf sides and consequently the spectroradiometrical response of reflected light. To the best of our knowledge, this is the first study describing a leaf-side-specific response to water regime in wheat using a spectroscopic approach.

The classical approaches for multispectral remote sensing evaluation of leaf and vegetation traits have usually been developed using the reflectance spectrum from the adaxial side of the leaves (Jacquemoud and Baret, 1990; Sims and Gamon, 2002; Lu and Lu, 2015). Although the adaxial leaf spectrum appeared to be more representative of the canopy-level data, the prediction of grain yield was clearly enhanced when abaxial rather than adaxial reflectance is employed, and this was irrespective of whether the full-range spectra or single SRIs were used (Table 4). Therefore, this study reveals that even for a species, such as wheat, with isobilateral leaves, spectra are different, and this may affect the assessment of yield.

Apart from constitutive differences, some anatomical traits of the abaxial leaf side (the epidermis thickness and the epidermis cell area) seemed to be less affected by changing water conditions than the adaxial side. This greater structural homogeneity across the abaxial leaf blade surface may

provide a less noisy spectral signal and better suitability for the prediction of yield from spectroscopy compared with the adaxial leaf side.

Supplementary data

Supplementary data are available at *JXB* online.

Fig. S1. Principal component analysis of reflectances at the leaf and canopy levels.

Fig. S2. Scanning electron micrographs of the epicuticular ultrastructure of flag leaves.

Table S1. Information on the spectral parameters used in this study.

Table S2. Table of means and significance of the two-way ANOVA for the spectral parameters.

Table S3. Significance of the two-way ANOVA of spectral indices for a subset of plots.

Acknowledgements

This study was supported by the Spanish project AGL2016-76527-R, MINECO. We thank the Goetz Instrument Program from the ASD PANalytical Company for providing us with the FieldSpec4 spectrometer. SCK is a recipient of a post-doctoral research grant (Juan de la Cierva IJCI-2014-20595) sponsored by MINECO. OVD is a recipient of a doctoral research grant (APIF) sponsored by the University of Barcelona.

References

Alexieva V, Sergiev I, Mapelli S, Karanov E. 2001. The effect of drought and ultraviolet radiation on growth and stress markers in pea and wheat. Plant, Cell and Environment **24,** 1337–1344.

Araus JL, Alegre L, Tapia L, Calafell R. 1986. Relationship between leaf structure and gas exchange in wheat leaves at different insertion levels. Journal of Experimental Botany **37,** 1323–1333.

Araus JL, Amaro T, Zuhair Y, Nachit MM. 1997. Effect of leaf structure and water status on carbon isotope discrimination in field-grown durum wheat. Plant, Cell and Environment **20,** 1484–1494.

Araus JL, Cabrera-Bosquet L, Serret MD, Bort J, Nieto-Taladriz MT. 2013. Comparative performance of $\delta^{13}C$, $\delta^{18}O$ and $\delta^{15}N$ for phenotyping durum wheat adaptation to a dryland environment. Functional Plant Biology **40,** 595–608.

Araus JL, Febrero A, Vendrell P. 1991. Epidermal conductance in different parts of durum wheat grown under Mediterranean conditions: the role of epicuticular waxes and stomata. Plant, Cell and Environment **14,** 545–558.

Araus JL, Tapia L, Alegre L. 1989. The effect of changing sowing date on leaf structure and gas exchange characteristics of wheat flag leaves grown under Mediterranean climate conditions. Journal of Experimental Botany **40,** 639–646.

Araus JL, Villegas D, Aparicio N, del Moral LFG, El Hani S, Rharrabti Y, Ferrio JP, Royo C. 2003. Environmental factors determining carbon isotope discrimination and yield in durum wheat under Mediterranean conditions. Crop Science **43,** 170–180.

Barnes JD, Balaguer L, Manrique E, Elvira S, Davison AW. 1992. A reappraisal of the use of DMSO for the extraction and determination of chlorophylls a and b in lichens and higher plants. Environmental and Experimental Botany **32,** 85–100.

Bianchi G, Figini ML. 1986. Epicuticular waxes of glaucous and nonglaucous durum wheat lines. Journal of Agricultural and Food Chemistry **34,** 429–433.

Bort J, Belhaj M, Latiri K, Kehel Z, Araus JL. 2014. Comparative performance of the stable isotope signatures of carbon, nitrogen and oxygen in assessing early vigour and grain yield in durum wheat. Journal of Agricultural Science **152,** 408–426.

Broge NH, Leblanc E. 2001. Comparing prediction power and stability of broadband and hyperspectral vegetation indices for estimation of green leaf area index and canopy chlorophyll density. Remote Sensing of Environment **76,** 156–172.

Cartelat A, Cerovic ZG, Goulas Y, *et al*. 2005. Optically assessed contents of leaf polyphenolics and chlorophyll as indicators of nitrogen deficiency in wheat (*Triticum aestivum* L.). Field Crops Research **91,** 35–49.

Carter GA. 1991. Primary and secondary effects of water content on the spectral reflectance of leaves. American Journal of Botany **78,** 916–924.

Carter GA, Knapp AK. 2001. Leaf optical properties in higher plants: linking spectral characteristics to stress and chlorophyll concentration. American Journal of Botany **88,** 677–684.

Ceccato P, Flasse S, Tarantola S, Jacquemoud S, Grégoire JM. 2001. Detecting vegetation leaf water content using reflectance in the optical domain. Remote Sensing of Environment **77,** 22–33.

Chakraborty U, Pradhan B. 2012. Oxidative stress in five wheat varieties (*Triticum aestivum* L.) exposed to water stress and study of their antioxidant enzyme defense system, water stress responsive metabolites and H_2O_2 accumulation. Brazilian Journal of Plant Physiology **24,** 117–130.

Chalker-Scott L. 1999. Environmental significance of anthocyanins in plant stress responses. Photochemistry and Photobiology **70,** 1–9.

Clark JB, Lister GR. 1975. Photosynthetic action spectra of trees: II. The relationship of cuticle structure to the visible and ultraviolet spectral properties of needles from four coniferous species. Plant Physiology **55,** 407–413.

Close DC, Beadle CL. 2003. The ecophysiology of foliar anthocyanin. Botanical Review **69,** 149–161.

Evans JR. 1999. Leaf anatomy enables more equal access to light and CO_2 between chloroplasts. New Phytologist **143,** 93–104.

Febrero A, Araus JL. 1994. Epicuticular wax load of near-isogenic barley lines differing in glaucousness. Scanning Microscopy **8,** 735–748.

Feret JB, François C, Asner GP, Gitelson AA, Martin RE, Bidel LP, Ustil SL, le Marie G, Jacquemoud S. 2008. PROSPECT-4 and 5: advances in the leaf optical properties model separating photosynthetic pigments. Remote Sensing of Environment **112,** 3030–3043.

Flexas J, Bota J, Galmes J, Medrano H, Ribas-Carbó M. 2006. Keeping a positive carbon balance under adverse conditions: responses of photosynthesis and respiration to water stress. Physiologia Plantarum **127,** 343–352.

Friedman J, Hastie T, Tibshirani R. 2010. Regularization paths for generalized linear models via coordinate descent. Journal of Statistical Software **33,** 1–22.

Gao BC. 1996. NDWI—a normalized difference water index for remote sensing of vegetation liquid water from space. Remote Sensing of Environment **58,** 257–266.

Gitelson A, Merzlyak MN. 1994. Spectral reflectance changes associated with autumn senescence of *Aesculus hippocastanum* L. and *Acer platanoides* L. leaves. Spectral features and relation to chlorophyll estimation. Journal of Plant Physiology **143,** 286–292.

Gitelson AA, Merzlyak MN, Chivkunova OB. 2001. Optical properties and nondestructive estimation of anthocyanin content in plant leaves. Photochemistry and Photobiology **74,** 38–45.

Gould KS, Neill SO, Vogelmann TC. 2002. A unified explanation for anthocyanins in leaves? Advances in Botanical Research **37,** 167–192.

Gutierrez M, Reynolds MP, Raun WR, Stone ML, Klatt AR. 2010. Spectral water indices for assessing yield in elite bread wheat genotypes under well-irrigated, water-stressed, and high-temperature conditions. Crop Science **50,** 197–214.

Hammad SA, Ali OA. 2014. Physiological and biochemical studies on drought tolerance of wheat plants by application of amino acids and yeast extract. Annals of Agricultural Sciences **59,** 133–145.

Hardisky MA, Smart RM, Klemas V. 1983. Growth response and spectral characteristics of a short *Spartina alterniflora* salt marsh irrigated with freshwater and sewage effluent. Remote Sensing of Environment **13,** 57–67.

Hernández I, Alegre L, Van Breusegem F, Munné-Bosch S. 2009. How relevant are flavonoids as antioxidants in plants? Trends in Plant Science **14,** 125–132.

Homolova L, Malenovský Z, Clevers JG, García-Santos G, Schaepman ME. 2013. Review of optical-based remote sensing for plant trait mapping. Ecological Complexity **15,** 1–16.

Izanloo A, Condon AG, Langridge P, Tester M, Schnurbusch T. 2008. Different mechanisms of adaptation to cyclic water stress in two South Australian bread wheat cultivars. Journal of Experimental Botany **59,** 3327–3346.

Jackson TJ, Chen D, Cosh M, Li F, Anderson M, Walthall C, Doriaswamy P, Hunt ER. 2004. Vegetation water content mapping using Landsat data derived normalized difference water index for corn and soybeans. Remote Sensing of Environment **92,** 475–482.

Jacquemoud S, Baret F. 1990. PROSPECT: a model of leaf optical properties spectra. Remote Sensing of Environment **34,** 75–91.

Jafarian T, Maghsoudi Moud A, Saffari VR. 2012. Water stress effects on winter and spring leaves anatomy of different wheat (*Triticum aestivum* L.) genotypes. Journal of Plant Physiology and Breeding **2,** 23–34.

Johnson DM, Smith WK, Vogelmann TC, Brodersen CR. 2005. Leaf architecture and direction of incident light influence mesophyll fluorescence profiles. American Journal of Botany **92,** 1425–1431.

Knapp AK, Vogelmann TC, McClean TM, Smith WK. 1988. Light and chlorophyll gradients within *Cucurbita* cotyledons. Plant, Cell and Environment **11,** 257–263.

Knapp A, Carter G. 1998. Variability in leaf optical properties among 26 species from a broad range of habitats. American Journal of Botany **85,** 940.

Kokaly RF. 2001. Investigating a physical basis for spectroscopic estimates of leaf nitrogen concentration. Remote Sensing of Environment **75,** 153–161.

Kozhoridze G, Orlovsky N, Orlovsky L, Blumberg DG, Golan-Goldhirsh A. 2016. Remote sensing models of structure-related biochemicals and pigments for classification of trees. Remote Sensing of Environment **186,** 184–195.

Liu HQ, Huete A. 1995. A feedback based modification of the NDVI to minimize canopy background and atmospheric noise. IEEE Transactions on Geoscience and Remote Sensing **33,** 457–465.

Loggini B, Scartazza A, Brugnoli E, Navari-Izzo F. 1999. Antioxidative defense system, pigment composition, and photosynthetic efficiency in two wheat cultivars subjected to drought. Plant Physiology **119,** 1091–1100.

Lu X, Lu S. 2015. Effects of adaxial and abaxial surface on the estimation of leaf chlorophyll content using hyperspectral vegetation indices. International Journal of Remote Sensing **36,** 1447–1469.

Lu S, Lu X, Zhao W, Liu Y, Wang Z, Omasa K. 2015. Comparing vegetation indices for remote chlorophyll measurement of white poplar and Chinese elm leaves with different adaxial and abaxial surfaces. Journal of Experimental Botany **66,** 5625–5637.

Ma D, Sun D, Wang C, Li Y, Guo T. 2014. Expression of flavonoid biosynthesis genes and accumulation of flavonoid in wheat leaves in response to drought stress. Plant Physiology and Biochemistry **80,** 60–66.

Main R, Cho MA, Mathieu R, O'Kennedy MM, Ramoelo A, Koch S. 2011. An investigation into robust spectral indices for leaf chlorophyll estimation. ISPRS Journal of Photogrammetry and Remote Sensing **66,** 751–761.

Martínez D, Guiamet J. 2004. Distortion of the SPAD 502 chlorophyll meter readings by changes in irradiance and leaf water status. Agronomie **24,** 41–46.

Mazza CA, Boccalandro HE, Giordano CV, Battista D, Scopel AL, Ballaré CL. 2000. Functional significance and induction by solar radiation of ultraviolet-absorbing sunscreens in field-grown soybean crops. Plant Physiology **122,** 117–126.

Merzlyak MN, Solovchenko AE, Smagin AI, Gitelson AA. 2005. Apple flavonols during fruit adaptation to solar radiation: spectral features and technique for non-destructive assessment. Journal of Plant Physiology **162,** 151–160.

Ollinger SV. 2011. Sources of variability in canopy reflectance and the convergent properties of plants. New Phytologist **189,** 375–394.

Peñuelas J, Filella I. 1998. Visible and near-infrared reflectance techniques for diagnosing plant physiological status. Trends in Plant Science **3,** 151–156.

Peñuelas J, Pinol J, Ogaya R, Filella I. 1997. Estimation of plant water concentration by the reflectance water index WI (R900/R970). International Journal of Remote Sensing **18,** 2869–2875.

Reicosky DA, Hanover JW. 1978. Physiological effects of surface waxes: I. Light reflectance for glaucous and nonglaucous *Picea pungens*. Plant Physiology **62,** 101–104.

Ripley B, Venables B, Bates DM, Hornik K, Gebhardt A, Firth D, Ripley MB. 2013. Package 'MASS'. CRAN R..

Serrano L, Peñuelas J, Ustin SL. 2002. Remote sensing of nitrogen and lignin in Mediterranean vegetation from AVIRIS data: decomposing biochemical from structural signals. Remote Sensing of Environment **81,** 355–364.

Shi SB, Chen WJ, Shi R, Li M, Zhang HG, Sun YN. 2014. PS II photochemical efficiency in flag leaf of wheat varieties and its adaptation to strong sun-light intensity on farmland of Xiangride in Qinghai Province, Northwest China. The Journal of Applied Ecology **25,** 2613–2622.

Sims DA, Gamon JA. 2002. Relationships between leaf pigment content and spectral reflectance across a wide range of species, leaf structures and developmental stages. Remote Sensing of Environment **81,** 337–354.

Soares AS, Driscoll SP, Olmos E, Harbinson J, Arrabaça MC, Foyer CH. 2008. Adaxial/abaxial specification in the regulation of photosynthesis and stomatal opening with respect to light orientation and growth with CO_2 enrichment in the C_4 species *Paspalum dilatatum*. New Phytologist **177,** 186–198.

Soares-Cordeiro AS, Driscoll SP, Arrabaça MC, Foyer CH. 2011. Dorsoventral variations in dark chilling effects on photosynthesis and stomatal function in *Paspalum dilatatum* leaves. Journal of Experimental Botany **62,** 687–699.

Steyn WJ, Wand SJE, Holcroft DM, Jacobs G. 2002. Anthocyanins in vegetative tissues: a proposed unified function in photoprotection. New Phytologist **155,** 349–361.

Taylor BR, Parkinson D, Parsons WF. 1989. Nitrogen and lignin content as predictors of litter decay rates: a microcosm test. Ecology **70,** 97–104.

Ter Braak CJ, Smilauer P. 2002. CANOCO reference manual and CanoDraw for Windows user's guide: software for canonical community ordination (version 4.5). http://library.wur.nl/WebQuery/wurpubs/fulltext/405659. Accessed 17 March 2017.

Terashima I, Sakaguchi S, Hara N. 1986. Intra-leaf and intracellular gradients in chloroplast ultrastructure of dorsiventral leaves illuminated from the adaxial or abaxial side during their development. Plant and Cell Physiology **27,** 1023–1031.

Tevini M, Braun J, Fieser G. 1991. The protective function of the epidermal layer of rye seedlings against ultraviolet-B radiation. Photochemistry and Photobiology **53,** 329–333.

Uddling J, Gelang-Alfredsson J, Piikki K, Pleijel H. 2007. Evaluating the relationship between leaf chlorophyll concentration and SPAD-502 chlorophyll meter readings. Photosynthesis Research **91,** 37–46.

Ustin SL, Gitelson AA, Jacquemoud S, Schaepman M, Asner GP, Gamon JA, Zarco-Tejada P. 2009. Retrieval of foliar information about plant pigment systems from high resolution spectroscopy. Remote Sensing of Environment **113,** 67–77.

Valifard M, Moradshahi A, Kholdebarin B. 2012. Biochemical and physiological responses of two wheat (*Triticum aestivum* L.) cultivars to drought stress applied at seedling stage. Journal of Agricultural Science and Technology **14,** 1567–1578.

Vogelmann TC, Evans JR. 2002. Profiles of light absorption and chlorophyll within spinach leaves from chlorophyll fluorescence. Plant, Cell and Environment **25,** 1313–1323.

Wang XQ, Wu WH, Assmann SM. 1998. Differential responses of abaxial and adaxial guard cells of broad bean to abscisic acid and calcium. Plant Physiology **118,** 1421–1429.

Warnes GR, Bolker B, Bonebakker L, *et al*. 2009. gplots: various R programming tools for plotting data. R package version, 2(4).

Willick IR, Lahlali R, Vijayan P, Muir D, Karunakaran C, Tanino KK. 2018. Wheat flag leaf epicuticular wax morphology and composition response to moderate drought stress is revealed by SEM, FTIR-ATR and synchrotron X-ray spectroscopy. Physiologia Plantarum **62,** 316–332.

Xue J, Su B. 2017. Significant remote sensing vegetation indices: a review of developments and applications. Journal of Sensors **2017,** 1353691.

Yousfi S, Serret MD, Márquez AJ, Voltas J, Araus JL. 2012. Combined use of $\delta^{13}C$, $\delta 18O$ and $\delta 15N$ tracks nitrogen metabolism and genotypic adaptation of durum wheat to salinity and water deficit. New Phytologist **194,** 230–244.

Zarco-Tejada PJ, Pushnik JC, Dobrowski S, Ustin SL. 2003. Steady-state chlorophyll a fluorescence detection from canopy derivative reflectance and double-peak red-edge effects. Remote Sensing of Environment **84,** 283–294.

Supplementary data

Article title: Leaf Dorsoventrality as a paramount factor determining spectral performance in field-grown wheat under contrasting water regimes

Authors: Omar Vergara-Diaz, Fadia Chairi, Rubén Vicente, Jose A Fernandez Gallego, Maria Teresa Nieto-Taladriz, Nieves Aparicio, Shawn C. Kefauver, José Luís Araus

The following Supplementary data is available for this article:

Figure S1. Principal component analysis of reflectances introduced as variables. Data points represent the sample measurements and the color labels are indicative of the three levels of measure, at the leaf level adaxial and abaxial reflectance are represented as green and red colour respectively and the canopy reflectance is respresented with the blue colour.

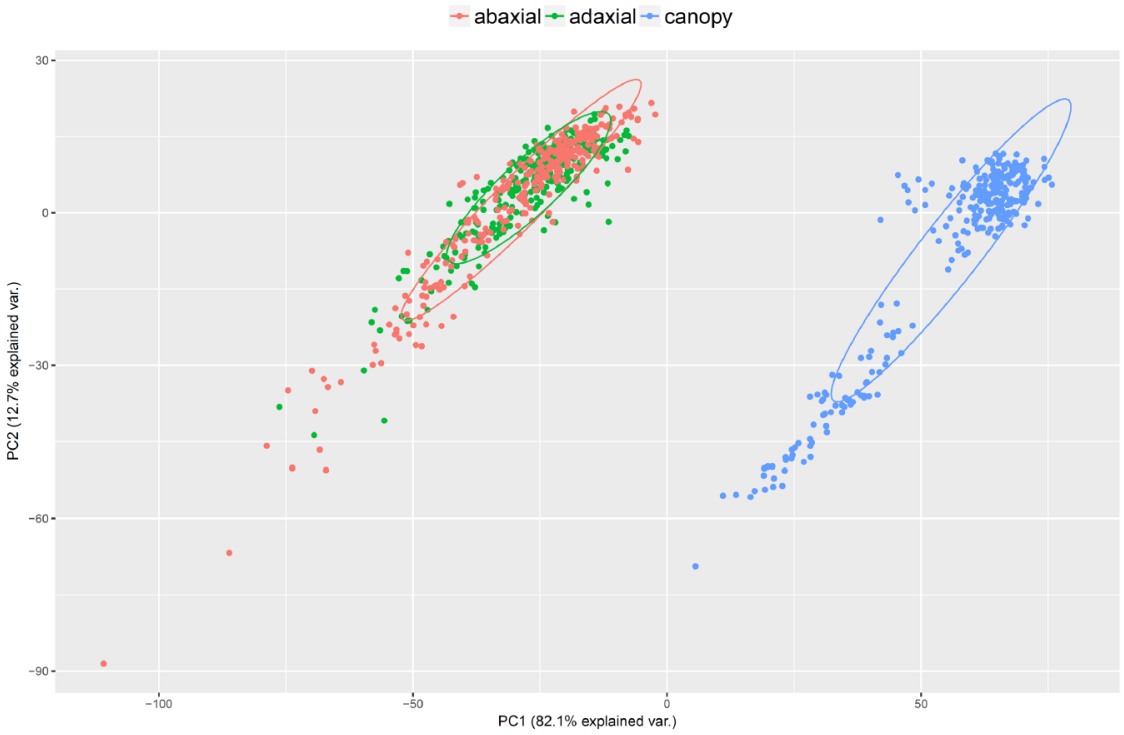

Figure S2. Scanning electron micrographs of the epicuticular ultrastructure of flag leaves. Images were taken from adaxial (A and C) and abaxial (B and D) surfaces of durum wheat grown under supplemental irrigation (A and B) and rainfed conditions (C and D) observed at 10000x magnification.

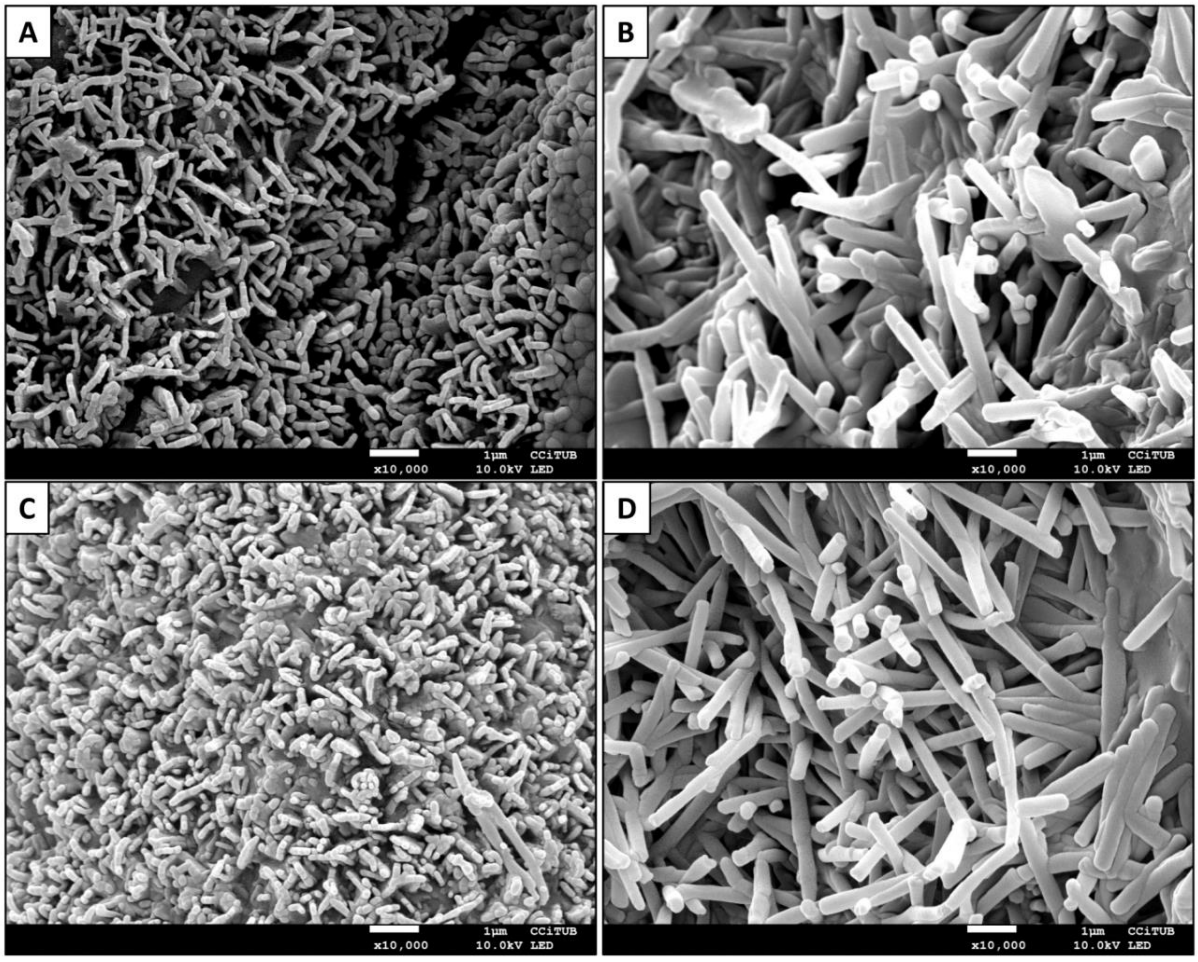

Table S1 Information on the spectral parameters used in this study, including their names and acronyms, target traits, formulations and citing literature. Subscripts refer to the wavelength used in the calculations of the spectral reflectance indices.

Index	Name	Target trait(s)	Formula	Literature
MSI	Moisture stress index	Water content	R_{1599} / R_{819}	Hunt & Rock, 1989
NDII	Normalised difference infrared index	Water content	$(R_{819} - R_{1649})/(R_{819} + R_{1649})$	Hardisky et al. 1983
NWI_1	Normalised difference water index 1	Water content	$(R_{970} - R_{900})/(R_{970} + R_{900})$	Babar et al. 2006
NWI_2	Normalised difference water index 2	Water content	$(R_{970} - R_{920})/(R_{970} + R_{920})$	Prasad et al. 2007
NWI_3	Normalised difference water index 3	Water content	$(R_{970} - R_{880})/(R_{970} + R_{880})$	Gao et al. 1995
NDWI	Normalised difference water index	Canopy water content	$(R_{857}-R_{1241})/(R_{857}+R_{1241})$	Gao 1996
NMDI	Normalised multi-band drought index	Drought status	$(R_{860}-(R_{1640} - R_{2130}))/(R_{860} + (R_{1640} - R_{2130}))$	Wang & Qu, 2007
WBI	Water band index	Canopy water status	R_{970} / R_{900}	Peñuelas et al. 1993
WI	Water index	Canopy water status	R_{900} / R_{970}	Peñuelas et al. 1993
$NDMI_1$	Normalised difference moisture index 1	Vegetation water content	$(R_{2200} - R_{1100})/(R_{2200} + R_{1100})$	Wilson & Sader, 2002
$NDMI_2$	Normalised difference moisture index 2	Moisture	$(R_{2247} - R_{1147})/(R_{2247} + R_{1147})$	Lobos et al. 2014
$NDMI_3$	Normalised difference moisture index 3	Moisture	$(R_{1650} - R_{830})/(R_{1650} - R_{850})$	Inoue et al. 2007
SWWI	Short Wave Water Index	Water content	(R_{1650} / R_{850})	Lobos et al. 2014
RGRR	Red green reflectance ratio	Anthocyanin content	R_{Red}/R_{Green}	Gamon & Surfus 1999
ARI	Anthocyanin reflectance index	Anthocyanin content	$R_{550}^{-1} - R_{700}^{-1}$	Gitelson et al. 2001
mARI	Modified anthocyanin reflectance index 1	Anthocyanin content	$R_{800} \times (R_{550}^{-1} - R_{700}^{-1})$	Gitelson et al. 2001
GATB	Gitelson Anthocyanin three	Anthocyanin content	$(R_{553\text{-}570}^{-1} - R_{690\text{-}710}^{-1}) \times R_{760\text{-}800}$	Gitelson et al. 2006

$PSSR_b$	Pigment-specific simple ratio	Chl b content	R_{800}/R_{635}	Blackburn, 1998
NDRE	Normalised difference red edge	Chlorophyll content	$(R_{790}-R_{720})/(R_{790}+R_{720})$	Barnes et al. 2000
PSRI	Plant senescing reflection index	Carotenoid to chlorophyll ratio	$(R_{680}-R_{500})1/R_{750}$	Merzlyak et al. 1999
SIPI	Structural independent pigment index	Carotenoid to chlorophyll a ratio	$(R_{800} - R_{445})/(R_{800} - R_{680})$	Peñuelas et al 1995;
PRI	Photochemical reflectance index	Photosynthetic light-use efficiency , Car/Chl ratio	$(R_{531} - R_{570})/(R_{531} + R_{570})$	Gamon et al. 1992
NPCI	Normalised pigment chlorophyll ratio index	Car/Chl a ratio; senescense, N status	$(R_{680}-R_{430})/(R_{430}+R_{680})$	Peñuelas et al. 1993
SRPI	Simple ratio pigment index	Car/Chl a ratio	R_{430}/R_{680}	Peñuelas et al. 1995
FRI	Flavonols reflectance index	Flavonol content	$(R_{410}^{-1} - R_{460}^{-1}) \times R_{800}$	Merzylak et al. 2005
NDNI	Normalised difference nitrogen index	Nitrogen content	$(\log (R_{1510}^{-1}) – \log (R_{1680}^{-1})) / (\log (R_{1510}^{-1}) + \log (R_{1680}^{-1}))$	Serrano et al 2002
NDLI	Normalized difference lignin index	Lignin content	$(\log (R_{1754}^{-1}) – \log (R_{1680}^{-1}))/(\log (R_{1754}^{-1}))+\log (R_{1680}^{-1}))$	Serrano et al. 2002
CAI	Cellulose absorption index	Dried plant material and cellulose	$0.5 \times(R_{2000} + R_{2200}) - R_{2100}$	Nagler et al. 2000
NDryMI	Normalized dry matter index	Dry matter content and water status	$(R_{1649}-R_{1722})/(R_{1649}+R_{1722})$	Hunt et al. 2012
$NDVI_1$	Normalised difference vegetation index	Green biomass	$(R_{800} - R_{670})/(R_{800} + R_{670})$	Rouse et al. 1974
GVI	Greenness Vegetation index	Green biomass	$(R_{682} - R_{553})/(R_{682} + R_{553})$	Not found
$NDVI_w$	Normalised difference vegetation index	Green biomass	$(R_{830} - R_{660})/(R_{830} + R_{660})$	Rouse et al. 1973
$NDVI_n$	Normalized difference vegetation index	Green biomass	$(R_{760} - R_{660})/(R_{760} + R_{660})$	Rouse et al. 1973
$GNDVI_n$	Green normalized difference vegetation index	Green biomass	$(R_{870} - R_{568})/(R_{870} + R_{568})$	Gitelson et al. 1996
$GNDVI_w$	Green normalized difference vegetation index	Green biomass	$(R_{830} - R_{560})/(R_{830} + R_{560})$	Gitelson et al. 1996

	band			
CRI_1	Carotenoid reflectance index 1	Carotenoid content	$(1/R_{510}) - (1/R_{550})$	Gitelson et al. 2002
CRI_2	Carotenoid reflectance index 2	Carotenoid content	$(1/R_{510}) - (1/R_{700})$	Gitelson et al. 2002
CRI_3	Carotenoid reflectance index 3	Carotenoid content	$R_{800} \times ((1/R_{520})-(1/R_{550}))$	Getilson et al. 2002
RARS-Car	Ratio analysis of reflectance spectra-Car	Carotenoid content	R_{746}/R_{513}	Chappelle et al. 1992
$PSSR_c$	Pigment-specific simple ratio-Car	Carotenoid content	R_{800}/R_{470}	Blackburn, 1998
ChlNDI	Chlorophyll normalised difference index	Chlorophyll a content	$(R_{705} - R_{445})/(R_{750} + R_{445})$	Datt, 1999
RECI	Red-edge Chlorophyll Index	Chlorophyll content	$(R_{770-800}/R_{720-730}) - 1$	Gitelson et al. 2003
mDATT	Modified Datt index	Chlorophyll content	$(R_{719} - R_{726})/(R_{719} - R_{743})$	Lu et al. 2015
TCI	Triangular chlorophyll index	Chlorophyll content	$1.2(R_{700}-R_{550})-1.5(R_{670}-R_{550}) \times (R_{700}/R_{670})^{0.5}$	Haboudane et al. 2008
TCARI	Transformed chlorophyll absorption reflectance index	Chlorophyll content	$3\times((R_{700}-R_{670})-0.2 \times (R_{700}-R_{550}) \times (R_{700}/R_{670}))$	Rondeaux et al. 1996
NPQI	Normalized Phaeophytinization Index	Chlorophyll degradation	$(R_{415}-R_{435})(R_{414}+R_{435})$	Barnes et al. 1992
mCARI	Modified chlorophyll absorption reflectance index	Chlorophyll content	$(1.5 \times (R_{800}-R_{670}) - 1.3 \times (R_{800}-R_{550}))/ \sqrt{((2 \times R_{800} + 1) \times (2 \times R_{800} +1) - (6 \times R_{800} - 5 \times \sqrt{R_{670}}) - 0.5)}$	Haboudane et al. 2004
CI	Carter index	Plant stress	R_{760} / R_{695}	Carter, 1994
$VREI_1$	Vogelmann red edge index 1	Chlorophyll content	(R_{740} / R_{720})	Vogelmann et al. 1993
$VREI_2$	Vogelmann red edge index 2	Chlorophyll content	$(R_{734} - R_{747})/(R_{715} + R_{726})$	Vogelmann et al. 1993
RENDVI	Red-Edge normalized difference index	Chlorophyll content	$(R_{750} - R_{705})/(R_{750} + R_{705})$	Gitelson & Merzlyak 1994
mRENDVI	Modified normalized difference index	Chlorophyll content	$(R_{750} - R_{705})/(R_{750} + R_{705} - 2 \times R_{445})$	Sims & Gamon 2002
MRCI	MERIS total chlorophyll index	Chlorophyll content	$(R_{750}-R_{710})/(R_{710}-R_{680})$	Dash & Curran 2004
$PSSR_a$	Pigment-specific simple ratio	Chl a content	R_{800}/R_{680}	Blackburn, 1998

GNDVI	Green normalized difference vegetation index	Green biomass	$(R_{800}-R_{550})/(R_{800}+R_{550})$	Daughtry et al. 2000
SR_1	Simple ratio	Green biomass	R_{900} / R_{680}	Rouse et al. 1973
SR_2	Simple ratio	Green biomass	R_{770} / R_{680}	Not found
SR_3	Simple ratio	Chlorophyll content	R_{750} / R_{700}	Gitelson & Merzlyak 1997
SR_4	Simple ratio 4	Chlorophyll content	R_{850} / R_{710}	Datt, 1999
mSR_1	Modified simple ratio 1	Chlorophyll content	$(R_{850} - R_{710})/(R_{850} - R_{680})$	Datt, 1999
mSR_2	Modified simple ratio 2	Chlorophyll content	$(R_{780} - R_{710})/(R_{780} - R_{680})$	Maccioni et al. 2001
mSR_3	Modified simple ratio 3	Chlorophyll content	$(R_{750} - R_{445})/(R_{705} - R_{445})$	Sims & Gamon 2002
mSR_4	Modified simple ratio 4	Leaf area index and biomass	$(R_{800}/R_{670}-1)/(\sqrt{(R_{800}/R_{670}+1)})$	Chen 1996
TVI	Triangular vegetation index	Leaf area index and Chlorophyll content	$0.5 \times (120 \times (R_{750}-R_{550}) - 200 \times (R_{670}-R_{550})$	Broge & Leblanc 2000
$mTVI_1$	Modified triangular vegetation index 1	Leaf area index	$1.2 (1.2 \times (R_{800}-R_{550}) – 2.5 \times (R_{670}-R_{550})$	Haboudane et al. 2004
$mTVI_2$	Modified triangular vegetation index 2	Leaf area index	$(1.5 \times (1.2 \times (R_{800}-R_{550}) - 2.5 \times (R_{670}-R_{800})))/ \sqrt{((2 \times R_{800} + 1) \times (2 \times R_{800} + 1)-(6 \times R_{800} - 5 \times \sqrt{R_{670}} - 0.5))}$	Haboudane et al. 2004
OSAVI	Optimized soil-adjusted vegetation index	Vegetation cover and biomass	$(1.5 \times (R_{800}-R_{670})/(R_{800}+R_{670}+0.16)$	Rondeaux et al. 1996
GI	Greeness index	Greenness	R_{554}/R_{677}	Zarco-Tejada et al. 2005
EVI_2	Enhanced vegetation index 2	Green biomass	$2.5 \times (R_{800}-R_{660})/(1+R_{800}+2.4*R_{660})$	Jiang et al. 2008
RDVI	Renormalised difference vegetation index	Green biomass	$(R_{800}-R_{670})/(\sqrt{R_{800}}+R_{670})$	Rougean & Breon 1995
TDVI	Transformed difference vegetation index	Vegetation cover and biomass	$\sqrt{(0.5 +((R_{NIR}-R_{Red})/(R_{NIR}+R_{Red})))}$	Deering et al. 1975
RVI	Ratio vegetation index	Vegetation cover and health	R_{NIR} / R_{Red}	Birth et al. 1968
OSAVI	Optimized soil-adjusted vegetation index	Vegetation cover and biomass	$(1.5*(R_{NIR} - R_{Red}))/(R_{NIR}+R_{red} + 0.16)$	Rondeaux et al. 1996
NDVI	Normalised difference vegetation index	Vegetation cover and biomass	$(R_{NIR} - R_{Red})/(R_{NIR} + R_{Red})$	Rouse et al. 1973

NLI	Non-linear index	Vegetation cover and biomass	$(R_{NIR}^2 - R_{Red})/(R_{NIR}^2 + R_{Red})$	Goel & Qin, 1994
mNLI	Modified non-linear index	Vegetation cover and biomass	$((R_{NIR}^2 - R_{Red}) \times 1.5)/((R_{NIR}^2 + R_{Red}) + 0.5)$	Yang et al. 2008
IPVI	Infrared percentage vegetation index	Vegetation cover and biomass	$R_{NIR}/(R_{NIR} + R_{Red})$	Crippen, 1990
GRVI	Green ratio vegetation index	Canopy cover	R_{NIR}/R_G	Sripada et al. 2006
EVI	Enhanced vegetation index	Canopy cover	$2.5 \times ((R_{NIR}-R_{Red})/(R_{NIR}+ 6 \times R_{Red}-7.5 \times R_B+1))$	Liu & Huete 1995
GNDVI	Green normalised difference vegetation index	Green biomass	$(R_{NIR} - R_G)/(R_{NIR} + R_G)$	Gitelson & Merzlyak 1998
RNDVI	Red normalised difference vegetation index	Healthy vegetation	$(R_{NIR-R})/ \sqrt{(R_{NIR}+R_{Red})}$	Roujean & Breon 1995
TCARI/OSAVI	Index Ratio	Chlorophyll content	TCARI/OSAVI	Haboudane et al. 2002
WI/NDVI	Index Ratio	Plant water content	WBI/NDVI	Peñuelas et al 1997
PROSPECT5 model				
Cab	Chlorophyll content			Jacquemoud & Barert 1990
Cxc	Carotenoid content			
EWT	Equivalent water thickness			

Table S2 Mean values of the spectral parameters for each water regime (R+, irrigated; R-, rainfed) and in each side of the leaf, together with the significance levels of the two-way analysis of variance.

Target trait	Water Regime		Leaf Side		Adaxial		Abaxial		Significance		
	R+	R-	adaxial	abaxial	R+	R-	R+	R-	P_{WR}	P_{LS}	P_{WRxLS}
Water content											
MSI	0.559	0.573	0.574	0.559	0.567	0.580	0.552	0.566	0.000	0.000	0.907
NDII	0.237	0.227	0.227	0.238	0.232	0.222	0.243	0.232	0.000	0.000	0.790
NWI_1	-0.016	-0.015	-0.016	-0.016	-0.016	-0.016	-0.016	-0.015	0.249	0.301	0.712
NWI_2	-0.016	-0.016	-0.016	-0.016	-0.016	-0.016	-0.016	-0.015	0.052	0.280	0.659
NWI_3	-0.015	-0.015	-0.015	-0.015	-0.015	-0.015	-0.015	-0.014	0.406	0.391	0.767
NDWI	0.042	0.037	0.039	0.040	0.041	0.037	0.043	0.038	0.000	0.007	0.845
NMDI	0.459	0.453	0.450	0.462	0.452	0.447	0.465	0.458	0.000	0.000	0.420
WBI	0.969	0.970	0.969	0.969	0.968	0.969	0.969	0.970	0.249	0.302	0.714
WI_2	1.032	1.032	1.032	1.032	1.033	1.032	1.032	1.031	0.249	0.299	0.711
$NDMI_1$	-0.578	-0.568	-0.572	-0.574	-0.577	-0.568	-0.579	-0.569	0.002	0.676	0.786
$NDMI_2$	-0.575	-0.568	-0.571	-0.572	-0.574	-0.568	-0.576	-0.568	0.016	0.804	0.826
$NDMI_3$	0.986	0.985	0.985	.987	0.986	0.984	0.987	0.987	0.010	0.000	0.135
SWWI	0.613	0.626	0.626	0.613	0.620	0.633	0.606	0.620	0.000	0.000	0.784
Anthocyanin											
ARI	-0.328	-0.452	-0.635	-0.144	-0.627	-0.644	-0.029	-0.259	0.000	0.000	0.001
mARI	-0.281	-0.387	-0.544	-0.124	-0.537	-0.551	-0.026	-0.222	0.000	0.000	0.001
RGRR	0.685	0.676	0.673	0.688	0.677	0.669	0.692	0.683	0.126	0.010	0.950
GATB	0.931	0.817	0.688	1.060	0.670	0.706	1.193	0.927	0.006	0.000	0.000
Carotenoids											
CRI_1	6.058	6.146	5.707	6.496	5.513	5.902	6.603	6.389	0.681	0.000	0.157
CRI_2	5.730	5.694	5.072	6.352	4.886	5.258	6.574	6.130	0.865	0.000	0.056
CRI_3	2.871	2.883	2.773	2.982	2.707	2.839	3.036	2.927	0.895	0.017	0.168
RARS-Car	10.370	10.275	9.978	10.667	9.834	10.122	10.907	10.428	0.646	0.001	0.066
$PSSR_c$	13.398	13.413	12.641	14.170	12.349	12.932	14.446	13.893	0.965	0.000	0.091
Chlorophyll											
ChlNDI	0.113	0.116	0.114	0.115	0.111	0.116	0.115	0.116	0.178	0.523	0.411
RECI	0.852	0.825	0.819	0.858	0.836	0.803	0.867	0.847	0.012	0.000	0.586
mDATT	0.324	0.329	0.332	0.322	0.329	0.335	0.320	0.323	0.000	0.000	0.213
mSR_1	0.792	0.785	0.785	0.792	0.788	0.782	0.795	0.789	0.038	0.023	0.921
mSR_2	0.788	0.782	0.781	0.788	0.785	0.778	0.791	0.785	0.035	0.020	0.915
mSR_3	7.826	8.112	7.767	8.171	7.905	7.629	7.747	8.596	0.576	0.431	0.273
TCARI	0.185	0.191	0.191	0.185	0.189	0.193	0.180	0.190	0.096	0.135	0.547
mCARI	0.134	0.138	0.133	0.139	0.130	0.136	0.138	0.140	0.444	0.243	0.773
CI	10.286	10.267	10.326	10.228	10.242	10.409	10.331	10.124	0.915	0.597	0.315
$VREI_1$	1.852	1.826	1.822	1.856	1.836	1.809	1.868	1.844	0.009	0.001	0.897
$VREI_2$	-0.199	-0.191	-0.189	-0.201	-0.194	-0.184	-0.205	-0.198	0.006	0.000	0.678
RENDVI	0.646	0.643	0.646	0.643	0.647	0.646	0.645	0.640	0.372	0.346	0.576
mRENDVI	0.764	0.758	0.762	0.760	0.766	0.758	0.761	0.759	0.217	0.696	0.522
MRCI	3.424	3.300	3.304	3.420	3.365	3.243	3.482	3.358	0.014	0.021	0.980
NDRE	0.388	0.381	0.379	0.390	0.384	0.375	0.393	0.387	0.021	0.002	0.683
$PSSR^a$	15.238	15.297	15.049	15.486	14.861	15.237	15.615	15.356	0.871	0.224	0.377
$PSSR^b$	13.580	13.340	13.054	13.866	12.915	13.193	14.245	13.488	0.428	0.007	0.087

NPQI	-0.002	-0.008	-0.021	0.011	-0.018	-0.024	0.013	0.008	0.000	0.000	0.661
Car/Chl ratio											
PSRI	-0.010	-0.010	-0.012	-0.008	-0.013	-0.012	-0.006	-0.009	0.069	0.000	0.000
SIPI	0.987	0.986	0.984	0.988	0.983	0.985	0.990	0.987	0.524	0.000	0.002
PRI	0.039	0.037	0.035	0.041	0.035	0.035	0.043	0.038	0.069	0.000	0.061
NPCI	-0.085	-0.082	-0.094	-0.073	-0.101	-0.086	-0.069	-0.078	0.464	0.000	0.001
SRPI	1.191	1.185	1.212	1.163	1.229	1.195	1.152	1.175	0.534	0.000	0.001
Other											
FRI	-0.337	-0.042	0.551	-0.930	0.402	0.701	-1.075	-0.784	0.000	0.000	0.955
TCARI/OSAVI	0.166	0.172	0.171	0.167	0.170	0.173	0.163	0.171	0.089	0.209	0.461
WBI/NDVI	1.118	1.117	1.111	1.124	1.113	1.108	1.123	1.125	0.842	0.024	0.572
Nitrogen content											
NDNI	0.311	0.306	0.310	0.307	0.313	0.307	0.310	0.304	0.000	0.027	0.939
Structural C											
NDLI	0.109	0.110	0.112	0.107	0.111	0.113	0.106	0.107	0.000	0.000	0.240
CAI	-0.017	-0.017	-0.019	-0.016	-0.019	-0.019	-0.016	-0.016	0.752	0.000	0.627
NDryMI	0.037	0.039	0.039	0.036	0.038	0.040	0.036	0.037	0.000	0.000	0.577
Narrow-band greenness											
$NDVI_1$	0.870	0.871	0.873	0.867	0.872	0.875	0.868	0.867	0.722	0.098	0.534
GVI	-0.338	-0.353	-0.357	-0.335	-0.351	-0.362	-0.325	-0.344	0.050	0.003	0.582
$NDVI_w$	0.869	0.869	0.871	0.867	0.870	0.873	0.868	0.866	0.855	0.228	0.417
$NDVI_n$	0.864	0.865	0.867	0.862	0.865	0.869	0.863	0.861	0.855	0.240	0.403
$GNDVI_n$	0.781	0.776	0.777	0.780	0.776	0.777	0.785	0.775	0.235	0.333	0.150
$GNDVI_w$	0.758	0.753	0.753	0.758	0.753	0.753	0.763	0.753	0.176	0.224	0.153
GNDVI	0.748	0.743	0.743	0.747	0.743	0.743	0.753	0.742	0.181	0.225	0.157
SR_1	15.527	15.588	15.344	15.771	15.149	15.540	15.905	15.637	0.867	0.243	0.368
SR_2	15.033	15.091	14.845	15.280	14.657	15.033	15.410	15.150	0.870	0.220	0.369
SR_3	6.81	6.78	6.867	6.724	6.839	6.895	6.788	6.660	0.716	0.150	0.355
SR_4	3.83	3.77	3.785	3.814	3.813	3.757	3.849	3.779	0.124	0.485	0.864
TVI	52.85	53.17	53.42	52.61	53.26	53.57	52.45	52.77	0.251	0.003	0.980
mTVI1	1.255	1.255	1.259	1.250	1.258	1.260	1.251	1.250	0.979	0.051	0.684
mTVI2	2.525	2.523	2.525	2.522	2.520	2.531	2.530	2.515	0.858	0.815	0.315
OSAVI	1.111	1.112	1.115	1.108	1.113	1.117	1.109	1.107	0.871	0.126	0.471
GI	2.148	2.212	2.211	2.150	2.184	2.237	2.113	2.187	0.915	0.597	0.315
EVI2	0.997	0.996	0.998	.995	0.996	1.000	0.998	0.991	0.671	0.502	0.264
RDVI	0.835	0.834	0.836	.833	0.835	0.836	0.835	0.831	0.678	0.293	0.328
Broad-band greenness											
TDVI	1.167	1.167	1.168	1.166	1.168	1.169	1.167	1.166	0.879	0.195	0.442
RVI	14.90	14.77	14.45	15.22	14.27	14.63	15.52	14.92	0.724	0.027	0.162
mSR_4	2.815	2.806	2.781	2.841	2.756	2.805	2.875	2.807	0.841	0.199	0.214
OSAVI	1.103	1.103	1.105	1.100	1.103	1.107	1.102	1.098	0.965	0.275	0.370
NDVI	0.862	0.863	0.865	0.860	0.863	0.867	0.862	0.859	0.885	0.228	0.432
NLI	0.843	0.843	0.844	0.841	0.843	0.846	0.843	0.839	0.998	0.363	0.382
mNLI	1.764	1.764	1.767	1.761	1.764	1.769	1.764	1.758	0.998	0.363	0.382
IPVI	0.931	0.932	0.933	0.930	0.932	0.933	0.931	0.930	0.885	0.228	0.432
GRVI	8.611	8.436	8.340	8.706	8.302	8.378	8.919	8.494	0.231	0.012	0.086
EVI	1.169	1.166	1.172	1.163	1.175	1.169	1.163	1.163	0.351	0.003	0.368
GNDVI	0.784	0.780	0.781	0.784	0.780	0.781	0.788	0.779	0.278	0.424	0.164
RNDVI	0.830	0.828	0.830	0.828	0.829	0.831	0.831	0.825	0.546	0.517	0.239
PROSPECT											
Cab	52.9	52.28	52.35	52.84	52.47	52.22	53.34	52.34	0.481	0.578	0.669
Cxc	13.64	13.84	13.54	13.93	13.15	13.94	14.12	13.74	0.627	0.353	0.164
EWT	0.013	0.012	0.012	0.012	0.013	0.012	0.013	0.012	0.001	0.968	0.846

Table S3 Significance levels of the two-way analysis of variance for a selection of spectral reflectance indices depending on water regime and on the side of the leaf in the subset of plots selected for the anatomical measurements.

	P_{WR}	P_{LS}	P_{WR*LS}
PRI	0.168	0.029	0.121
ARI	0.026	< 0.001	0.005
mARI	0.038	< 0.001	0.005
NDLI	0.540	< 0.001	0.961
CAI	0.156	0.012	0.802
MSI	0.515	0.371	0.872
PSRI	0.061	0.025	< 0.001
NDWI	0.014	0.219	0.853
NMDI	0.112	0.005	0.778
NDNI	< 0.001	0.347	0.924
MDATT	0.128	0.027	0.597
$NDMI_3$	0.248	0.020	0.792
Chl – RM	0.003	0.011	0.425
NDryMI	< 0.001	0.008	0.752

CHAPTER 4

Metabolome profiling supports the key role of the spike in wheat yield performance

Omar Vergara-Diaz, Thomas Vatter, Rubén Vicente, Toshihiro Obata, Teresa Nieto-Taladriz, Nieves Aparicio, Shawn Carlisle Kefauver, Alisdair Fernie, José Luis Araus

Submitted to:
Journal of Experimental Botany

ABSTRACT

Although the relevance of spike bracts in stress acclimation and contribution to yield was recently revealed, the metabolome of this organ and its response to water stress is still unknown. The metabolite profiles of flag leaves, glumes and lemmas were characterized under contrasting field water regimes in five durum wheat cultivars. Water conditions during growth were characterized through spectral vegetation indices, canopy temperature and isotope composition. Spike bracts exhibited better coordination of carbon and nitrogen metabolisms than the flag leaves in terms of photorespiration, nitrogen assimilation and respiration paths. This coordination facilitated an accumulation of organic and amino acids in spike bracts, especially under water stress. The metabolomic response to water stress also involved an accumulation of antioxidant and drought tolerance related sugars, particularly in the spikes. Furthermore, certain cell wall, respiratory and protective metabolites were associated with genotypic outperformance and yield stability. In addition, grain yield was strongly predicted by leaf and spike bracts metabolomes independently. This study supports the role of the spike as a key organ during wheat grain filling, particularly under stress conditions and provides information fundamental to explore new ways to improve wheat productivity including important biomarkers for yield prediction.

Title: Metabolome profiling supports the key role of the spike in wheat yield performance

Authors

Omar Vergara-Diaz[1], omarvergaradiaz@gmail.com

Thomas Vatter[1], thomasva@gmx.de

Rubén Vicente[1,2], vicenteperez.ruben@gmail.com

Toshihiro Obata[2], tobata2@unl.edu

Maria Teresa Nieto-Taladriz, mtnieto@inia.es

Nieves Aparicio Gutierrez, apagutni@itacyl.es

Shawn Carlisle Kefauver[1], sckefauver@ub.edu

Alisdair Fernie[2], Fernie@mpimp-golm.mpg.de

José Luis Araus[1*], jaraus@ub.edu

[1]Integrative Crop Ecophysiology Group, Plant Physiology Section, Faculty of Biology, University of Barcelona. Diagonal 643, 08028 Barcelona, SPAIN

[2]Max Planck Institute of Molecular Plant Physiology. Am Mühlenberg 1, 14476 Potsdam, GERMANY

*corresponding author: José Luis Araus, Faculty of Biology, University of Barcelona. Diagonal 643, 08028 Barcelona, SPAIN. Telephone number: (+34) 934021469

Date of submission: 30 July 2019

Number of tables and figures: 5 tables and 6 figures (all for colour online-only and none for colour in print)

Word count: 6314

Supplementary data: 2 tables and 3 figures

Title: Metabolome profiling supports the key role of the spike in wheat yield performance

Running title: Spike versus leaf metabolome and yield performance in wheat

Abstract

Although the relevance of spike bracts in stress acclimation and contribution to yield was recently revealed, the metabolome of this organ and its response to water stress is still unknown. The metabolite profiles of flag leaves, glumes and lemmas were characterized under contrasting field water regimes in five durum wheat cultivars. Water conditions during growth were characterized through spectral vegetation indices, canopy temperature and isotope composition. Spike bracts exhibited better coordination of carbon and nitrogen metabolisms than the flag leaves in terms of photorespiration, nitrogen assimilation and respiration paths. This coordination facilitated an accumulation of organic and amino acids in spike bracts, especially under water stress. The metabolomic response to water stress also involved an accumulation of antioxidant and drought tolerance related sugars, particularly in the spikes. Furthermore, certain cell wall, respiratory and protective metabolites were associated with genotypic outperformance and yield stability. In addition, grain yield was strongly predicted by leaf and spike bracts metabolomes independently. This study supports the role of the spike as a key organ during wheat grain filling, particularly under stress conditions and provides information fundamental to explore new ways to improve wheat productivity including important biomarkers for yield prediction.

Abbreviations

CQAs, caffeoylquinic acids; DR, detection rate; DHA, dehydroascorbate; GABA, γ-aminobutyric acid; GNY, grain nitrogen yield; GY, grain yield; HI, harvest index; HY, high yielding; LY, low yielding; PH, plant height; Pyr, pyruvate; TKW, thousand kernel weight; WS, water stress; 2OG, 2-oxoglutarate.

Introduction

The projections of the effects of global change, including increases in temperature and dryness in many regions, threaten crop production in the coming years (Field *et al.*, 2014; Asseng *et al.*, 2015). Wheat is particularly sensitive to drought at the flowering and grain filling stages, while more than 50% of the land where wheat is grown is already affected by periodic droughts (Pfeiffer *et al.*, 2005). Durum wheat is the primary crop in the south and east of the Mediterranean basin with the European Union being the leading global producer (Lidon *et al.*, 2014). In addition, genetic gain in the post-green revolution wheats has stagnated or even declined (Chairi *et al.*, 2018). In this sense, wheat breeding for water stress tolerance is urgent, particularly in regions that are highly sensitive to global

climate change such as the Mediterranean Basin (Field *et al.*, 2014). Strategies to combat these challenges should involve enhancing stress resilience and progressing field-based high-throughput phenotyping.

Multi-omics techniques have recently been used for the characterization of wheat performance under water stress (Vicente *et al.*, 2018*b*; Michaletti *et al.*, 2018). These are crucial to understand the underlying molecular mechanisms of plant responses that confer genotypic resilience to stress conditions. Water stress is known to trigger major reprogramming of plant metabolism including a decrease in photosynthetic carbon metabolism via restriction in CO_2 diffusion and inhibition of CO_2 assimilation (Tezara *et al.*, 1999), whereas photorespiration and the accumulation of reactive oxygen species increases (Ergen *et al.*, 2009). Furthermore, water stress generally inhibits nitrogen assimilation and stimulates amino acid catabolism, while the accumulation of certain amino acids can function as osmoprotectants or signaling molecules (Xu and Yu, 2006; Bown and Shelp, 2016; Ullah *et al.*, 2017). For instance, an accumulation has long been documented for certain amino acids such as proline, γ-aminobutyryc acid (GABA) and isoleucine in wheat leaves in response to water stress (Ibrahim and Abdellatif, 2016; Lou *et al.*, 2018; Michaletti *et al.*, 2018). However, no previous evidence for a functional role of these metabolites has been reported in spike bracts.

In the last few years, far more attention has been paid to the role of photosynthetic organs other than the leaf blades in plant stress acclimation, with the spikes being particularly relevant. Indeed, the spike has been shown to be a major contributor of photosynthates (Sanchez-Bragado *et al.*, 2014). Some studies have revealed that the contribution of wheat bracts to grain filling is considerable due to their higher and/or more steady photosynthesis, high carbon refixation rates, delayed senescence and high-water use efficiency compared to the flag leaves, particularly under water stress conditions (Tambussi *et al.*, 2007; Sanchez-Bragado *et al.*, 2014*a*; Jia *et al.*, 2015; Merah *et al.*, 2017; Vicente *et al.*, 2018*b*). In addition, an up-regulation of nitrogen and respiration metabolism has been reported in wheat spikes under water stress, revealing that spike bracts are active sites for nitrogen assimilation (Vicente *et al.*, 2018*b*). In sharp contrast, the metabolic and transcriptomic profiles of leaves and roots in cereals have been used for predicting complex agronomic traits including yield (Riedelsheimer *et al.*, 2012*a*,*b*; Obata *et al.*, 2015; Xu *et al.*, 2016; de Abreu e Lima *et al.*, 2017). However, the metabolome of wheat spike bracts and their response to water stress has not been characterized and, in fact, the metabolic role of the spike is not yet understood to any depth. In the present work we aimed to i) characterize the metabolome of the flag leaf and spike bracts -specifically the spike glumes and lemmas- in durum wheat in response to water stress, ii) explore the existence of organ-specific metabolic traits and physiological functions, iii) identify metabolites associated with genotypic outperformance, and iv) model metabolite-grain yield association.

Materials and Methods

Plant material and experimental set up

Field trials were carried out during the 2014/15 growing season at three locations with different growth conditions in Spain. Agronomic information together with weather, irrigation and soil information are detailed in Table 1.

The study is based on five durum wheat (*Triticum turgidum* L. subsp *durum* (Desf) Husn.) modern (i.e. semidwarf) commercial varieties released during the last thirty years in Spain. The varieties Sula, Dorondon, Pelayo, Don Sebastian and Kiko Nick, registered in the years 1994, 1999, 2003, 2004 and 2009, respectively, were selected from a panel of 20 semi-dwarf post-Green-Revolution varieties as they have been demonstrated to be representative of yield performance variability under water stress conditions while neither phenology differences -days to heading- nor genotype per environment interaction were shown (Chairi *et al.*, 2018; Fig. S1).

For each trial, plants were sown in a randomized block design with three replicates and four growing conditions were considered. First, two rainfed trials in Colmenar de Oreja and Zamadueñas that are highly restrictive environments were grouped as water stress (WS) conditions. Second, the supplemental irrigation trial of Zamadueñas and the rainfed trial of El Majano which is characterized as a high yielding environment due to its closeness to the Guadalquivir River (i.e. high-water table level) were hereafter considered as high yielding (HY) conditions. Trial grouping was further supported by yield and carbon isotope data of the same plant material in retrospective studies (Chairi *et al.*, 2018; Medina *et al.*, 2019) (Fig. 1) as well as by the similarities in metabolite variability between the rainfed and irrigated trials of Zamadueñas (Table S2).

Plant height (PH) was measured at grain filling. At harvest, grains were dried in an oven at 60ºC for 48 hours to steady weight and grain yield (GY) was determined by harvesting the whole plot. In addition, total biomass was measured and the number of grains spike^{-1} was counted in a set of 10 plants per plot. Then, thousand kernel weight (TKW) and harvest index (HI) were calculated.

Spectral and thermal field measurements

The flag leaf, spike and canopy spectral signatures were measured around midday on sunny days with a FieldSpec4 (ASD Inc. PANalytical Company, Boulder, USA) full-range portable spectroradiometer. The reflectance spectra of three flag leaves and three spikes were recorded for each plot with an ASD leaf clip accessory. Canopy spectra were measured with a pistol grip coupled by an optical fiber to the FieldSpec4 spectrometer. Measurements were made one meter above the plot canopy in a zenithal plane and the reflectance was calibrated every 15-20 minutes with a Spectralon white reference panel. Spectra were acquired at the crop development stages of anthesis and grain filling, which are

69 and 74 in the Zadoks scale (Zadoks *et al.*, 1974) respectively, on 13 April and 11 May in El Majano, 12 and 25 May in Colmenar de Oreja and 15 and 28 May in Zamadueñas. Then, three water-related spectral reflectance indices were calculated: the Normalized Difference Water Index (NDWI; Gao, 1996), the Normalized Water Index (NWI; Babar et al., 2006) and the Normalized Difference Moisture Index (NDMI; Lobos et al., 2014).

Canopy temperature was acquired in the afternoon (about 4PM) from a remotely piloted aircraft system flown in clear sky conditions using a Mikrokopter Oktokopter 6S12 XL eight rotor UAV (HiSystems GmbH, Moomerland, Germany) at an above ground level altitude of 50 m. A FLIR Tau2 640 (FLIR Systems, Nashua, NH, USA) thermal camera was mounted on a MK HiSight SLR2 camera platform and programmed for continuous capture with an image acquisition rate of 20 s^{-1}, a resolution of 640 x 520 pixels and an estimated ground spatial resolution of 54 mm per pixel. Thermal images were exported using the TEAX ThermoViewer v1.3.12 and converted to 32bit temperature in Celsius using a custom batch processing macro function in FIJI software (Schindelin *et al.*, 2012).

Leaf and spike metabolite profiling and isotope analyses

Three flag leaf blades and three spikes per plot were harvested and immediately frozen in dry ice at the stages of anthesis and middle grain filling on the same dates mentioned before. All glumes and lemmas of each of the three collected spikes per replicate were separated, and the three partitioned organs were ground in liquid nitrogen. Although awns can be important photosynthetic bracts contributing to yield (Sanchez-Bragado *et al.*, 2016) they are more affected by early senescence and were discarded in the current work. One hundred milligrams of fresh material powder from 360 samples were used for gas chromatography-mass spectrometry (GC-MS).

Metabolite extraction and derivatization were performed as an adaptation of the procedure described in Lisec et al. (2006) and Witt et al. (2012). One μl of each sample solution was injected into a gas chromatography time-of-flight mass spectrometry (GC–TOF–MS) system (Pegasus III, Leco, St Joseph, USA). The chromatogram was evaluated using GC-TOF-MS ChromaTOF software (Pegasus, LECO, St Joseph, USA). Peaks in the chromatograms were manually annotated and ion intensity was determined using TagFinder software (Luedemann *et al.*, 2011) and with a reference library derived from the Golm Metabolome-Database for compound identification (Kopka *et al.*, 2005).

The stable carbon (^{13}C:^{12}C) isotope ratio as well as the nitrogen concentration (%N) were measured in the flag leaves at grain filling and in mature grain dry matter using an elemental analyzer (Flash 1112 EA; Thermo Finnigan, Bremen, Germany) coupled with an isotope ratio mass spectrometer (Delta C IRMS, Thermo Finnigan) operating in a continuous flow mode. Samples of 0.7–1 mg of leaf and grain dry matter from each plot, together with reference materials, were weighed and sealed into tin capsules. Measurements were conducted at the Scientific Facilities of the University of

Barcelona. Isotopic values were expressed in composition notation (δ) as follows: $\delta^{13}C$ (‰) $=[(^{13}C/^{12}C)_{sample}/(^{13}C/^{12}C)_{standard}]-1$, where 'sample' refers to plant material and 'standard' to international secondary standards of known ^{13}C:^{12}C ratios (IAEA CH7 polyethylene foil, IAEA CH6 sucrose, and USGS 40 L-glutamic acid) calibrated against Vienna Pee Dee Belemnite calcium carbonate with an analytical precision (standard deviation) of 0.10‰. Grain nitrogen yield (GNY) was then calculated as the product of GY and grain %N per plot.

Statistical analysis

R 3.5.1 (R Core Team, 2018) was used for conducting multivariate ANOVAs and heatmap analyses were undertaken with the GPLOTS package (Warnes *et al.*, 2009). Principal component analysis (PCA) and correlation network analyses were performed with the PCA3D and QGRAPH packages, respectively (Epskamp *et al.*, 2012; January Weiner, 2017). Figures were drawn with SigmaPlot 10.0 (Systat Software Inc., San Jose, CA, USA).

The metabolite data used for the prediction models of GY were first revised so that those metabolites with more than 10% missing data over all samples were removed from the dataset. The remaining missing values were then interpolated with the DMwR package (Torgo, 2016) with the K-Nearest Neighbor Classification method using RStudio 3.2.2.

Yield prediction models were performed with flag leaves and spike bracts metabolite profiles at the anthesis and grain filling stages and by considering an additional $\log_2$-transformation of metabolite intensities. Individual (i.e. single plot) metabolic data for the HY and WS conditions were combined into one dataset. Identification of metabolite GY associations and GY prediction based on metabolite data was performed using least absolute shrinkage and selection operator (LASSO) regression. LASSO is a penalized logistic regression that can handle large number of predictors, which are in turn highly collinear, and precise variable selection and prediction despite small sample size. Analysis was carried out with SAS software 9.4 (SAS Institute Inc., Cary, NC, USA) applying the *proc glmselect* procedure. To increase the robustness of the results, five-fold cross-validation (CV) was conducted. In total 100 CV runs (20 times five-fold CV) were performed. For these, 100 subsets were extracted from the full dataset. Each of the subsets comprised 75% of the data points and was randomly selected. The subsets were taken as training sets for the identification of metabolite grain yield associations and for the estimation of their effects. The remaining 25% of the data was used as a validation set. To estimate the proportion of variance in grain yield explained by the model, the unbiased estimator Adj-R^2 (Draper and Smith, 1981) was calculated for each subset. As a measure of accuracy, the root mean square error (RMSE) was calculated. Effects for each metabolite were extracted as a regression coefficient of the respective metabolite directly from the LASSO model. In addition, the count of each metabolite over all training sets was recorded and referred to as the

detection rate. This value was taken as a measure of importance of the specific metabolite grain yield association. To determine the predictive ability of the full model for grain yield, the regression estimates, obtained using the training sets, were used to predict the grain yield value of the remaining 25% of data forming the validation sets. The predictive ability was defined to be the squared Pearson product-moment correlation between predicted and observed phenotypic values. The statistics provided for each model (R^2, Adj-R^2, RMSE, and metabolite effect for the training and validation sets) were averaged across all 100 CV runs to obtain the results.

In addition to the predictive ability that was estimated based on the validation dataset by combining data of HY and WS conditions, the predictive ability of the models was tested in HY and WS conditions separately. For this, multiple regression was performed by setting the metabolites that showed a detection rate of at least 70% according to the LASSO variable selection.

Results

All the agronomic traits studied decreased significantly under water stress (WS) conditions compared to the high yielding (HY) environment (Table 2); biomass decreased by 24.6%, grain yield (GY) by 37.3%, grain nitrogen yield (GNY) by 27%, thousand kernel weight (TKW) by 19.1%, harvest index (HI) by 13.8% and the number of grains spike^{-1} by 10.3%. In addition, genotypic differences were detected in GY, TKW and in the number of grains spike^{-1}. GY was significantly higher in Pelayo and Sula, followed by Kiko Nick and Dorondon with intermediate GYs, and, lastly, Don Sebastian showed the lowest grain yield. TKW was higher in Don Sebastian, Pelayo and Kiko Nick and lower in Sula and Dorondon. The number of grains spike^{-1} was higher in Dorondon and Sula, intermediate in Pelayo and lower in Kiko Nick and Don Sebastian. Grain nitrogen content was significantly higher under WS conditions, whereas it was significantly lower in the genotypes Dorondon and Sula, intermediate in Kiko Nick and Pelayo and higher in Don Sebastian.

At both growth stages canopy temperature was significantly higher under WS conditions (Table 3). The three spectral reflectance indices selected for the assessment of canopy, leaf and spike water status (NDMI, NDWI and NWI) showed a significantly higher water signal under HY conditions compared to WS conditions at both growth stages. Both leaf and grain $\delta^{13}C$ were significantly higher under WS conditions. No significant genotype per environment interaction was obtained for any of these agronomic or phenotypic traits.

Metabolome differences between organs and growth stages

Marked differences in the metabolite profiles were in part attributed to inter-organ and growth stage variability. At anthesis, the PCA (Fig. 1) explained up to 61.9% of metabolome variance with samples

being grouped according to the organ and growing environment. The separation between spike bracts and environments was less clear at grain filling. Several environments per organ and/or stage interactions were significant because metabolic changes were closely associated with the organ whereas many metabolites showed differential increasing or decreasing phenological patterns.

Except for Asp, malate, raffinose, *trans*-caffeate and threonate, which were more abundant in the leaves, there was a significantly larger accumulation of metabolites in the spike organs compared to flag leaves (Fig. 2). Additionally, the phenylpropanoids 3-*cis* and 3-*trans*-caffeoylquinic acids (CQAs), were only detected in the leaves. Concerning metabolomic differences between the two studied spike organs, many of the detected metabolites had accumulated to higher levels in the glumes than in the lemmas. Many amino acids (Hyp, Pro, 5-oxoproline, Orn, Thr, Trp and GABA) and sugars (Fru, Glc, Suc, *myo*-inositol-P, Rha), as well as many metabolites involved in respiration and photorespiration (isocitrate, succinate, 3-phosphoglycerol, Gly, Ser, glycolate and glycerate) as well as ascorbate metabolism (threonate, galactonate-1,4-lactone and glucarate-1,4-lactone) accumulated to significantly higher levels in glumes than in lemmas. In contrast, some sugars (erythrose, trehalose and maltose) and metabolites involved in respiration (2OG and Pyr) were more abundant in lemmas than in glumes.

Most of amino acids and all photorespiration intermediates decreased in all organs and conditions from anthesis to grain filling (Fig. 2). Regarding major carbohydrates, Suc, Glc and Fru contents decreased in all organs from anthesis to the grain filling stage under WS whereas in HY conditions metabolic variation depended on the organ in particular. Lastly, trehalose, erythrose, Fuc and maltose increased in leaves but decreased in spike organs from anthesis to grain filling. The relative contents of aromatic amino acids, Orn and threonate were higher during grain filling compared to anthesis in all organs and conditions and DHA, His and Lys content in spike bracts were also increased at grain filling. With respect to respiratory metabolites, some were generally increased (isocitrate, citrate, malate) and other decreased (2OG, fumarate and pyruvate) from anthesis to the grain filling stage and these changes were more pronounced under WS conditions.

Changes in the metabolome due to water stress

Wide differences in the metabolomes of leaves and spike organs were found between WS and HY conditions, with these changes being partly dependent on the organ studied and phenological stage (Fig. 3). In the following section, results are presented for the first sampling (anthesis) because at grain-filling, the differences in metabolite abundances between water conditions were less contrasted than at anthesis but the main trends were still comparable.

In all the studied organs, Fru, Glc and Suc contents increased significantly under WS compared to HY conditions. Similarly, raffinose, maltose, isomaltose and trehalose were generally increased in the

spike organs, whereas erythrose increased in the flag leaves under WS. Galactinol decreased significantly in all the organs, particularly in the spikes, whereas *myo*-inositol and *myo*-inositol-P decreased in leaves and lemmas. Regarding cell wall metabolites, the Fuc relative content decreased in the flag leaves and lemmas, with Rha increasing in the leaves and glumes, whereas cellobiose increased only in glumes.

In the case of amino acids, WS generally induced an increase in all the studied organs, but this increase was particularly pronounced in the spikes. In both spike organs Val, Ala, Asp, Gln, Met, Thr, Ile, Lys, Trp, Hyp, GABA, β-Ala, 5-oxoproline, Pro, Orn and His increased in response to WS. Additionally, Tyr, Phn, Hse, Glu and Arg content also increased in glumes under WS. In the leaves, Hyp, Arg, Lys and Pro increased significantly but Asn decreased under WS.

Whereas in leaves the relative content of photorespiratory metabolites decreased (glycerate, glycolate and Ser), in the spike bracts an increasing significant trend was observed under WS. In relation to the glycolytic pathway, Pyr decreased significantly in the leaves under WS. In the tricarboxylic acid (TCA) cycle, different changes were observed. In leaves 2OG, succinate and fumarate decreased, and citrate increased under WS. In the spike bracts malate increased under WS, whereas isocitrate increased and succinate decreased significantly in the lemmas alone, and fumarate decreased only in glumes. With regards to energy and nucleic acid metabolism, the nicotinate and adenine content increased significantly in glumes and lemmas. Meanwhile in leaves and lemmas, AMP increased and phosphate decreased under WS.

In addition, 3-phosphoglycerol increased in the spikes under WS whereas phenylpropanoids decreased significantly in the flag leaf (3-*cis*-caffeoilquinic acid, *trans*-caffeate and quinic acid) and in lemmas (quinic acid). The relative content of other secondary metabolites related to ascorbate metabolism (glucarate-1,4-lactone, galactonate-1,4-lactone and threonate) increased significantly in glumes but in leaves a variable trend was evidenced. Furthermore, in bracts there was a significant general increase across aromatic compounds.

Genotypic differences in metabolite profiles

Two genotypes contrasting in their performance under the two water conditions were considered: Pelayo, as a high yielding genotype, and Don Sebastian, as a low yielding genotype. The metabolite profiles of flag leaves, lemmas and glumes differed significantly between the two genotypes within each growing stage and environmental condition (Fig. 4).

In leaves, Pelayo generally exhibited higher levels of major sugars, glycan-related sugars and others (Suc, Fru, Fuc, Xyl, Rha and isocitrate) than in Don Sebastian, whereas the opposite occurred with phenylpropanoids, aromatics, some amino acids and other metabolites (CQAs, *trans*-caffeate

hydroxy-pyridines, adenine, GABA, Gly, Trp, Orn, Ser, glycolate, galactinol and trehalose). In the two spike bracts, Pelayo showed generally higher contents of 4-hydroxy-*trans*-cinnamate and isocitrate compared with Don Sebastian, while in lemmas there was higher contents of threonate and glycerate and in glumes higher levels of Fru, isomaltose, Fuc and Xyl in Pelayo than in Don Sebastian.

At anthesis, spike bracts of Don Sebastian exhibited in general higher content in most of amino acids at anthesis and other metabolites such as DHA, malate and 3-phosphoglycerol than Don Sebastian. In contrast, the opposite trend was observed at grain filling but no significant differences between genotypes (except for Hyp in lemmas) were detected. It is likely that the higher amino acid contents in bracts of Don Sebastian at anthesis were due to lower rates of spike growth, while N assimilation continued to be active. In addition, the higher grain %N in Don Sebastian would likely be a consequence of the remobilization of N compounds to its lower number of grains spike^{-1} rather than a higher rate of N assimilation occurring in Don Sebastian compared to Pelayo.

Predicting yield from metabolite profiles

The metabolome of the flag leaf blade and spike bracts proved strongly associated with GY and the closest fitting regression models were obtained when the metabolite profiles at anthesis were employed (Table 4). The metabolite profiles of leaves (raw metabolite intensity) explained up to 73.6% (Adj-R^2) of GY variability in the training set and 65.2% of yield variability in the validation set (RMSE=0.882). The metabolite profiles of the lemmas (log_2-transformed metabolite intensity) explained up to 83.4% of yield variability in the training set and 65.5% in the validation set (RMSE=0.878). Finally, the glume metabolite profiles (raw metabolite intensity) explained 78.4% of yield variability in the training set and 56.2% in the validation set (RMSE=0.975). At the grain filling stage, the metabolite profiles of leaves, glumes and lemmas still explained much of the GY variability; 63.8%, 45.7% and 35.8% for the validation sets, respectively (Table 4).

The metabolites with the highest detection rate (DR) in the LASSO variable selection, along with their positive or negative effect on yield, are shown in Table 5. Calculation of the DR revealed variation in the importance of metabolite-GY associations between organs and growth stages. Whereas amino acids generally related to yield negatively, some organic acids and sugars related to protective, osmotic or cell wall metabolisms affected yield positively (Table 5). Thus, correlations of leaf and spike bracts metabolites with GY were particularly strong for fucose (positive correlation) and proline (negative correlation) (Fig. S3).

In the multiple regression models (using metabolites with DR≥70%), the metabolite profiles of leaves, lemmas and glumes significantly predicted yield variability in the whole set of data at anthesis as well as in the WS and HY growing conditions, separately (Fig. 5A). In this analysis, the lemma metabolome provided the most accurate yield prediction from its metabolite profile, explaining up to 83.9% of

yield variability, followed by leaves (Adj-R^2= 0.764) and glumes (Adj-R^2=0.712) for the whole set of data. Despite all regressions being significant, under WS the metabolite variability always enhanced the yield prediction accuracy compared to HY conditions.

GY variance explained by the metabolites for the three organ-specific models showed that in leaves Fuc and Pro jointly explained above 36% of GY variation, succinate and glucarate-1,4-lactone explained about 28% and the remaining explained 12% of yield variation (Fig. 5B). In bracts, Val explained between 25 to 34% and isomaltose between 10 to 19% of yield variation in lemmas and glumes, respectively. Besides, in lemmas malate and Hyp jointly reached 32% of yield variation, raffinose and glycerol explained almost 12% whereas succinate, threonate and GABA content jointly explained 5% of yield variation. Additionally, in glumes, the remaining Glu, N-acetylserine and *myo*-inositol jointly explained above 18% of yield variation.

At anthesis, the Pro (and usually Hyp) contents of the leaves, lemmas and glumes were associated with decreasing PH, biomass, HI, number of spikes m^{-2} and TKW and with increasing $\delta^{13}C$ (Fig. S2). Respiratory metabolites in both leaves and spike bracts were largely positively associated with increasing PH, biomass, HI, spikes m^{-2} and TKW. In leaves and glumes, the sugar alcohols (glycerol, galactinol and *myo*-inositol) were positively correlated with increasing HI, TKW, biomass, spikes m^{-2} and grains $spike^{-1}$. However, 3-phosphoglycerol in bracts was negatively correlated with PH and HI and strongly positively correlated with $\delta^{13}C$. By contrast, amino acids in the leaves and bracts were generally positively associated with increasing spikes m^{-2}, PH, HI and with decreasing grains $spike^{-1}$ and biomass. Most amino acids also correlated negatively with $\delta^{13}C$, except Ala, Glu and β-Ala in the spikes, which correlated positively with this parameter. Several sugars (mostly maltose, isomaltose, Fru, and Glc, but in some cases Rha, trehalose, raffinose and erythrose) correlated negatively with spikes m^{-2}, biomass, PH and HI, but positively correlated with grain $\delta^{13}C$. Fuc content in leaves and lemmas correlated positively with the number of grains m^{-2}, GNY, HI, and Biomass

Discussion

In this study, the decrease in biomass, GY and all yield components under WS conditions compared with the high yielding trials was associated with water stress as shown by the increase in leaf $\delta^{13}C$, an even larger increase in grain $\delta^{13}C$ (Table 3) and the strong negative correlation between $\delta^{13}C$ and grain yield across genotypes, plots and trials (adj.R^2 = 0.405; p-value < 0.0001; not shown)(Araus *et al.*, 2003, 2013). In addition, thermal and spectral indices also evidenced the better water status in the high yielding trials at both the canopy and plant levels (Zarco-Tejada *et al.*, 2004; Araus and Cairns, 2014).

Genotypic differences in final yield among the five genotypes tested were partly explained by the decreased number of grains spike^{-1}, which may be the consequence of smaller spike size together with a poorer grain set due to water stress (Farooq *et al.*, 2014).

Metabolic overview of wheat flag leaves and spike bracts and their phenology-associated changes

The observed higher levels of the majority of detected metabolites in glumes and lemmas compared to flag leaves (Fig. 2) may be a consequence of i) the closeness to the grain (Bort *et al.*, 1995) and ii) the active metabolic role of spikes as sink organs, but iii) also due to their role in assimilation and refixation (Tambussi *et al.*, 2007; Vicente *et al.*, 2018*b*). Higher levels of the major sugars and of most of the amino acids in the spike bracts, particularly in the glumes, may indicate the significant contribution of wheat bracts to grain carbon, via photosynthesis and carbon refixation, and of nitrogen, via primary assimilation and/or recycling, particularly under water stress (Tambussi *et al.*, 2007; Sanchez-Bragado *et al.*, 2014*a*; Jia *et al.*, 2015; Merah *et al.*, 2017; Vicente *et al.*, 2018*b*). Higher levels of photorespiratory and TCA-cycle intermediates in the spikes suggest the occurrence of considerable photorespiratory rates, recycling of ammonia and provision of carbon skeletons which facilitated the increased synthesis and/or accumulation of amino acids in the spike bracts (Keys and Leegood, 2002).

The ascorbate dependent detoxification machinery seemed to be increased in glumes, which is in agreement with recent work at the transcript and enzyme activity levels (Lou *et al.*, 2018; Vicente *et al.*, 2018*b*). Furthermore, some sugars in lemmas (trehalose, maltose and erythrose) could have relevant functions as sugar storage, signaling and water stress tolerance (Martínez-Barajas *et al.*, 2011; Alam *et al.*, 2014; Ilhan *et al.*, 2015; Ibrahim and Abdellatif, 2016). In contrast, higher raffinose and malate content in leaves may be evidence the accumulation of photosynthates (Van den Ende, 2013) and/or a role in osmotic regulation (Acosta-Motos *et al.*, 2017) among other functions. Unlike spikes, the outstanding detection of phenylpropanoids in leaves may act as sun-screens and antioxidants (Masuda *et al.*, 2008; Cheynier *et al.*, 2013).

Concerning metabolome changes from anthesis to grain filling (Fig. 2), most metabolites decreased in leaves and spike bracts, which can be attributed to sugar and amino acid catabolism and remobilization to the grains. However, in spikes the aromatic and urea-cycle amino acids showed increasing trends over time, mainly under WS conditions, suggesting amino acid catabolism and N remobilization (Hildebrandt et al., 2015). The increased intermediates of the TCA-cycle in the spikes, mainly under WS, could meet the increasing demand for amino and organic acids, via anaplerotic reactions, for their remobilization to the grain. Moreover, the increase in DHA and threonate levels

in the spike bracts suggest that antioxidant machinery was likely involved in the maintenance of spike functioning at the end of plant cycle (Lou *et al.*, 2018).

Water stress effects on flag leaf and spike metabolomes

Water stress impacted broadly on leaf and spike bract metabolomes, particularly at the anthesis stage with a remarkable accumulation of major sugars and the amino acids Pro, Hyp and Lys (Fig. 3, 6). These changes were likely due to growth cessation and a reduction in the consumption of metabolites and may participate in cell osmotic adjustment (Obata and Fernie, 2012). At grain filling, water stress-induced differences were mostly observed in the spike bracts (Table S1), which displayed a greater metabolic response than flag leaves (Tambussi *et al.*, 2007; Jia *et al.*, 2015; Merah *et al.*, 2017).

The water stress-induced increase in amino acid content was remarkably more prominent in spike bracts than in flag leaves (Fig. 3). In Vicente et al. (2018), an upregulation of *NR*, *NIR* and *GS2* genes, the key enzymes in the primary N assimilation pathway, was observed in durum wheat spikes, in contrast to flag leaves under water stress. These changes, together with the increase in several organic and amino acids in the present study, support an optimal coordination of carbon and nitrogen metabolism in spikes for the provision of nitrogen-rich compounds to the developing grain. This coordination was previously observed in durum wheat leaves (Vicente *et al.*, 2018*a*), but has not previously been observed in spikes.

In concordance with the changes observed in gene expression (Vicente *et al.*, 2018*b*), respiratory intermediates generally decreased in leaves, while they increased in spike bracts under WS. The strong decrease in 2-oxogluatarate (a key metabolite required for ammonia assimilation) in leaves, could indicate a breakdown in the link between C and N metabolism under WS, while no changes were observed in spike bracts. At the same time, the increased photorespiration intermediates in spike organs in response to WS could be attributed to higher rates of photorespiration under drought (Timm *et al.*, 2013). This may support an enhancement of N recycling in coordination with respiratory metabolism, thereby contributing to the increased biosynthesis of amino acids in spike bracts (Rachmilevitch *et al.*, 2004; Zhao *et al.*, 2015). In addition, the remarkable increase of the branched chain amino acids in spikes under WS may be physiologically relevant as alternative respiratory substrates under stress, either directly via electron transfer to the flavoprotein complex or indirectly via the TCA-cycle from their catabolic products (Obata and Fernie, 2012; Hildebrandt *et al.*, 2015).

Unlike leaves, the increase of other sugars in spikes, particularly glumes, (raffinose, maltose, isomaltose and trehalose) may prevent oxidative damage (Van den Ende, 2013) and could contribute to water stress tolerance (Martínez-Barajas *et al.*, 2011; Ibrahim and Abdellatif, 2016) which partly explains the strong performance of spikes under stress (Tambussi *et al.*, 2007; Vicente *et al.*, 2018*b*).

Other water stress-induced metabolic changes concern structural elements (cell wall related sugars, phenylpropanoids and Hyp) perhaps promoting a modulation in the composition of the cell wall and membranes and cell wall thickening (Zhao *et al.*, 2015) assisting in tolerance of water stress.

Recent studies have reported higher antioxidant enzyme activities and transcript abundances in wheat spikes compared to flag leaves (Kong *et al.*, 2015; Lou *et al.*, 2018; Vicente *et al.*, 2018*b*). In our study, the increased precursors of ascorbate in glumes and leaves may be as a consequence of a higher sun-exposition during the reproductive period of the crop. Complementarily, the moderate increase in aromatic amino acids in glumes under WS could be evidence of an increasing demand for precursors for the synthesis of antioxidants (e.g. flavonoids) (Bowne *et al.*, 2012). The accumulation of other metabolites (GABA, 5-oxoproline, adenine and aromatics) in spike bracts under WS could also have a protective function (Noctor *et al.*, 2012; Sukrong *et al.*, 2012; Hildebrandt *et al.*, 2015; Bown and Shelp, 2016).

Genotypic metabolic variation

Genotypic differences associated with yield performance (Fig. 4, 6) involved two main metabolic events: changes in cell structural elements and carbon assimilation.

Firstly, in Pelayo (HY genotype) the accumulation of cell-wall monosaccharides, involved in glycan-structures synthesis, in the leaves and cinnamic acids, related with lignin composition, in the spikes suggest that alterations in the cell wall and membranes may occur contributing to drought acclimation and yield stability (Vanholme *et al.*, 2010; Salvador *et al.*, 2013; Quan *et al.*, 2016). By contrast, the increase in leaf phenylpropanoids and precursors in Don Sebastian (LY genotype) may result in an increase in lignin deposition and consequently an inhibition of growth (Bubna *et al.*, 2011).

Secondly, increasing photosynthates in the leaves and glumes of the HY genotype suggest enhanced carbon assimilation including refixation (Zhao *et al.*, 2015) and carbon remobilization to the grain. The generally increased isocitrate content in leaves and bracts of Pelayo could be associated with energy metabolism, but also with secondary metabolism (Araújo *et al.*, 2014) and with the accumulation of carbon compounds when N is limited (Popova and Pinheiro de Carvalho, 1998). Further research on this topic may clarify how isocitrate contributes to genotypic outperformance.

Prediction of yield by spike bracts and flag leaf metabolomes

The LASSO statistical approach has proven its performance in metabolomic data sets with improvements over standard linear regression models, including PLS-based models (Bujak *et al.*, 2016). Obata et al. (2015) predicted satisfactorily maize grain yield from the leaf metabolome, revealing metabolic traits that may contribute to yield maintenance under abiotic stress conditions.

In our study using wheat, the spike bract metabolome, particularly of the lemmas, proved to be as determinant for final crop yield determination as the leaves, confirming the relevance of spike metabolism (Sanchez-Bragado *et al.*, 2014*a*; Vicente *et al.*, 2018*b*).

The negative association of amino acids with yield (Table 5, Fig. 5B) supports the concept that some metabolites classically assumed to have a drought-tolerance role (e.g. proline) (Saeedipour, 2013) were instead stress indicators that accumulated as compatible solutes and osmoprotectants. Interestingly, in the spikes Val rather than Pro seemed to play a key role as indicator of stress severity and yield losses, likely functioning as osmoprotectants and/or substrate for further energetic reactions (Araujo *et al.*, 2010; Hildebrandt *et al.*, 2015). Also, 3-phosphoglycerol in spike bracts appeared to be an excellent indicator of water stress as inferred by its strong correlation with grain $\delta^{13}C$ (Fig. S2) which increases with increasing water stress throughout crop growth.

In leaves, Fuc may confer firmer and more resistant cell walls (Reiter *et al.*, 1993), while succinate most likely feeds energetic and anaplerotic pathways, thus showed interesting metabolic targets for higher yields (Fig. S3). In the spike bracts, HY performance was positively associated with, among other things i) ascorbate and glutathione-related metabolites (*N*-acetylserine and threonate) which make up an essential antioxidant system and have a role in plant development and stress responses (Noctor *et al.*, 2012), ii) *myo*-inositol as an abiotic stress tolerance inducer (Obata *et al.*, 2015), iii) GABA and glycerol likely involved in osmotic adjustment, redox control and carbon-nitrogen balance (Chen and Jiang, 2010; Bouché and Fromm, 2004; Batushansky *et al.*, 2014). Therefore, the existence of active antioxidant and osmoprotective machinery in spike bracts is likely to have enabled appropriate functioning of other metabolic processes such as C and N assimilation during water stress conditions (Kong *et al.*, 2015) or counteracted the typically higher temperatures observed in bracts compared to leaves (Vicente *et al.*, 2018*b*), contributing positively to crop yield.

Finally, the positive correlation of leaf and spike bract respiratory intermediates and sugar alcohols with grain yield and most of the agronomical yield components (Fig. S2), including HI and TKW, suggests a direct or indirect role of these metabolites in grain filling that should be studied further.

Concluding remarks

Our study revealed that the spike bract metabolome is strongly responsive to water stress, and far more noticeably than the flag leaf. Unlike leaves, a strong coordination between C and N metabolisms via primary nitrogen assimilation, the photorespiratory nitrogen cycle and the TCA-cycle was evidenced in wheat spikes, particularly under WS, culminating in an active biosynthesis of organic and amino acids (Fig. 6). Additionally, the levels of carbon fixation and/or refixation in spikes were remarkable as inferred by the levels of photosynthates. The superior physiological outperformance of the spikes compared to the flag leaf under WS was furthermore related to an

active antioxidant machinery. Moreover, metabolite-GY association models indicated the key metabolites associated with genotypic outperformance, highlighting the association of respiratory, cell wall and antioxidant metabolites with water stress acclimation and yield stability. Drought resilience may be mediated, at least in part, by the high performance of the spikes. These findings therefore indicate that spike metabolic traits are a suitable breeding target. The results from the current study provide information fundamental to the understanding of wheat physiology as well as providing important biomarkers for yield prediction.

Supplementary data

Table S1. Metabolite means

Table S2. Metabolite change in Zamadueñas

Fig. S1. Yield variability

Fig. S2. Correlation network

Acknowledgments

We thank Jesús Mérida for field trial design and management and Max Plank technicians for their assistance. This work was supported by the Spanish Ministry of Economy and Competitiveness (MEC) [grant number AGL2016-76527- R]. S.C.K. is the recipient of a Juan de la Cierva Research grant from the MEC [IJCI2014-20595]. O.V.D. is the recipient of the APIF fellowship sponsored by the University of Barcelona. We thank the Goetz Instrument Program from the ASD PANalytical Company for providing us with the FieldSpec4 spectrometer.

References

de Abreu e Lima F, Westhues M, Cuadros-Inostroza Á, Willmitzer L, Melchinger AE, Nikoloski Z. 2017. Metabolic robustness in young roots underpins a predictive model of maize hybrid performance in the field. The Plant Journal **90**, 319–329.

Acosta-Motos J, Ortuño M, Bernal-Vicente A, *et al.* 2017. Plant Responses to Salt Stress: Adaptive Mechanisms. Agronomy **7**, 18.

Alam MM, Nahar K, Hasanuzzaman M, Fujita M. 2014. *Trehalose-induced drought stress tolerance: A comparative study among different Brassica species*.

Araujo WL, Ishizaki K, Nunes-Nesi A, *et al.* 2010. Identification of the 2-Hydroxyglutarate and Isovaleryl-CoA Dehydrogenases as Alternative Electron Donors Linking Lysine Catabolism to the

Electron Transport Chain of Arabidopsis Mitochondria. THE PLANT CELL ONLINE **22**, 1549–1563.

Araújo WL, Martins AO, Fernie AR, Tohge T. 2014. 2-Oxoglutarate: linking TCA cycle function with amino acid, glucosinolate, flavonoid, alkaloid, and gibberellin biosynthesis. Frontiers in Plant Science **5**, 552.

Araus JL, Cabrera-Bosquet L, Serret MD, Bort J, Nieto-Taladriz MT. 2013. Comparative performance of δ13C, δ18O and δ15N for phenotyping durum wheat adaptation to a dryland environment. Functional Plant Biology **40**, 595.

Araus JL, Cairns JE. 2014. Field high-throughput phenotyping: the new crop breeding frontier. Trends in plant science **19**, 52–61.

Araus JL, Kefauver SC, Zaman-Allah M, Olsen MS, Cairns JE. 2018. Translating High-Throughput Phenotyping into Genetic Gain. Trends in Plant Science **23**, 451–466.

Araus JL, Villegas D, Aparicio N, del Moral LFG, El Hani S, Rharrabti Y, Ferrio JP, Royo C. 2003. Environmental Factors Determining Carbon Isotope Discrimination and Yield in Durum Wheat under Mediterranean Conditions. Crop Science **43**, 170.

Asseng S, Ewert F, Martre P, *et al.* 2015. Rising temperatures reduce global wheat production. Nature Climate Change **5**, 143–147.

Babar MA, Reynolds MP, van Ginkel M, Klatt AR, Raun WR, Stone ML. 2006. Spectral Reflectance Indices as a Potential Indirect Selection Criteria for Wheat Yield under Irrigation. Crop Science **46**, 578.

Batushansky A, Kirma M, Grillich N, Toubiana D, Pham PA, Balbo I, Fromm H, Galili G, Fernie AR, Fait A. 2014. Combined Transcriptomics and Metabolomics of Arabidopsis thaliana Seedlings Exposed to Exogenous GABA Suggest Its Role in Plants Is Predominantly Metabolic. Molecular Plant **7**, 1065–1068.

Bort J, Brown RH, Araus JL. 1995. Lack of C4 photosynthetic metabolism in ears of C3 cereals. Plant, Cell and Environment **18**, 697–702.

Bouché N, Fromm H. 2004. GABA in plants: just a metabolite? Trends in Plant Science **9**, 110–115.

Bown AW, Shelp BJ. 2016. Plant GABA: Not Just a Metabolite. Trends in plant science **21**, 811–813.

Bowne JB, Erwin TA, Juttner J, Schnurbusch T, Langridge P, Bacic A, Roessner U. 2012. Drought Responses of Leaf Tissues from Wheat Cultivars of Differing Drought Tolerance at the Metabolite Level. Molecular Plant **5**, 418–429.

Bubna GA, Lima RB, Zanardo DYL, dos Santos WD, Ferrarese M de LL, Ferrarese-Filho O. 2011. Exogenous caffeic acid inhibits the growth and enhances the lignification of the roots of soybean (Glycine max). Journal of Plant Physiology **168**, 1627–1633.

Bujak R, Daghir-Wojtkowiak E, Kaliszan R, Markuszewski MJ. 2016. PLS-Based and Regularization-Based Methods for the Selection of Relevant Variables in Non-targeted Metabolomics Data. Frontiers in Molecular Biosciences **3**, 35.

Chairi F, Vergara-Diaz O, Vatter T, Aparicio N, Nieto-Taladriz MT, Kefauver SC, Bort J, Serret MD, Araus JL. 2018. Post-green revolution genetic advance in durum wheat: The case of Spain. Field Crops Research **228**, 158–169.

Chen H, Jiang J-G. 2010. Osmotic adjustment and plant adaptation to environmental changes related to drought and salinity. Environmental Reviews **18**, 309–319.

Cheynier V, Comte G, Davies KM, Lattanzio V, Martens S. 2013. Plant phenolics: Recent advances on their biosynthesis, genetics, and ecophysiology. Plant Physiology and Biochemistry **72**, 1–20.

Draper NR, Smith H. 1981. *Applied Regression Analysis*.

Van den Ende W. 2013. Multifunctional fructans and raffinose family oligosaccharides. Frontiers in plant science **4**, 247.

Epskamp S, Cramer AOJ, Waldorp LJ, Schmittmann VD, Borsboom D. 2012. qgraph : Network Visualizations of Relationships in Psychometric Data. Journal of Statistical Software **48**, 1–18.

Ergen NZ, Thimmapuram J, Bohnert HJ, Budak H. 2009. Transcriptome pathways unique to dehydration tolerant relatives of modern wheat. Functional & Integrative Genomics **9**, 377–396.

Farooq M, Hussain M, Siddique KHM. 2014. Drought Stress in Wheat during Flowering and Grain-filling Periods. Critical Reviews in Plant Sciences **33**, 331–349.

Field CB, Barros VR, Intergovernmental Panel on Climate Change. Working Group II D, *et al.* 2014. *Climate change 2014 : impacts, adaptation, and vulnerability : Working Group II contribution to the fifth assessment report of the Intergovernmental Panel on Climate Change*.

Gao B. 1996. NDWI—A normalized difference water index for remote sensing of vegetation liquid water from space. Remote Sensing of Environment **58**, 257–266.

Hildebrandt TM, Nunes Nesi A, Araújo WL, Braun H-P. 2015. Amino Acid Catabolism in Plants. Molecular Plant **8**, 1563–1579.

Ibrahim HA, Abdellatif YMR. 2016. Effect of maltose and trehalose on growth, yield and some biochemical components of wheat plant under water stress. Annals of Agricultural Sciences **61**, 267–274.

Ilhan S, Ozdemir F, Bor M. 2015. Contribution of trehalose biosynthetic pathway to drought stress tolerance of *Capparis ovata* Desf (T Elzenga, Ed.). Plant Biology **17**, 402–407.

January Weiner M. 2017. *Package 'pca3d' Type Package Title Three Dimensional PCA Plots*.

Jia S, Lv J, Jiang S, Liang T, Liu C, Jing Z. 2015. Response of wheat ear photosynthesis and photosynthate carbon distribution to water deficit. Photosynthetica **53**, 95–109.

Keys AJ, Leegood RC. 2002. Photorespiratory Carbon and Nitrogen Cycling: Evidence from Studies of Mutant and Transgenic Plants. Photosynthetic Nitrogen Assimilation and Associated Carbon and Respiratory Metabolism. Dordrecht: Kluwer Academic Publishers, 115–134.

Kong L, Sun M, Xie Y, Wang F, Zhao Z. 2015. Photochemical and antioxidative responses of the glume and flag leaf to seasonal senescence in wheat. Frontiers in Plant Science **6**, 358.

Kopka J, Schauer N, Krueger S, *et al.* 2005. GMD@CSB.DB: the Golm Metabolome Database. Bioinformatics **21**, 1635–1638.

Lidon F, Almeida A, Leitao A, Silva M, Pinheiro N, Macas B, Costa R. 2014. A synoptic overview of durum wheat production in the Mediterranean region and processing following the European Union requirements. Emirates Journal of Food and Agriculture **26**, 693.

Lisec J, Schauer N, Kopka J, Willmitzer L, Fernie AR. 2006. Gas chromatography mass spectrometry–based metabolite profiling in plants. Nature Protocols **1**, 387–396.

Lobos GA, Matus I, Rodriguez A, Romero-Bravo S, Araus JL, del Pozo A. 2014. Wheat genotypic variability in grain yield and carbon isotope discrimination under Mediterranean conditions

assessed by spectral reflectance. Journal of Integrative Plant Biology **56**, 470–479.

Lou L, Li X, Chen J, Li Y, Tang Y, Lv J. 2018. Photosynthetic and ascorbate-glutathione metabolism in the flag leaves as compared to spikes under drought stress of winter wheat (Triticum aestivum L.). PLoS ONE.

Luedemann A, von Malotky L, Erban A, Kopka J. 2011. TagFinder: Preprocessing Software for the Fingerprinting and the Profiling of Gas Chromatography–Mass Spectrometry Based Metabolome Analyses. Methods in molecular biology (Clifton, N.J.).255–286.

Martínez-Barajas E, Delatte T, Schluepmann H, de Jong GJ, Somsen GW, Nunes C, Primavesi LF, Coello P, Mitchell RAC, Paul MJ. 2011. Wheat grain development is characterized by remarkable trehalose 6-phosphate accumulation pregrain filling: tissue distribution and relationship to SNF1-related protein kinase1 activity. Plant physiology **156**, 373–81.

Masuda T, Yamada K, Akiyama J, Someya T, Odaka Y, Takeda Y, Tori M, Nakashima K, Maekawa T, Sone Y. 2008. Antioxidation Mechanism Studies of Caffeic Acid: Identification of Antioxidation Products of Methyl Caffeate from Lipid Oxidation. Journal of Agricultural and Food Chemistry **56**, 5947–5952.

Medina S, Vicente R, Nieto-Taladriz MT, Aparicio N, Chairi F, Vergara-Diaz O, Araus JL. 2019. The Plant-Transpiration Response to Vapor Pressure Deficit (VPD) in Durum Wheat Is Associated With Differential Yield Performance and Specific Expression of Genes Involved in Primary Metabolism and Water Transport. Frontiers in Plant Science **9**, 1994.

Merah O, Evon P, Monneveux P. 2017. Participation of Green Organs to Grain Filling in Triticum turgidum var durum Grown under Mediterranean Conditions. International journal of molecular sciences **19**.

Michaeli S, Fromm H. 2015. Closing the loop on the GABA shunt in plants: are GABA metabolism and signaling entwined? Frontiers in plant science **6**, 419.

Michaletti A, Naghavi MR, Toorchi M, Zolla L, Rinalducci S. 2018. Metabolomics and proteomics reveal drought-stress responses of leaf tissues from spring-wheat. Scientific Reports **8**, 5710.

Noctor G, Mhamdi A, Chaouch S, Han Y, Neukermans J, Marquez-Garcia B, Queval G, Foyer CH. 2012. Glutathione in plants: an integrated overview. Plant, Cell & Environment **35**, 454–484.

Obata T, Fernie AR. 2012. The use of metabolomics to dissect plant responses to abiotic stresses. **69**, 3225–3243.

Obata T, Witt S, Lisec J, Palacios-Rojas N, Florez-Sarasa I, Yousfi S, Araus JL, Cairns JE, Fernie AR. 2015. Metabolite Profiles of Maize Leaves in Drought, Heat, and Combined Stress Field Trials Reveal the Relationship between Metabolism and Grain Yield. Plant physiology **169**, 2665–83.

Pfeiffer W, Trethowan R, Ginkel M, Ortiz-Monasterio I, Rajaram S. 2005. Breeding for abiotic stress tolerance in wheat. Abiotic stresses plant resistance through breeding and molecular approaches. No. CIS-4737. CIMMYT, 401–489.

Popova TN, Pinheiro de Carvalho MÂ. 1998. Citrate and isocitrate in plant metabolism. Biochimica et Biophysica Acta (BBA) - Bioenergetics **1364**, 307–325.

Quan N, Anh L, Khang D, *et al.* 2016. Involvement of Secondary Metabolites in Response to Drought Stress of Rice (Oryza sativa L.). Agriculture **6**, 23.

R Core Team. 2018. R: A Language and Environment for Statistical Computing.

Rachmilevitch S, Cousins AB, Bloom AJ. 2004. Nitrate assimilation in plant shoots depends on

photorespiration. Proceedings of the National Academy of Sciences of the United States of America **101**, 11506–10.

Reiter WD, Chapple CC, Somerville CR. 1993. Altered growth and cell walls in a fucose-deficient mutant of Arabidopsis. Science (New York, N.Y.) **261**, 1032–5.

Riedelsheimer C, Czedik-Eysenberg A, Grieder C, Lisec J, Technow F, Sulpice R, Altmann T, Stitt M, Willmitzer L, Melchinger AE. 2012*a*. Genomic and metabolic prediction of complex heterotic traits in hybrid maize. Nature Genetics **44**, 217–220.

Riedelsheimer C, Lisec J, Czedik-Eysenberg A, Sulpice R, Flis A, Grieder C, Altmann T, Stitt M, Willmitzer L, Melchinger AE. 2012*b*. Genome-wide association mapping of leaf metabolic profiles for dissecting complex traits in maize. Proceedings of the National Academy of Sciences of the United States of America **109**, 8872–7.

Saeedipour S. 2013. Relationship of Grain Yield, ABA and Proline Accumulation in Tolerant and Sensitive Wheat Cultivars as Affected by Water Stress. Proceedings of the National Academy of Sciences, India Section B: Biological Sciences **83**, 311–315.

Salvador VH, Lima RB, dos Santos WD, Soares AR, Böhm PAF, Marchiosi R, Ferrarese M de LL, Ferrarese-Filho O. 2013. Cinnamic acid increases lignin production and inhibits soybean root growth. PloS one **8**, e69105.

Sanchez-Bragado R, Elazab A, Zhou B, Serret MD, Bort J, Nieto-Taladriz MT, Araus JL. 2014*a*. Contribution of the ear and the flag leaf to grain filling in durum wheat inferred from the carbon isotope signature: Genotypic and growing conditions effects. Journal of Integrative Plant Biology **56**, 444–454.

Sanchez-Bragado R, Molero G, Reynolds MP, Araus JL. 2014*b*. Relative contribution of shoot and ear photosynthesis to grain filling in wheat under good agronomical conditions assessed by differential organ δ13C. Journal of experimental botany **65**, 5401–13.

Sanchez-Bragado R, Molero G, Reynolds MP, Araus JL. 2016. Photosynthetic contribution of the ear to grain filling in wheat: a comparison of different methodologies for evaluation. Journal of Experimental Botany **67**, 2787–2798.

Schindelin J, Arganda-Carreras I, Frise E, *et al.* 2012. Fiji: an open-source platform for biological-image analysis. Nature Methods **9**, 676–682.

Sengupta S, Mukherjee S, Basak P, Majumder AL. 2015. Significance of galactinol and raffinose family oligosaccharide synthesis in plants. Frontiers in plant science **6**, 656.

Sukrong S, Yun K-Y, Stadler P, Kumar C, Facciuolo T, Moffatt BA, Falcone DL. 2012. Improved Growth and Stress Tolerance in the Arabidopsis oxt1 Mutant Triggered by Altered Adenine Metabolism. Molecular Plant **5**, 1310–1332.

Tambussi EA, Bort J, Guiamet JJ, Nogués S, Araus JL. 2007. The Photosynthetic Role of Ears in C_3 Cereals: Metabolism, Water Use Efficiency and Contribution to Grain Yield. Critical Reviews in Plant Sciences **26**, 1–16.

Tezara W, Mitchell VJ, Driscoll SD, Lawlor DW. 1999. Water stress inhibits plant photosynthesis by decreasing coupling factor and ATP. Nature **401**, 914–917.

Timm S, Florian A, Wittmiss M, Jahnke K, Hagemann M, Fernie AR, Bauwe H. 2013. Serine Acts as a Metabolic Signal for the Transcriptional Control of Photorespiration-Related Genes in Arabidopsis. PLANT PHYSIOLOGY **162**, 379–389.

Ullah N, Yüce M, Neslihan Öztürk Gökçe Z, Budak H. 2017. Comparative metabolite profiling of drought stress in roots and leaves of seven Triticeae species. BMC Genomics **18**, 969.

Vanholme R, Demedts B, Morreel K, Ralph J, Boerjan W. 2010. Lignin biosynthesis and structure. Plant physiology **153**, 895–905.

Vicente R, Martínez-Carrasco R, Pérez P, Morcuende R. 2018*a*. New insights into the impacts of elevated CO 2 , nitrogen, and temperature levels on the regulation of C and N metabolism in durum wheat using network analysis. New Biotechnology **40**, 192–199.

Vicente R, Vergara-Díaz O, Medina S, Chairi F, Kefauver SC, Bort J, Serret MD, Aparicio N, Araus JL. 2018*b*. Durum wheat ears perform better than the flag leaves under water stress: Gene expression and physiological evidence. Environmental and Experimental Botany **153**, 271–285.

Vogt T. 2010. Phenylpropanoid Biosynthesis. Molecular Plant **3**, 2–20.

Witt S, Galicia L, Lisec J, Cairns J, Tiessen A, Araus JL, Palacios-Rojas N, Fernie AR. 2012. Metabolic and Phenotypic Responses of Greenhouse-Grown Maize Hybrids to Experimentally Controlled Drought Stress. Molecular Plant **5**, 401–417.

Xu S, Xu Y, Gong L, Zhang Q. 2016. Metabolomic prediction of yield in hybrid rice. The Plant Journal **88**, 219–227.

Xu Z-Z, Yu Z-W. 2006. Nitrogen metabolism in flag leaf and grain of wheat in response to irrigation regimes. Journal of Plant Nutrition and Soil Science **169**, 118–126.

Zadoks JC, Chang TT, Konzak CF. 1974. A decimal code for the growth stages of cereals. Weed Research **14**, 415–421.

Zarco-Tejada PJ, Berjon a., Miller JR. 2004. Stress Detection in Crops with Hyperspectral Remote Sensing and Physical Simulation Models. Airborne Imaging Spectroscopy Workshop, 1–5.

Zhao Y, Zhao J, Zhao C, *et al.* 2015. A metabolomics study delineating geographical location-associated primary metabolic changes in the leaves of growing tobacco plants by GC-MS and CE-MS. Nature Publishing Group.

Tables

Table 1. Geographic, climatic, agronomic, and soil information for each study site. Colmenar de Oreja and El Majano experimental stations belong to the Instituto Nacional de Investigación y Tecnología Agraria y Alimentaria (INIA) of Spain and Zamadueñas experimental station belong to the Instituto Tecnológico Agrario de Castilla y León (ITACyL).

	Zamadueñas experimental station	Colmenar de Oreja experimental station	El Majano experimental station
Altitude (mamsl)	700	590	20
Coordinates	41º 42' N, 4º 42' W	40º 04' N, 3º 31' W	37°14' N, 6°03' W
Mean Temp.[b] (ºC)	10.73	13.01	14.5
Max. mean Temp.[b] (ºC)	17.45	21.45	21.6
Min. mean Temp.[b] (ºC)	4.64	5.36	8.3
Precipitation[b] (mm)	258.4	206.8	161.8
Sowing date	24.11.2014	21.11.2014	11.12.2014
Harvest date	22.07.2015	20.07.2015	11.06.2015
Sowing density (seeds m^{-2})	250	250	250
Plot surface (m^2)	10.5 (7x1.5)	10.5 (7x1.5)	10.5 (7x1.5)
Irrigation provided[a] (mm)	125	-	-
Fertilization			
1st application	300 kg ha^{-1} NPK 8:15:15	400 kg ha^{-1} NPK 15:15:15	500 kg ha^{-1} NPK 15:15:15
2nd application	300 kg ha^{-1} CAN 27%N	150 kg ha^{-1} Urea 46%	100 kg ha^{-1} Urea 46%
Soil texture	Loam	Clay-loam	Silty clay loam
Soil pH	8.44	8.1	7.6

[a]in the irrigated treatment

[b]during the growing season

Table 2. Means of grain yield (GY), grain nitrogen yield (GNY), biomass, thousand kernel weight (TKW), harvest index (HI), number of grains spike^{-1}, grain and leaf nitrogen concentration for the high yielding (HY) and water stress (WS) conditions and for each genotype along with the significance level of the respective two-way ANOVA. Values for conditions are averaged over genotypes and values for genotypes are averaged over conditions. Letters correspond to Tukey's b separation. P-values are for conditions (P_C), genotypes (P_G) and the interaction (P_{CxG}).

	GY (Mg ha^{-1})	GNY (kg ha^{-1})	Biomass (Mg ha^{-1})	HI (%)	TKW (g)	Grains Spike^{-1}	Grain N (%)	Leaf N (%)
Conditions								
HY	6.98	165.3	19.53	36.04	49.48	34.62	2.39	3.92
WS	4.38	120.6	14.72	31.06	40.03	31.04	2.70	3.99
Genotypes								
Pelayo	6.26b	152.2	18.10	34.45ab	46.11b	33.05b	2.52ab	3.99
Kiko Nick	5.84ab	147.9	17.66	33.03ab	48.03b	28.01a	2.55ab	4.04
Dorondon	5.27ab	128.9	15.13	36.47b	38.77a	40.32c	2.38a	3.86
Sula	6.04b	138.0	17.83	33.64ab	40.74a	37.31c	2.50a	3.82
Don Sebastian	4.98a	135.5	17.40	30.64a	50.11b	25.45a	2.75b	4.01
Max.	8.24	203.5	35.14	43.15	63.80	51.10	3.48	4.83
Min.	3.18	71.7	9.45	17.10	27.90	21.40	0.98	2.71
CV (%)	25.9	21.6	24.3	17.9	17.3	21.8	14.5	9.4
ANOVA								
P_C	0.000	0.000	0.000	0.002	0.000	0.002	0.000	0.375
P_G	0.005	0.086	0.261	0.094	0.000	0.000	0.005	0.519
P_{C*G}	0.063	0.517	0.716	0.935	0.918	0.166	0.104	0.788

Table 3. Means of canopy temperature (T), the canopy normalized difference moisture index (NDMI), the leaf normalized difference water index (NDWI) and the spike normalized water index (NWI) at the anthesis and grain filling stages and grain and leaf stable carbon isotope composition ($\delta^{13}C$) at grain filling under high yielding (HY) and water stress (WS) conditions and for each genotype, along with the significance level of the respective two-way ANOVA. Values for conditions are averaged over genotypes and values for genotypes are averaged over conditions. Letters correspond to Tukey's b separation. P-values are for conditions (P_C), genotypes (P_G) and the interaction (P_{CxG}).

	Anthesis				Grain filling					
	T	Canopy NDMI	Leaf NDWI	Spike NWI	T	Canopy NDMI	Leaf NDWI	Spike NWI	Grain $\delta^{13}C$ (‰)	Leaf $\delta^{13}C$ (‰)
Conditions										
HY	15.71	-.792	0.0442	-0.061	26.09	-.695	0.0462	-0.061	-26.65	-28.47
WS	18.22	-.747	0.0395	-0.068	33.44	-.607	0.0394	-0.071	-25.03	-27.85
Genotypes										
Pelayo	17.40	-0.773	0.0402	-0.065 ab	29.96	-.654	0.0412	-0.065	-26.00	-28.11
Kiko Nick	17.29	-0.761	0.0413	-0.068 a	31.53	-.644	0.043	-0.074	-26.16	-28.50
Dorondon	17.61	-0.766	0.0414	-0.065 ab	30.77	-.633	0.0401	-0.061	-26.04	-28.16
Sula	17.32	-0.782	0.0466	-0.067 a	31.16	-.651	0.0478	-0.066	-26.00	-27.94
Don Sebastian	17.31	-0.767	0.0398	-0.058 b	31.53	-.674	0.0422	-0.065	-25.49	-28.12
ANOVA										
P_C	0.000	0.000	0.000	0.000	0.000	0.001	0.015	0.005	0.000	0.000
P_G	0.952	0.683	0.058	0.007	0.952	0.885	0.145	0.150	0.699	0.196
P_{C*G}	0.994	0.957	0.842	0.599	0.987	0.993	0.347	0.648	0.995	0.675

Table 4. LASSO regression models for the prediction of grain yield from leaf, glume and lemma metabolite profiles (metabolites as predictor variables) at the anthesis and grain filling stages. Regression models were performed using raw metabolite intensity (upper part of table) and log_2-transformed metabolite intensity. The statistics represent the mean across the 100 cross-validation runs.

	Anthesis stage			Grain filling stage		
	R^2	Adj R^2	RMSE	R^2	Adj R^2	RMSE
Raw intensity						
Leaves						
Training set	0.801	0.736	0.758	0.774	0.702	0.805
Validation set	0.684	0.652	0.882	0.673	0.638	0.891
Glumes						
Training set	0.837	0.768	0.679	0.612	0.508	1.040
Validation set	0.602	0.562	0.975	0.437	0.381	1.180
Lemmas						
Training set	0.845	0.762	0.709	0.514	0.385	1.160
Validation set	0.651	0.616	0.925	0.252	0.178	1.370
Log_2-transformed intensity						
Leaves						
Training set	0.855	0.788	0.669	0.808	0.741	0.744
Validation set	0.645	0.609	0.908	0.659	0.623	0.909
Glumes						
Training set	0.850	0.784	0.653	0.736	0.642	0.885
Validation set	0.582	0.539	0.998	0.507	0.457	1.110
Lemmas						
Training set	0.897	0.834	0.589	0.758	0.633	0.891
Validation set	0.687	0.655	0.878	0.417	0.358	1.210

R^2, coefficient of determination; Adj-R^2, adjusted coefficient of determination; RMSE, root mean square error.

Table 5. Ten metabolites at anthesis and grain filling showing the highest importance in yield prediction models based on 100 cross-validation runs and their effect on yield.

	Leaves			Glumes			Lemmas		
	metabolite	effect	DR (%)	metabolite	effect	DR (%)	metabolite	Effect	DR (%)
Anthesis									
	fucose	+	100	Val	-	93	Val	-	99
	rhamnose	-	100	isomaltose	-	84	malate	-	98
	Pro	-	99	Glu	-	83	Hyp	-	97
	succinate	+	98	N-acetylSer	+	82	glycerol	+	96
	glucarate-1,4-lactone	-	77	*myo*-inositol	+	77	threonate	+	79
	uracil	+	73	cellobiose	-	69	GABA	+	75
	galactonate	+	58	glycerol-3P	-	67	succinate	+	74
	Trp	-	58	malate	-	66	raffinose	-	71
	3-*cis*-caffeoylquinic acid	-	49	Asn	-	64	isomaltose	-	71
	Asp	-	48	maltose	-	63	Ala	-	63
Grain filling									
	fucose	+	100	fucose	+	100	trehalose	+	100
	rhamnose	-	100	rhamnose	-	100	Asp	-	99
	Trp	-	98	Trp	+	99	Hyp	-	98
	phosphate	+	93	Glu	-	92	xylose	+	94
	tyramine	-	88	Hyp	-	91	phosphate	+	85
	Asn	+	87	Ala	+	66	citrate	-	84
	β-Ala	-	79	salicylate	-	62	isocitrate	+	65
	maltose	+	70	tyramine	+	53	4hydroxypyridine	+	64
	Pro	-	68	xylose	+	49	succinate	-	63
	erythrose	-	38	trehalose	+	44	4-hydroxy-*trans*-cinnamate	+	59

DR, detection rate in 100 cross validation runs; +/- , positive/negative effect of each metabolite on grain yield.

Figure legends

Figure 1. Principal component analysis of metabolite profiles of leaves, glumes and lemmas at the anthesis (A) and grain filling stages (B). Individuals are numbered in the graph and labeled in the legend by the five cultivars: DO, Dorondon; DS, Don Sebastian; KN, Kiko Nick; PE, Pelayo; SU, Sula; and by the four environments: HYE1 and HYE2, high yielding environments 1 and 2 (corresponding to the irrigated trial of Zamadueñas and to El Majano trial, respectively); WSE1 and WSE2, water stress environments 1 and 2 (corresponding to the rainfed trials of Aranjuez and Zamadueñas, respectively).

1, HYE1 leaf KN; **2**, HYE1 leaf PE; **3**, HYE1 leaf DO**; 4**, HYE1 leaf DS; **5**, HYE1 leaf SU; **6**, HYE2 leaf KN; **7**, HYE2 leaf PE; **8**, HYE2 leaf DO; **9**, HYE2 leaf DS; **10**, HYE2 leaf SU; **11**, WS1 leaf KN; **12**, WS1 leaf PE; **13**, WS1 leaf DO; **14**, WS1 leaf DS; **15**, WS1 leaf SU; **16**, WS2 leaf KN; **17**, WS2 leaf PE; 18, WS2 leaf DO; **19**, WS2 leaf DS; **20**, WS2 leaf SU; **21**, HYE1 glume KN; **22**, HYE1 glume PE; **23**, HYE1 glume DO; **24**, HYE1 glume DS; **25**, HYE1 glume SU; **26**, HYE2 glume KN; **27**, HYE2 glume PE; **28**, HYE2 glume DO; **29**, HYE2 glume DS; **30**, HYE2 glume SU; **31**, WS1 glume KN; **32**, WS1 glume PE; **33**, WS1 glume DO; **34**, WS1 glume DS; **35**, WS1 glume SU; **36**, WS2 glume KN; **37**, WS2 glume PE; **38**, WS2 glume DO; **39**, WS2 glume DS; **40**, WS2 glume SU; **41**, HYE1 lemma KN; **42**, HYE1 lemma PE; **43**, HYE1 lemma DO; **44**, HYE1 lemma DS; **45**, HYE1 lemma SU; **46**, HYE2 lemma KN; **47**, HYE2 lemma PE; **48**, HYE2 lemma DO; **49**, HYE2 lemma DS; **50**, HYE2 lemma SU; **51**, WS1 lemma KN; **52**, WS1 lemma PE; **53**, WS1 lemma DO; **54**, WS1 lemma DS; **55**, WS1 lemma SU; **56**, WS2 lemma KN; **57**, WS2 lemma PE; **58**, WS2 lemma DO; **59**, WS2 lemma DS; **60**, WS2 lemma SU.

Figure 2. Heatmap of the metabolite profiles of leaves, lemmas and glumes at the anthesis (A) and grain filling (GF) stages under high yielding (HY) and water stress (WS) conditions. P-values are shown for the organ (P_o) and stage (P_s) factors and their interaction (P_{o*s}). The red-blue color scale was obtained from Z-score transformation of actual values. Black color indicates those metabolites not detected.

Figure 3. Water stress-induced changes in metabolite content at anthesis. Blue-red color scale represents log_2-fold change, blue means higher metabolite content under water stress conditions and red stands for higher content under high yielding conditions. Black color indicates those metabolites not detected. *, p-value < 0.05; **, p-value < 0.01; ***, p-value < 0.001.

Figure 4. Genotypic differences in metabolite content between the drought-tolerant genotype Pelayo and the drought sensitive genotype Don Sebastian in leaves, lemmas and glumes at anthesis (S1) and grain filling (S2) under high yielding (HY) and water stress (WS) conditions. The blue-red color scale represents log_2-fold change, blue means higher metabolite content in Pelayo and red stands for higher content in Don Sebastian. Asterisks indicate significant genotypic differences. *, p-value < 0.05; **, p-value < 0.01; ***, p-value < 0.001

Figure 5. Multiple regression models with the variables selected by 70% of model runs (A) and their respective relative importance analyses for the variables (B). Blue: fitted line for HY, red: fitted line for WS, dotted line: fitted line for WS and HY conditions combined. Below, doted bars indicate metabolites negatively affecting grain yield (GY) and horizontal pattern bars indicate metabolites positively affecting GY.

Figure 6. Illustration of the principal metabolic trends shown in leaves and spike bracts in response to water stress and in the high yielding scenario. Blue and red colours refer to increasing and decreasing metabolic paths, respectively. Genotypic changes in yield components refer to the two-ways ANOVA by selecting the genotypes Pelayo and Don Sebastian only (data not shown). aa, amino acids; GNY, grain nitrogen yield; GY, grain yield; HI, harvest index; TKW, thousand kernel weigth.

Figure 1

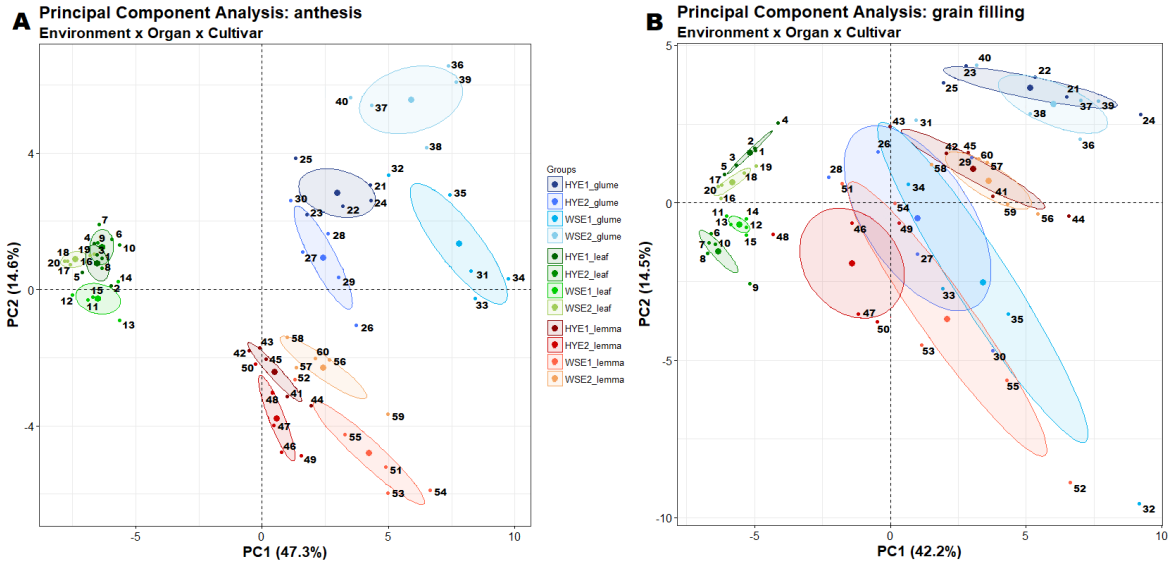
A
Principal Component Analysis: anthesis
Environment x Organ x Cultivar
PC1 (47.3%)
PC2 (14.6%)
Groups
HYE1_glume
HYE2_glume
WSE1_glume
WSE2_glume
HYE1_leaf
HYE2_leaf
WSE1_leaf
WSE2_leaf
HYE1_lemma
HYE2_lemma
WSE1_lemma
WSE2_lemma
B
Principal Component Analysis: grain filling
Environment x Organ x Cultivar
PC1 (42.2%)
PC2 (14.5%)

Figure 2

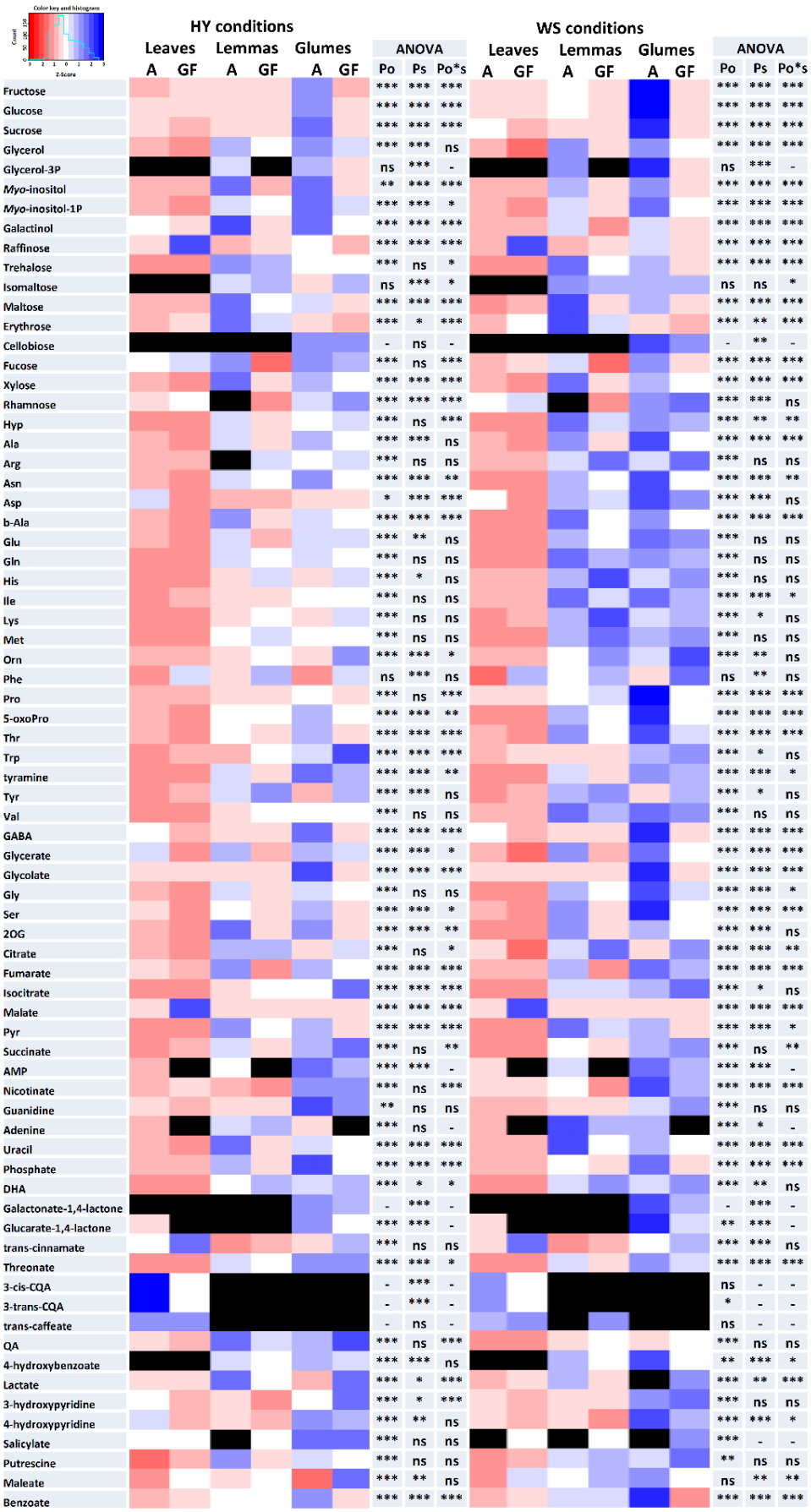
Color key and histogram
Count
Z-Score
HY conditions
WS conditions
Leaves
Lemmas
Glumes
A
GF
ANOVA
Po
Ps
Po*s
Fructose
Glucose
Sucrose
Glycerol
Glycerol-3P
Myo-inositol
Myo-inositol-1P
Galactinol
Raffinose
Trehalose
Isomaltose
Maltose
Erythrose
Cellobiose
Fucose
Xylose
Rhamnose
Hyp
Ala
Arg
Asn
Asp
b-Ala
Glu
Gln
His
Ile
Lys
Met
Orn
Phe
Pro
5-oxoPro
Thr
Trp
tyramine
Tyr
Val
GABA
Glycerate
Glycolate
Gly
Ser
2OG
Citrate
Fumarate
Isocitrate
Malate
Pyr
Succinate
AMP
Nicotinate
Guanidine
Adenine
Uracil
Phosphate
DHA
Galactonate-1,4-lactone
Glucarate-1,4-lactone
trans-cinnamate
Threonate
3-cis-CQA
3-trans-CQA
trans-caffeate
QA
4-hydroxybenzoate
Lactate
3-hydroxypyridine
4-hydroxypyridine
Salicylate
Putrescine
Maleate
Benzoate

Figure 3

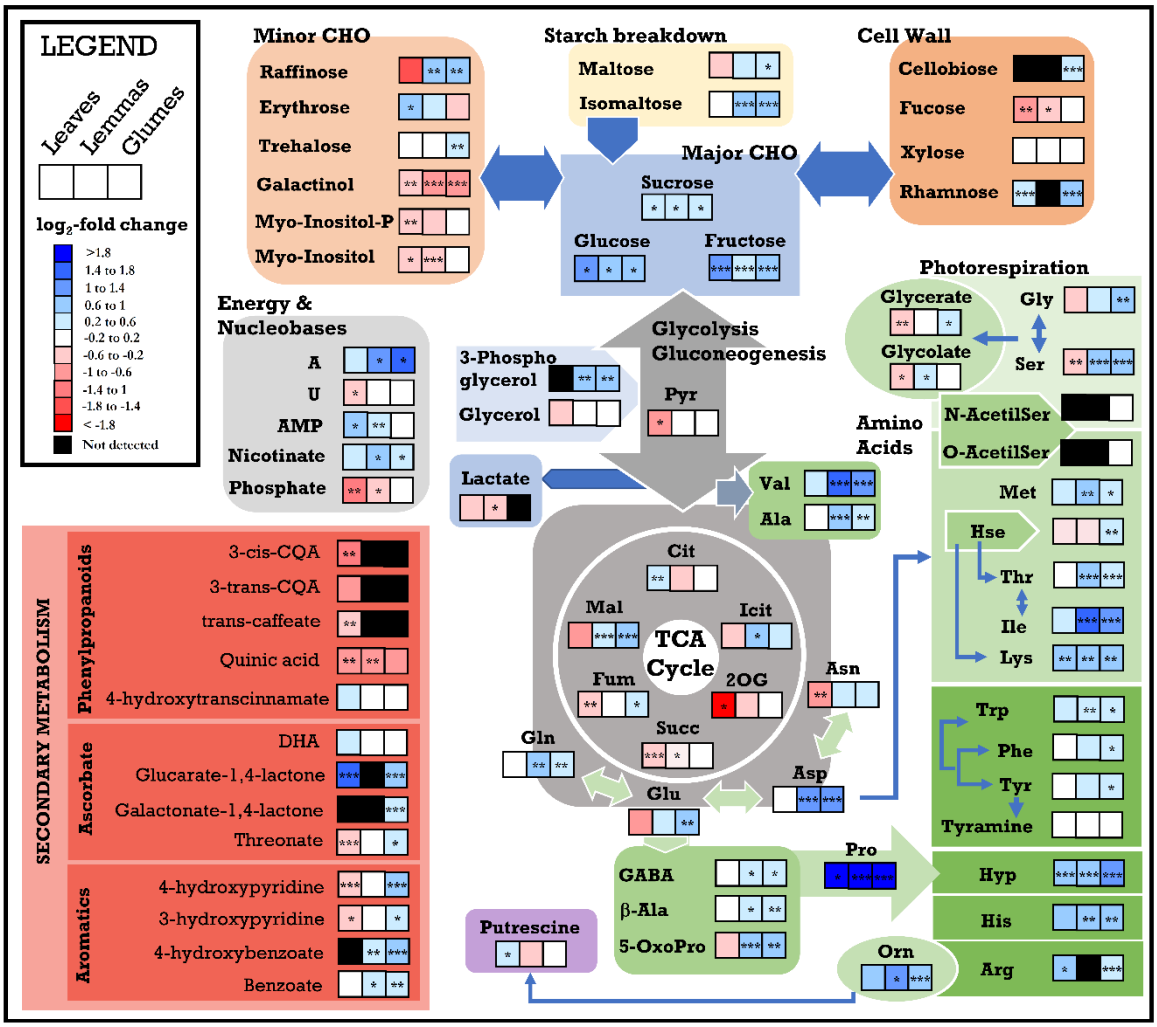
LEGEND
Leaves
Lemmas
Glumes
log2-fold change
>1.8
1.4 to 1.8
1 to 1.4
0.6 to 1
0.2 to 0.6
-0.2 to 0.2
-0.6 to -0.2
-1 to -0.6
-1.4 to 1
-1.8 to -1.4
< -1.8
Not detected
Minor CHO
Raffinose
Erythrose
Trehalose
Galactinol
Myo-Inositol-P
Myo-Inositol
Starch breakdown
Maltose
Isomaltose
Cell Wall
Cellobiose
Fucose
Xylose
Rhamnose
Major CHO
Sucrose
Glucose
Fructose
Photorespiration
Glycerate
Glycolate
Gly
Ser
Energy & Nucleobases
A
U
AMP
Nicotinate
Phosphate
Glycolysis
Gluconeogenesis
3-Phospho glycerol
Glycerol
Pyr
Lactate
Amino Acids
N-AcetilSer
O-AcetilSer
Val
Ala
Met
Hse
Thr
Ile
Lys
Cit
Mal
Icit
TCA Cycle
Fum
2OG
Succ
Asn
Gln
Asp
Glu
Trp
Phe
Tyr
Tyramine
Pro
GABA
β-Ala
5-OxoPro
Hyp
His
Arg
Orn
Putrescine
SECONDARY METABOLISM
Phenylpropanoids
3-cis-CQA
3-trans-CQA
trans-caffeate
Quinic acid
4-hydroxytranscinnamate
Ascorbate
DHA
Glucarate-1,4-lactone
Galactonate-1,4-lactone
Threonate
Aromatics
4-hydroxypyridine
3-hydroxypyridine
4-hydroxybenzoate
Benzoate

Figure 4

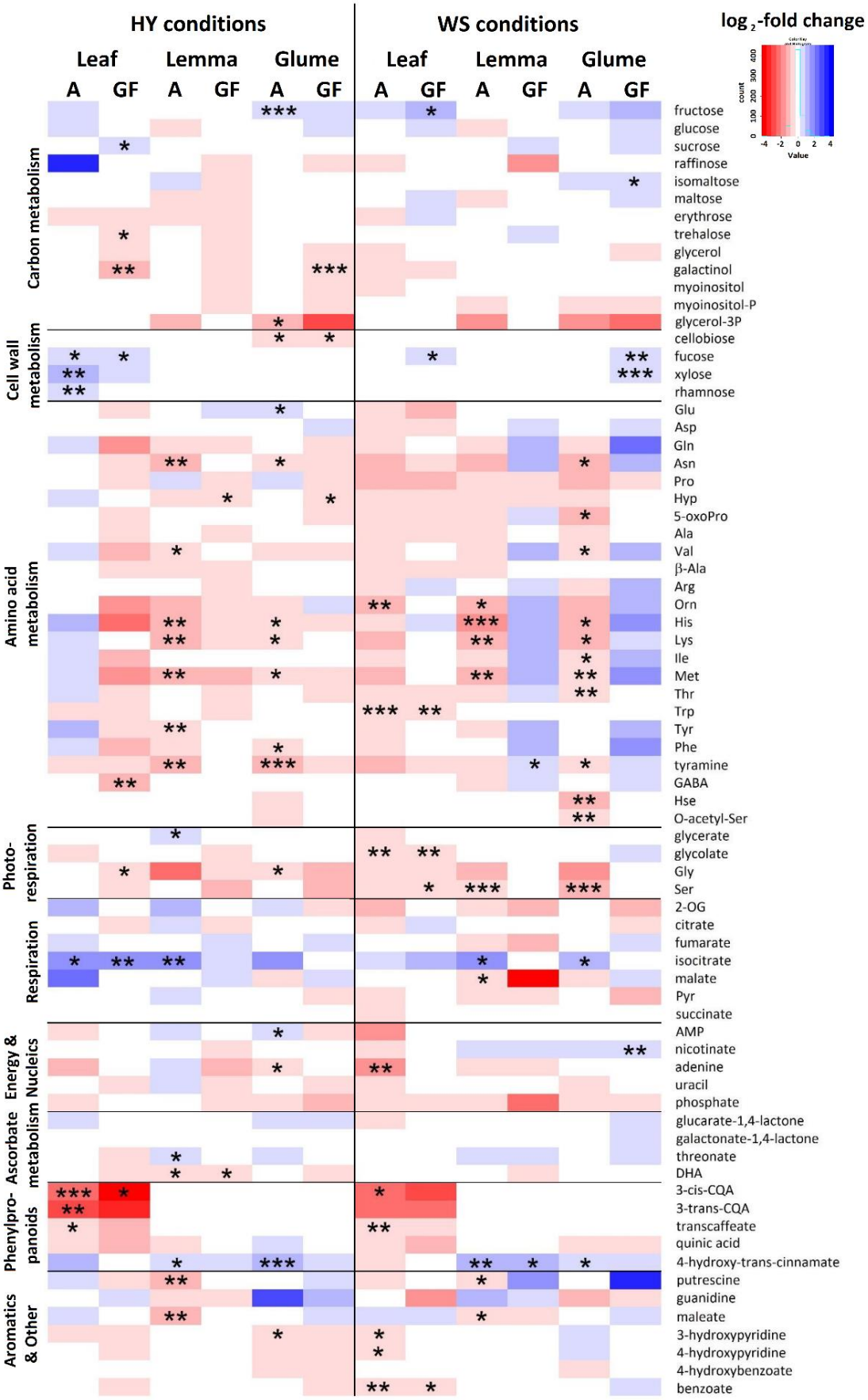
HY conditions
WS conditions
log2-fold change
Leaf
Lemma
Glume
A
GF
Carbon metabolism
Cell wall metabolism
Amino acid metabolism
Photo-respiration
Respiration
Energy & Nucleics
Ascorbate metabolism
Phenylpro-panoids
Aromatics & Other
fructose
glucose
sucrose
raffinose
isomaltose
maltose
erythrose
trehalose
glycerol
galactinol
myoinositol
myoinositol-P
glycerol-3P
cellobiose
fucose
xylose
rhamnose
Glu
Asp
Gln
Asn
Pro
Hyp
5-oxoPro
Ala
Val
β-Ala
Arg
Orn
His
Lys
Ile
Met
Thr
Trp
Tyr
Phe
tyramine
GABA
Hse
O-acetyl-Ser
glycerate
glycolate
Gly
Ser
2-OG
citrate
fumarate
isocitrate
malate
Pyr
succinate
AMP
nicotinate
adenine
uracil
phosphate
glucarate-1,4-lactone
galactonate-1,4-lactone
threonate
DHA
3-cis-CQA
3-trans-CQA
transcaffeate
quinic acid
4-hydroxy-trans-cinnamate
putrescine
guanidine
maleate
3-hydroxypyridine
4-hydroxypyridine
4-hydroxybenzoate
benzoate

Figure 5

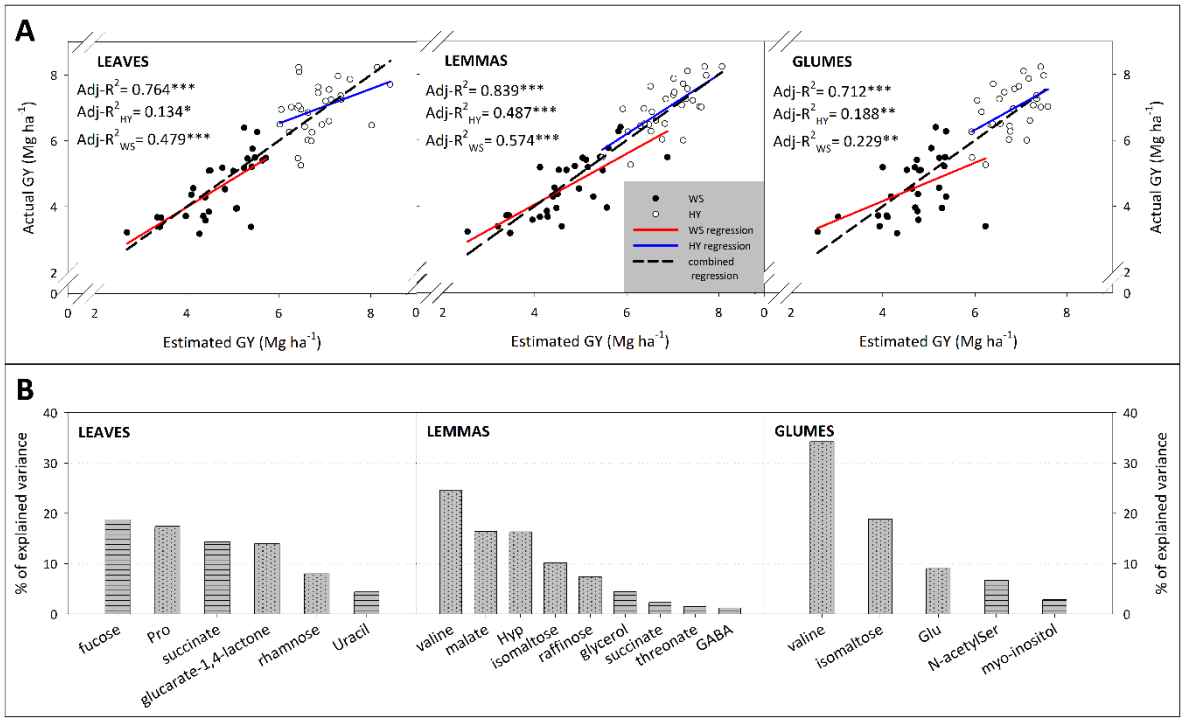
A
LEAVES
Adj-R2= 0.764***
Adj-R2 HY= 0.134*
Adj-R2 WS= 0.479***
LEMMAS
Adj-R2= 0.839***
Adj-R2 HY= 0.487***
Adj-R2 WS= 0.574***
GLUMES
Adj-R2= 0.712***
Adj-R2 HY= 0.188**
Adj-R2 WS= 0.229**
WS
HY
WS regression
HY regression
combined regression
Actual GY (Mg ha-1)
Estimated GY (Mg ha-1)
B
% of explained variance
fucose
Pro
succinate
glucarate-1,4-lactone
rhamnose
Uracil
valine
malate
Hyp
isomaltose
raffinose
glycerol
succinate
threonate
GABA
valine
isomaltose
Glu
N-acetylSer
myo-inositol

Figure 6

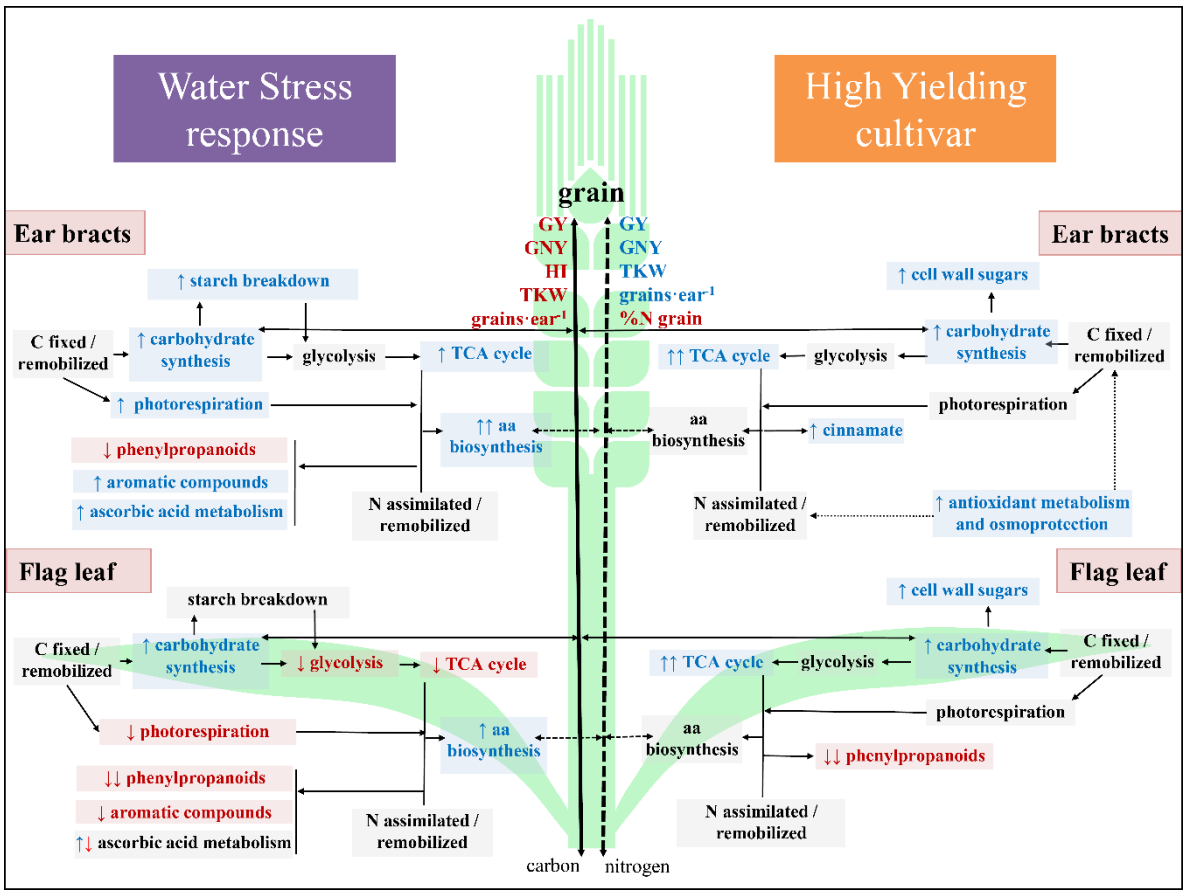
Water Stress response
High Yielding cultivar
grain
GY
GNY
HI
TKW
grains·ear⁻¹
GY
GNY
TKW
grains·ear⁻¹
%N grain
Ear bracts
Ear bracts
↑ starch breakdown
C fixed / remobilized
↑ carbohydrate synthesis
glycolysis
↑ TCA cycle
↑ photorespiration
↓ phenylpropanoids
↑ aromatic compounds
↑ ascorbic acid metabolism
N assimilated / remobilized
↑↑ aa biosynthesis
aa biosynthesis
↑ cell wall sugars
↑ carbohydrate synthesis
C fixed / remobilized
↑↑ TCA cycle
glycolysis
photorespiration
↑ cinnamate
N assimilated / remobilized
↑ antioxidant metabolism and osmoprotection
Flag leaf
Flag leaf
starch breakdown
C fixed / remobilized
↑ carbohydrate synthesis
↓ glycolysis
↓ TCA cycle
↓ photorespiration
↓↓ phenylpropanoids
↓ aromatic compounds
↑↓ ascorbic acid metabolism
N assimilated / remobilized
↑ aa biosynthesis
aa biosynthesis
↑ cell wall sugars
↑ carbohydrate synthesis
C fixed / remobilized
↑↑ TCA cycle
glycolysis
photorespiration
↓↓ phenylpropanoids
N assimilated / remobilized
carbon
nitrogen

Supplementary material

Title

Metabolome profiling supports the key role of the spike in wheat yield performance

Table S1. Differences in the relative content of metabolites between growing conditions in leaves, lemmas and glumes at anthesis and grain filling expressed as log_2-fold change (log_2-FC) together with the corresponding statistical significance (p-value). Positive log_2-FC values indicate higher relative content under water stress conditions and negative log_2-FC values indicate higher content under high yielding conditions.

	Anthesis						Grain filling					
	Leaf		Lemma		Glume		Leaf		Lemma		Glume	
	log_2-FC	p-value	log_2-FC	p-value	log_2-FC	p-value	log_2-FC	p-value	log_2-FC	p-value	log_2-FC	p-value
Carbon metabolism												
Fru	1.31	0.000	0.56	0.000	0.95	0.000	0.35	0.053	0.48	0.006	0.55	0.028
Glc	1.37	0.000	0.85	0.000	0.84	0.000	0.17	0.307	0.54	0.002	0.59	0.034
Suc	0.36	0.016	0.37	0.011	0.39	0.014	0.12	0.631	0.09	0.506	0.23	0.064
raffinose	-1.68	0.164	0.65	0.003	0.58	0.008	0.12	0.591	0.50	0.351	0.15	0.549
isomaltose	-	-	0.80	0.000	0.88	0.000	-	-	0.05	0.673	0.04	0.835
maltose	-0.28	0.075	0.28	0.254	0.53	0.026	-0.33	0.026	-0.10	0.660	-0.10	0.573
glycerol	-0.25	0.225	0.14	0.220	0.06	0.553	-0.17	0.583	-0.13	0.491	-0.40	0.076
galactinol	-0.57	0.005	-0.66	0.000	-0.67	0.000	-0.09	0.553	-0.84	0.000	-0.39	0.007
trehalose	-0.05	0.072	0.19	0.114	0.50	0.002	-0.30	0.019	-0.76	0.000	-0.29	0.064
erythrose	0.76	0.046	0.56	0.148	-0.42	0.654	0.75	0.002	-0.08	0.816	-	-
myo-inositol	-0.21	0.016	-0.31	0.000	-0.14	0.068	0.08	0.448	0.21	0.381	0.02	0.922
*myo*inositol-1-P	-0.33	0.001	-0.25	0.132	-0.08	0.566	-	-	-0.11	0.461	-0.36	0.061
glycerol-3P	-	-	0.95	0.008	0.99	0.008	-	-	-	-	-0.38	0.526
Amino acid metabolism												
Hyp	0.80	0.001	0.65	0.000	1.07	0.000	0.47	0.066	0.57	0.003	0.52	0.037
Ala	-0.15	0.047	0.43	0.000	0.51	0.002	-0.07	0.669	-0.06	0.699	-0.06	0.570
Asn	-0.74	0.001	0.43	0.117	0.35	0.168	-0.26	0.409	0.26	0.612	0.17	0.690
Asp	-0.18	0.115	1.27	0.000	1.34	0.000	0.52	0.208	1.15	0.000	1.01	0.001
b-Ala	-0.08	0.512	0.25	0.038	0.39	0.004	0.59	0.001	0.31	0.059	0.07	0.648
Glu	-0.63	0.149	0.42	0.144	0.74	0.006	0.44	0.146	0.76	0.016	0.57	0.012
Gln	-0.20	0.437	0.81	0.005	0.44	0.007	-0.24	0.648	0.54	0.194	0.62	0.423
His	0.82	0.126	0.94	0.001	0.64	0.004	0.13	0.751	0.74	0.166	0.60	0.298
Ile	0.38	0.156	1.49	0.000	1.00	0.000	0.12	0.735	0.75	0.015	0.70	0.056
Lys	0.88	0.004	0.94	0.002	0.76	0.001	0.29	0.212	1.13	0.037	0.44	0.409
Met	0.44	0.276	0.69	0.001	0.55	0.004	-0.07	0.872	0.67	0.146	0.93	0.103
Orn	0.86	0.157	1.04	0.015	0.89	0.001	0.16	0.868	1.06	0.073	0.46	0.456
Phe	-0.13	0.630	0.21	0.139	0.43	0.035	0.11	0.772	0.06	0.824	0.27	0.527
Pro	2.98	0.028	2.96	0.000	2.47	0.000	1.33	0.069	1.27	0.005	1.19	0.011
5-oxoproline	-0.20	0.225	0.68	0.001	0.65	0.004	0.07	0.691	0.23	0.428	0.18	0.622
Thr	-0.14	0.104	0.83	0.000	0.51	0.000	0.16	0.344	0.49	0.016	0.40	0.052

Trp	0.22	0.187	0.33	0.006	0.31	0.012	0.42	0.005	-0.26	0.026	-0.25	0.045
tyramine	0.07	0.181	-0.04	0.941	-0.11	0.358	0.67	0.015	-0.01	0.938	-0.07	0.615
Tyr	-0.03	0.255	0.22	0.185	0.44	0.017	0.17	0.502	0.05	0.856	-0.03	0.934
Val	0.38	0.067	1.63	0.000	1.12	0.000	0.08	0.803	0.76	0.011	0.68	0.085
GABA	0.06	0.663	0.20	0.049	0.27	0.015	0.38	0.117	0.08	0.707	0.03	0.870
Arg	0.82	0.018	-	-	0.56	0.000	0.42	0.135	0.99	0.045	0.88	0.147
Hse	-	-	-	-	0.58	0.002	-	-	-	-	-	-
N-acetyl-Ser	-	-	-	-	0.07	0.616	-	-	-	-	-	-
O-acetyl-Ser	-	-	-	-	-0.05	0.815	-	-	-	-	-	-
Photorespiration												
glycerate	-0.54	0.003	0.10	0.196	0.20	0.014	-0.38	0.154	0.06	0.770	-0.10	0.502
glycolate	-0.21	0.026	0.18	0.022	0.12	0.118	0.04	0.838	0.04	0.748	-0.14	0.461
Gly	-0.34	0.121	0.37	0.533	0.84	0.006	-0.44	0.030	0.44	0.055	0.33	0.263
Ser	-0.43	0.002	0.78	0.000	0.78	0.000	-0.04	0.863	0.36	0.181	0.33	0.249
Respiration												
2OG	-2.56	0.015	-0.48	0.077	-0.08	0.789	-0.74	0.543	0.01	0.915	0.75	0.098
citrate	0.45	0.003	-0.32	0.316	0.00	0.990	-0.18	0.459	0.32	0.144	0.42	0.034
fumarate	-0.30	0.005	-0.15	0.398	0.38	0.017	0.08	0.696	0.33	0.260	0.33	0.204
isocitrate	-0.33	0.478	0.71	0.012	0.52	0.055	-0.22	0.209	0.35	0.163	0.14	0.492
MALATE	-0.88	0.145	0.59	0.000	0.99	0.000	0.00	0.979	1.15	0.320	-0.94	0.007
pyruvate	-0.92	0.023	0.14	0.508	-0.02	0.868	-0.44	0.050	0.26	0.563	0.53	0.230
succinate	-0.54	0.000	-0.18	0.040	0.08	0.409	-0.14	0.339	0.05	0.815	-0.03	0.866
Cell Wall												
cellobiose	-	-	-	-	0.50	0.000	-	-	-	-	-0.05	0.859
fucose	-0.65	0.001	-0.35	0.003	-0.06	0.446	-0.45	0.000	-	-	-0.68	0.000
xylose	0.00	0.994	-0.08	0.571	0.02	0.893	-0.14	0.366	-0.02	0.848	-0.21	0.022
rhamnose	0.45	0.000	-	-	0.61	0.000	0.42	0.000	-	-	0.13	0.269
Energy & Nucleic												
AMP	0.86	0.037	0.58	0.005	0.15	0.270	-	-	-	-	0.14	0.630
nicotinate	0.34	0.064	0.65	0.027	0.41	0.033	0.02	0.897	0.16	0.344	-0.22	0.044
guanidine	-1.87	0.137	0.37	0.266	-1.12	0.340	0.64	0.156	0.23	0.353	0.05	1.000
Adenine	0.22	0.623	1.06	0.019	1.41	0.032	-	-	0.01	0.992	-	-
uracil	-0.48	0.019	0.16	0.263	0.15	0.314	0.23	0.447	0.80	0.004	0.09	0.758
phosphate	-1.20	0.002	-0.49	0.039	-0.19	0.372	-0.72	0.028	-0.11	0.842	-0.69	0.078
Ascorbate metabolism												
DHA	0.22	0.124	0.10	0.414	-0.02	0.617	0.17	0.314	0.07	0.633	0.19	0.163
glucarate-1,4-lactone	1.53	0.000	-	-	0.74	0.000	-	-	-	-	0.81	0.025
galactonate-1,4-lactone	-	-	-	-	0.38	0.000	-	-	-	-	0.04	0.759
threonate	-0.30	0.000	0.19	0.062	0.29	0.001	0.04	0.704	0.02	0.907	-0.11	0.227
Phenylpropanoids												
4-hydroxy-*trans*-cinnamate	0.51	0.138	0.14	0.340	0.12	0.432	0.02	0.943	-0.16	0.397	-0.36	0.067
3-*cis*-CQA	-1.03	0.007	-	-	-	-	0.07	0.966	-	-	-	-
3-*trans*-CQA	-0.80	0.088	-	-	-	-	-0.16	0.811	-	-	-	-
trans-caffeate	-0.31	0.008	-	-	-	-	-0.02	0.808	-	-	-	-
quinic acid	-0.95	0.001	-0.90	0.002	-0.62	0.101	-0.74	0.026	-0.33	0.157	-0.85	0.002
Aromatics & Other												
4-hydroxybenzoate	-	-	0.41	0.006	0.72	0.001	-	-	0.26	0.103	-0.04	0.874
benzoate	-0.12	0.202	0.20	0.033	0.26	0.006	0.09	0.498	0.14	0.259	-0.40	0.018

3-hydroxypyridine	-0.39	0.000	0.13	0.347	0.60	0.000	-0.20	0.237	-	-	-0.13	0.404
4-hydroxypyridine	-0.39	0.034	0.03	0.819	0.29	0.037	-0.24	0.214	-0.08	0.544	-0.10	0.627
lactate	-0.33	0.059	-0.23	0.032	-	-	-0.28	0.092	-0.50	0.119	-0.25	0.468
malonate	-	-	-	-	-	-	-	-	-	-	-0.93	0.000
salicylate	-	-	-	-	-	-	0.07	0.609	-	-	-0.09	0.160
putrescine	0.46	0.013	-0.28	0.110	-0.14	0.513	0.09	0.711	-	-	0.84	0.340
maleate	-0.22	0.512	0.33	0.094	3.92	0.482	0.16	0.590	0.33	0.260	-0.94	0.014

Table S2. Metabolite content change (log_2-fold change) between the Zamadueñas rainfed and Zamadueñas irrigated trials at anthesis stage. Blue color is indicative of increasing metabolite under WS environment. *, p-value < 0.05; **, p-value < 0.01; ***, p-value < 0.001; ns, non-significant.

Metabolites	Leaves	Lemmas	Glumes
5-oxoproline	0.45**	0.51**	0.22ns
Ala	-0.41***	0.20*	0.36*
Arg	0.38**		0.18ns
Asn	-0.70*	-0.28ns	0.24ns
Asp	0.22ns	2.09***	1.89***
β-Ala	-0.34ns	0.21ns	0.39*
GABA	0.16ns	0.09ns	-0.05ns
Gln	0.22ns	0.60*	0.10ns
Glu	1.93**	1.15**	1.25**
His	0.31ns	0.57ns	0.05ns
Hse			0.32ns
Hyp	1.29***	1.00***	1.20***
Ile	-0.26ns	1.38***	0.85***
Lys	0.15ns	0.23ns	-0.03ns
Met	-0.22ns	0.60*	0.33ns
N-acetyl-Ser			-0.71***
O-acetyl-Ser			-0.54**
Orn	0.64ns	0.15ns	0.01ns
Phe	-1.56***	-0.08ns	-0.02ns
Pro	4.56***	3.09***	2.45***
Thr	0.02ns	0.73***	0.44***
Trp	-0.28ns	-0.31*	-0.19ns
Tyr	-1.44***	0.20ns	0.11ns
tyramine	-0.23ns	0.14ns	-0.06ns
Val	-0.06ns	1.47***	1.00***
3-hydroxypyridine	-0.33**	-0.09ns	0.59*
4-hydroxybenzoate		0.29ns	0.44ns
4-hydroxypyridine	-0.30*	0.00ns	0.35ns
benzoate	-0.35*	0.13ns	-0.02ns
lactate	-0.29ns	-0.22ns	

maleate	-0.29ns	0.12ns	0.11ns
putrescine	0.29ns	-0.20ns	-0.19ns
DHA	-0.13ns	0.27*	0.05ns
galactonate-1,4-lactone			0.55***
glucarate-1,4-lactone	1.43***		1.02***
threonate	-0.44***	-0.02ns	0.13ns
erythrose	0.46ns	0.69**	ns
Fru	1.02***	0.72***	0.88***
galactinol	-0.64***	-0.05ns	-0.19ns
Glc	1.18***	1.22***	1.22***
glycerol	-1.05***	-0.23*	-0.29**
glycerol-3P		1.26***	1.27***
isomaltose		0.82***	0.94***
maltose	0.28ns	0.52*	0.95ns
myo-inositol	-0.13ns	0.00ns	-0.02ns
*myo*inositol-1-P	-0.12ns	0.31ns	0.05ns
Raf	-0.74ns	0.51ns	0.75*
Suc	0.80***	1.04***	1.15***
trehalose	0.19ns	0.52***	0.90***
cellobiose			0.90***
fucose	-0.80***	-0.19*	0.01ns
rhamnose	0.25ns		0.43***
xylose	-0.34*	-0.32***	-0.24*
Adenine	-0.60ns	0.17ns	-0.56ns
AMP	0.76ns	0.75*	0.23ns
guanidine	-0.85ns	-0.55ns	-1.54ns
nicotinate	-0.47**	-0.14ns	-0.05ns
phosphate	0.03ns	-0.16ns	0.06ns
uracil	-1.15***	-0.16ns	-0.06ns
3-*cis*-CQA	-0.25ns		
3-*trans*-CQA	-0.14ns		
4-hydroxy-*trans*-cinnamate	0.31ns	0.27ns	0.00ns
quinic acid	-0.24ns		
trans-caffeate	-0.14ns		
Gly	-0.38*	0.38ns	0.52ns
glycerate	-0.33**	0.14ns	0.14ns
glycolate	-0.28*	0.02ns	0.20*
Ser	0.21ns	0.67***	0.79***
2OG	0.33ns	0.07ns	0.14ns
citrate		-2.04***	-2.43***
fumarate	-0.33ns	0.07ns	0.64**
isocitrate		-0.28ns	-0.33ns
malate	-0.37ns	0.79***	0.87*
pyruvate	-0.67**	0.34ns	0.01ns
succinate	-0.43***	-0.28*	-0.18ns

Figures

Figure S1. Mean values of grain yield in a collection of twenty post-green revolution durum wheat genotypes under high yielding (HY) and water stress (WS) conditions as indicated in the Materials and Methods. Red bars correspond to the five selected genotypes in this study.

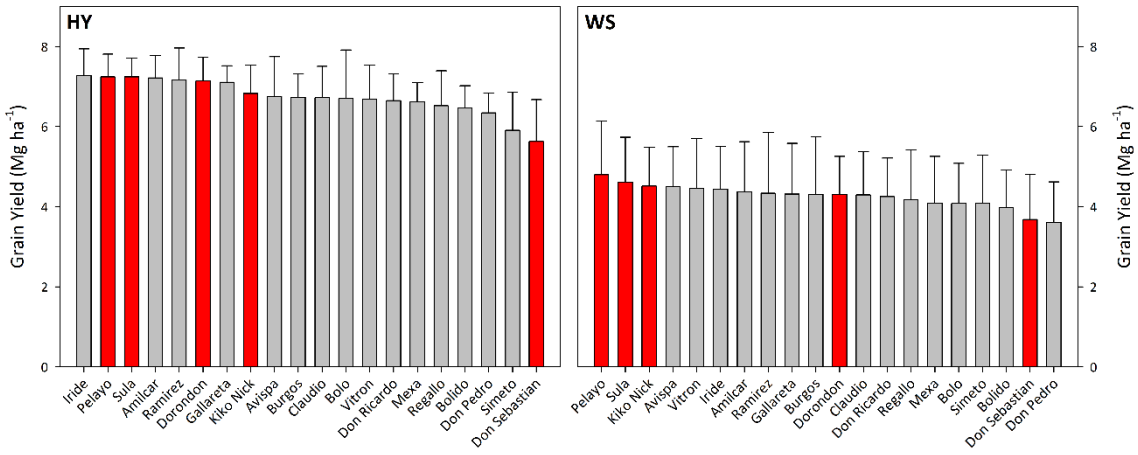

Figure S2. Correlation networks between metabolite contents and agronomic and physiological traits. The maximum alpha value was fixed at 0.001 and weaker correlations were omitted. Green lines stand for positive correlations and red lines for negative correlations. Greater line thickness indicates higher correlation coefficients.

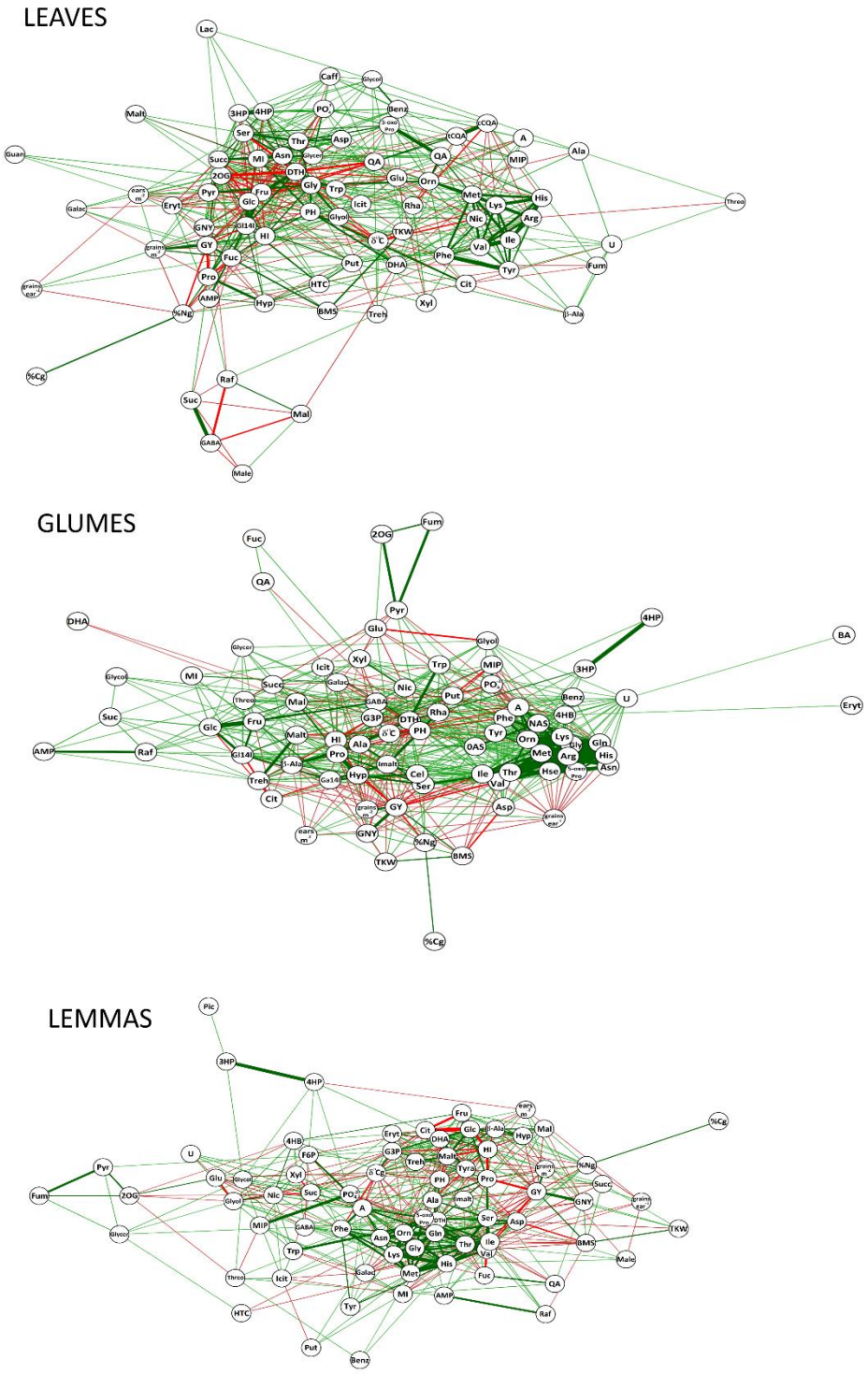

2OG, 2-oxoglutarate; cCQA, 3-cis-caffeoylquinic acid; 3HP, 3-hydroxypyridine; G3P, 3-phosphoglycerol; tCQA, 3-trans-caffeoylquinic acid; 4HB, 4-hydroxybenzoate; Hyp, 4-hydroxyproline;

4HP, 4-hydroxypyridine; 4HP, 4-hydroxypyridine; HTC, 4-hydroxy-trans-cinnamate; 5-oxoPro, 5-oxoproline; A,adenine; AMP, adenosine monophosphate; Ala, alanine; Arg, arginine; Asn, asparagine; Asp, aspartate; β-Ala, β-alanine; Benz, benzoate; BA, benzylalcohol; BMS, biomass; $\delta^{13}C$, carbon isotope composition; Cel, cellobiose; Cit, citrate; DTH, days to heading; DHA, dehydroascorbate; ears m^{-2}, ears per square meter; Eryt, erythrose; Fru, fructose; F6P, fructose-6-phosphate; Fuc, fucose; Fum, fumarate; Galac, galactinol; Ga14l, galactonate-1,4-lactone; GABA, γ-aminobutyric acid; Gl14l, glucarate-1,4-lactone; Glc, glucose; Glu, glutamate; Gln, glutamine; Glycer, glycerate; Glyol, glycerol; Gly, glycine; Glyol, glycolate; %Cg, grain carbon concentration; %Ng, grain nitrogen concentration; GNY, grain nitrogen yield; GY, grain yield; grains ear^{-1}, grains per ear; grains m^{-2}, grains per square meter; Guan, guanidine; HI, harvest index; His, histidine; Hse, Homoserine; Icit, isocitrate; Ile, isoleucine; Imalt, isomaltose; Lac, lactate; Lys, lysine; Mal, malate; Male, maleate; Malt, maltose; Met, methionine; MI, myo-inositol; MIP, myoinositol-1-P; NAS, N-acetyl-Serine; Nic, nicotinate; OAS, O-acetyl-Serine; Orn, ornithine; Phe, phenylalanine; phosphate, PO_4^{3-}; Pic, picolinate; PH, plant height; Pro, proline; Put, putrescine; Pyr, pyruvate; QA, quinic acid; Raf, raffinose; Rha, rhamnose; Ser, serine; Succ, succinate; Suc, sucrose; TKW, thousand kernel weight; Threo, threonate; Thr, threonine; Caff, trans-caffeate; Treh, trehalose; Trp, tryptophan; Tyra, tyramine; Tyr, tyrosine; U, uracil; Val, valine; Xyl, xylose.

Figure S3. Scatter plots between grain yield and fucose (Fuc), proline (Pro) and hydroxyproline (Hyp) relative content in leaves, glumes or lemmas at anthesis and grainfilling stages. *, p-value < 0.05; **, p-value < 0.01; ***, p-value < 0.001; ns, non-significant.

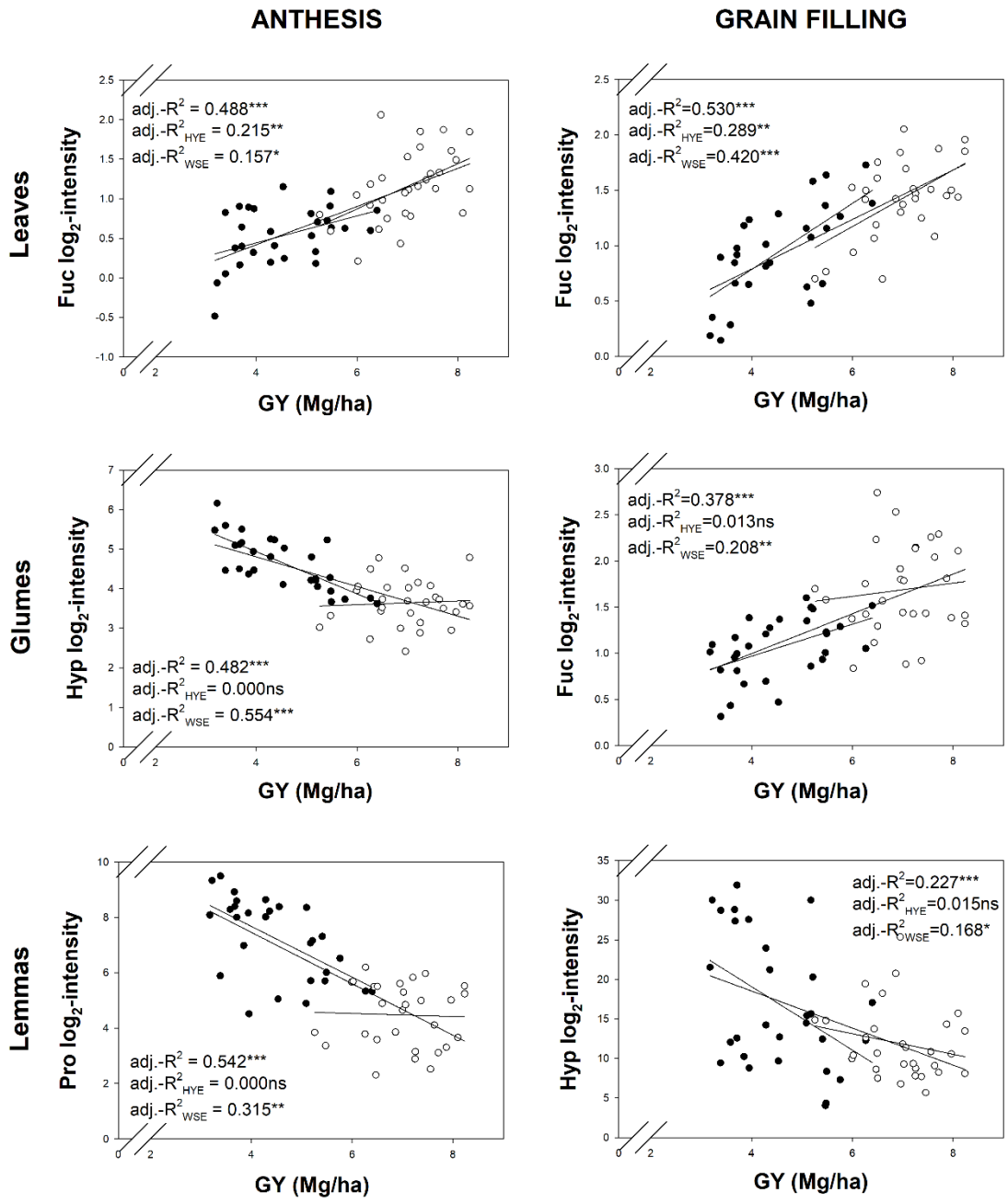

CHAPTER 5

Assessing durum wheat ear and leaf metabolomes in the field through hyperspectral data

Omar Vergara-Diaz, Thomas Vatter,
Shawn Carlisle Kefauver, Toshihiro Obata,
Alisdair R. Fernie, José Luis Araus

Submitted to:
The Plant Journal

ABSTRACT

Hyperspectral techniques are currently used to retrieve information concerning plant biophysical traits, predominantly targeting pigments, water and nitrogen-protein contents, structural elements, and the leaf area index. Even so, hyperspectral data could be more extensively exploited to overcome the breeding challenges being faced under global climate change by advancing high throughput field phenotyping. In this study, we explore the potential of field spectroscopy to predict the metabolite profiles in flag leaves and ear bracts in durum wheat. The full range reflectance spectra (VIS-NIR-SWIR) of flag leaves, ears and canopies were recorded in a collection of contrasting genotypes grown in four environments under different water regimes. GC-MS metabolite profiles were analysed in the flag leaves, ear bracts, glumes and lemmas. The results from regression models exceeded 50% of the explained variation (adj-R^2 in the validation sets) for at least 15 metabolites in each plant organ, whereas their errors were considerably low. The best regressions were obtained for malate (82%), glycerate and serine (63%) in leaves; *myo*-inositol (81%) in lemmas; glycolate (80%) in glumes; sucrose in leaves and glumes (68%); GABA in leaves and glumes (61% and 71%, respectively); proline and glucose in lemmas (74% and 71%, respectively) and glumes (72% and 69%, respectively). The selection of wavebands in the models and the performance of the models based on canopy and VIS-organ spectra and yield prediction are discussed. We feel that this technique will likely be of interest due to its broad applicability in ecophysiology research, plant breeding programs and the agri-food industry.

Assessing durum wheat ear and leaf metabolomes in the field through hyperspectral data

Omar Vergara-Diaz[1], Thomas Vatter[1], Shawn Carlisle Kefauver[1], Toshihiro Obata[2], Alisdair R. Fernie[2], José Luis Araus[1*]

[1] Integrative Crop Ecophysiology Group, Plant Physiology Section, Faculty of Biology, University of Barcelona. Diagonal 643, 08028 Barcelona, SPAIN

[2] Max Planck Institute of Molecular Plant Physiology. Am Mühlenberg 1, 14476 Potsdam, GERMANY

*corresponding author: José Luis Araus, Faculty of Biology, University of Barcelona. Diagonal 643, 08028 Barcelona, SPAIN. Telephone number: (+34) 934021469

Summary

Hyperspectral techniques are currently used to retrieve information concerning plant biophysical traits, predominantly targeting pigments, water and nitrogen-protein contents, structural elements, and the leaf area index. Even so, hyperspectral data could be more extensively exploited to overcome the breeding challenges being faced under global climate change by advancing high throughput field phenotyping. In this study, we explore the potential of field spectroscopy to predict the metabolite profiles in flag leaves and ear bracts in durum wheat. The full range reflectance spectra (VIS-NIR-SWIR) of flag leaves, ears and canopies were recorded in a collection of contrasting genotypes grown in four environments under different water regimes. GC-MS metabolite profiles were analyzed in the flag leaves, ear bracts, glumes and lemmas. The results from regression models exceeded 50% of the explained variation (adj-R^2 in the validation sets) for at least 15 metabolites in each plant organ, whereas their errors were considerably low. The best regressions were obtained for malate (82%), glycerate and serine (63%) in leaves; *myo*-inositol (81%) in lemmas; glycolate (80%) in glumes; sucrose in leaves and glumes (68%); GABA in leaves and glumes (61% and 71%, respectively); proline and glucose in lemmas (74% and 71%, respectively) and glumes (72% and 69%, respectively). The selection of wavebands in the models and the performance of the models based on canopy and VIS-organ spectra and yield prediction are discussed. We feel that this technique will likely be of interest due to its broad applicability in ecophysiology research, plant breeding programs and the agri-food industry.

Keywords

Breeding, ear bracts, flag leaf, LASSO, metabolome, yield, spectroscopy, wheat,

Significance statement

The study of the light reflected from plant surfaces can inform us about compositional traits. The development of this technique is critical for advances in field phenotyping and thereby plant breeding. This study aims to predict the metabolite profiles of wheat leaves and ear bracts from hyperspectral data recorded in the field. Key sugars, organic acids and amino acids in central metabolism were satisfactorily predicted, illustrating the great potential of this technique.

Introduction

The current urgency to obtain crops that are more resilient to climate change or with improved quality traits requires new technical and methodological advances that overcome the plant phenotyping bottleneck (Araus and Cairns, 2014). In this sense, spectroradiometric techniques offer potential opportunities not only at the laboratory level, but by using portable imaging systems (or even imaging from satellites), also in the field. In this manner plant performance can be assessed in single tissues or plants or in entire crops or even whole ecosystems.

The development of high spectral resolution systems has been driven by the need for quantitative estimation of plant biochemical and physiological traits as well as characterising canopy architecture. Spectroscopic studies at the laboratory scale were the basis for the development of field evaluation systems that are nowadays used in agricultural and ecological monitoring and research. Plant pigments, including chlorophyll, carotenoids and anthocyanins, are the most studied traits and have been precisely retrieved from leaf and canopy spectral reflectance data (Homolová *et al.*, 2013). In addition, the retrieval of data on plant macronutrients, mainly nitrogen and phosphorus (Mutanga *et al.*, n.d.; Pimstein *et al.*, 2011), canopy water content (Clevers *et al.*, 2010), some structural components such as lignin and cellulose (Kokaly *et al.*, 2009) or even plant polyphenols (Skidmore *et al.*, 2009; Kokaly and Skidmore, 2015) have also been reported. Recent studies have addressed the use of hyperspectral reflectance for the evaluation of diverse physiological traits such as photosystem functioning, maximal Rubisco activity and dark respiration (Lobos *et al.*, 2019; Coast *et al.*, 2019; Silva-Perez *et al.*, 2018). Furthermore, the biophysical and structural traits of single plants and communities (including crops), such as leaf mass per area, leaf area index or plant height greatly affect the reflectance spectra and may thus also potentially be estimated by this reason (Yang *et al.*, 2016; Olsoy *et al.*, 2016). These advances can undoubtedly serve as excellent tools in plant ecophysiology studies, including the assessment of nutritional and water status, and potentially offer a great contribution to plant phenotyping and agronomy.

From a different perspective, recent studies have reported close relationships between the plant metabolome, yield performance and stress resilience (Obata *et al.*, 2015). In addition, novel studies have revealed that in cereals such as wheat, the ears can perform as major photosynthetic organs

during grain filling and have great relevance during plant N-assimilation and antioxidant metabolism, particularly under stress conditions (Sanchez-Bragado *et al.*, 2014; Tambussi *et al.*, 2007; Vicente *et al.*, 2018). The use of molecular spectroscopy includes but is not limited to the pharmaceutical and agri-food industries (Osborne, 2000; Luypaert *et al.*, 2007). In this sense, the possibility of predicting certain leaf and ear metabolites from remotely sensed data, particularly under field conditions, might enable *in vivo* metabolomics (metabolite characterization) and open the door to a new generation of plant phenotyping approaches. However, the retrieval of information pertaining to biochemical compounds has not yet been addressed in terms of broad metabolite profiles. Furthermore, the assessment of plant biochemical traits at the canopy scale still faces considerable limitations due to canopy structure and density, while such assessments in ear bracts could also be challenging due to their morphoanatomical and compositional characteristics.

In this study we set out to predict the metabolite profiles of wheat flag leaves and ear bracts, as well as grain yield, using the visible-near infrared-short waved infrared (VIS-NIR-SWIR) reflectance spectra of plant flag leaves, ears and plot canopies by least absolute shrinkage and selection operator (LASSO) regression. Although the prediction of grain yield from hyperspectral data using canopy or leaf reflectance in cereals (Weber *et al.*, 2012) including wheat (Garriga *et al.*, 2017; Montesinos-López *et al.*, 2017; Hernandez *et al.*, 2015) is not novel, the use of the ear spectrum for prediction has not been tested so far. Secondly, we aim to assess which wavebands of the spectrum are related to specific metabolites or groups of metabolites.

Results

Spectral overview and grain yield association (or grain yield prediction)

Leaf, ear and canopy spectra were clearly separated by both principal component (PC) analysis of original reflectance (Fig. 1 upper) and derivative (Fig. 1 lower) spectra and explained 94.3% and 71.0% of the data variability, respectively. The contribution of the wavebands to the PCs and hence to the group separation was clearer when the derivative spectra were employed, although the cumulative percentage of variance decreased compared to that of original reflectance. PC1 was principally determined by the reflectance in the VIS (R_{500}, R_{550}, R_{650} and R_{680}) and NIR (R_{830}, R_{880}, R_{1000} and R_{1225}) bands, while PC2 was mainly affected by the derivative spectra in the SWIR (R_{1750}, R_{2040} and $R_{2300\text{-}2400}$) but also in certain wavebands in the NIR (R_{1060} and R_{1400}).

Grain yield prediction models using leaf, ear and canopy spectra (sample size = 288) explained above 80% of yield variability in the training sets and up to 74.0%, 72.8% and 72.1% in the validation sets of the leaf, ear and canopy models, respectively (Table 1). In the models that used leaf and canopy spectra, prediction accuracy was slightly increased when applying spectral information recorded at the grain filling stage (RMSE = 0.783 and 0.813, respectively), whereas ear spectra at anthesis

provided the best prediction accuracy (RMSE = 0.802). Leaf and ear spectral information explained a slightly higher proportion of grain yield as compared to the canopy spectral data, but the differences were minor (Table 1).

Waveband selection in the yield prediction models differed according to the measured trait: the specific organ spectrum and the canopy spectrum (Fig. 2). In the case of the model based on the leaf spectrum, the highest detection rate occurred in the violet (400-440 nm) and in the red-edge (780 nm) wavebands as well as in the first part of the NIR (895-1000 nm) region (and precisely in the SWIR 2310 nm). In the case of the canopy spectrum-based model for yield prediction, the highest detection rates principally occurred in the terminal region of the NIR (1360-1400 nm) and in the SWIR (1800 nm, 2065 nm and 2280-2385 nm). Secondarily, some detection peaks were shown in the VIS-NIR range (515 nm, 760 nm, 1023 nm, 1130 nm). Finally, in the case of the ear spectrum model, the selection of wavebands exhibited an intermediate performance compared to the two other models; the highest detection rates were found in the violet and blue region (400-490 nm), in the first part of the NIR (800-880 nm, 985 nm, 1085 nm) and in the SWIR region (2210 nm, 2305 nm, 2385 nm).

Metabolite-spectrum association in leaves and ears

GC-MS based metabolite profiling of wheat flag leaves and ear bracts detected 66 metabolites for leaves, 70 metabolites for glumes and 64 metabolites for lemmas, 60 of which were detected in all tissues (Table 2). In general terms, diverse regions of the leaf and ear spectra were identified as closely correlated with much of the metabolite content (Fig. 3). However, the strength of correlations was not uniform throughout the spectrum and depended on the measured organ (i.e. on the specificity between the organ spectrum and tissue metabolome).

In leaves, the highest correlations between derivative spectrum and leaf metabolites were observed in the VIS region of the spectrum (400-770 nm) but also in certain NIR wavebands (about 1200 nm and 1350 nm) and SWIR (about 1500 nm, 1800 nm, 2000 nm, 2150 nm and 2200 nm) and included, among others, many amino acids (threonine, serine, alanine, GABA, aspartate, asparagine and β-alanine), organic acids (glycolate, glycerate, fumarate, citrate and pyruvate) and sugars (*myo*-inositol, glycerol, sucrose and xylose). Less prominently, another group of leaf metabolites was more correlated with the NIR-SWIR regions (centred on 1200 nm, 1500 nm, 1800 nm, 2000 nm and 2200 nm) such as glycine, arginine, dehydroascorbate, 2-oxoglutarate, tryptophan, hydroxyproline, and proline; whereas predominantly some sugars (fucose, raffinose, trehalose, *myo*-inositol-P and erythrose) and amino acids (lysine, phenylalanine, methionine) correlated moderately with reflectance spectra in the VIS and SWIR regions. Correlation between ear bract metabolites and the ear spectrum showed similar trends. For several metabolites -particularly in lemmas- higher coefficients were observed in the NIR-SWIR spectral regions (about 1100 nm, 1275-1450 nm, 1500-

1700 nm, 1750 nm, 1850 nm and about 2000-2200 nm) and to a minor extent in the VIS (centred on 450 nm, 600 nm and 750 nm). According to their coefficients of correlation, in lemmas the strongest association was found for the sugars xylose, glucose, maltose and the sugar derivatives glycerol and *myo*-inositol; for the organic acids pyruvate, fumarate succinate and glycerate; and for the amino acids β-alanine, threonine, serine and GABA. Following this trend, in glumes the strongest correlations were found for the sugars and sugar derivatives - fructose, glucose, sucrose, *myo*-inositol, *myo*-inositol-P, maltose and raffinose; for the organic acids glycerate and glycolate; and for the amino acids GABA, serine, threonine, asparagine, proline and alanine.

Regarding the positive or negative relationships between the derivative reflectance and metabolite content some general trends can be mentioned, although these are not applicable for all metabolites because metabolite-spectrum specificity occurred. In ear bracts, most metabolites correlated positively with the derivative spectrum in the wavebands 695-780 nm, 990-1055 nm, 1225-1260 nm, 1470-1690 nm and 2020-2225 nm, whereas they correlated negatively with the derivative reflectance centred on 400-475 nm, 550-625 nm, 925-975 nm, 1075-1175 nm, 1260-1460 nm, 1700-1790 nm, 1815-1890 nm, 1920-2010 nm and 2250-2400 nm. Note that the strengths of these correlations as well as the concrete range of these wavebands were metabolite-dependent. However, some ear amino acids (tyrosine, phenylalanine and tryptophan) and organic acids (citrate, threonate and isocitrate) exhibited the opposite trend in terms of their correlation coefficient with the derivative spectrum, at least in the wavebands centred on 1350 nm and 1550 nm. Unlike the ears, the relationship between the derivative spectrum and metabolite content in leaves was still more heterogeneous. For many metabolites, higher positive correlation coefficients were observed for the wavebands 555-676 nm, 720-800 nm and secondarily in the regions centred on 1100 nm, 1350 nm, 1800 nm and 2200 nm. Conversely, the derivative reflectance wavebands that negatively correlated were primarily 400-553 nm and 680-717 nm and secondarily in wavebands centred on 1190 nm, 1475 nm, 2000 nm and 2150 nm. Even so, for some metabolites (most of them amino acids) the opposite correlation coefficients were observed, particularly in wavebands around 1500 nm and 2000 nm (Fig. 3).

Metabolite estimation models using the VIS-NIR-SWIR organ spectrum

Flag leaf and ear bract metabolites were targeted as response variables and predicted from leaf and ear full-range spectra, respectively. From this collection, the overall results showed that LASSO regression models were able to explain more than 30% of the variability for 32 metabolites in lemmas, 36 metabolites in leaves and 40 metabolites in glumes according to the adj-R^2 in their validation sets (n=120) (Table 3). A higher proportion of explained variance was generally achieved when the metabolite content was expressed as $\log_2$-transformed relative content and the spectra were introduced as original reflectance. For at least 15 metabolites in leaves and ears, prediction

models achieved more than 50% of explained variation according to their adj-R^2 in the validation sets (Fig. 4). These metabolites were predominantly sugars (glucose, sucrose, fructose, raffinose, maltose, xylose, rhamnose, fucose and erythrose), sugar alcohols (*myo*-inositol, 3-phosphoglycerol, galactinol and glycerol), organic acids (malate, citrate, glycerate, fumarate, glycolate and pyruvate) and amino acids (proline, serine, threonine, GABA, alanine and tryptophan). Considering the range of variation within the metabolites and their standard deviations in the data set (in their respective original intensity or the log2-transformed intensity), the considerably low RMSE in the models indicated the good to very good prediction accuracies of these models. The strength of the prediction for each metabolite depended partly on the tissue (i.e. the best prediction models in each tissue did not always match the same metabolites).

According to the adjusted determination coefficients in the validation sets, the best predicted metabolites of leaves were the organic acids malate (82%) and glycerate (63%), the amino acids serine (63%), GABA (61%) and alanine (61%), and sucrose (68%) (Fig. 4). In the case of the lemma's metabolites, higher prediction robustness was shown for *myo*-inositol (81%), proline (74%), glucose (71%), glycerate (63%) and maltose (60%). Finally, in glumes the highest proportions of metabolite content variance were obtained for the organic acids glycolate (80%) and glucarate-1,4-lactone (64%), for the amino acids proline (72%) and GABA (71%), and for the sugars 3-phosphoglycerol (72%), glucose (69%), sucrose (68%), maltose (61%) and raffinose (60%).

Metabolite estimation models using the VIS-organ spectrum and the canopy spectrum

In comparison to the prediction models using the full range spectra of leaves and ears, there was an evident loss of a proportion of variance explained in the metabolite prediction models when only the VIS spectrum was employed. Even so, some metabolites were considerably well predicted; for seven metabolites in leaves, eleven metabolites in glumes, and three metabolites in lemmas the proportion of variance explained by the model exceeded 50% in the validation sets (Fig. 4). The highest determination coefficients of the regressions were shown for *myo*-inositol (Adj-R^2 = 58-71%) and glucose (Adj-R^2 = 57-60%) in ear bracts, glycerate (Adj-R^2 = 59%) in lemmas and glycolate (Adj-R^2 = 63%) in glumes. Finally, in leaves the highest proportions of phenotypic variance explained were found for serine (Adj-R^2 = 65%), malate (Adj-R^2 = 62%), glycerate (Adj-R^2 = 60%) and sucrose (Adj-R^2 = 57%). On the other hand, the use of canopy spectra for the estimation of the leaf and ear bract metabolite profiles (Fig. 4) resulted, on average, in slightly worse determination coefficients relative to the VIS-NIR-SWIR models. The best estimation models based on Adj-R^2 values were obtained for malate (71%), glycerate (69%), serine (65%) and phosphate (61%) in leaves; for *myo*-inositol (76%) and glycerate (64%) in lemmas; and for GABA (75%), glycolate (74%), glycerol-3-P (64%), phosphate (63%), *myo*-inositol (63%), glucose (63%) and proline (60%) in glumes. It is, however, worth mentioning that in some cases the metabolite variance explained from the canopy spectra slightly

surpassed the VIS-NIR-SWIR models from individual organ spectra, as in the case of phosphate in leaves and glumes; GABA and *myo*-inositol in glumes; citrate, putrescine and threonine in leaves; and glycerol-3-P, uracil, alanine, trehalose and fucose in lemmas.

Waveband selection in metabolite estimation models

Figure 5 presents the detection rates of wavebands throughout the VIS-NIR-SWIR spectrum for certain metabolite estimation models using the respective organ spectrum or the canopy spectrum. Regardless of the specific metabolite prediction model, common trends in waveband selection were clear. When the canopy spectrum was employed the 1300-1400 nm and 2200-2400 nm regions were mainly selected with secondary bands around 1700 nm, whereas when the organ (i.e. leaf and ear) spectra were used, the 400-500 nm region was selected principally and the secondary wavebands lay between 600-700 nm, 800-1000nm and 2200-2400 nm.

Waveband selection for the prediction of metabolites such as serine and glycerate in leaves and lemmas varied depending on the organ measured. Some spectral regions were selected in both models (i.e. leaf metabolites vs. leaf spectrum; lemma metabolites vs. ear spectrum) in the prediction of serine (about 400 nm and 800 nm) and glycerate (about 400 nm), but many other wavebands selected were model/organ-dependent (Fig. 5). Similarly, when GABA and sucrose were compared, some wavebands were commonly selected from both leaf and ear spectra (around 400 nm for GABA and around 450 nm, 850-900 nm and 1700 nm for sucrose) while other wavebands were selected differentially between models. Furthermore, the prediction models for lemma and glume proline from the ear spectrum selected wavebands around 400-500 nm, 600-700 nm and 1700-1800 nm in both cases. On the other hand, waveband selection also differed depending on the spectrum used, whether it was the canopy spectrum or that of the respective organ. For instance, in the prediction of leaf metabolites some selected wavebands were coincident in organ and canopy models (around 1350 nm for serine, 2400 nm for GABA, 2350 nm for malate and 600 nm for sucrose) but many others were specifically detected in the canopy or organ models. For prediction of lemma metabolites, the wavebands detected in both the canopy and organ models were around 400 nm and 2350 nm for serine; 450 nm, 800 nm and 2400 nm for glycerate; 400 nm for *myo*-inositol; and 2300-2400 nm for glucose (Fig. 5). Finally, in the case of glume metabolite prediction, wavebands around 400 nm and 1350 nm for GABA; 450 nm, 1000 nm and 2250-2400 nm for sucrose and 400 nm for 3-phosphoglycerol were detected in both scaling approaches.

Regarding waveband selection from the canopy spectrum for estimation of metabolites in the leaves and ear bracts, a certain amount of specificity between wavebands and metabolites was observed. For instance, canopy models selected around 750 nm, 1350 nm and 2350 nm for leaf and lemma

serine, 1350 nm and 2350 nm for leaf and lemma glycerate, and 1350 nm and 2400 nm for leaf and glume sucrose.

Discussion

Previous work addressing grain yield prediction achieved 70.7% and 69.5% of the explained variability from leaf and canopy VIS-NIR-SWIR spectra, respectively, through application of PLS regression models (Weber *et al.*, 2012). While this previous study was performed in maize, the present work in wheat slightly improved this accuracy by achieving up to 74% of the explained yield with the use of LASSO regression, which has proven its greater performance over standard linear regression models (Bujak *et al.*, 2016). Also, similar to the leaf and canopy spectra, for the first time a relationship was established between the ear spectrum and final yield (adj-R^2 = 73% in validation set) in terms of explained variance.

The most relevant wavelengths for predicting grain yield have previously been associated with photosynthetic capacity (495–680 nm), the red inflection point (680–780 nm) and plant water status (900, 970, and 1450 nm, 1150–1260 nm, and 1520–1540 nm) (Hernandez *et al.*, 2015; Weber *et al.*, 2012). In the current work, the strong detection of violet-blue (400-490 nm) wavebands in leaf and ear-based models was likely associated with chlorophyll absorption and amino acid-protein absorption (Schmid, 2001). Additional detection peaks in the NIR wavelengths in leaf (780 nm, 895-1000 nm) and ear-based models (800-880 nm, 985 nm, 1085 nm) may be partly associated with structural discontinuities in the tissues (i.e. cell layers, interfaces and mesophyll structure), water content, brown pigment content (i.e. carotenoids and flavonoids) (Peñuelas and Filella, 1998; Ceccato *et al.*, 2001; Homolová *et al.*, 2013) and sugar concentration (900-990 nm) (Golic *et al.*, 2003). Also, important detection peaks in the SWIR region in ear-based models (2210 nm, 2305 nm, 2385 nm) and to a weaker extent in leaf-based models (2310 nm) can be related to absorptions by amino acid-protein, sugars, lignin, and/or cellulose (Thulin *et al.*, 2014) among others. In the case of the canopy-based yield prediction model, the most relevant wavebands detected could be associated with protein, sugar and/or cellulose absorptions (2065 nm, 2280-2385 nm). The other important detection peak located in the 1360-1400 nm waveband has been previously attributed to the absorption of organic carbon in soils (Homhuan *et al.*, 2016), specifically cellulose, lignin and/or sugar absorptions (Curran *et al.*, 1992; Ben-Dor *et al.*, 1997). Additional wavelengths detected in the VIS (480 nm, 515 nm) and NIR regions (760 nm, 1023 nm, 1130 nm) could be related to photosynthetic capacity, water vapour and N-H bond absorption features (Lugassi *et al.*, 2014; Ben-Dor *et al.*, 1997). Thus, in our study, yield performance was associated with photosynthetic traits, water content and brown pigment content in both leaves and ear bracts and specifically with sugar, amino acids-protein and structural elements (i.e. cellulose and lignin), particularly in bracts. For its part, waveband detection in canopy-based models reveals the importance of the 1360-1400 nm peak

as a likely indicator of biomass quantity and quality in the plot (i.e. organic carbon including structural elements), and in turn these are related to grain yield (Reynolds *et al.*, 2007), while other peaks may be attributed to photosynthetic activity, nitrogen and water content signals.

In the literature, spectroscopic studies addressing the retrieval of plant (leaf) biochemicals have mostly targeted pigments, nitrogen-protein, structural elements (cellulose and lignin) and mineral compounds (e.g. phosphorus and potassium) (Thulin *et al.*, 2014; Kokaly *et al.*, 2009; Skidmore *et al.*, 2009). However, to the best of our knowledge, the estimation of specific plant metabolites through VIS-NIR-SWIR spectral data in the field is still non-existent. This work has shown, for the first time, the robust capabilities of hyperspectral field-sensors for the non-destructive estimation of leaf and ear metabolite profiles. From the metabolites detected in wheat leaves and ear bracts by GC-MS profiling, about one quarter were satisfactorily predicted with accuracies over 50% (in the validation sets) including many sugars, amino acids and organic acids that play a central role in primary and secondary metabolism. Among them, some can be highlighted for their relevance in plant physiological functioning: i) major sugars involved in photosynthetic metabolism, carbon partitioning and storage (sucrose, fructose and glucose); ii) other sugars and sugar alcohols associated with protective functions, osmotic adjustment and stress tolerance (raffinose, maltose, glycerol, 3-phosphoglycerol and *myo*-inositol) (Obata *et al.*, 2015; Ibrahim and Abdellatif, 2016; Van den Ende, 2013); iii) amino acids such as proline, GABA, alanine, aspartate and tryptophan, with some of them involved in osmotic regulation, signalling and in the synthesis of secondary metabolites (Hildebrandt *et al.*, 2015; Chen and Jiang, 2010; Bown and Shelp, 2016); iv) photorespiration intermediates (glycerate, serine and glycolate); and v) other organic acids (malate, fumarate and pyruvate) related to osmoprotection and respiratory metabolism (Acosta-Motos *et al.*, 2017). By contrast, the unsatisfactory estimation of some metabolites (e.g. ornithine, lysine, glycine, 2-oxoglutarate, glutamate, fucose, arginine, methionine, isoleucine and valine) could be, among other reasons, due to the fact that (i) they do not exhibit any differentiable or appreciable spectral absorption, (ii) their spectral signal were (mostly) masked by other major spectral signals such as water and pigments and/or (iii) their amounts or the range of sample variation were small, which did not favour a good fit to the models.

Knowledge of the VIS-NIR-SWIR spectral features (spectral signals in plant reflectance) of the metabolites that we have characterised here has been considerably limited because typically other approaches have been used such as UV, MIR, X-ray, Raman or FTIR spectroscopy (Zhu *et al.*, 2011; Barth, 2000; Meyer *et al.*, 2017). This contrasts with the broader information available on generic constituents such as protein-N and sugars across many wavebands of the VIS-NIR-SWIR spectrum. For instance, the N-protein content has been mainly retrieved from three broad spectral regions: the red-edge region (680–780 nm), the NIR region around 1200 nm and the SWIR region where three

main protein absorption features are located around 1680 nm, 2050 nm and 2170 nm (Homolová *et al.*, 2013; Kumar *et al.*, 2002; Thulin *et al.*, 2014), whereas absorption in the blue (around 405 nm) and in the NIR (895-990 nm) has been associated with the total amino acid content (Bao *et al.*, 2012). For its part, absorption wavebands for sugar (and particularly starch) have been reported in the NIR (around 900 nm) and in the SWIR (1450 nm, 1700 nm, 1950 nm, 2100 nm, 2250 nm, 2300 nm and 2350 nm) (Kuska *et al.*, 2018).

When examining organ spectral properties in this study, the blue region proved to be the most relevant waveband for metabolite prediction (Fig. 5), regardless of the metabolite examined. In the same way, in all canopy models the 1300-1400 nm and 2200-2400 nm regions were always the best determinants for metabolite prediction, and were coincident with some of the absorption bands associated with sugars and N compounds. In addition, the existence of some metabolites (e.g. serine, proline, GABA, sucrose or glycerate) that were easily predicted in two or three tissues may be because (i) these compounds had prominent absorptions in at least some of the wavebands and (ii) their variation was closely related to the spectral signal of other traits like water, nitrogen and pigments. Besides, some degree of specificity between certain metabolites and the spectra used could be associated with morpho-anatomical particularities affecting the reflected radiation such as cuticle thickness and composition, the level of differential cell packing, or organ shape (e.g. flatness) (Ollinger, 2011; Carter and Knapp, 2001).

On the other hand, metabolite prediction models based on canopy reflectance or on the VIS organ spectrum still proved robust although in a minor extent than those using VIS-NIR-SWIR organ spectrum. These results encourage the up-scaling of data collection via UAVs as hyperspectral sensors become more affordable, which has been proposed for assessment of mineral constituents (Skidmore *et al.*, 2009), whereas the employment of VIS field spectrometers could be a low-cost robust alternative. High spatial resolution hyperspectral imaging from UAVs along with image segmentation techniques (Fernandez-Gallego *et al.*, 2018; Parraga *et al.*, 2019; Gracia-Romero *et al.*, 2019) might also enable the simultaneous and yet separate retrieval of the spectra of different crop canopy components such as flag leaves and ears. Altogether, these advances open the door for non-invasive and rapid field monitoring of key traits in flag leaves and/or ear bracts associated with photosynthesis and photorespiration, sugar accumulation, and stress-response and drought-tolerance metabolites. In this way it would be possible to study spatial-temporal variation in metabolite content (at least in some cases) and their response to stress conditions. In conclusion, this technique may be of interest for its broad applicability in plant breeding programs, ecophysiology research, and the agri-food industry. Future research may develop additional spectral transformations and automate metabolite retrieval models with spectral-managing software in order to make these data accessible to potential users such as breeders and ecophysiologists. In this

sense, previous computing efforts in radiative transfer models, currently included in ARTMO (Verrelst *et al.*, 2016; Verrelst *et al.*, 2015; Feret *et al.*, 2008; Atzberger *et al.*, 2003), which were developed for the retrieval of biophysical traits (chlorophyll, brown pigments, leaf water content, leaf area index and fluorescence) at the canopy and leaf levels are excellent precedents and may pave the way for collection of metabolite content data.

Experimental procedures

Plant material and experimental set up

Field trials were carried out during the 2014/15 growing season at three locations: in north Spain at the experimental station of Zamadueñas (Valladolid), belonging to the Instituto Tecnológico Agrario de Castilla y León (ITACyL), in central Spain at the experimental station of Colmenar de Oreja (Madrid), and in south Spain at the experimental station of El Majano (Seville), both belonging to the Instituto Nacional de Investigación y Tecnología Agraria y Alimentaria (INIA) of Spain. Geographic and agronomic information, together with weather, irrigation and soil information are detailed in Table 3.

Plant material consisted of 24 commercial durum wheat (*Triticum turgidum* L. subsp *durum* (Desf) Husn.) varieties released during the last thirty years in Spain. The varieties Don Sebastian, Dorondon, Kiko Nick, Pelayo and Sula (Chairi *et al.*, 2018) were selected as representative of yield performance variability and subsequently used for metabolite profiling and spectral prediction models.

For each trial, plants were sown in randomized block designs with three replicates. A total of four growing conditions were considered: three rainfed trials (one rainfed trial at each of the experimental stations) and one supplemental irrigated trial at Zamadueñas. While the rainfed environments of Colmenar and Zamadueñas are highly restrictive, the rainfed trial of El Majano is characterized as a high yielding environment due to its closeness to the Guadalquivir River (i.e. high level water table). At harvest, grains were dried in an oven at 60ºC for 48 hours and grain yield (GY) was determined.

Spectral field measurements

The flag leaf, ear and canopy spectral signatures were measured around midday on sunny days with a Field-Spec4 (ASD Inc. PANalytical Company, Boulder, USA) full-range portable spectroradiometer. The reflectance spectra of three flag leaves and three ears were recorded for each plot with an ASD leaf clip accessory assembled on an ASD standard plant contact probe provided with a halogen bulb coupled to the FieldSpec4 spectrometer with an optical fibre. Canopy spectra were measured with a pistol grip coupled to the optical fibre. Measurements were made one metre above the plot canopy in a zenithal plane and the reflectance was calibrated every 15-20 minutes with a Spectralon white

reference panel. Spectra were acquired at the crop development stages of anthesis and grain filling, which are stages 69 and 74 in the Zadoks scale (Zadoks *et al.*, 1974), respectively, on 13 April and 11 May at El Majano, 12 and 25 May at Colmenar de Oreja, and 15 and 28 May at Zamadueñas. For the prediction models the spectra were tested as original reflectance spectra and as derivative-transformed reflectance spectra.

Leaf and ear metabolite profiling and isotope analyses

Three flag leaf blades and three ears per plot were harvested and immediately frozen in dry ice at the anthesis and middle grain filling stages on the same dates mentioned before. Then, the glumes and lemmas of the ears were separated, and the three organs were ground in liquid nitrogen. One hundred milligrams of powdered fresh material of each of the 360 samples were used for gas chromatography-mass spectrometry (GC-MS).

Metabolite extraction and derivatisation were performed as an adaptation of the procedure described in Lisec et al. (2006) and Witt et al. (2012). One μl of each sample was used to inject into a gas chromatography-time of flight- mass spectrometry (GC–TOF–MS) system (Pegasus III, Leco, St Joseph, USA). The relative changes in the metabolite pools were analysed using GC-TOF-MS ChromaTOF software (Pegasus, LECO, St Joseph, USA). Peaks in the chromatograms were manually annotated and ion intensity was determined by the aid of TagFinder (Luedemann *et al.*, 2011) using a reference library derived from the Golm Metabolome-Database for compound identification (Kopka *et al.*, 2005).

Statistical analysis

R 3.5.1 (R Core Team, 2018) was used for conducting principal component analysis (PCA) with the PCA3D package (January Weiner, 2017). Figures were drawn with SigmaPlot 10.0 (Systat Software Inc., San Jose, CA, USA).

Grain yield and metabolite prediction models were performed with canopies, flag leaves and ears reflectance spectra. To fit the models for grain yield and for metabolite predictions, individual (i.e. single plot) leaf, ear and canopy spectra were used and data for the HY and WS conditions were combined into one dataset. Identification of spectrum-metabolite and spectrum-GY associations and their predictions based on spectral data was performed using least absolute shrinkage and selection operator (LASSO) regression. Analysis was carried out with SAS software 9.4 (SAS Institute Inc., Cary, NC, USA) applying the *proc glmselect* procedure. To increase the robustness of the results, five-fold cross-validation (CV) was conducted. In total 100 CV runs (20 times five-fold CV) were performed. For these 100 subsets were extracted from the full dataset. Each subset comprised 75% of the data points each, randomly selected. The subsets were taken as training sets for the identification of

spectrum metabolite and grain yield associations and for the estimation of their effects. The remaining 25% of the data was used as validation set. To estimate the proportion of variance in the grain yield and the metabolite relative content explained by the model, the unbiased estimator Adj-R^2 (Draper and Smith, 1981) was calculated for each subset. As a measure of accuracy, the root mean square error (RMSE) was calculated. Effects for each waveband were extracted as a regression coefficient of the respective waveband directly from the LASSO model. In addition, the count of each waveband over all training sets was recorded and referred to as the detection rate. This value was taken as a measure of importance of the associations of grain yield and metabolite content with specific wavebands. To determine the predictive ability of the full model for grain yield and for each metabolite, the regression estimates, obtained using the training sets, were used to predict the grain yield and metabolite value of the remaining 25% of data forming the validation sets. The predictive ability was defined to be the squared Pearson product-moment correlation between predicted and observed phenotypic values. The statistics provided for each model (R^2, Adj-R^2, RMSE, and waveband effect for the training and validation sets) were averaged across all 100 CV runs to obtain the final results.

Before running LASSO regression models, the regions from 350 to 400 nm and 2400 to 2500 nm were removed from all reflectance data to avoid the noisy bands in the spectra. Additionally, in plant canopy spectra the region from 1800 to 2000 nm was also removed because it is strongly affected by water vapour absorption.

Acknowledgements

We thank Nieves Aparicio, Maria Teresa Nieto-Taladriz and Jesús Mérida for field trial design and management and Max Plank technicians for their assistance. This work was supported by the Spanish Ministry of Economy and Competitiveness (MEC) [grant number AGL2016-76527- R]. S.C.K. is the recipient of a Juan de la Cierva Research grant from the MEC [IJCI2014-20595]. O.V.D. is the recipient of an APIF fellowship sponsored by the University of Barcelona. J.L.A. acknowledges the support of the ICREA Academia, the Government of Catalonia, Spain. We thank the Goetz Instrument Program from the ASD PANalytical Company for providing us with the FieldSpec4 spectrometer. All authors declare not to have any conflict of interest.

References

Acosta-Motos, J., Ortuño, M., Bernal-Vicente, A., et al. (2017) Plant Responses to Salt Stress: Adaptive Mechanisms. *Agronomy*, **7**, 18. Available at: http://www.mdpi.com/2073-4395/7/1/18 [Accessed August 23, 2018].

Araus, J.L. and Cairns, J.E. (2014) Field high-throughput phenotyping: the new crop breeding frontier. *Trends Plant Sci.*, **19**, 52–61. Available at: http://www.ncbi.nlm.nih.gov/pubmed/24139902 [Accessed July 19, 2018].

Atzberger, C., Jarmer, T., Schlerf, M., Kotz, B. and Werner, W. (2003) Retrieval of wheat bio-physical attributes from hyperspectral data and SAILH+ PROSPECT radiative transfer model. *3rd EARSeL Work. Imaging Spectrosc.*, 473–482. Available at: http://www.researchgate.net/publication/228798770_Retrieval_of_wheat_bio-physical_attributes_from_hyperspectral_data_and_SAILH_PROSPECT_radiative_transfer_model/file/9fcfd50a356a730d97.pdf.

Bao, Y., Kong, W., He, Y., Liu, F., Tian, T. and Zhou, W. (2012) Quantitative Analysis of Total Amino Acid in Barley Leaves under Herbicide Stress Using Spectroscopic Technology and Chemometrics. *Sensors*, **12**, 13393–13401. Available at: http://www.ncbi.nlm.nih.gov/pubmed/23202000 [Accessed May 10, 2019].

Barth, A. (2000) The infrared absorption of amino acid side chains. *Prog. Biophys. Mol. Biol.*, **74**, 141–173. Available at: https://www.sciencedirect.com/science/article/pii/S0079610700000213 [Accessed May 10, 2019].

Ben-Dor, E., Inbar, Y. and Chen, Y. (1997) The reflectance spectra of organic matter in the visible near-infrared and short wave infrared region (400–2500 nm) during a controlled decomposition process. *Remote Sens. Environ.*, **61**, 1–15. Available at: https://www.sciencedirect.com/science/article/abs/pii/S0034425796001204 [Accessed May 2, 2019].

Bown, A.W. and Shelp, B.J. (2016) Plant GABA: Not Just a Metabolite. *Trends Plant Sci.*, **21**, 811–813. Available at: http://www.ncbi.nlm.nih.gov/pubmed/27542324 [Accessed August 27, 2018].

Bujak, R., Daghir-Wojtkowiak, E., Kaliszan, R. and Markuszewski, M.J. (2016) PLS-Based and Regularization-Based Methods for the Selection of Relevant Variables in Non-targeted Metabolomics Data. *Front. Mol. Biosci.*, **3**, 35. Available at: http://journal.frontiersin.org/Article/10.3389/fmolb.2016.00035/abstract [Accessed July 6, 2018].

Carter, G.A. and Knapp, A.K. (2001) Leaf optical properties in higher plants: linking spectral characteristics to stress and chlorophyll concentration. *Am. J. Bot.*, **88**, 677–84. Available at: http://www.ncbi.nlm.nih.gov/pubmed/11302854 [Accessed November 27, 2018].

Ceccato, P., Flasse, S., Tarantola, S., Jacquemond, S. and Grégoire, J.-M. (2001) Detecting vegetation water content using reflectance in the optical domain. *Remote Sens. Environ.*, **77**, 22–33.

Chairi, F., Vergara-Diaz, O., Vatter, T., Aparicio, N., Nieto-Taladriz, M.T., Kefauver, S.C., Bort, J., Serret, M.D. and Araus, J.L. (2018) *Post-green Revolution genetic advance in durum wheat: the case of Spain*,.

Chen, H. and Jiang, J.-G. (2010) Osmotic adjustment and plant adaptation to environmental changes related to drought and salinity. *Environ. Rev.*, **18**, 309–319. Available at: http://www.nrcresearchpress.com/doi/10.1139/A10-014 [Accessed September 5, 2018].

Clevers, J.G.P.W., Kooistra, L. and Schaepman, M.E. (2010) Estimating canopy water content using hyperspectral remote sensing data. *Int. J. Appl. Earth Obs. Geoinf.*, **12**, 119–125. Available at: https://ac-els-cdn-com.sire.ub.edu/S0303243410000103/1-s2.0-S0303243410000103-main.pdf?_tid=c267b335-52b9-41c7-b40f-

8fd26faaf7e1&acdnat=1548067130_e16a47357c4a8f1ed42cc1cd54e20131 [Accessed January 21, 2019].

Coast, O., Shah, S., Ivakov, A., et al. (2019) Predicting dark respiration rates of wheat leaves from hyperspectral reflectance. *Plant. Cell Environ.*, pce.13544. Available at: https://onlinelibrary.wiley.com/doi/abs/10.1111/pce.13544 [Accessed April 10, 2019].

Curran, P.J., Dungan, J.L., Macler, B.A., Plummer, S.E. and Peterson, D.L. (1992) Reflectance Spectroscopy of Fresh Whole Leaves for the Estimation of Chemical Concentration. *Remote Sens. Environ.*, **39**, 153–166. Available at: https://pdf.sciencedirectassets.com/271745/1-s2.0-S0034425700X0171X/1-s2.0-0034425792901335/main.pdf?x-amz-security-token=AgoJb3JpZ2luX2VjELz%252F%252F%252F%252F%252F%252F%252F%252F%252F%252FwEaCXVzLWVhc3QtMSJIMEYCIQD58U2O2nBK%252B75nWSCka7FQhmnuRrinllaztWO8pUyhFwIhAMPaLb6Ve%252 [Accessed May 2, 2019].

Draper, N.R. and Smith, H. (1981) *Applied Regression Analysis*, Available at: http://link.springer.com/10.1007/b98890.

Ende, W. Van den (2013) Multifunctional fructans and raffinose family oligosaccharides. *Front. Plant Sci.*, **4**, 247. Available at: http://www.ncbi.nlm.nih.gov/pubmed/23882273 [Accessed June 19, 2018].

Feret, J.B., François, C., Asner, G.P., Gitelson, A.A., Martin, R.E., Bidel, L.P.R., Ustin, S.L., Maire, G. le and Jacquemoud, S. (2008) PROSPECT-4 and 5: Advances in the leaf optical properties model separating photosynthetic pigments. *Remote Sens. Environ.*, **112**, 3030–3043.

Fernandez-Gallego, J.A., Kefauver, S.C., Gutiérrez, N.A., Nieto-Taladriz, M.T. and Araus, J.L. (2018) Wheat ear counting in-field conditions: high throughput and low-cost approach using RGB images. *Plant Methods*, **14**, 22. Available at: https://plantmethods.biomedcentral.com/articles/10.1186/s13007-018-0289-4 [Accessed June 3, 2019].

Garriga, M., Romero-Bravo, S., Estrada, F., Escobar, A., Matus, I.A., Pozo, A. del, Astudillo, C.A. and Lobos, G.A. (2017) Assessing Wheat Traits by Spectral Reflectance: Do We Really Need to Focus on Predicted Trait-Values or Directly Identify the Elite Genotypes Group? *Front. Plant Sci.*, **8**, 280. Available at: http://www.ncbi.nlm.nih.gov/pubmed/28337210 [Accessed May 15, 2019].

Golic, M., Walsh, K. and Lawson, P. (2003) Short-Wavelength Near-Infrared Spectra of Sucrose, Glucose, and Fructose with Respect to Sugar Concentration and Temperature. *Appl. Spectrosc.*, **57**, 139–145. Available at: http://www.ncbi.nlm.nih.gov/pubmed/14610949 [Accessed May 8, 2019].

Gracia-Romero, A., Kefauver, S.C., Fernandez-Gallego, J.A., et al. (2019) UAV and Ground Image-Based Phenotyping: A Proof of Concept with Durum Wheat. *Remote Sens.*, **11**, 1244. Available at: https://www.mdpi.com/2072-4292/11/10/1244 [Accessed June 17, 2019].

Hernandez, J., Lobos, G.A., Matus, I., Pozo, A. Del, Silva, P., Galleguillos, M., Atzberger, C. and Thenkabail, P.B. (2015) Using Ridge Regression Models to Estimate Grain Yield from Field Spectral Data in Bread Wheat (Triticum Aestivum L.) Grown under Three Water Regimes. , **7**, 2109–2126. Available at: www.mdpi.com/journal/remotesensingArticle [Accessed May 15, 2019].

Hildebrandt, T.M., Nunes Nesi, A., Araújo, W.L. and Braun, H.-P. (2015) Amino Acid Catabolism in Plants. *Mol. Plant*, **8**, 1563–1579. Available at: https://www.sciencedirect.com/science/article/pii/S1674205215003664 [Accessed June 11, 2018].

Homhuan, S., Pansak, W., Lawawirojwong, S. and Narongrit, C. (2016) Laboratory Spectroscopy Assessments of Rainfed Paddy Soil Samples on Visible and Near-Infrared Spectroscopy Reflectance for Estimating Soil Organic Carbon. *Air, Soil Water Res.*, 9–77. Available at: https://journals.sagepub.com/doi/pdf/10.4137/ASWR.S40173 [Accessed May 2, 2019].

Homolová, L., Malenovský, Z., Clevers, J.G.P.W., García-Santos, G. and Schaepman, M.E. (2013) Review of optical-based remote sensing for plant trait mapping. *Ecol. Complex.*, **15**, 1–16.

Ibrahim, H.A. and Abdellatif, Y.M.R. (2016) Effect of maltose and trehalose on growth, yield and some biochemical components of wheat plant under water stress. *Ann. Agric. Sci.*, **61**, 267–274. Available at: https://www.sciencedirect.com/science/article/pii/S0570178316300173 [Accessed July 5, 2018].

January Weiner, M. (2017) *Package "pca3d" Type Package Title Three Dimensional PCA Plots*, Available at: https://cran.r-project.org/web/packages/pca3d/pca3d.pdf [Accessed September 19, 2018].

Kokaly, R.F., Asner, G.P., Ollinger, S. V., Martin, M.E. and Wessman, C.A. (2009) Characterizing canopy biochemistry from imaging spectroscopy and its application to ecosystem studies. *Remote Sens. Environ.*, **113**, S78–S91. Available at: http://dx.doi.org/10.1016/j.rse.2008.10.018.

Kokaly, R.F. and Skidmore, A.K. (2015) Plant phenolics and absorption features in vegetation reflectance spectra near 1.66 µm. *Int. J. Appl. Earth Obs. Geoinf.*, **43**, 55–83. Available at: https://www.sciencedirect.com/science/article/pii/S0303243415000112 [Accessed April 1, 2019].

Kopka, J., Schauer, N., Krueger, S., et al. (2005) GMD@CSB.DB: the Golm Metabolome Database. *Bioinformatics*, **21**, 1635–1638. Available at: https://academic.oup.com/bioinformatics/article-lookup/doi/10.1093/bioinformatics/bti236 [Accessed June 13, 2018].

Kumar, L., Schmidt, K., Dury, S. and Skidmore, A. (2002) Imaging Spectrometry and Vegetation Science. In Springer, Dordrecht, pp. 111–155. Available at: http://link.springer.com/10.1007/978-0-306-47578-8_5 [Accessed May 9, 2019].

Kuska, M.T., Behmann, J. and Mahlein, A.-K. (2018) Conference paper Potential of hyperspectral imaging to detect and identify the impact of chemical warfare compounds on plant tissue. *Pure Appl. Chem*, **90**, 1615–1624. Available at: https://doi.org/10.1515/pac-2018-0102 [Accessed May 2, 2019].

Lisec, J., Schauer, N., Kopka, J., Willmitzer, L. and Fernie, A.R. (2006) Gas chromatography mass spectrometry–based metabolite profiling in plants. *Nat. Protoc.*, **1**, 387–396. Available at: http://www.nature.com/doifinder/10.1038/nprot.2006.59 [Accessed June 13, 2018].

Lobos, G., Escobar-Opazo, A., Estrada, F., et al. (2019) Spectral Reflectance Modeling by Wavelength Selection: Studying the Scope for Blueberry Physiological Breeding under Contrasting Water Supply and Heat Conditions. *Remote Sens.*, **11**, 329. Available at: http://www.mdpi.com/2072-4292/11/3/329 [Accessed March 29, 2019].

Luedemann, A., Malotky, L. von, Erban, A. and Kopka, J. (2011) TagFinder: Preprocessing Software for the Fingerprinting and the Profiling of Gas Chromatography–Mass Spectrometry Based Metabolome Analyses. In *Methods in molecular biology (Clifton, N.J.)*. pp. 255–286. Available at: http://www.ncbi.nlm.nih.gov/pubmed/22351182 [Accessed June 13, 2018].

Lugassi, R., Chudnovsky, A., Zaady, E., et al. (2014) Spectral Slope as an Indicator of Pasture Quality. *Remote Sens.*, **7**, 256–274. Available at: http://www.mdpi.com/2072-4292/7/1/256

[Accessed May 2, 2019].

Luypaert, J., Massart, D.L. and Heyden, Y. Vander (2007) Near-infrared spectroscopy applications in pharmaceutical analysis. *Talanta*, **72**, 865–883. Available at: https://www.sciencedirect.com/science/article/pii/S003991400600823X [Accessed May 10, 2019].

Meyer, F., Blum, M., Benkert, A., et al. (2017) X-ray Emission Spectroscopy of Proteinogenic Amino Acids at All Relevant Absorption Edges. *J. Phys. Chem. B*, **121**, 6549–6556. Available at: http://pubs.acs.org/doi/10.1021/acs.jpcb.7b04291 [Accessed May 10, 2019].

Montesinos-López, O.A., Montesinos-López, A., Crossa, J., Campos, G. de los, Alvarado, G., Suchismita, M., Rutkoski, J., González-Pérez, L. and Burgueño, J. (2017) Predicting grain yield using canopy hyperspectral reflectance in wheat breeding data. *Plant Methods*, **13**. Available at: https://www.ncbi.nlm.nih.gov/pmc/articles/PMC5209864/ [Accessed May 15, 2019].

Mutanga, O., Skidmore, A.K. and Prins, H.H.T. Predicting in situ pasture quality in the Kruger National Park, South Africa, using continuum-removed absorption features. Available at: www.elsevier.com/locate/rse [Accessed January 21, 2019].

Obata, T., Witt, S., Lisec, J., Palacios-Rojas, N., Florez-Sarasa, I., Yousfi, S., Araus, J.L., Cairns, J.E. and Fernie, A.R. (2015) Metabolite Profiles of Maize Leaves in Drought, Heat, and Combined Stress Field Trials Reveal the Relationship between Metabolism and Grain Yield. *Plant Physiol.*, **169**, 2665–83. Available at: http://www.ncbi.nlm.nih.gov/pubmed/26424159 [Accessed July 6, 2018].

Ollinger, S. V. (2011) Sources of variability in canopy reflectance and the convergent properties of plants. *New Phytol.*, **189**, 375–394.

Olsoy, P.J., Mitchell, J.J., Levia, D.F., Clark, P.E. and Glenn, N.F. (2016) Estimation of big sagebrush leaf area index with terrestrial laser scanning. *Ecol. Indic.*, **61**, 815–821. Available at: https://www.sciencedirect.com/science/article/pii/S1470160X15005853 [Accessed January 21, 2019].

Osborne, B.G. (2000) Near-Infrared Spectroscopy in Food Analysis. In *Encyclopedia of Analytical Chemistry*. Chichester, UK: John Wiley & Sons, Ltd. Available at: http://doi.wiley.com/10.1002/9780470027318.a1018 [Accessed May 10, 2019].

Parraga, A., Doering, D., Atkinson, J.G., Bertani, T., Oliveira Andrades Filho, C. de, Souza, M.R.Q. de, Ruschel, R. and Susin, A.A. (2019) Wheat Plots Segmentation for Experimental Agricultural Field from Visible and Multispectral UAV Imaging. In Springer, Cham, pp. 388–399. Available at: http://link.springer.com/10.1007/978-3-030-01054-6_28 [Accessed June 3, 2019].

Peñuelas, J. and Filella, L. (1998) Visible and near-infrared reflectance techniques for diagnosing plant physiological status. *Trends Plant Sci.*, **3**, 151–156.

Pimstein, A., Karnieli, A., Bansal, S.K. and Bonfil, D.J. (2011) Exploring remotely sensed technologies for monitoring wheat potassium and phosphorus using field spectroscopy. *F. Crop. Res.*, **121**, 125–135. Available at: https://ac-els-cdn-com.sire.ub.edu/S0378429010003151/1-s2.0-S0378429010003151-main.pdf?_tid=ffebdfb7-01cd-4d58-b804-ac9fdaca3c3d&acdnat=1548066813_c495b5594968a56097cd32efc3911912 [Accessed January 21, 2019].

R Core Team (2018) R: A Language and Environment for Statistical Computing. Available at: https://www.r-project.org/.

Reynolds, M.R., Calderini, C., Condon, A. and Vargas, M. (2007) Association of source/sink traits with yield, biomass and radiation use efficiency among random sister lines from three wheat crosses in a high-yield environment. *J. Agric. Sci.*, **145**, 3–16. Available at: https://repository.cimmyt.org/xmlui/bitstream/handle/10883/2540/89761.pdf [Accessed May 30, 2019].

Sanchez-Bragado, R., Elazab, A., Zhou, B., Serret, M.D., Bort, J., Nieto-Taladriz, M.T. and Araus, J.L. (2014) Contribution of the ear and the flag leaf to grain filling in durum wheat inferred from the carbon isotope signature: Genotypic and growing conditions effects. *J. Integr. Plant Biol.*, **56**, 444–454. Available at: http://www.ncbi.nlm.nih.gov/pubmed/24028829 [Accessed July 9, 2018].

Schmid, F.-X. (2001) Biological Macromolecules: UV-visible Spectrophotometry. In *Encyclopedia of Life Sciences*. Chichester, UK: John Wiley & Sons, Ltd. Available at: http://doi.wiley.com/10.1038/npg.els.0003142 [Accessed May 30, 2019].

Silva-Perez, V., Molero, G., Serbin, S.P., Condon, A.G., Reynolds, M.P., Furbank, R.T. and Evans, J.R. (2018) Hyperspectral reflectance as a tool to measure biochemical and physiological traits in wheat. *J. Exp. Bot.*, **69**, 483–496. Available at: http://www.ncbi.nlm.nih.gov/pubmed/29309611 [Accessed May 15, 2019].

Skidmore, A.K., Ferwerda, J.G., Mutanga, O., Wieren, S.E. Van, Peel, M., Grant, R.C., Prins, H.H.T., Bektas Balcik, F. and Venus, V. (2009) Forage quality of savannas — Simultaneously mapping foliar protein and polyphenols for trees and grass using hyperspectral imagery. *Remote Sens. Environ.*, **114**, 64–72. Available at: https://ac-els-cdn-com.sire.ub.edu/S0034425709002521/1-s2.0-S0034425709002521-main.pdf?_tid=86da70f0-4c70-463c-8458-64130ae05307&acdnat=1548067429_b314d72da353a4d9e23374d73a0a9084 [Accessed January 21, 2019].

Tambussi, E.A., Bort, J., Guiamet, J.J., Nogués, S. and Araus, J.L. (2007) The Photosynthetic Role of Ears in C $_3$ Cereals: Metabolism, Water Use Efficiency and Contribution to Grain Yield. *CRC. Crit. Rev. Plant Sci.*, **26**, 1–16. Available at: http://www.tandfonline.com/doi/abs/10.1080/07352680601147901 [Accessed July 5, 2018].

Thulin, S., Hill, M.J., Held, A., Jones, S. and Woodgate, P. (2014) Predicting Levels of Crude Protein, Digestibility, Lignin and Cellulose in Temperate Pastures Using Hyperspectral Image Data. *Am. J. Plant Sci.*, **05**, 997–1019. Available at: http://www.scirp.org/journal/doi.aspx?DOI=10.4236/ajps.2014.57113 [Accessed May 7, 2019].

Verrelst, J., Rivera, J.P., Gitelson, A., Delegido, J., Moreno, J. and Camps-Valls, G. (2016) Spectral band selection for vegetation properties retrieval using Gaussian processes regression. *Int. J. Appl. Earth Obs. Geoinf.*, **52**, 554–567. Available at: http://dx.doi.org/10.1016/j.jag.2016.07.016 [Accessed May 28, 2019].

Verrelst, J., Rivera, J.P. and Moreno, J. (2015) ARTMO's Global Sensitivity Analysis (GSA) toolbox to quantify driving variables of leaf and canopy radiative transfer models. , **2**, 2015–2031. Available at: http://ipl.uv.es/artmo/. [Accessed May 28, 2019].

Vicente, R., Vergara-Díaz, O., Medina, S., Chairi, F., Kefauver, S.C., Bort, J., Serret, M.D., Aparicio, N. and Araus, J.L. (2018) Durum wheat ears perform better than the flag leaves under water stress: Gene expression and physiological evidence. *Environ. Exp. Bot.*, **153**, 271–285. Available at: https://linkinghub.elsevier.com/retrieve/pii/S0098847218301795 [Accessed June 19, 2018].

Weber, V.S., Araus, J.L., Cairns, J.E., Sanchez, C., Melchinger, A.E. and Orsini, E. (2012) Prediction of grain yield using reflectance spectra of canopy and leaves in maize plants grown under different water regimes. *F. Crop. Res.*, **128**, 82–90. Available at: https://pdf.sciencedirectassets.com/271162/1-s2.0-S0378429012X00029/1-s2.0-S0378429011004205/main.pdf?x-amz-security-token=AgoJb3JpZ2luX2VjEPv%2F%2F%2F%2F%2F%2F%2F%2F%2FwEaCXVzLWVhc3QtMSJGMEQCIBz0%2FoDe7TzIWzwkgOEJ%2B2nJ1RW2zJMCGSiix2CWFR9SAiAmw3Xkhfhz [Accessed April 24, 2019].

Witt, S., Galicia, L., Lisec, J., Cairns, J., Tiessen, A., Araus, J.L., Palacios-Rojas, N. and Fernie, A.R. (2012) Metabolic and Phenotypic Responses of Greenhouse-Grown Maize Hybrids to Experimentally Controlled Drought Stress. *Mol. Plant*, **5**, 401–417. Available at: https://www.sciencedirect.com/science/article/pii/S1674205214601283 [Accessed June 13, 2018].

Yang, X., Tang, J., Mustard, J.F., Wu, J., Zhao, K., Serbin, S. and Lee, J.E. (2016) Seasonal variability of multiple leaf traits captured by leaf spectroscopy at two temperate deciduous forests. *Remote Sens. Environ.*, **179**, 1–12. Available at: http://dx.doi.org/10.1016/j.rse.2016.03.026.

Zadoks, J.C., Chang, T.T. and Konzak, C.F. (1974) A decimal code for the growth stages of cereals. *Weed Res.*, **14**, 415–421. Available at: http://doi.wiley.com/10.1111/j.1365-3180.1974.tb01084.x [Accessed October 1, 2018].

Zhu, G., Zhu, X., Fan, Q. and Wan, X. (2011) Raman spectra of amino acids and their aqueous solutions. *Spectrochim. Acta Part A Mol. Biomol. Spectrosc.*, **78**, 1187–1195. Available at: https://www.sciencedirect.com/science/article/pii/S1386142510007043 [Accessed May 9, 2019].

Tables

Table 1. Performance of leaf, ear and canopy spectra for the prediction of grain yield using LASSO models. Statistics are provided for the training and validation sets.

	Leaf spectrum				Ear spectrum				Canopy spectrum			
	R^2	Adj-R^2	RMSE	Spectral transformation	R^2	Adj-R^2	RMSE	Spectral transformation	R^2	Adj-R^2	RMSE	Spectral transformation
Anthesis												
Training set	0.871	0.816	0.659	Original	0.928	0.869	0.554	First	0.883	0.806	0.678	First
Validation set	0.715	0.710	0.828	reflectance	0.733	0.728	0.802	derivative	0.665	0.659	0.897	derivative
Grain filling												
Training set	0.907	0.848	0.598	Original	0.923	0.854	0.587	First	0.925	0.863	0.569	Original
Validation set	0.744	0.740	0.783	reflectance	0.700	0.695	0.852	derivative	0.726	0.721	0.813	reflectance

Table 2. LASSO regression models for the prediction of leaf and ear bract metabolites from leaf and ear reflectance, respectively. The LASSO statistics provided were the adjusted coefficient of determination (adj-R^2) and the root mean squared error (RMSE). Descriptive statistics of metabolite relative intensities are maximum and minimum values (MAX and MIN), mean and standard deviation (SD) values. The best model (mod) in terms of proportion of explained variance is shown for each metabolite, the acronyms of the models are: RR, raw metabolite intensity combined with original reflectance; RD, raw metabolite intensity combined with the first derivative spectra; LR, log_2-transformed metabolite intensity combined with original reflectance; LD, log_2-transformed metabolite intensity combined with the first derivative spectra.

	Leaves							Lemmas							Glumes						
	LASSO model			Descriptive Statistics				LASSO model			Descriptive Statistics				LASSO model			Descriptive Statistics			
metabolite	adj-R^2	RMSE	mod	MAX	MIN	MEAN	SD	adj-R^2	RMSE	mod	MAX	MIN	MEAN	SD	adj-R^2	RMSE	mod	MAX	MIN	MEAN	SD
malate	0.817	20.630	RD	131.012	1.679	55.755	28.483	0.018	23.63	RR	108.73	0.3	4.51	15.194	0.56	0.981	LR	4.821	-2.193	1.449	1.511
sucrose	0.684	2.380	RD	13.134	0.127	4.119	4.354	0.173	2.250	RR	11.292	0.087	6.533	2.502	0.681	0.754	LD	6.148	1.680	3.858	1.360
glycerate	0.634	0.56	LR	3.189	-0.799	1.687	0.959	0.634	0.519	LD	3.452	-0.044	2.159	0.887	0.315	0.427	LD	3.578	1.313	2.597	0.526
serine	0.626	0.653	LR	2.140	-2.224	0.349	1.197	0.581	0.67	LR	3.396	-1.348	1.569	1.074	0.565	0.764	LD	3.966	-1.185	1.991	1.205
GABA	0.614	0.583	RD	2.963	0.009	1.000	0.969	0.235	0.33	RD	1.868	0.036	0.822	0.385	0.705	0.93	LR	3.120	-3.206	0.648	1.751
alanine	0.605	0.415	LD	3.471	0.508	2.365	0.675	0.428	4.270	RD	27.883	2.428	12.686	5.775	0.426	0.544	LR	5.358	1.899	3.720	0.736
raffinose	0.592	1.630	LR	7.525	-0.526	4.033	2.618	0.484	0.926	LR	6.819	-0.184	2.296	1.314	0.598	1.080	LR	6.644	-0.641	3.457	1.753
tryptophan	0.583	0.379	LD	2.699	-0.22	1.211	0.603	0.269	0.405	LR	2.942	0.684	1.611	0.481	0.357	0.384	LR	4.224	1.594	2.589	0.489
erythrose	0.578	0.89	LD	7.783	2.117	5.040	1.410	0.223	181.94	RD	867.34	12.38	281.84	212.818	0.035	0.831	LD	8.980	4.420	5.635	0.946
glycerol	0.568	0.741	LD	3.794	-1.302	1.330	1.148	0.388	3.550	RD	26.730	1.381	9.952	4.695	0.394	3.690	RD	22.057	1.769	10.939	4.842
aspartate	0.554	0.644	RD	2.121	-4.224	1.446	0.993	0.395	1.110	LR	2.729	-3.729	0.243	1.454	0.333	1.130	LD	3.221	-3.966	0.672	1.413
pyruvate	0.551	0.571	LR	5.708	0.141	2.030	1.238	0.186	1.480	LR	9.534	1.993	7.010	1.668	0.251	1.370	LR	9.812	3.148	6.465	1.591
proline	0.499	1.370	LR	8.675	0.714	4.050	1.970	0.736	1.05	LR	9.92	2.09	6.09	2.087	0.724	1.250	LR	12.016	1.674	6.960	2.451
citrate	0.462	0.709	LD	4.218	-0.126	2.522	1.004	0.501	0.903	LD	6.428	1.356	4.386	1.312	0.341	0.836	LD	6.376	1.107	4.184	1.091
trehalose	0.454	0.473	LD	3.861	0.462	2.006	0.651	0.323	0.618	LR	6.835	3.067	5.396	0.771	0.355	0.531	LD	6.421	2.772	4.837	0.682
putrescine	0.448	6.840	RR	57.265	1.149	10.633	9.652	0.087	0.95	LD	7.737	2.441	4.852	1.004	0.071	1.130	LR	9.318	2.343	4.606	1.199
threonate	0.448	0.375	LD	4.640	1.964	3.136	0.518	0.221	0.393	LD	3.852	1.493	2.354	0.452	0.237	2.150	RD	15.400	2.862	8.412	2.491
threonine	0.445	0.429	LD	2.832	0.267	1.850	0.597	0.526	0.558	LR	4.560	0.17	2.819	0.838	0.568	0.581	LR	4.582	0.298	3.138	0.92
phenylalanine	0.409	0.672	LR	4.523	-1.091	1.481	0.898	0.057	0.595	LR	4.207	0.247	1.883	0.623	0.096	0.68	LR	5.177	0.679	1.688	0.736
quinic acid	0.405	0.687	LR	4.138	0.265	2.004	0.905	0.382	0.632	LR	5.012	0.872	3.128	0.821	0.42	5.140	RD	35.917	2.857	11.209	7.227
phosphate	0.397	1.220	LR	3.368	-3.707	-0.195	1.593	0.356	1.150	LR	6.702	0.3	3.457	1.466	0.571	1.340	LR	7.089	-6.115	4.111	2.119
4-hydroxypyridine	0.39	0.488	LR	2.062	-0.948	0.503	0.634	0.255	0.424	RD	2.905	0.396	1.269	0.501	0.095	0.673	LR	2.883	-0.454	1.409	0.713
uracil	0.39	2.180	RD	14.908	0.623	4.426	2.857	0.502	1.016	LD	6.870	-0.896	4.713	1.494	0.402	0.828	LR	6.356	0.558	4.437	1.101
glucose	0.371	0.697	RD	4.897	0.16	1.509	0.906	0.705	0.564	LD	4.005	-0.674	1.526	1.081	0.687	1.280	LR	6.541	-2.531	2.572	2.358
glycolate	0.364	0.439	LD	3.663	1.155	2.716	0.56	0.121	0.376	LD	3.621	1.292	2.775	0.41	0.795	15.080	RR	102.07	0.434	38.516	34.164

isocitrate	0.363	2.100	RD	15.540	0.144	3.391	2.909	0.209	24.000	RR	127.148	1.568	39.847	27.574	0.23	1.090	LR	7.702	0.358	5.741	1.286
fructose	0.335	0.777	LD	2.355	-1.916	0.588	0.97	0.506	0.852	RD	6.260	0.689	2.560	1.249	0.567	1.195	LR	4.999	-3.807	1.708	1.856
fumarate	0.335	0.5	LD	1.688	-1.626	0.209	0.625	0.568	1.130	LR	3.302	-2.735	0.213	1.755	0.148	0.727	LD	3.555	-0.441	1.656	0.797
tyrosine	0.325	0.631	LR	4.162	-0.406	1.587	0.784	0.022	1.960	RR	36.880	2.494	8.556	5.625	0.16	0.692	LD	5.504	1.295	2.419	0.769
hydroxyproline	0.319	0.594	LR	3.664	0.021	1.390	0.741	0.351	9.640	RD	76.884	4.011	20.536	12.512	0.459	9.350	RR	84.173	5.315	20.934	13.314
nicotinate	0.309	1.520	RD	9.857	1.333	4.027	1.870	0.389	1.780	RD	22.492	0.64	3.303	2.810	0.272	2.960	RD	35.958	3.689	8.797	4.041
asparagine	0.303	0.98	LR	4.218	-0.721	1.932	1.198	0.369	1.250	LR	8.539	0.787	5.309	1.602	0.409	1.460	LR	8.893	0.668	5.596	1.934
lysine	0.288	0.795	LR	5.968	1.418	3.557	0.953	0.139	1.150	LR	9.605	3.431	5.761	1.249	0.13	1.060	LD	9.456	3.369	5.613	1.145
myo-inositol	0.288	0.341	LR	3.650	1.604	2.818	0.412	0.807	0.53	LR	5.776	1.590	4.179	1.246	0.587	0.554	LR	5.960	2.648	4.560	0.884
oxoglutarate	0.266	1.320	LD	9.106	2.314	4.171	1.648	0.357	1.350	LR	12.137	4.853	8.965	1.702	0.126	1.440	LR	12.128	5.456	9.044	1.552
glutamate	0.264	1.170	LD	5.277	-1.253	1.908	1.384	0.212	9.490	RD	72.298	1.191	13.584	11.144	0.117	10.950	RD	88.247	1.615	18.001	12.199
glycine	0.255	0.65	LR	2.400	-0.922	0.653	0.762	0.185	0.861	LR	6.500	0.629	2.445	0.962	0.309	0.902	LR	5.881	-0.517	2.792	7.877
fucose	0.252	0.438	LR	2.058	-0.485	1.006	0.513	0.313	0.463	LR	2.356	-0.766	1.614	0.653	0.496	0.34	LD	2.738	0.314	1.618	0.489
DHA	0.249	0.6	LR	5.361	1.804	3.916	0.705	0.232	12.600	RD	98.266	10.486	36.682	14.742	0.182	9.620	RR	73.590	14.574	38.107	10.878
maleate	0.237	3.750	RR	24.910	0.368	4.595	4.429	0.163	3.750	RD	22.401	0.221	6.308	4.219	0.255	1.140	LD	5.525	-2.086	2.400	1.387
arginine	0.235	0.73	LD	5.807	1.150	2.825	0.843	0.098	1.490	LD	8.947	2.559	5.549	1.603	0.29	89.370	RD	828.093	2.523	71.833	106.049
benzoate	0.234	0.374	LD	1.637	-0.144	0.677	0.435	0.057	0.418	LR	1.984	-0.312	1.019	0.434	0.371	0.843	RR	5.346	0.302	2.272	1.087
β-alanine	0.233	0.592	LD	3.372	0.022	1.785	0.689	0.542	0.508	LD	5.049	1.891	3.400	0.767	0.365	3.890	RD	27.908	3.391	11.888	5.019
myo-inositol-P	0.231	0.329	LD	4.022	2.375	3.177	0.385	0.374	0.548	LR	6.957	4.069	5.413	0.708	0.581	0.518	LR	7.461	4.481	6.056	0.821
methionine	0.211	0.957	LR	7.998	1.935	3.988	1.105	0.077	1.210	LR	10.507	4.125	7.366	1.269	0.26	1.550	LD	11.030	-2.361	7.022	1.868
maltose	0.187	0.523	LD	5.647	2.182	3.847	0.588	0.595	43.83	RD	345.81	15.53	91.9	73.396	0.612	24.950	RD	253.052	17.679	62.711	44.139
succinate	0.181	3.330	RD	27.082	4.189	9.763	3.879	0.374	0.488	LD	5.730	2.745	4.181	0.629	0.118	10.680	RD	76.296	14.794	29.504	11.843
histidine	0.174	1.060	LR	6.442	-0.236	2.363	1.194	0.087	1.240	LR	8.303	1.853	4.498	1.312	0.122	1.210	LR	8.532	1.551	4.349	1.301
ornithine	0.171	1.070	LR	5.270	-1.304	0.908	1.201	0.191	1.650	LR	8.424	-2.208	3.854	1.858	0.166	1.420	LD	9.047	-1.210	4.751	1.607
xylose	0.17	0.453	LR	1.712	-0.602	0.428	0.501	0.542	0.487	LD	3.506	0.194	1.685	0.731	0.311	0.39	LD	3.475	-0.133	1.745	0.485
pyroglutamate	0.149	0.58	LR	2.275	-0.917	0.423	0.639	0.279	0.819	LR	4.610	0.29	2.742	0.974	0.353	1.060	LR	5.293	-0.419	2.932	1.340
AMP	0.146	2.850	RD	22.340	1.068	4.286	3.752	0.038	0.73	LR	5.397	2.091	3.691	0.759	0.421	0.816	LD	5.974	1.252	4.480	1.100
thydroxypyridine	0.14	0.524	LR	2.303	-0.627	0.907	0.572	0.213	0.424	RD	4.137	0.652	2.177	0.756	0.084	1.500	RR	10.620	1.183	3.724	1.616

isoleucine	0.124	0.754	LR	4.880	0.126	1.879	0.819	0.272	0.821	LR	6.228	2.118	3.941	0.972	0.348	0.857	LR	6.799	1.406	4.093	1.074
tyramine	0.118	0.588	LD	2.558	-1.594	0.428	0.639	0.394	3.010	RR	19.628	2.119	7.749	3.984	0.047	4.570	RR	22.137	2.812	13.353	4.682
glutamine	0.115	0.923	LR	7.589	1.236	3.387	1.010	0.263	1.170	LR	8.949	2.860	6.076	1.373	0.22	1.630	LR	9.993	0.097	5.799	1.885
t-hydroxy-cinnamate	0.05	0.915	RR	5.730	0.799	2.326	0.979	0.159	0.915	RR	82.751	3.946	31.847	15.513	0.057	24.300	RR	147.561	15.294	54.096	25.337
valine	0.048	0.618	LR	3.377	-0.782	0.602	0.646	0.302	0.832	LR	4.705	0.5	2.357	1.002	0.287	0.893	LR	5.608	-0.025	2.508	1.068
galactinol	0.041	0.51	LR	1.174	-1.504	-0.184	0.524	0.525	0.669	RR	4.855	0.146	1.390	0.993	0.403	0.595	RR	5.127	0.309	1.491	0.794
adenine	0.033	1.020	LR	6.470	2.134	3.579	1.051	0.15	111.050	RD	942.301	5.956	124.015	136.890	0.389	1.040	LD	9.444	2.830	5.464	1.429
lactate	0.026	0.646	LR	2.953	-0.854	1.385	0.664	0.328	0.842	LR	3.913	-1.280	2.020	1.049	-	-	-	-	-	-	-
3-phosphoglycerol	-	-	-	-	-	-	-	0.53	1.134	RD	9.282	0.123	2.006	1.872	0.717	1.160	LR	3.678	-4.509	-0.692	2.242
isomaltose	-	-	-	-	-	-	-	0.104	0.551	LD	3.208	-0.042	1.445	0.586	0.293	0.533	LD	3.336	0.15	1.194	0.647
4-hydroxybenzoate	-	-	-	-	-	-	-	0.252	0.546	LD	4.533	0.625	2.603	0.648	0.348	0.702	LR	5.434	0.344	2.968	0.893
rhamnose	0.561	0.31	LR	4.655	2.059	3.501	0.478	-	-	-	-	-	-	-	0.356	0.398	LD	5.567	3.326	4.354	0.508
glucaratelactone	0.414	0.811	LR	3.177	-1.540	0.643	1.108	-	-	-	-	-	-	-	0.642	0.808	LR	6.095	-0.009	3.454	1.385
transcaffeate	0.074	0.446	LR	4.896	2.441	3.162	0.472	-	-	-	-	-	-	-	-	-	-	-	-	-	-
c-CQA	0.371	1.640	LR	4.386	-3.617	0.275	2.102	-	-	-	-	-	-	-	-	-	-	-	-	-	-
t-CQA	0.569	1.580	LR	6.582	-3.565	1.818	2.444	-	-	-	-	-	-	-	-	-	-	-	-	-	-
cellobiose	-	-	-	-	-	-	-	-	-	-	-	-	-	-	0.134	2.960	RR	19.711	3.269	8.753	3.253
galactonate-1,4-lactone	-	-	-	-	-	-	-	-	-	-	-	-	-	-	0.292	0.424	RD	2.917	0.692	1.652	0.515
malonate	-	-	-	-	-	-	-	-	-	-	-	-	-	-	0.267	0.657	LD	4.387	0.222	1.971	0.794
N-acetylserine	-	-	-	-	-	-	-	-	-	-	-	-	-	-	0.185	0.504	LD	2.320	-0.238	1.127	0.577
O-acetylserine	-	-	-	-	-	-	-	-	-	-	-	-	-	-	0.425	0.367	LD	3.110	0.382	1.858	0.521

Table 3. Geographic, climatic, agronomic, and soil information for each study site. Colmenar de Oreja and El Majano experimental stations belong to the Instituto Nacional de Investigación y Tecnología Agraria y Alimentaria (INIA) of Spain and Zamadueñas experimental station belongs to the Instituto Tecnológico Agrario de Castilla y León (ITACyL).

	Zamadueñas experimental station	Colmenar de Oreja experimental station	El Majano experimental station
Altitude (mamsl)	700	590	20
Coordinates	41º 42' N, 4º 42' W	40º 04' N, 3º 31' W	37°14' N, 6°03' W
Mean Temp.[b] (ºC)	10.73	13.01	14.5
Max. mean Temp.[b] (ºC)	17.45	21.45	21.6
Min. mean Temp.[b] (ºC)	4.64	5.36	8.3
Precipitation[b] (mm)	258.4	206.8	161.8
Sowing date	24.11.2014	21.11.2014	11.12.2014
Harvest date	22.07.2015	20.07.2015	11.06.2015
Sowing density (seeds m^{-2})	250	250	250
Plot surface (m^2)	10.5 (7x1.5)	10.5 (7x1.5)	10.5 (7x1.5)
Irrigation provided[a] (mm)	125	180	-
Fertilisation			
1st application	300 kg ha^{-1} NPK 8:15:15	400 kg ha^{-1} NPK 15:15:15	500 kg ha^{-1} NPK 15:15:15
2nd application	300 kg ha^{-1} CAN 27%N	150 kg ha^{-1} Urea 46%	100 kg ha^{-1} Urea 46%
Soil texture	Loam	Clay-loam	Silty clay loam
Soil pH	8.44	8.1	7.6

[a]in the irrigated treatment

[b]during the growing season

Figure legends

Figure 1. Means of leaf, ear and canopy VIS-NIR-SWIR reflectance spectra (upper left) and the first derivative reflectance spectra (lower left). Standard deviations are plotted in grey. Principal component analysis of the reflectance spectra (upper in middle) and the first derivative spectra (lower in middle) and the corresponding waveband contribution in the first two components (upper and lower right). HY, high yielding environment; R-, rainfed environment.

Figure 2. Detection rate (%) of wavebands in the VIS-NIR-SWIR spectrum in the yield prediction models performed from leaf, ear and canopy spectra (n=288).

Figure 3. Heatmap showing the correlation coefficients between the wavebands in the first derivative reflectance spectra of leaves and ears and the metabolite profiles of leaves, glumes and lemmas.

Figure 4. Bar plot showing the proportion of explained variance (adj-R^2 in the validation sets) of leaf (A) glume (B) and lemma (C) metabolites in the LASSO regression models based on the VIS-NIR-SWIR organ spectrum, the VIS organ spectrum and the canopy spectrum.

Figure 5. Waveband detection rates in the prediction models for a selection of leaf, glume and lemma metabolites. Green lines correspond to the detection rate of the models based on the VIS-NIR-SWIR organ spectrum, blue lines indicate the detection rate of wavebands when using the canopy spectrum. GABA, γ-aminobutyric acid; Glc, glucose; Pro, proline; Ser, serine; Suc, sucrose.

Figures

Figure 1

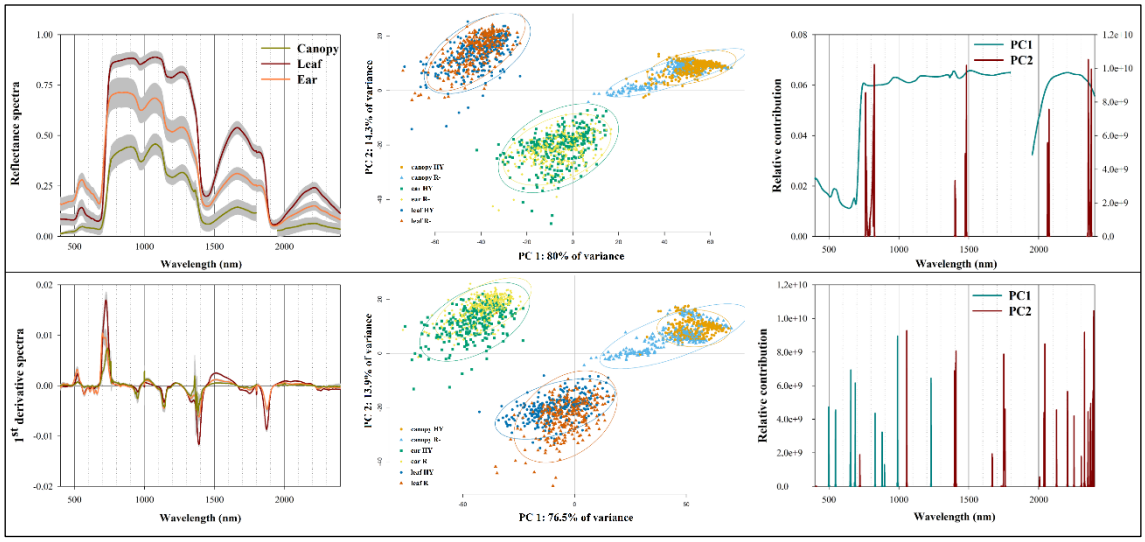

Figure 2

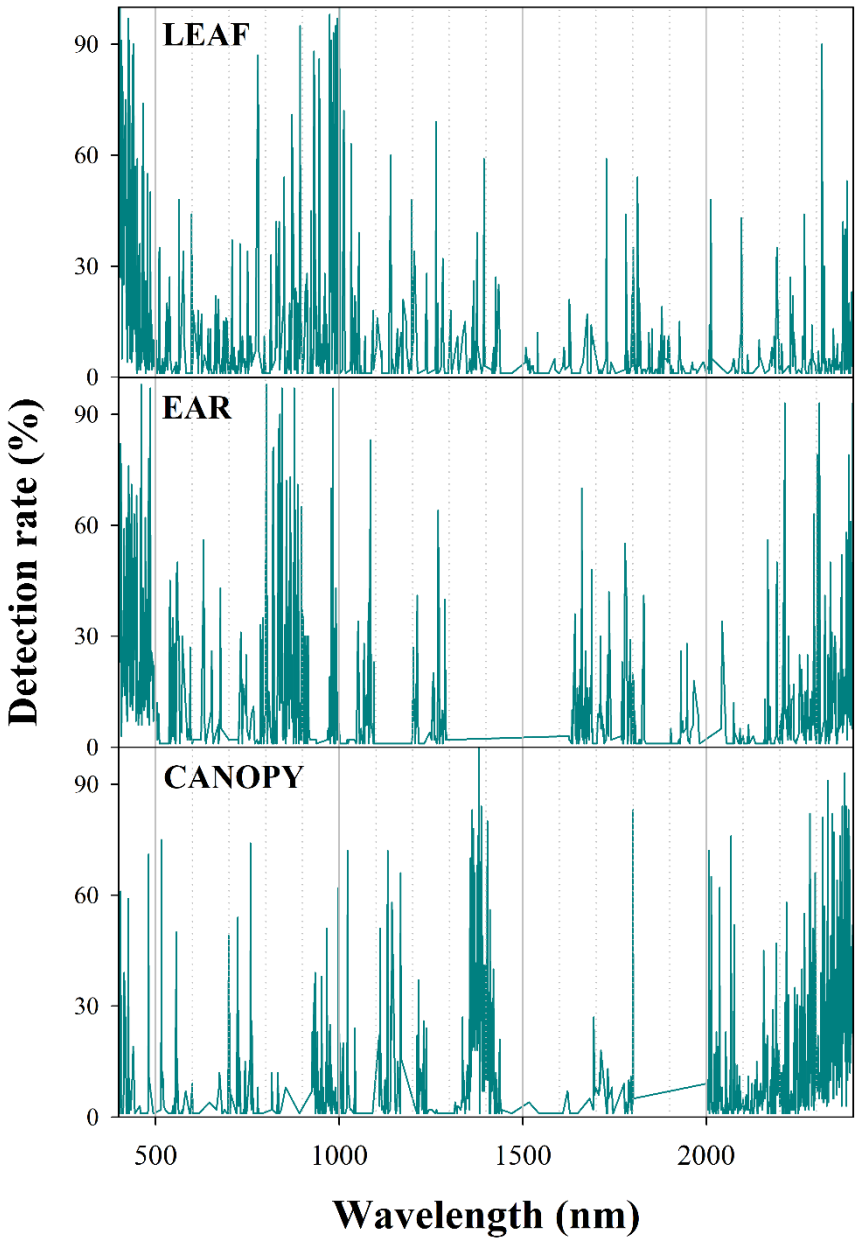
LEAF
EAR
CANOPY
Detection rate (%)
0
30
60
90
500
1000
1500
2000
Wavelength (nm)

Figure 3

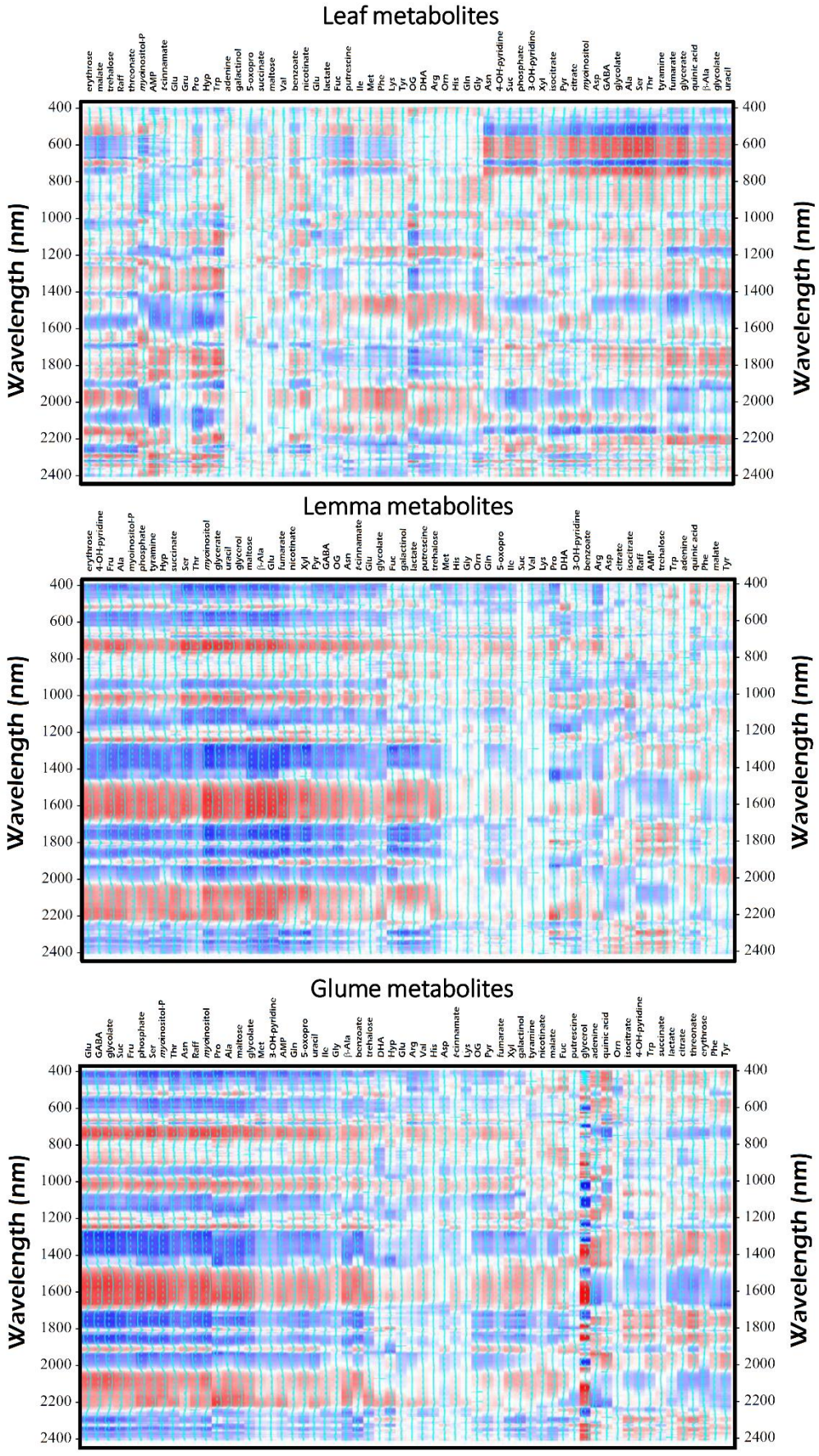
Leaf metabolites
erythrose malate trehalose Raff threonate myoinositol-P AMP t-cinnamate Glu Gru Pro Hyp Trp adenine galactinol 5-oxopro succinate maltose Val benzoate nicotinate Glu lactate Fuc putrescine Ile Met Phe Lys Tyr OG DHA Arg Orn His Gln Gly Asn 4-OH-pyridine Suc phosphate 3-OH-pyridine Xyl isocitrate Pyr citrate myoinositol Asp GABA glycolate Ala Ser Thr tyramine fumarate glycerate quinic acid β-Ala glycolate uracil
Wavelength (nm)
400 600 800 1000 1200 1400 1600 1800 2000 2200 2400
Lemma metabolites
erythrose 4-OH-pyridine Fru Ala myoinositol-P phosphate tyramine Hyp succinate Ser Thr myoinositol glycerate uracil glycerol maltose β-Ala Glu fumarate nicotinate Xyl Pyr GABA OG Asn t-cinnamate Glu glycolate Fuc galactinol lactate putrescine trehalose Met His Gly Orn Gln 5-oxopro Ile Suc Val Lys Pro DHA 3-OH-pyridine benzoate Arg Asp citrate isocitrate Raff AMP trehalose Trp adenine quinic acid Phe malate Tyr
Wavelength (nm)
400 600 800 1000 1200 1400 1600 1800 2000 2200 2400
Glume metabolites
Glu GABA glycolate Suc Fru phosphate Ser myoinositol-P Thr Asn Raff myoinositol Pro Ala maltose glycolate Met 3-OH-pyridine AMP Gln 5-oxopro uracil Ile Gly β-Ala benzoate trehalose DHA Hyp Glu Arg Val His Asp t-cinnamate Lys OG Pyr fumarate Xyl galactinol tyramine nicotinate malate Fuc putrescine glycerol adenine quinic acid Orn isocitrate 4-OH-pyridine Trp succinate lactate citrate threonate erythrose Phe Tyr
Wavelength (nm)
400 600 800 1000 1200 1400 1600 1800 2000 2200 2400

Figure 4

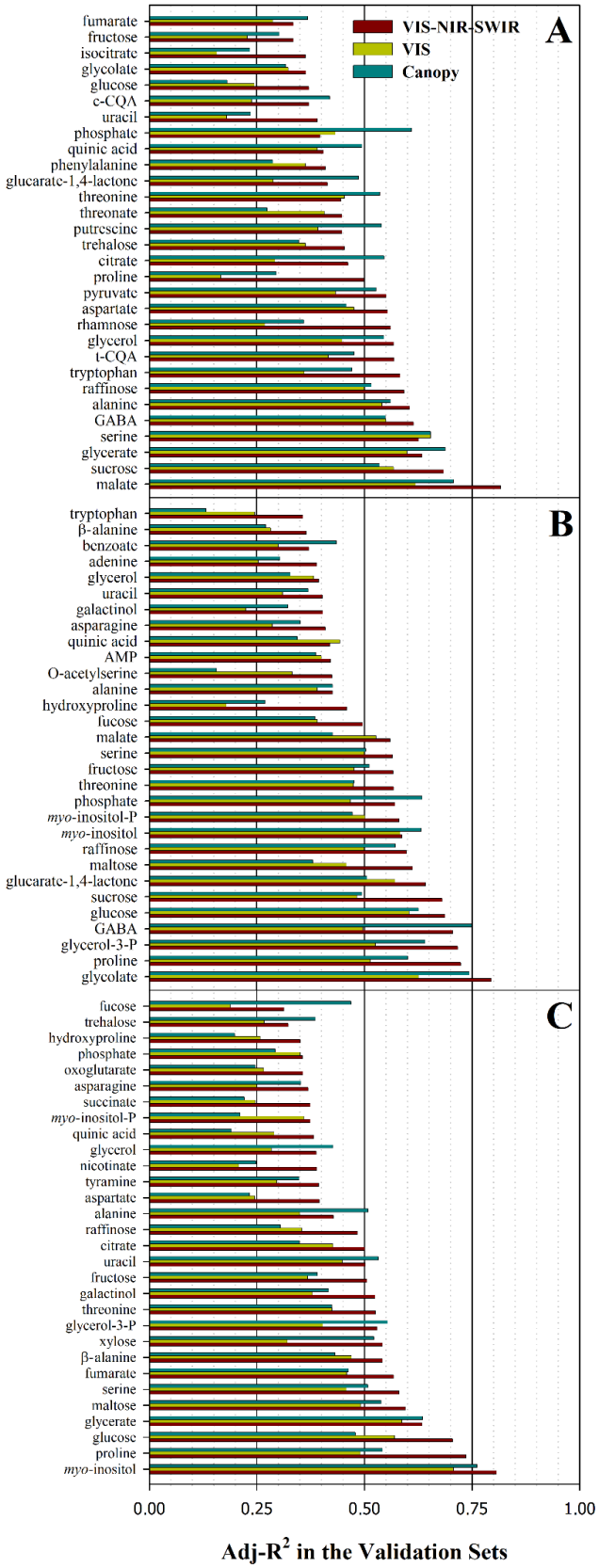
VIS-NIR-SWIR
VIS
Canopy
A
fumarate
fructose
isocitrate
glycolate
glucose
c-CQA
uracil
phosphate
quinic acid
phenylalanine
glucarate-1,4-lactone
threonine
threonate
putrescine
trehalose
citrate
proline
pyruvate
aspartate
rhamnose
glycerol
t-CQA
tryptophan
raffinose
alanine
GABA
serine
glycerate
sucrose
malate
B
tryptophan
β-alanine
benzoate
adenine
glycerol
uracil
galactinol
asparagine
quinic acid
AMP
O-acetylserine
alanine
hydroxyproline
fucose
malate
serine
fructose
threonine
phosphate
myo-inositol-P
myo-inositol
raffinose
maltose
glucarate-1,4-lactone
sucrose
glucose
GABA
glycerol-3-P
proline
glycolate
C
fucose
trehalose
hydroxyproline
phosphate
oxoglutarate
asparagine
succinate
myo-inositol-P
quinic acid
glycerol
nicotinate
tyramine
aspartate
alanine
raffinose
citrate
uracil
fructose
galactinol
threonine
glycerol-3-P
xylose
β-alanine
fumarate
serine
maltose
glycerate
glucose
proline
myo-inositol
0.00
0.25
0.50
0.75
1.00
Adj-R2 in the Validation Sets

Figure 5

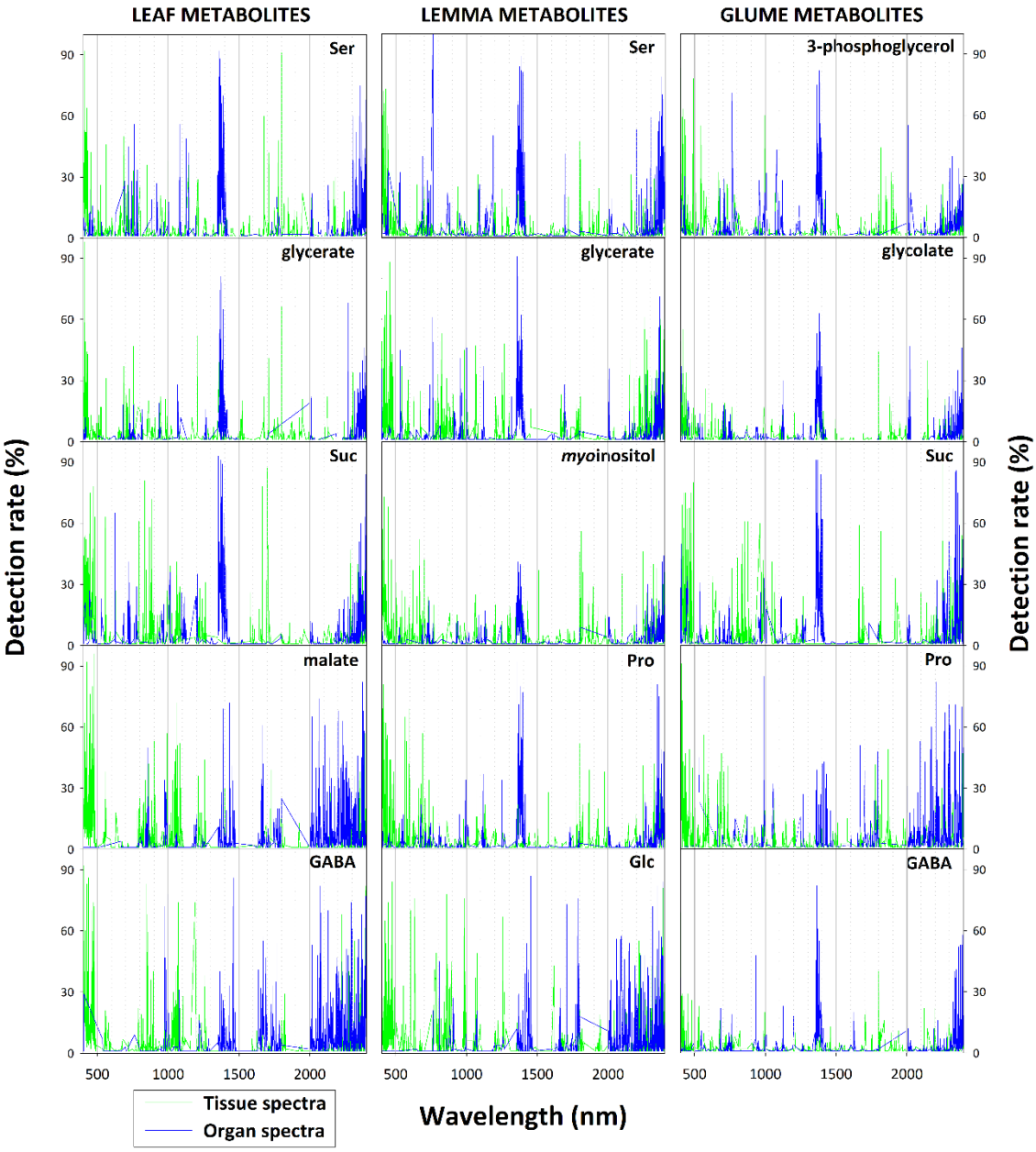
LEAF METABOLITES
LEMMA METABOLITES
GLUME METABOLITES
Ser
Ser
3-phosphoglycerol
glycerate
glycerate
glycolate
Suc
myoinositol
Suc
malate
Pro
Pro
GABA
Glc
GABA
Detection rate (%)
Detection rate (%)
Wavelength (nm)
Tissue spectra
Organ spectra

DISCUSSION

DISCUSSION

The current thesis represents a multidimensional attempt to investigate avenues to improve crop phenotyping. To that end, a range of traits involved in the response to the environment and performance of maize and wheat, the two major crop species worldwide, together with novel phenotyping approaches were investigated: i) crop yield performance under diverse stress conditions, ii) genotypic variability providing opportunities to breed for, iii) phenotyping approaches from low-cost to frontier technologies, iv) plant morphoanatomical and composition traits that affect phenotyping and v) metabolomics of wheat tissues, particularly focusing on the ear as a new frontier in field phenotyping. In a broad sense, we feel that these studies have contributed to the advancement of field phenotyping aimed for breeding and even crop management, while providing new insights in ecophysiology, particularly identifying traits for further selection. Therefore, the different chapters integrated in this thesis have succeeded in characterizing plant-crop traits from a broad range of methods and provided useful advances to be applied not only in field phenotyping, but also for plant monitoring and even basic plant research.

Exploring new traits for wheat adaptation to the environment

In the last years, the growing interest in plant phenotyping research is not casual and has to do with the urgency to obtain resilient crops, to understand plant stress responses and to overcome plant breeding shortcomings. Thus, plant phenotyping has become the backbone of most studies in ecology, agronomy and ecophysiology exploring plant functional diversity, compare the performance of species or study plant responses to the environment (Granier and Vile, 2014; Rahaman *et al.*, 2015). The phenotypic plant responses to either biotic or abiotic stresses are multidimensional and include morpho-anatomic, physiological and molecular variations leading to mechanisms of acclimation or avoidance. Also, in the case of wheat, in most of plant ecophysiology studies far more attention has been paid to the role of the flag leaf (e.g. traditionally considered as the main photosynthetic organ contributing to grain filling). Instead, the understanding of the metabolism of non-laminar organs such as the ear may provide further insights on wheat ecophysiology and opportunities to breed for.

In our work in yellow rusted durum wheat (Vergara-Diaz *et al.*, 2015), changes in yield components interrelationships and phenology (days to heading) were associated with disease incidence and grain yield. Thus early-heading genotypes, mitigated the incidence of the disease through a mechanism of avoidance, therefore exhibiting higher yields. Previous works proposed to optimize phenology traits, especially the timing of reproductive stages, with respect to the historic or predicted future occurrence of different types of stresses (Zheng *et al.*, 2015). Our study was limited to sixteen commercial varieties; therefore, it could be equivocal to extrapolate this conclusion to a wider

collection of genotypes. In other words, the obtention of genetically resistant varieties may not be necessarily linked to short-cycle varieties but undoubtedly this trait permits to better scape from this disease and accumulate higher yields.

In other work with wheat, leaf anatomy traits (epidermis and mesophyll metrics) were shown to be modulated by dorsoventrality and water stress, with consequent variations on their associated spectral signal (Vergara-Díaz *et al.*, 2018). Also, the pigments (chlorophyll, anthocyanin and carotenoids) 'spectral signal variation suggested possible side-specific photochemical changes in response to water regime. It was proposed that water stress induces structural and pigment changes in the leaf that tends to reduce dorsoventral differences (functioning) in the leaf and consequently the spectroradiometrical response. Despite of the limitations of this study, it seems clear that acclimation mechanisms of plants in response to stress are complex and multidimensional and should be carefully/thoroughly addressed. Moreover, even in a species like wheat traditionally considered as having isobilateral amphistomatous leaves, dorsoventrality may affect the performance of the remote sensing assessed vegetation indices.

In wheat leaves and roots, osmotic stress imposition generally involves an alteration of nitrogen assimilation machinery affecting protein synthesis (i.e. accumulation of free amino acids) and sugar content, triggering expression patterns of dehydration-responsive, carbon-metabolism, and nitrogen-related genes (Annunziata *et al.*, 2016; Yousfi *et al.*, 2016; Brini *et al.*, 2007; Fàbregas and Fernie, 2019). Whereas the leaves and the roots have been the main plant organs targeted given their role as photosynthetic organs or capturing resources (water and nutrients) for the plants other plant parts have attracted less attention in the past. However, in the case of wheat, the exploration of the role other plant organs, such as wheat ears, is attracting increasing attention as these may enhance the understanding of underlying mechanisms implicated in plant acclimation while providing new opportunities for breeding. In this line of work, our study in wheat metabolite profiling (Vergara-Diaz *et al.,* submitted *a*) supports previous evidences from other approaches (isotopes, transcriptome and enzyme activity studies) that highlighted the role of ears as photosynthetic organs contributing to grain filling and nitrogen assimilation and its enhanced antioxidant metabolism, particularly under water stress conditions (Vicente *et al.*, 2018; Sanchez-Bragado *et al.*, 2014; Lou *et al.*, 2018; Tambussi *et al.*, 2007). We proposed the outperformance of spikes under water stress to be associated with i) strong coordination of nitrogen assimilation, photorespiratory nitrogen cycle and TCA cycle, ii) remarkable levels of carbon fixation and/or refixation and iii) an active antioxidant machinery. Thus, our work evidenced that ear bracts metabolism is strongly responsive to water stress and concluded that drought resilience of wheat may be mediated by the high performance of the ear. Besides, photosynthetic non-laminar tissues and the inflorescence have been reported to contribute to grain carbon in a major extent than the flag leaves (Merah *et al.*, 2017; Sanchez-Bragado, *et al.*, 2014;

Sanchez-Bragado *et al.*, 2016). Thus, although many advances have been done in this field recently, there is still much to know from ear metabolism. For instance, ear contribution to grain filling is highly variable according to environment and genetic factors (Merah *et al.*, 2017; Zhu *et al.*, 2009), so future work must address how to assure the heritability of ear outperformance traits, from which breeding to improve wheat drought tolerance may benefit.

Detecting genotypic variability for breeding

Plant phenotyping may provide valuable information for breeding as long as genotypic variability exists and can be detected. In the works included in the current thesis, genotypic differences for diverse categories of traits have been identified even in small panels/collection of genotypes.

Although leaf or crop plot colour (derived from RGB imagers) may appear as a simple or even naive traits, they have demonstrated to integrate phenotypic information that succeeded in detecting genotypic variability associated with traits of interest. For instance, genotypic differences in plot colour traits (RGB indices) were closely associated with yellow rust disease incidence and were accurate predictors of grain yield (Vergara-Diaz *et al.*, 2015). Instead, in the assayed panel of genotypes under disease conditions, stomatal conductance and canopy temperature depression, both parameters being closely associated with plant water status, failed to capture genotypic differences, although changes in water status associated to yellow rust have been reported(Smith *et al.*, 1986; Awad *et al.*, 2015). When measuring stomatal conductance in the field, the limited the number of biological replicates (leaves per plot), given the time elapsed by each measurement, the daily patterns of this trait and the changing weather conditions (wind and sunlight) may involve methodological problems leading to ambiguous results. Canopy temperature measured plot by plot may have some comparatively advantages but so far sudden changes in weather prevented to asses genotypic differences in tolerance to yellow rust. In contrast, the almost-instantaneous record of the complete field trials (particularly when using thermal cameras mounted in aerial platforms) may solve some of the limitations inherent to ground (i.e. individual plot level) measurements of canopy temperature and likely provide better results (Araus et al. 2018).

In the work developed in maize (Vergara-Díaz *et al.*, 2016) addressing genotypic variability under different nitrogen fertilization regimes, the performance of leaf and plot colour traits, was the key point of the study. Unlike spectroradiometrical approaches, like NDVI and SPAD-readings, we concluded that (RGB) colour traits offer opportunities for the assessment of genotypic variability in grain yield and leaf nitrogen content within each nitrogen fertilization level. Thus, RGB-derived genotypic characterization may provide information fundamental for the selection of the most

efficient genotypes in terms of grain production and nitrogen uptake, responding to the needs of breeding for nitrogen deficiency tolerance in maize.

A last insight on genotypic variability can be extracted from the metabolic study of wheat organs under water stress (Vergara-Diaz et al., submitted a). We concluded that genotypic high-yielding behaviour was mainly associated with alterations in cell wall metabolism and with carbon assimilation in the leaf and spike bracts. We considered that the reported metabolic changes may have contributed to drought acclimation and yield stability, thus, the study targets potentially interesting metabolites for molecular breeding. Even so, further mechanistic investigation is needed to set the basis of these changes observed at the metabolic level while the use of a wider collection of genotypes may enable to identify other sources of variation contributing to stress resilience. In that context genotypic differences in metabolites may be assessed in a non-destructively manner using hyperspectral approach as detailed below (Vergara-Diaz et al., submitted b).

Phenotyping through proximal sensing: from the low cost to the frontier sensors

At present, most of what is considered high-throughput phenotyping is based on remote sensing (Araus *et al.*, 2018). Imaging systems, including RGB, multi/hyper-spectral, fluorescence and thermal sensors, can be deployed on diverse types of platforms: in controlled environments (chambers), "pheno-mobiles", fixed platforms permanently stationed in a given site or in aerial platforms (i.e. drones). Among the panoply of new techniques in plant biology for phenotyping, the most frequently deployed and versatile are the RGB based technologies, as they have demonstrated to be high-throughput, while being straightforward from an operational point of view and low-cost (Rahaman *et al.*, 2015; Araus *et al.*, 2018). In our research, RGB-derived phenotyping proved to be highly versatile and high-throughput method for the retrieval of plant-crop traits under nitrogen deficiency and disease conditions.

Prior to our research on yellow rust in wheat, many studies used RGB images of leaves for the detection and classification of diseases and/or for the quantification of disease incidence (Kampmann and Hansen, 1994; Camargo and Smith, 2009). Also, recent works, still employing leaf images, have developed complex image processing systems, including the integration to deep learning machines and sophisticated statistics that successfully characterized diverse diseases symptoms and spread severity even in many plant species (Mohanty *et al.*, 2016; Johannes *et al.*, 2017). Therefore, RGB-assisted disease phenotyping may be of great importance not only for breeding and management but also for improving the efficacy of fungicides and new biological control treatments. While we feel that these advances are interesting, particularly when integrated in automated phenotyping platforms,

these are still away from end users 'management because of their operational complexity and lack of representativeness of cultivars in the field. For instance, one disease-resistant genotype exhibiting healthy leaves when tested in pots, may eventually show low vigour (i.e. low biomass and tillering rate) in the field, which is not detectable with leaf images, and may provide ambiguous information. While detection and identification algorithms are key for disease management, their final application should be tested in the field at plot scale of measurements which may provide most valuable information for final users: breeders, ecophysiologists and phytopathologists. Our approach (Vergara-Diaz *et al.*, 2015) was much more straightforward as we did not aim to detect and classify the disease (i.e. necrosed areas, yellowish or orange spots and stripes). Instead, zenithal images at the ground level (that may be upscaled at the aerial level) enabled to catch high definition colour traits of a representative plot area, that were indicative not only of disease spread, but also of biomass and green cover. Therefore, the presented approach was more representative of genotype by environment performance and satisfactorily integrated information regarding yield losses and grain yield. Subsequently, this method proved to detect efficiently maize lethal necrosis disease incidence in a study where I was co-author (Kefauver *et al.*, 2015) which demonstrated its broad use for biotic stress assessment. Although recent work assessing disease conditions and yield performance at the aerial level encountered some limitations (Liu *et al.*, 2018), it is the opinion of authors that biotic stress assessment may benefit from the implementation of RGB-based phenotyping at the aerial scale. The employment of other sensing methods (thermal, hyperspectral and florescence) may provide more complex phenotypic output and may be employed for in-field early (visual-asymptomatic) detection of plant diseases, which in fact is the larger challenge together with the distinction of phenotypic signal between biotic and abiotic stresses, which frequently overlap (Calderón *et al.*, 2013; Pauli *et al.*, 2016).

The other RGB-phenotyping approach presented in the current thesis addressed maize performance under diverse nitrogen fertilization conditions (Vergara-Díaz *et al.*, 2016). The first works proposing the use of RGB sensors for the retrieval of maize traits were performed at the lab and aimed to estimate chlorophyll content as compared to the performance of SPAD-meter (Kawashima and Nakatani, 1998), since chlorophyll content is closely associated with nitrogen status. Following research aimed to determine leaf nitrogen concentration using leaf images (Mercado-Luna *et al.*, 2010; Ali *et al.*, 2013). Jia *et al.* (2014) estimated satisfactorily the aboveground nitrogen accumulation (rather than its concentration in leaf area basis) as derived from biomass cover from plot images. Although the relevance of these results is undoubtedly, it should be noted that the intrinsic association between green cover, biomass and total nitrogen accumulation sets certain degree of uncertainty in the basis of nitrogen estimation. Although in our research, higher robustness in the prediction of leaf nitrogen was shown when employing leaf-RGB derived indices, the canopy RGB indices were still good indicators of plant nitrogen. In agreement with our work, more recent studies (Chen *et al.*, 2018) found CIE-Lab RGB indices to be closely related with leaf nitrogen content, while other works comparing RGB

and NDVI methods to predict grain yield in wheat (Fernández *et al.*, 2019) obtained quite similar results. Also, recent evaluation of RGB and multispectral sensors mounted at remotely piloted aircrafts (RPA; this term is nowadays preferred instead of the more popular term of unmanned aerial vehicle, UAV) for the assessment of nitrogen accumulation in rice showed the better performance of RGB indices than the multispectral indices, except by red-edge multispectral indices (Zheng *et al.*, 2018). In this line of research, RGB-derived phenotyping is providing novel methods for crop traits evaluation, such as detection and quantification of crop cover, height and volume (Pádua *et al.*, 2018), plant emergence and leaf area quantification (Li *et al.*, 2019), or the effect of mineral deficiency on dynamic leaf growth and colour (Sun *et al.*, 2018). Thus, we consider that the integration of RGB sensors with other imagery sensors in aerial platforms, together with novel computing systems for image segmentation and data extraction, will be key for the acquisition and further evaluation of large phenotypic datasets (i.e. hundreds to thousands of genotypes).

Even so, frontier technologies like field spectroscopy may provide high-dimensional phenotypic data contributing to basic and applied research. In Vergara-Díaz *et al.* (2018) field spectroscopy was employed for the analysis of leaf dorsoventrality as compared to water stress effect in wheat, and their interaction. Thereby, we could dissect and discuss the major biochemical and biophysical changes associated with dorsoventrality and water stress and their implications. Although spectral indices can be informative, they use less than 1% of the spectra, whereas the employment of the full spectra data (acquired through hyperspectral sensors) can better inform on physiological processes and biochemical compositions besides of ecological applications (Turner *et al.*, 2003; Pauli *et al.*, 2016). Thus, the capability of hyperspectral sensors for the estimation of the metabolite content of plant organs in wheat was investigated (Vergara-Díaz et al., submitted b). Although the spectral signatures of plant organs and canopies are jointly influenced by environmental and plant structural characteristics (i.e. canopy architecture and organs anatomy)(Homolová *et al.*, 2013; Peñuelas and Filella, 1998), they still proved to contain valuable information regarding biochemical composition (Vergara-Díaz et al., submitted b). In consideration of our findings, much efforts can be dedicated in the development of in-field metabolic phenotyping through hyperspectral information. However, still certain aspects must be carefully addressed: i) validation of this method in plant material grown under different stressor conditions, ii) using a wider range of genotypic variability or even comparing different species, iii) testing the possible interferences of stress-associated anatomy changes and iv) further validate the retrieval robustness with analytical measurements of metabolite concentration rather than the relative metabolite content.

Deeping in the prediction capability: from grain yield to metabolic profile

The studies conforming the present thesis, although deploying multiple analytical and statistical approaches, converge in the estimation of crop-plant traits, principally the grain yield but also

composition traits, including a wide range of metabolites. It is worth to mention that many factors (e.g. seasonal variability, variation in the sensors and methodology used and the different stress conditions evaluated) may interfere affecting the results of predictive models. Also, the statistical approaches performed were specific for each case of study so a strict comparison of their robustness and accuracy could be equivocal/ambiguous. That said, we hereafter provide a tentative comparison of the diverse methods used in crop-plant traits estimation.

In the case of yield, RGB-derived phenotypic data, solely or in combination, with a phenology trait (days to heading) explained together between 68 to 72% of yield variation (Vergara-Diaz *et al.*, 2015; Vergara-Díaz *et al.*, 2016). For its part, the application of spectroscopic methods either with the employment of formulated spectral reflectance indices or with variable selection methods from the whole spectra of leaves, ears and canopies could enhance the prediction of grain yield, achieving between 73 to 90% and 72 to 75% (in the validation sets) of explained yield variability, respectively (Vergara-Díaz *et al.*, 2018; Vergara-Díaz *et al.,* submitted b). From these spectroscopic studies it was concluded that i) canopy spectrum generally permit to predict yield with higher precision as it integrates phenotypic information regarding biomass and green cover, closely associated with yield, ii) ear spectrum is indicative of final yield even in some case reaching the precision of canopy spectrum-based models and iii) the use of leaf abaxial spectrum instead of the adaxial enhances yield prediction likely due to its greater structural homogeneity. Finally, yield prediction based on metabolite profiles of leaves and ear bracts also yielded very good results, as grain yield explained variation ranged between 74 to 83% in the training sets and between 56 to 66% in the validation sets, with lemma's metabolite profile providing the most robust prediction followed by the leaves and glumes profiles. Nevertheless, direct prediction of yield using the spectral signature was stronger than yield prediction based on metabolite profiles. All methods developed have key strengths i) field spectroscopy may provide the most robust prediction and permits to deep into the traits associated with yield (by documenting the relationship between specific wavebands of the spectrum with crop-plant constituents or biophysical traits), ii) RGB methods represent the most cost-effective phenotyping tool of high operational simplicity while providing high-throughput data and iii) metabolite-yield association studies permit to dissect metabolic responses related to yield while providing potential biomarkers for breeding.

Regarding leaf nitrogen content assessment, highest prediction accuracy at the single leaf level was given by SPAD-meter (82% of explained variation) but, as previously explained, leaf nitrogen differences across genotypes within fertilization levels was far better detected by RGB-derived indices, although their prediction of leaf nitrogen content across treatments was more modest (69% of explained variation)(Vergara-Díaz *et al.*, 2016). In other words, RGB vegetation indices appear as more

robust than the spectral measurement derived from a leaf chlorophyll meter, as a phenotypic approach to assess the genotypic variability of maize to different levels of N fertilization.

Lastly, the use of field spectroscopy permitted to quantitatively estimate several leaf and ear bracts metabolites with considerable high prediction accuracy (Vergara-Diaz *et al.,* submitted b), since for at least fifteen metabolites per organ, models exceeded 50% of explained variation (validation sets). Many of these metabolites are of great relevance as they are representative of or modulate plant physiological processes, so that their non-destructive estimation is a highly valuable information for molecular and ecophysiological studies as well as for breeding programs. For instance, this could be applied to track carbon assimilation, its partitioning and storage, protective and osmotic adjustment responses, nitrogen assimilation, signaling and for the assessment of photorespiration and respiratory functioning, which are currently some of the promising fields of study in molecular biology (Clément *et al.*, 2018; Eisenhut *et al.*, 2019).

Future challenges and concerns in plant phenotyping research

There exists a perception regarding the cost and complexity of new phenotyping methods which may limit their adoption by the private sector or public research (Araus *et al.*, 2018). However, many fields of research, from molecular biology to data science, are called to jointly overcome these worries convincingly. One key concern refers to the validation of the HTP methods in the field and the reliability of the extrapolation of phenotypic data from controlled environments to real (field) conditions. This is because controlled systems are unable to replicate environmental variables influencing complex traits such as grain yield and drought tolerance (Pauli *et al.*, 2016; but see: Yadav *et al.*, 2019 for opposite results). For instance, molecular studies revealed that plant responses to drought can vary dramatically between the greenhouse and the field, emphasizing the importance of field-based research (Lovell *et al.*, 2016; Pauli *et al.*, 2016). Even, transcriptomic and metabolic adjustment can change due to the type of treatment with which stress is imposed (e.g. dehydration of detached leaves or water withholding for imposing water stress under controlled environments) as well as to the severity and duration of the imposed stress (both in the field and in controlled systems) (Fàbregas and Fernie, 2019). Thus, basic standards in terms of stress imposition and evaluation will need to be adopted (Fàbregas and Fernie, 2019). Also, recent works have evidenced different molecular mechanisms occurring in shoots and roots in response to drought (e.g. activation/deactivation of resource uptake, upregulation of transport and biosynthesis of amino acids and hormones) (Gargallo-Garriga *et al.*, 2015; Rasheed *et al.*, 2016), whereas novel works on wheat ear performance also highlighted its great responsiveness to water stress (Vicente *et al.*, 2018; Vergara-Díaz *et al.,* submitted a; Sanchez-Bragado *et al.*, 2016). Therefore, future phenotyping must

address spatially different (i.e. intra-plant) responses coping with stress, deepening in wheat ecophysiology while providing potential phenotypic traits for breeding for stress resilience.

Spectacular advances have been done in HTP, such as the combination of numerous high-precision sensors (sensor fusion) in phenotyping platforms, for the prediction of complex plant physical traits and three-dimensional structure, and capturing physiological and growth dynamics as well as stress-responsive traits (Deery *et al.*, 2014; Chen *et al.*, 2014). However, there is a need to evaluate whether the data generated by HTP is capturing true biological signal and if that signal is worth the investment of resources (Pauli *et al.*, 2016). For this, future research must contemplate the promotion of open-source and low-cost hardware solutions; for instance, through smartphones and tablets apps meeting the demands of researchers and farmers. Other concerns for the adoption of HTP encompass operational issues such as the need to develop more mobile methods adapted to real conditions. For instance, many phenotyping platforms are purpose-developed for a specific research so that they are not commonly transferable to other crops and field designs (Pauli *et al.*, 2016). Instead, the use of sensors-equipped small aerial vehicles (i.e. RPAS) can be pervasive across experimental designs and species although they mostly capture canopies phenotypic traits.

Extensive phenotyping and multi-omics characterization generate vast amount of data from which biological meaning must be extracted. In this sense, part of the current challenges in phenotyping concerns data and computer sciences, as these must provide the tools for the acquisition, processing (management) and integration of multidimensional data while ensuring operational simplicity and data accessibility. Also, there is room for improving the characterization of the environment, whereas phenotyping methods must be simple and clear and preferably affordable in order to ensure reproducibility and reliability of the data, while promoting a wide adoption of common protocols for phenotyping.

CONCLUSIONS

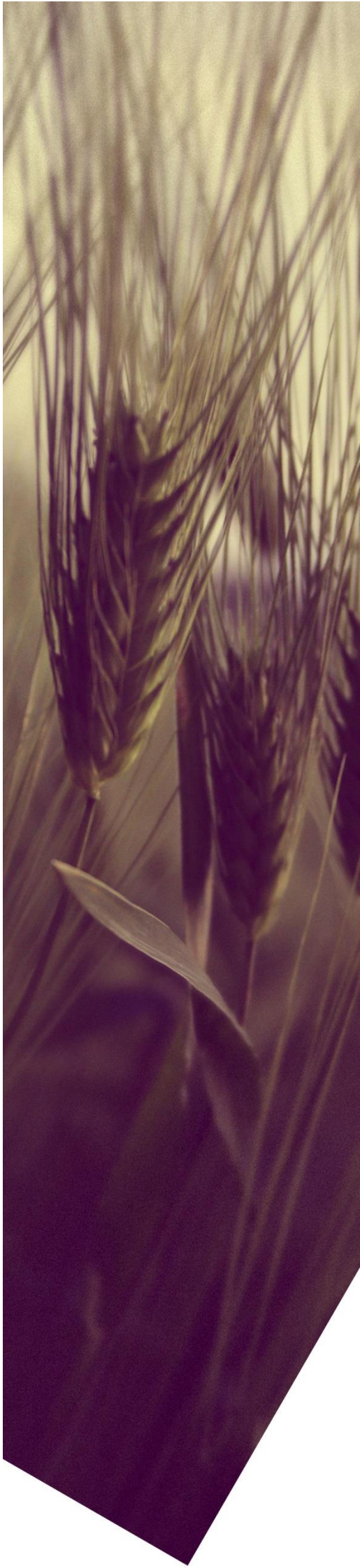

CONCLUSIONS

Plant phenotyping and, in a broad sense, plant biology research still must elucidate many aspects of plant adaptation to stresses, including how to identify stress resilience and which are the phenotypic traits indicative of stress tolerance. While these challenges are huge, it is evident that the intense development of very diverse phenotyping systems is paying off, as reported in the conclusions of this thesis:

i) RGB-derived phenotyping is an efficient and cost-effective tool that can be easily implemented in plant research, breeding and crop management. RGB-based vegetation indices (in this case by a parameterization or colour to HIS, CIE-Lab and CIE-Luv colour spaces) obtained from plot images are reliable indicators of green cover (vegetation coverage and oppositely, soil exposure) while provide numeric information of colour balance in the image (e.g. if mean colour tends to dark green, yellowish green, bluish green or red).

ii) These RGB colour components can be closely associated with a broad range of phenomena that generate a visible colour signal such as growth and yield traits, physiological processes (e.g. active photosynthetic area and senescence), disease spread and leaf nitrogen concentration. .

iii) On the other hand, field spectroscopy represents a frontier technology for phenotyping that can be intended for the disclosure of more complex and hidden plant traits in relation to their composition, anatomy and physiological status.

iv) The interactions between plant reflectance spectrum, leaf anatomy and environmental conditions are intricated and must be carefully addressed. While water stress triggers anatomy and biochemical modulation in plants that can be detected and evaluated from hyperspectral sensors, constitutive differences between leaf sides (leaf dorsoventral differences) affect leaf reflectance spectrum even in a larger extent than water stress does.

v) Nevertheless, dorsoventral differences (at the anatomical level and at the biochemical spectral signal level) are less evident under rainfed conditions, as compared to well-watered conditions.

vi) While the greater structural homogeneity of the abaxial leaf side may favour a less noisy spectral signal, the adaxial leaf side is still more representative of canopy reflectance, which should be considered for future spectroscopic research in wheat.

vii) Metabolome characterisation of wheat enables to better understand how plant tissues suffer from and adapt to stress contributing to elucidate their physiologic role and offering new ways to improve wheat productivity and resilience.

viii) The marked accumulation of organic and amino acids in spike bracts, particularly under water stress, is facilitated by a better coordination of carbon and nitrogen metabolisms in terms of photorespiration, nitrogen assimilation and respiration paths as compared to that of the flag leaf, whereas water stress induced accumulation of antioxidants and drought tolerance related sugars, particularly in the bracts, support the outperformance of the spike as compared to the flag leaf.

ix) Metabolite-yield association permits to reveal metabolites related to genotypic outperformance and yield stability.

x) Field spectroscopy can be high-throughput tool intended for internal phenotyping of metabolite profiles of wheat leaves and ears.

xi) Important metabolites implicated in sugar, photorespiration, osmoprotection, and secondary metabolisms can be estimated with considerably high robustness, which could likely be of interest for ecophysiologists, plant breeders and the agri-food industry.

xii) Although the regression models, based on organ full-range reflectance spectrum, achieve the higher robustness, models based on canopy and organ-VIS spectra still appear promising and offer potential opportunities.

RESUM GENERAL DE LA TESI

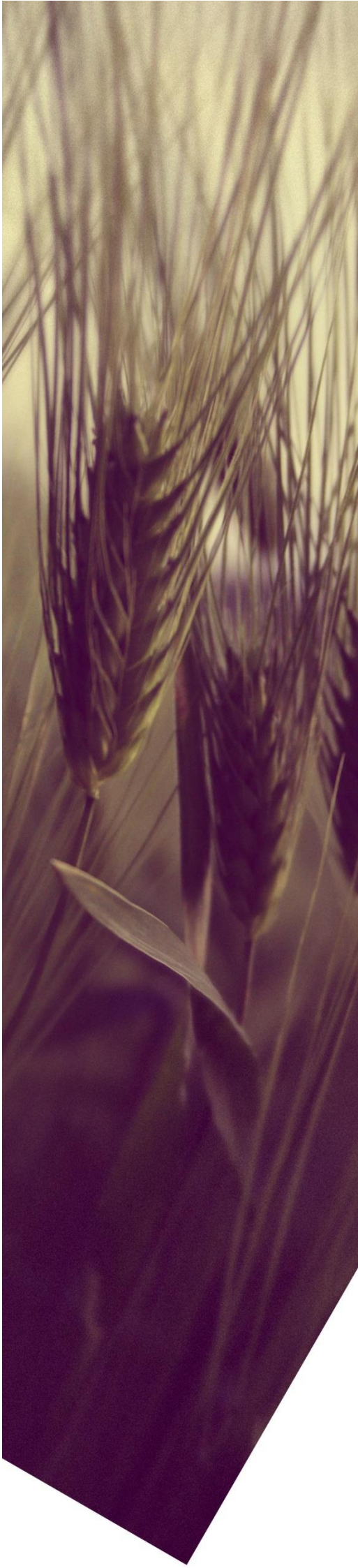

RESUM GENERAL DE LA TESI

Introducció

L'escalfament global està afectant ja els sistemes biològics i físics d'arreu del món, i ha assolit recentment 1ºC per sobre dels nivells preindustrials, incrementant 0.2ºC per dècada. Malgrat això, moltes regions del món, particularment poblades, han experimentat un increment de temperatura superior a 1.5ºC per sobre dels nivells preindustrials. A més a més, el canvi climàtic, ha comportat un increment de la freqüència d'onades de calor, nombre i intensitat de dies calorosos i de fenòmens de pluges molt intenses. Cal tenir en compte, però, que el canvi global té un fort component regional. A Europa, per exemple, els increments de temperatura observats i projectats es donen als extrems latitudinals. Els canvis de precipitació observada i projectada són menys evidents, tot i que generalment s'accepta que s'ha produït un increment de precipitació al nord d'Europa i un decrement al sud. Aquestes tendències probablement es magnifiquin properament, mentre que la freqüència d'episodis de sequeres i pluges intenses també s'agreugi a conseqüència del canvi global. Tot plegat repercutirà en la disponibilitat de recursos hídrics al subsol i en superfície així com també en un increment de risc d'erosió.

L'avenç de l'agricultura moderna, amb l'obtenció de varietats altament productives i l'ús massiu de fertilitzants i d'altres productes va comportar un increment de la producció arreu del món però també va tenir efectes nocius sobre els agro-ecosistemes. Actualment, l'agricultura ocupa bona part des sòls útils i utilitza una part important dels recursos hídrics continentals, particularment a zones del sud d'Europa. L'increment de temperatura pot tenir efectes greus en el desenvolupament i producció dels cultius principals mentre que n'incrementa la demanda hídrica. Com a resultat, ja s'ha reportat pèrdues greus de producció d'alguns cultius i s'ha projectat que a nivell mundial s'incrementin aquestes pèrdues, tot i que a nivell regional algunes zones en puguin resultar beneficiades. El canvi climàtic també pot tenir efectes sobre la distribució i supervivència de malalties i plagues que puguin agreujar el manteniment de la seguretat alimentaria. Molts estudis han identificat efectes positius de l'increment de CO_2 ambiental com ara una optimització de l'ús de l'aigua, malgrat això l'increment de la demanda hídrica dels cultius i els processos fisiològics d'aclimatació posen en qüestió els beneficis a llarg termini.

Per tant, els sistemes agrícoles requereixen urgentment un cert grau d'adaptació per tal de fer front aquests problemes, reduint la seva pròpia contribució al canvi climàtic i incrementar la producció mundial per tal de satisfer l'increment de demanda global. Per a tal fi, l'agricultura haurà de fer ús de tot un seguit d'estratègies des de canvis en sistemes de maneig agrícola fins a la millora de varietats.

Algunes de les estratègies poden ser i) ajustar dates de sembra i collita, ii) ús de varietats de cicle curt, iii) implementació de tècniques d'agricultura de conservació, iv) canvis dels usos de sòl, v) implementació de sistemes de reg altament eficients i vi) canvi de les varietats o espècies cultivades. Malgrat això, només amb la millora vegetal es podran obtenir varietats més resilients als escenaris del canvi climàtic.

Els cereals són un grup divers de monocotiledònies herbàcies i anuals de distribució cosmopolita, la domesticació i el cultiu de les quals va permetre l'assentament de les poblacions humanes fa aproximadament 12000 anys. La domesticació va comportar un increment de la mida dels grans i una pèrdua de la seva capacitat de dormició i dispersió. Actualment, la meitat del consum calòric de la població mundial prové directament dels cereals, essent el blat i el blat de moro els més cultivats. Pel que fa a l'anatomia i al desenvolupament, el blat té fulles isobilaterals alternes que consten de beina i làmina, la tija està composta de nus i entrenús mentre que els fillols tenen la mateixa estructura que la tija principal. La tija és fistulosa, tret da'ls nusos, i a la posició terminal hi trobem la fulla bandera i l'espiga. El blat té rels primàries inicialment i al filloleig en desenvolupa de secundàries. L'espiga és una inflorescència amb un raquis que suporta les espiguetes envoltades per glumes, les quals contenen les flors, envoltades per la lema i la pàlea. El carpel conté l'estigma i tres estams i el gra resultant consta de testa i capa d'aleurona a l'exterior, i d'endosperma, escutel i embrió a l'interior. Els estadis de desenvolupament del blat són germinació i creixement de les plàntules, filloleig, elongació de les tiges, espigueig, floració, ompliment del gra i maduresa, i s'acostuma a quantificar amb l'escala de Zadoks. D'altra banda, el blat de moro és important no només pel consum humà sinó també per l'animal i pels seus productes derivats. El seu origen es donà a la regió Mesoamericana, probablement a partir d'una espècie Teosinte anual. A diferència del blat, té metabolisme C4, és alt i té una sola tija, fulles oposades, la inflorescència masculina és forma a l'àpex mentre que la femenina (panotxa) es forma entre la fulla i la tija a una secció mitja de la planta. El seu desenvolupament es divideix en vegetatiu i reproductiu en funció del nombre de fulles formades i el grau de maduresa dels grans en formació.

Les plantes estar sotmeses a diferents factors que minven el seu potencial genètic de creixement i reproducció. Generalment es divideixen en estressos biòtics, com plagues i fongs, i abiòtics com l'excés de calor o la manca d'aigua. Per una banda l'estrès hídric succeeix quan l'absorció d'aigua de la planta és menor que la demanda evaporativa. Per adaptar-s'hi, les plantes engeguen tot un seguit de mecanismes d'aclimatació a nivell anatòmic, fisiològic i metabòlic. L'efecte i severitat dependrà en part de l'estadi fenològic de la planta. En el cas del blat, la fase més crítica es dona entre el filloleig i l'antesi, afectant negativament el nombre de grans. Si l'estrès hídric afecta entre l'antesi i l'ompliment del gra, es produeix una acceleració del desenvolupament i una reducció de l'ompliment del gra amb

la conseqüent reducció del pes del gra. En el cas del blat de moro, l'estrès hídric causa un increment de l'interval entre l'alliberament del pol·len i l'emergència dels estigmes. L'estrès per excés de calor provoca un accelerament del desenvolupament en detriment de la fertilitat. Malgrat que la transpiració pot refrigerar els teixits, l'excés de calor sovint és acompanyat per una manca de disponibilitat d'aigua. Les deficiències nutricionals ocasionen un estrès sobre les plantes provocant disfuncions metabòliques i limitació del creixement. La baixa fertilitat és un dels factor més limitants sobre la producció global com ara a les regions subsaharianes, per això incrementar l'eficiència en l'ús dels nutrients és un punt clau. D'altra banda, múltiples organismes poden originar un estrès biòtic a les plantes i poden causar pèrdues de producció. Un problema afegit derivat del canvi global és l'entrada de nous agents causals de malalties i plagues que eventualment poden causar problemes importants sobre ecosistemes i cultius pel que l'obtenció de varietats resistents és essencial.

L'estudi del funcionament o fisiologia del vegetals en resposta a les condicions ambientals es coneix com ecofisiologia. El conjunt de característiques que un organisme pot mostrar es coneix com fenotip, que en un sentit ampli inclou la seva variabilitat morfològica, fisiològica o bioquímica, i la seva caracterització es coneix com fenotipat. Així, el fenotip es refereix al resultat de la interacció del genotip amb l'ambient al llarg del seu desenvolupament. El conjunt de fenotips d'un organisme rep el nom de fenoma. Alguns autors diferencien el fenotip intern constituït pel genoma i proteoma (entre d'altres), del fenotip extern referit als trets que es poden mesurar amb tècniques no invasives. El desenvolupament de la bioinformàtica i de sistemes de fenotipat d'alt rendiment ha de contribuir a connectar el genotip al fenotip. El fenotipat convencional integrat en programes de millora s'ha basat en la caracterització del creixement i de les components de rendiment. A més a més, altres tècniques emprades han estat la caracterització del vigor inicial, del contingut de clorofil·les, del funcionament de la fotosíntesi o de la conductància estomàtica. Altres tècniques en recerca han estat l'anàlisi composicional, morfològic i anatòmic. Totes aquestes tècniques són útil per caracteritzar l'estrès a la planta i per seleccionar ecotips, el seu ús rutinari al camp no és factible.

Tanmateix, l'ús de tècniques no destructives de detecció remota aporta una basta informació que pot ser emprada en ecofisiologia, agronomia i per caracteritzar fenotips al camp. Per a aquest fi, els sensors tenen diferents rangs de mesura i poden implementar-se a diferents escales des del seu ús a nivell de camp fins al nivell de satèl·lits passant per plataformes aèries. Majorment els sensors utilitzats són càmeres RGB, multi/híper-espectrals i tèrmiques. També és clau considerar la resolució espacial i espectral que es requereix en funció dels trets d'interès i de l'escala de mesura. Quan s'ha emprat tècniques d'espectroscòpia, l'aproximació clàssica ha estat el desenvolupament de nombrosos índexs de vegetació associats a trets com la biomassa aèria, la cobertura vegetal, el contingut hídric i pigmentari, principalment. Els últims avenços amb aquestes tècniques han permès fins i tot la caracterització en profunditat del funcionament dels fotosistemes i de l'avaluació de trets biofísics i

bioquímics complexes. D'altra banda, l'ús de sensors RGB representa una alternativa de baix cost, maneig senzill i alt rendiment, motius pels quals s'està expandint el seu ús. Així, s'ha emprat per avaluar el creixement vegetal o les deficiències minerals. Finalment, l'ús de sensors tèrmics permet avaluar en temps real l'estatus hídric de plantes o cultius i és útil pel maneig de cultius i per la selecció de cultivars tolerants a la sequera.

D'altra banda, el desenvolupament i integració de tècniques d'alt rendiment de caracterització molecular pot revelar les respostes fenotípiques complexes que confereixen resiliència genotípica a cert estrès. En particular, la metabolòmica és el resultat de l'expressió gènica i l'activitat enzimàtica en un moment donat, la qual cosa representa una eina d'alt rendiment per entendre les respostes fisiològiques a l'ambient. Per exemple, l'estrès hídric desencadena una resposta de reprogramació metabòlica incloent-hi una inhibició de l'assimilació de nitrogen, una aturada del creixement o una resposta d'osmoprotecció.

En resum, aquesta tesi és un recull d'estudis on s'empren tècniques de fenotipat RGB, híper-espectral i metabolòmica per a la caracterització del comportament de genotips de blat dur i blat de moro sota diverses condicions estressants.

Objectius

Aquesta tesi té com a objectiu contribuir a l'avenç del fenotipat de camp i de l'ecofisiologia proporcionant mètodes i enfocaments d'àmplia aplicació des dels de baix cost i senzills fins als més innovadors i sofisticats. Per a aquest fi, s'han caracteritzats genotips de blat i blat de moro en condicions de camp i sota diferents condicions estressants. Els objectius específics, corresponents a cada capítol són els següents:

i) Relacionar els índexs de vegetació RGB i altres trets fenotípics amb la incidència de la malaltia del rovell lineal del blat predint el rendiment i les pèrdues de rendiment amb aquests trets.

ii) Avaluar la deficiència de nitrogen en una panel de genotips de blat de moro, tot desenvolupant eines de fenotipat assequibles i de fàcil maneig. Comparar la robustesa dels índexs de vegetació RGB amb d'altres com l'NDVI per la predicció del rendiment i del nitrogen foliar, així com avaluar la variabilitat dins de cada nivell d'aplicació de nitrogen.

iii) Investigar l'efecte del règim hídric i de la dorsoventralitat foliar en blat sobre les característiques de la reflectància. Elucidar quins són els trets fisiològics, anatòmics i bioquímics responsables i quines són les implicacions alhora de predir el rendiment.

iv) Caracteritzar el metaboloma de fulles i bràctees de blat en resposta a l'estrès hídric. Investigar l'existència de respostes metabòliques específiques de cada teixit i estudiar l'associació entre els metabòlits i el rendiment.

v) Investigar l'estimació del contingut de metabòlits a partir d'informació híper-espectral a nivell de fulla, espiga i capçada. Avaluar la relació entre determinades bandes de l'espectre de reflectància amb certs metabòlits.

Capítol 1

El fong biotròfic *Puccinia striiformis* f. sp. *tritici* és l'agent causant del rovell groc lineal al blat. D'entre els anys 2010 al 2013, una nova soca d'aquest patogen (Warrior/Ambition), contra la qual les varietats de blat cultivades al present no presenten resistència, va aparèixer i es va propagar ràpidament. Això ha posat en perill la producció de cereals a bona part d'Europa. S'ha considerat que la recerca de noves fonts de resistència en vers aquesta soca és la solució més eficient i segura per tal de garantir una alta producció de gra. Per a tal fi, el desenvolupament de tècniques de fenotipat de camp de baix cost i alt rendiment hi pot contribuir de manera considerable. En aquest estudi s'analitzen els índexs de vegetació d'imatges digitals vermell, verd i blau (RGB, de l'anglès red-green-blue) preses de les capçades dels cultivars en condicions de camp. Es va avaluar la seva precisió i robustesa per a la predicció del rendiment de gra i per l'avaluació de la severitat de la malaltia en comparació amb altres mesures de camp com ara l'índex de vegetació de la diferència normalitzada (NDVI), el contingut foliar de clorofil·la (SPAD), la conductància estomàtica i la temperatura de la capçada. A més a més, també es va discutir sobre les components del rendiment i paràmetres agronòmics en relació amb el rendiment i amb la severitat de la malaltia. Els índexs basats en RGB van demostrar ser uns predictor precisos del rendiment de gra i de les pèrdues de rendiment de gra associades al rovell groc (R^2 = 0.581 i R^2 = 0.536, respectivament) sobrepassant de lluny l'habilitat predictiva del NDVI (R^2 = 0.118 i R^2 = 0.128, respectivament). En comparació amb el rendiment potencial, es va trobar que la presència de la malaltia estava correlacionada amb reduccions en el nombre de grans per espiga, en el nombre de grans per metre quadrat, amb el pes mig del gra i amb

l'índex de collita. Les pèrdues de rendiment de gra en presència del rovell groc van ser també més elevades en aquelles varietats de floració més tardana. Finalment, la combinació d'índexs basats en RGB juntament amb el nombre de dies fins l'espigat van ser capaços d'explicar el 70.9% de la variabilitat del rendiment de gra i el 62.7% de les pèrdues de rendiment.

Capítol 2

La producció dels cultius de blat de moro està limitada a nivell mundial per la disponibilitat de nitrogen, particularment als sòls pobres de les regions tropicals i subtropicals. El desenvolupament de tècniques de fenotipat de camp i de monitoreig assequibles i d'alt rendiment és clau per tal de millorar el cultiu de blat de moro sota condicions de fertilització baixa en nitrogen. En aquest estudi es proposen diversos índexs de vegetació derivats d'imatges digitals del vermell, verd i blau (RGB, de l'anglès red-green-blue) a nivell de fulla i de capçada com a eines de baix cost per a la millora vegetal i pel maneig de la fertilització. Aquests es van comparar amb el rendiment de l'índex de vegetació de la diferència normalitzada (NDVI) mesurat a nivell de camp i des d'una plataforma aèria, així com amb el contingut foliar de clorofil·la i d'altres paràmetres referents a la composició i estructura foliar a l'estadi de floració. Un conjunt de deu híbrids crescuts sota cinc règims de nitrogen diferents i en condicions hídriques òptimes van ser avaluats a l'estació experimental del CIMMYT de Harare (Zimbabwe). El rendiment de gra i la concentració de nitrogen foliar entre nivells de fertilització es van poder predir de manera robusta a partir de la majoria d'aquests índexs RGB (amb $R^2 \sim 0.7$) sobrepassant el poder de predicció del NDVI i del contingut foliar de clorofil·les. A més a més, els índexs RGB van sobrepassar el rendiment del NDVI en quant a l'avaluació de les diferències genotípiques en el rendiment de gra i en la concentració de nitrogen foliar per a cada nivell de fertilització nitrogenada. Tot i això, el millor predictor de la concentració de nitrogen foliar entre els cinc ambients de fertilització va ser el contingut foliar de clorofil·les però els seu comportament dins de cada nivell de fertilització nitrogenada va resultar ineficient. Els altres trets foliars avaluats també van resultar ser ineficients com a paràmetres pel fenotipat. Es va concloure que l'adopció de tècniques de fenotipat basades en índexs RGB pot contribuir de manera significativa al progrés de la millora vegetal i del maneig apropiat de la fertilització.

Capítol 3

Els efectes de la dorsoventralitat de les fulles i la seva interacció amb canvis induïts ambientalment en la resposta espectral de les fulles son encara insuficientment coneguts i entesos, particularment

en fulles isobilaterals. En aquest estudi s'ha investigat el comportament espectral de vint-i-quatre genotips de blat dur crescuts en condicions de camp a dues ubicacions. A totes dues, es va cultivar en condicions d'irrigació i de secà. La reflectància espectral de la fulla bandera en l'espectre continu del VIS-NIR-SWIR (visible-infraroig proper-infraroig d'ona curta) es va enregistrar per les bandes adaxial i abaxial de les fulles així com també a nivell de capçada. A més a més, altres trets relacionats amb l'estatus hídric i amb el rendiment de gra van ser també avaluats. També, es van mesurar paràmetres anatòmics de la fulla bandera en un subconjunt de cinc genotips.

Els trets espectrals estudiats van resultar més afectats per la banda de la fulla més que no pas pel règim hídric. Les diferències dorsiventrals a la fulla van suggerir l'ocurrència d'un major contingut de pigments accessoris a la banda abaxial de la fulla, mentre que les diferències entre règims hídrics van estar relacionades amb uns continguts de clorofil·la, nitrogen i aigua més elevats al tractament irrigat. Aquestes variacions van ser associades també amb canvis anatòmics. A més a més, les diferències dorsiventrals van ser menys acusades en el tractament de secà, la qual cosa va suggerir l'existència de respostes específiques de cada banda de la fulla a nivell anatòmic i bioquímic. Finalment, la precisió en la predicció del rendiment va millorar quan es va fer servir l'espectre de la banda abaxial de la fulla enlloc del de la banda adaxial. Es va concloure que la importància de la dorsoventralitat sobre els trets espectrals és fonamental, fins i tot en fulles isobilaterals.

Capítol 4

La rellevància de les bràctees de l'espiga en l'aclimatació a l'estrès així com la seva contribució al rendiment ha estat recentment revelada. Tot i així, el metaboloma d'aquest òrgan i la seva resposta a l'estrès hídric encara són encara desconeguts. En aquest estudi, els perfils metabòlics de les fulles bandera, de les glumes i de les lemes van ser caracteritzats en condicions de règims hídrics contrastants per a cinc genotips de blat dur. Les condicions hídriques durant el creixement van ser caracteritzades a través d'índexs de vegetació espectral, de la temperatura de la capçada i de la composició isotòpica de carboni.

Les bràctees de l'espiga varen exhibir una major coordinació dels metabolismes del carboni i nitrogen en comparació a la fulla bandera en termes de les vies de fotorespiració, assimilació de nitrogen i respiració. Aquesta coordinació va facilitar l'acumulació d'aminoàcids i àcids orgànics a les bràctees de l'espiga, especialment sota condicions d'estrès hídric. La resposta metabolòmica a l'estrès hídric també va implicar una acumulació de sucres relacionats amb funcions antioxidants i de tolerància a la sequera, particularment a les espigues. A més a més, certs metabòlits relacionats amb el

metabolisme de la paret cel·lular, la respiració i d'altres amb funcions protectores es van relacionar amb un millor comportament genotípic i amb l'estabilitat del rendiment. També, el rendiment de gra va ser predit de manera robusta a partir dels metabolomes de fulles i bràctees de manera independent. Aquest estudi recolza el rol de l'espiga com a òrgan clau durant l'ompliment del gra al blat, particularment en condicions d'estrès, i proporciona informació fonamental per a explorar noves vies per a la millora de la productivitat de blat, incloent-hi bio-marcadors importants per a la predicció del rendiment.

Capítol 5

A l'actualitat, les tècniques híper-espectrals s'utilitzen per a la recuperació d'informació pel que fa a trets biofísics de les plantes, i predominantment s'han centrat en el continguts de components com ara els pigments fotosintètics i accessoris, en l'aigua, en el nitrogen o proteïnes, en elements estructurals com ara la lignina o d'altres com l'índex d'àrea foliar. Tot i això, la informació híper-espectral encara pot ser explotada de manera més extensiva per tal de superar els reptes en la millora vegetal en el context del canvi global i avançar en el fenotipat de camp d'alt rendiment. En aquest estudi, explorem el potencial de l'espectroscòpia de camp per a la predicció dels perfils metabòlics de la fulla bandera i de les bràctees de l'espiga a blat dur. L'espectre de reflectància de rang complert (VIS-NIR-SWIR) de les fulles bandera, de les espigues i de les capçades van ser enregistrats a una col·lecció de genotips contrastants crescuts a quatre ambients sota diferents règims hídrics. El perfils metabòlics de les fulles bandera i de dues bràctees de l'espiga, la lema i la gluma, van ser analitzats mitjançant GC-MS.

Els resultats dels models de regressió van sobrepassar el 50% de variació explicada (adj-R^2 als conjunts de validació) per a almenys 15 metabòlits de cada òrgan estudiat, mentre que els seus respectius errors van ser considerablement baixos. Les millors regressions es van obtenir per al malat (82%), glicerat i serina (63%) a fulles; per al *mio*-inositol (81%) a lemes; pel glicolat (80%) a glumes; per la sucrosa a fulles i glumes (68%); per GABA a fulles i glumes (61% i 71% respectivament); per la prolina i la glucosa a lemes (74% i 71%, respectivament) i glumes (72% i 69%, respectivament). També es discuteixen la selecció de bandes d'ona als models i el comportament dels diferents models basats en l'espectre de la capçada i de l'espectre visible dels respectius òrgans, així com la predicció del rendiment. Considerem que aquesta tècnica pot probablement ésser d'interès per la seva àmplia aplicabilitat en la investigació ecofisiològica, en programes de millora vegetal així com en la industria agro-alimentària.

Conclusions

El fenotipat vegetal, i en sentit ampli, la recerca en biologia vegetal encara ha d'elucidar molts aspectes de l'adaptació de les plantes a l'estrès, incloent com identificar la resiliència a l'estrès i quins son els trets fenotípics indicatius de la tolerància a l'estrès. Malgrat que els reptes són encara considerables, també és evident que l'intens desenvolupament de molt diversos sistemes de fenotipat està donant els seus fruits, com es reporta a les conclusions d'aquesta tesi.

i) El fenotipat derivat de RGB és una eina eficient i econòmica que pot ser fàcilment implementada en la recerca i millora vegetal i en el maneig de cultius. Els índexs de vegetació basats en sensors RGB (en aquest cas a partir de la parametrització del color als espais del color HIS, CIE-Lab i CIE-Luv) obtinguts a partir d'imatges a nivell de parcel·la són indicadors fiables de la coberta verda i proporcionen informació numèrica del balanç de color a la imatge.

ii) Aquests components RGB del color s'associen estretament amb un ampli ventall de trets que generin una senyal visible, com ara el creixement i els rendiment, processos fisiològics, dispersió de malalties així com el contingut foliar de nitrogen.

iii) D'altra banda, l'espectroscòpia de camp és una tecnologia d'avantguarda que pot ser empleada per elucidar trets de les plantes més complexos en relació a la seva composició, anatomia i estatus fisiològic.

iv) Les interaccions entre la reflectància espectral de les plantes, l'anatomia foliar i les condicions ambientals són intricades i han de ser adreçades de manera curosa. Si ve l'estrès hídric desencadena una modulació anatòmica i bioquímica a les plantes que pot ser detectada i avaluada amb sensors híper-espectrals, d'altres factors com les diferències constitutives entre les bandes de la fulla (diferències dorsiventrals) també afecten la reflectància fins i tot en major grau que no pas l'estrès hídric.

v) Malgrat això, les diferències dorsiventrals (a nivell anatòmic i les bioquímiques inferides a partir de la seva senyal espectral) són menys evidents sota condicions de secà que no pas en condicions d'adequada irrigació.

vi) Mentre que la major homogeneïtat estructural de la banda abaxial de la fulla pot proporciona una senyal espectral més nítida, la banda adaxial de la fulla continua essent més representativa de la reflectància de la capçada, la qual cosa ha de ser considerat en futurs estudis espectroscòpics en blat.

vii) La caracterització metabolòmica del blat permet un millor enteniment de com els teixits vegetals pateixen l'estrès i com se n'adapten, tot contribuint a elucidar el seu rol fisiològic i oferint noves vies per a millorar la productivitat del blat i la seva resiliència.

viii) La destacada acumulació d'aminoàcids i àcids orgànics a les bràctees de l'espiga, particularment sota condicions d'estrès hídric, és facilitada per una millor coordinació dels metabolismes del carboni i del nitrogen en termes de fotorespiració, assimilació de nitrogen i respiració en comparació a la fulla bandera. La particular acumulació a les bràctees de sucres i d'altres metabòlits relacionats amb funcions antioxidants i de tolerància a la sequera recolza el millor comportament de l'espiga en comparació a la fulla bandera.

ix) L'estudi de l'associació entre metabòlits i rendiment permet revelar aquells relacionats amb el millor comportament genotípic i amb l'estabilitat del rendiment.

x) L'espectroscòpia de camp pot ser una eina d'alt rendiment quan s'utilitza pel fenotipat intern dels perfils metabòlics de les fulles i espigues de blat.

xi) És possible d'estimar amb una robustesa considerablement elevada tot un seguit de metabòlits implicats en el metabolisme dels sucres, de la fotorespiració, de l'osmoprotecció així com metabòlits secundaris, la qual cosa pot ser d'ampli interès pels ecofisiòlegs, milloradors i per la industria agro-alimentaria.

xii) Tot i que les millors prediccions de metabòlits s'obtenen a partir de l'espectre de rang complert dels òrgans, els models basats en l'espectre de la capçada i de l'espectre visible de l'òrgan per sí sol són prometedors i ofereixen altres oportunitats potencials.

REFERENCES

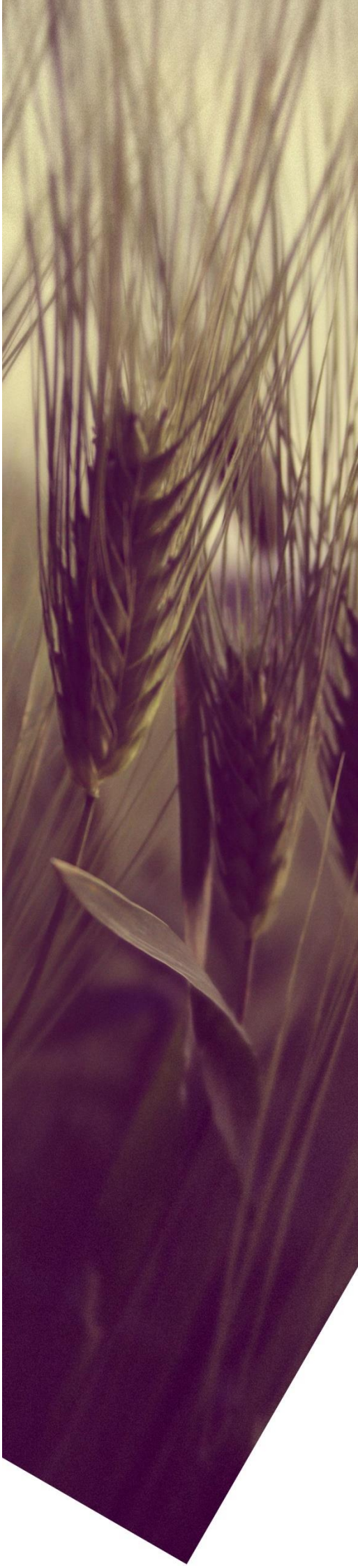

REFERENCES

Abreu e Lima, F. de, Westhues, M., Cuadros-Inostroza, Á., Willmitzer, L., Melchinger, A.E. and Nikoloski, Z. (2017) Metabolic robustness in young roots underpins a predictive model of maize hybrid performance in the field. *Plant J.*, **90**, 319–329. Available at: http://www.ncbi.nlm.nih.gov/pubmed/28122143 [Accessed August 23, 2018].

Acevedo, E., Fereres, E., Giménez, C. and Srivastava, J.P. (1991) *Improvement and management of winter cereals under temperature, drought and salinity stresses*, Instituto Nacional de Investigaciones Agrarias.

Adamsen, F.G., Pinter, P.J., Barnes, E.M., LaMorte, R.L., Wall, G.W., Leavitt, S.W. and Kimball, B.A. (1999) Measuring Wheat Senescence with a Digital Camera. *Crop Sci.*, **39**, 719. Available at: https://www.crops.org/publications/cs/abstracts/39/3/CS0390030719 [Accessed July 3, 2019].

Ali, M., Al-Ani, A., Eamus, D. and Tan, D. (2013) An Algorithm Based on the RGB Colour Model to Estimate Plant Chlorophyll and Nitrogen Contents. In *International Conference on Sustainable Environment and Agriculture*. International Association of Computer Science & Information Technology Press, pp. 52–56. Available at: https://opus.lib.uts.edu.au/handle/10453/28424 [Accessed August 8, 2019].

Allen, M.R., Dube, O.P., Solecki, W., et al. (2018) *Framing and Context. In: Global Warming of 1.5°C. An IPCC Special Report on the impacts of global warming of 1.5°C above pre-industrial levels and related global greenhouse gas emission pathways, in the context of strengthening the global response to the*,.

Almacellas, J., López Querol, A., Álvaro Sánchez, F., Serra Gironella, J., Capellades Pericas, G. and Marín Sánchez, y J.P. (2013) *La roya amarilla de los trigos, un problema emergente*,.

Andrade-Sanchez, P., Gore, M.A., Heun, J.T., Thorp, K.R., Carmo-Silva, A.E., French, A.N., Salvucci, M.E. and White, J.W. (2014) Development and evaluation of a field-based high-throughput phenotyping platform. *Funct. Plant Biol.*, **41**, 68. Available at: http://www.publish.csiro.au/?paper=FP13126 [Accessed July 3, 2019].

Annunziata, M.G., Ciarmiello, L.F., Woodrow, P., Maximova, E., Fuggi, A. and Carillo, P. (2016) Durum Wheat Roots Adapt to Salinity Remodeling the Cellular Content of Nitrogen Metabolites and Sucrose. *Front. Plant Sci.*, **7**, 2035. Available at: http://www.ncbi.nlm.nih.gov/pubmed/28119716 [Accessed September 3, 2019].

Aquino, A., Diago, M.P., Millán, B. and Tardáguila, J. (2017) A new methodology for estimating the grapevine-berry number per cluster using image analysis. *Biosyst. Eng.*, **156**, 80–95. Available at: https://www.sciencedirect.com/science/article/pii/S1537511016300940 [Accessed August 6, 2019].

Araus, J.L. and Cairns, J.E. (2014) Field high-throughput phenotyping: the new crop breeding frontier. *Trends Plant Sci.*, **19**, 52–61. Available at: http://www.ncbi.nlm.nih.gov/pubmed/24139902 [Accessed July 19, 2018].

Araus, J.L. and Kefauver, S.C. (2018) Breeding to adapt agriculture to climate change: affordable phenotyping solutions. *Curr. Opin. Plant Biol.*, **45**, 237–247. Available at: https://www.sciencedirect.com/science/article/pii/S1369526618300098 [Accessed July 5, 2019].

Araus, J.L., Kefauver, S.C., Zaman-Allah, M., Olsen, M.S. and Cairns, J.E. (2018) Translating High-Throughput Phenotyping into Genetic Gain. *Trends Plant Sci.*, **23**, 451–466. Available at: https://www.sciencedirect.com/science/article/pii/S1360138518300207 [Accessed August 7, 2018].

Araus, J.L., Slafer, G.A., Royo, C. and Serret, M.D. (2008) Breeding for Yield Potential and Stress Adaptation in Cereals. *CRC. Crit. Rev. Plant Sci.*, **27**, 377–412. Available at: http://www.tandfonline.com/doi/abs/10.1080/07352680802467736 [Accessed July 3, 2019].

Awad, Y.M., Abdullah, A.A., Bayoumi, T.Y., Abd-Elsalam, K. and Hassanien, A.E. (2015) Early Detection of Powdery Mildew Disease in Wheat (Triticum aestivum L.) Using Thermal Imaging Technique. In Springer, Cham, pp. 755–765. Available at: http://link.springer.com/10.1007/978-3-319-11310-4_66 [Accessed August 15, 2019].

Awika, J.M. (2011) *Advances in Cereal Science: Implications to Food Processing and Health Promotion*, Available at: https://pubs.acs.org/doi/10.1021/bk-2011-1089.ch001. [Accessed June 5, 2019].

Barbour, M.M., Fischer, R.A., Sayre, K.D. and Farquhar, G.D. (2000) Oxygen isotope ratio of leaf and grain material correlates with stomatal conductance and grain yield in irrigated wheat. *Funct. Plant Biol.*, **27**, 625. Available at: http://www.publish.csiro.au/?paper=PP99041 [Accessed August 21, 2019].

Barriopedro, D., Fischer, E.M., Luterbacher, J., Trigo, R.M. and García-Herrera, R. (2011) The hot summer of 2010: redrawing the temperature record map of Europe. *Science*, **332**, 220–4. Available at: http://www.ncbi.nlm.nih.gov/pubmed/21415316 [Accessed July 2, 2019].

Beleggia, R., Platani, C., Nigro, F., Vita, P. De, Cattivelli, L. and Papa, R. (2013) Effect of genotype, environment and genotype-by-environment interaction on metabolite profiling in durum wheat (Triticum durum Desf.) grain. *J. Cereal Sci.*, **57**, 183–192. Available at: https://www.sciencedirect.com/science/article/pii/S0733521012001828 [Accessed September 3, 2019].

Beniston, M., Stephenson, D.B., Christensen, O.B., et al. (2007) Future extreme events in European climate: an exploration of regional climate model projections. *Clim. Change*, **81**, 71–95. Available at: http://link.springer.com/10.1007/s10584-006-9226-z [Accessed July 2, 2019].

Bindi, M. and Olesen, J.E. (2011) The responses of agriculture in Europe to climate change. *Reg. Environ. Chang.*, **11**, 151–158. Available at: http://link.springer.com/10.1007/s10113-010-0173-x [Accessed July 2, 2019].

Boegh, E., Soegaard, H., Broge, N., Hasager, C.B., Jensen, N.O., Schelde, K. and Thomsen, A. (2002) Airborne multispectral data for quantifying leaf area index, nitrogen concentration, and photosynthetic efficiency in agriculture. *Remote Sens. Environ.*, **81**, 179–193. Available at: https://www.sciencedirect.com/science/article/abs/pii/S003442570100342X [Accessed July 3, 2019].

Bown, A.W. and Shelp, B.J. (2016) Plant GABA: Not Just a Metabolite. *Trends Plant Sci.*, **21**, 811–813. Available at: http://www.ncbi.nlm.nih.gov/pubmed/27542324 [Accessed August 27, 2018].

Brini, F., Hanin, M., Lumbreras, V., Irar, S., Pagès, M. and Masmoudi, K. (2007) Functional characterization of DHN-5, a dehydrin showing a differential phosphorylation pattern in two Tunisian durum wheat (Triticum durum Desf.) varieties with marked differences in salt and drought tolerance. *Plant Sci.*, **172**, 20–28. Available at: https://www.sciencedirect.com/science/article/pii/S0168945206002111 [Accessed September 3, 2019].

Bundy, J.G., Davey, M.P. and Viant, M.R. (2009) Environmental metabolomics: a critical review and future perspectives. *Metabolomics*, **5**, 3–21. Available at: http://link.springer.com/10.1007/s11306-008-0152-0 [Accessed September 3, 2019].

Cabrera-Bosquet, L., Crossa, J., Zitzewitz, J. von, Serret, M.D. and Luis Araus, J. (2012) High-throughput Phenotyping and Genomic Selection: The Frontiers of Crop Breeding ConvergeF. *J. Integr. Plant Biol.*, **54**, 312–320. Available at: http://www.ncbi.nlm.nih.gov/pubmed/22420640 [Accessed July 3, 2019].

Cabrera-Bosquet, L., Sánchez, C. and Araus, J.L. (2009) Oxygen isotope enrichment ($\Delta^{18}O$) reflects yield potential and drought resistance in maize. *Plant. Cell Environ.*, **32**, 1487–1499. Available at: http://doi.wiley.com/10.1111/j.1365-3040.2009.02013.x [Accessed August 21, 2019].

Cairns, J.E., Hellin, J., Sonder, K., Araus, J.L., MacRobert, J.F., Thierfelder, C. and Prasanna, B.M. (2013)

Adapting maize production to climate change in sub-Saharan Africa. *Food Secur.*, **5**, 345–360. Available at: http://link.springer.com/10.1007/s12571-013-0256-x [Accessed July 3, 2019].

Calderón, R., Navas-Cortés, J.A., Lucena, C. and Zarco-Tejada, P.J. (2013) High-resolution airborne hyperspectral and thermal imagery for early detection of Verticillium wilt of olive using fluorescence, temperature and narrow-band spectral indices. *Remote Sens. Environ.*, **139**, 231–245. Available at: https://www.sciencedirect.com/science/article/abs/pii/S0034425713002435 [Accessed August 28, 2019].

Camargo, A. and Smith, J.S. (2009) An image-processing based algorithm to automatically identify plant disease visual symptoms. *Biosyst. Eng.*, **102**, 9–21. Available at: https://www.sciencedirect.com/science/article/pii/S1537511008002870 [Accessed August 6, 2019].

Casadesús, J., Kaya, Y., Bort, J., et al. (2007) Using vegetation indices derived from conventional digital cameras as selection criteria for wheat breeding in water-limited environments. *Ann. Appl. Biol.*, **150**, 227–236. Available at: http://doi.wiley.com/10.1111/j.1744-7348.2007.00116.x [Accessed July 3, 2019].

Chairi, F., Vergara-Diaz, O., Vatter, T., Aparicio, N., Nieto-Taladriz, M.T., Kefauver, S.C., Bort, J., Serret, M.D. and Araus, J.L. (2018) Post-green revolution genetic advance in durum wheat: The case of Spain. *F. Crop. Res.*, **228**, 158–169. Available at: https://www.sciencedirect.com/science/article/pii/S0378429017321081 [Accessed September 14, 2018].

Chen, D., Neumann, K., Friedel, S., Kilian, B., Chen, M., Altmann, T. and Klukas, C. (2014) Dissecting the Phenotypic Components of Crop Plant Growth and Drought Responses Based on High-Throughput Image Analysis. *Plant Cell*, **26**, 4636–4655. Available at: http://www.ncbi.nlm.nih.gov/pubmed/25501589 [Accessed August 28, 2019].

Chen, Z., Wang, X. and Wang, H. (2018) Preliminary research on total nitrogen content prediction of sandalwood using the error-in-variable models based on digital image processing. *PLoS One*, **13**. Available at: https://www.ncbi.nlm.nih.gov/pmc/articles/PMC6103514/ [Accessed August 7, 2019].

Ciais, P., Reichstein, M., Viovy, N., et al. (2005) Europe-wide reduction in primary productivity caused by the heat and drought in 2003. *Nature*, **437**, 529–533. Available at: http://www.nature.com/articles/nature03972 [Accessed July 2, 2019].

Ciscar, J.-C., Iglesias, A., Feyen, L., et al. (2011) Physical and economic consequences of climate change in Europe. *Proc. Natl. Acad. Sci.*, **108**, 2678–2683. Available at: https://www.pnas.org/content/108/7/2678 [Accessed July 2, 2019].

Clément, G., Moison, M., Soulay, F., Reisdorf-Cren, M. and Masclaux-Daubresse, C. (2018) Metabolomics of laminae and midvein during leaf senescence and source–sink metabolite management in Brassica napus L. leaves. *J. Exp. Bot.*, **69**, 891–903. Available at: https://academic.oup.com/jxb/article/69/4/891/4105913 [Accessed July 15, 2019].

Coast, O., Shah, S., Ivakov, A., et al. (2019) Predicting dark respiration rates of wheat leaves from hyperspectral reflectance. *Plant. Cell Environ.*, pce.13544. Available at: https://onlinelibrary.wiley.com/doi/abs/10.1111/pce.13544 [Accessed April 10, 2019].

Confalonieri, R., Paleari, L., Foi, M., et al. (2017) PocketPlant3D: Analysing canopy structure using a smartphone. *Biosyst. Eng.*, **164**, 1–12. Available at: https://www.sciencedirect.com/science/article/pii/S1537511017306384 [Accessed August 6, 2019].

Daccache, A. and Lamaddalena, N. (2010) Climate change impacts on pressurised irrigation systems. *Proc. Inst. Civ. Eng. - Eng. Sustain.*, **163**, 97–105. Available at: http://www.icevirtuallibrary.com/doi/10.1680/ensu.2010.163.2.97 [Accessed July 2, 2019].

Deery, D., Jimenez-Berni, J., Jones, H., Sirault, X. and Furbank, R. (2014) Proximal Remote Sensing Buggies and Potential Applications for Field-Based Phenotyping. *Agronomy*, **4**, 349–379. Available at: http://www.mdpi.com/2073-4395/4/3/349 [Accessed August 27, 2019].

Djanaguiraman, M., Prasad, P.V. V., Boyle, D.L. and Schapaugh, W.T. (2011) High-Temperature Stress and Soybean Leaves: Leaf Anatomy and Photosynthesis. *Crop Sci.*, **51**, 2125. Available at: https://www.crops.org/publications/cs/abstracts/51/5/2125 [Accessed August 21, 2019].

EEA (2009) *Water Resources Across Europe – Confronting Water Scarcity and Drought.*, Luxembourg.

Eisenhut, M., Roell, M. and Weber, A.P.M. (2019) Mechanistic understanding of photorespiration paves the way to a new green revolution. *New Phytol.*, **223**, 1762–1769. Available at: https://onlinelibrary.wiley.com/doi/abs/10.1111/nph.15872 [Accessed September 9, 2019].

Ennajeh, M., Vadel, A.M., Cochard, H. and Khemira, H. (2015) Comparative impacts of water stress on the leaf anatomy of a drought-resistant and a drought-sensitive olive cultivar. *J. Hortic. Sci. Biotechnol.*, **85**, 289–294. Available at: http://www.tandfonline.com/doi/full/10.1080/14620316.2010.11512670 [Accessed August 21, 2019].

Ergen, N.Z., Thimmapuram, J., Bohnert, H.J. and Budak, H. (2009) Transcriptome pathways unique to dehydration tolerant relatives of modern wheat. *Funct. Integr. Genomics*, **9**, 377–396. Available at: http://www.ncbi.nlm.nih.gov/pubmed/19330365 [Accessed August 27, 2018].

Eubanks, M.W. (1997) Molecular analysis of crosses between Tripsacum dactyloides and Zea diploperennis (Poaceae). *Theor. Appl. Genet.*, **94**, 707–712. Available at: http://link.springer.com/10.1007/s001220050469 [Accessed July 29, 2019].

Fàbregas, N. and Fernie, A.R. (2019) The metabolic response to drought. *J. Exp. Bot.*, **70**, 1077–1085. Available at: http://www.ncbi.nlm.nih.gov/pubmed/30726961 [Accessed August 30, 2019].

FAO (2013) *Statistical yearbook 2013, World Food and Agriculture*, Available at: http://faostat.fao.org/.

Feng, Y.-L., Fu, G.-L. and Zheng, Y.-L. (2008) Specific leaf area relates to the differences in leaf construction cost, photosynthesis, nitrogen allocation, and use efficiencies between invasive and noninvasive alien congeners. *Planta*, **228**, 383–390. Available at: http://www.ncbi.nlm.nih.gov/pubmed/18392694 [Accessed July 3, 2019].

Fernández, E., Gorchs, G. and Serrano, L. (2019) Use of consumer-grade cameras to assess wheat N status and grain yield. *PLoS One*, **14**, e0211889. Available at: http://www.ncbi.nlm.nih.gov/pubmed/30768611 [Accessed August 7, 2019].

Ferrara, R.M., Trevisiol, P., Acutis, M., Rana, G., Richter, G.M. and Baggaley, N. (2010) Topographic impacts on wheat yields under climate change: two contrasted case studies in Europe. *Theor. Appl. Climatol.*, **99**, 53–65. Available at: http://link.springer.com/10.1007/s00704-009-0126-9 [Accessed July 2, 2019].

Field, C.B., Barros, V.R., Intergovernmental Panel on Climate Change. Working Group II, D., et al. (2014) *Climate change 2014 : impacts, adaptation, and vulnerability : Working Group II contribution to the fifth assessment report of the Intergovernmental Panel on Climate Change*,.

Fischer, T., Byerlee, D. and Edmeades, G. (2014) *Crop yields and global food security. Will yield increase continue to feed the world?*, Available at: https://www.aciar.gov.au/node/12101.

Flexas, J., Bota, J., Galmés, J., Medrano, H. and Ribas-Carbó, M. (2006) Keeping a positive carbon balance under adverse conditions: responses of photosynthesis and respiration to water stress. *Physiol. Plant.*, **127**, 343–352. Available at: http://doi.wiley.com/10.1111/j.1399-3054.2006.00621.x [Accessed July 3, 2019].

García-Ruiz, J.M., López-Moreno, J.I., Vicente-Serrano, S.M., Lasanta–Martínez, T. and Beguería, S. (2011)

Mediterranean water resources in a global change scenario. *Earth-Science Rev.*, **105**, 121–139. Available at: https://www.sciencedirect.com/science/article/pii/S0012825211000134 [Accessed July 2, 2019].

Gargallo-Garriga, A., Sardans, J., Pérez-Trujillo, M., et al. (2015) Opposite metabolic responses of shoots and roots to drought. *Sci. Rep.*, **4**, 6829. Available at: http://www.nature.com/articles/srep06829 [Accessed September 2, 2019].

Goderniaux, P., Brouyère, S., Blenkinsop, S., Burton, A., Fowler, H.J., Orban, P. and Dassargues, A. (2011) Modeling climate change impacts on groundwater resources using transient stochastic climatic scenarios. *Water Resour. Res.*, **47**. Available at: https://agupubs.onlinelibrary.wiley.com/doi/full/10.1029/2010WR010082 [Accessed July 2, 2019].

Goodess, C., Jacob, D., Deque, M., Guttierez, J., Huth, R., Kendon, E., Leckebusch, G., Lorenz, P. and Pavan, V. (2009) Downscaling methods, data and tools for input to impacts assessments. Available at: https://ueaeprints.uea.ac.uk/31098/ [Accessed July 2, 2019].

Granier, C. and Vile, D. (2014) Phenotyping and beyond: modelling the relationships between traits. *Curr. Opin. Plant Biol.*, **18**, 96–102. Available at: https://www.sciencedirect.com/science/article/pii/S1369526614000259 [Accessed August 6, 2019].

Großkinsky, D.K., Pieruschka, R., Svensgaard, J., Rascher, U., Christensen, S., Schurr, U. and Roitsch, T. (2015) Phenotyping in the fields: dissecting the genetics of quantitative traits and digital farming. *New Phytol.*, **207**, 950–952. Available at: http://doi.wiley.com/10.1111/nph.13529 [Accessed September 3, 2019].

Großkinsky, D.K., Syaifullah, S.J. and Roitsch, T. (2018) Integration of multi-omics techniques and physiological phenotyping within a holistic phenomics approach to study senescence in model and crop plants. *J. Exp. Bot.*, **69**, 825–844. Available at: http://www.ncbi.nlm.nih.gov/pubmed/29444308 [Accessed September 3, 2019].

Guardiola-Albert, C. and Jackson, C. (2011) Potential Impacts of Climate Change on Groundwater Supplies to the Doñana Wetland, Spain. *Wetlands*, **31**, 907–920.

Homolová, L., Malenovský, Z., Clevers, J.G.P.W., García-Santos, G. and Schaepman, M.E. (2013) Review of optical-based remote sensing for plant trait mapping. *Ecol. Complex.*, **15**, 1–16.

Houle, D., Govindaraju, D.R. and Omholt, S. (2010) Phenomics: the next challenge. *Nat. Rev. Genet.*, **11**, 855–866. Available at: http://www.nature.com/articles/nrg2897 [Accessed June 19, 2019].

IPCC (2014a) *Climate Change 2014 Impacts, Adaptation, and Vulnerability. Part A: Global and Sectoral Aspects. Working Group II Contribution to the Fifth Assessment Report of the Intergovernmental Panel on Climate Change*, Available at: https://www.ipcc.ch/site/assets/uploads/2018/02/WGIIAR5-PartA_FINAL.pdf.

IPCC (2014b) *Climate change 2014 Impacts, Adaptation and Vulnerability. Part B: Regional Aspects. Working Group II. Contribution to the fifth assessment report of the International Panel on Climate Change*, Available at: https://www.ipcc.ch/site/assets/uploads/2018/02/WGIIAR5-PartB_FINAL.pdf.

Jacob, D. and Podzun, R. (2010) Global warming below 2°C relative to pre-industrial level: How might climate look like in Europe. *Nov. Acta Leopoldina*, 71–76.

Jia, B., He, H., Ma, F., Diao, M., Jiang, G., Zheng, Z., Cui, J. and Fan, H. (2014) Use of a digital camera to monitor the growth and nitrogen status of cotton. *ScientificWorldJournal.*, **2014**, 602647. Available at: http://www.ncbi.nlm.nih.gov/pubmed/24723817 [Accessed August 7, 2019].

Johannes, A., Picon, A., Alvarez-Gila, A., Echazarra, J., Rodriguez-Vaamonde, S., Navajas, A.D. and Ortiz-Barredo, A. (2017) Automatic plant disease diagnosis using mobile capture devices, applied on a

wheat use case. *Comput. Electron. Agric.*, **138**, 200–209. Available at: https://www.sciencedirect.com/science/article/pii/S016816991631050X [Accessed August 6, 2019].

Jones, R.A. and Qualset, C.O. (1984) Breeding Crops for Environmental Stress Tolerance. In *Applications of Genetic Engineering to Crop Improvement*. Dordrecht: Springer Netherlands, pp. 305–340. Available at: http://www.springerlink.com/index/10.1007/978-94-009-6207-1_10 [Accessed August 23, 2019].

Kampmann, H.H. and Hansen, O.B. (1994) Using colour image analysis for quantitative assessment of powdery mildew on cucumber. *Euphytica*, **79**, 19–27. Available at: http://link.springer.com/10.1007/BF00023572 [Accessed July 3, 2019].

Kawashima, S. and Nakatani, M. (1998) An Algorithm for Estimating Chlorophyll Content in Leaves Using a Video Camera. *Ann. Bot.*, **81**, 49–54. Available at: https://academic.oup.com/aob/article-lookup/doi/10.1006/anbo.1997.0544 [Accessed August 7, 2019].

Kefauver, S.C., El-Haddad, G., Vergara-Diaz, O. and Araus, J.L. (2015) RGB picture vegetation indexes for High-Throughput Phenotyping Platforms (HTPPs). In C. M. U. Neale and A. Maltese, eds. International Society for Optics and Photonics, p. 96370J. Available at: http://proceedings.spiedigitallibrary.org/proceeding.aspx?doi=10.1117/12.2195235 [Accessed August 9, 2019].

Kjellström, E., Nikulin, G., Hansson, U., Strandberg, G. and Ullerstig, A. (2011) 21st century changes in the European climate: uncertainties derived from an ensemble of regional climate model simulations. *Tellus A Dyn. Meteorol. Oceanogr.*, **63**, 24–40. Available at: https://www.tandfonline.com/doi/full/10.1111/j.1600-0870.2010.00475.x [Accessed July 2, 2019].

Kobata, T., Palta, J.A. and Turner, N.C. (1992) Rate of Development of Postanthesis Water Deficits and Grain Filling of Spring Wheat. *Crop Sci.*, **32**, 1238. Available at: https://www.crops.org/publications/cs/abstracts/32/5/CS0320051238 [Accessed August 23, 2019].

Kokaly, R.F., Asner, G.P., Ollinger, S. V., Martin, M.E. and Wessman, C.A. (2009) Characterizing canopy biochemistry from imaging spectroscopy and its application to ecosystem studies. *Remote Sens. Environ.*, **113**, S78–S91. Available at: http://dx.doi.org/10.1016/j.rse.2008.10.018.

Kokaly, R.F. and Skidmore, A.K. (2015) Plant phenolics and absorption features in vegetation reflectance spectra near 1.66 µm. *Int. J. Appl. Earth Obs. Geoinf.*, **43**, 55–83. Available at: https://www.sciencedirect.com/science/article/pii/S0303243415000112 [Accessed April 1, 2019].

Konzmann, M., Gerten, D. and Heinke, J. (2013) Climate impacts on global irrigation requirements under 19 GCMs, simulated with a vegetation and hydrology model. *Hydrol. Sci. J.*, **58**, 88–105. Available at: http://www.tandfonline.com/doi/abs/10.1080/02626667.2013.746495 [Accessed July 2, 2019].

Lavalle, C., Micale, F., Houston, T.D., Camia, A., Hiederer, R., Lazar, C., Conte, C., Amatulli, G. and Genovese, G. (2009) Climate change in Europe. 3. Impact on agriculture and forestry. A review. *Agron. Sustain. Dev.*, **29**, 433–446. Available at: http://link.springer.com/10.1051/agro/2008068 [Accessed July 2, 2019].

Lenderink, G. and Meijgaard, E. van (2008) Increase in hourly precipitation extremes beyond expectations from temperature changes. *Nat. Geosci.*, **1**, 511–514. Available at: http://www.nature.com/articles/ngeo262 [Accessed July 2, 2019].

Li, B., Xu, X., Han, J., Zhang, L., Bian, C., Jin, L. and Liu, J. (2019) The estimation of crop emergence in potatoes by UAV RGB imagery. *Plant Methods*, **15**, 15. Available at: https://plantmethods.biomedcentral.com/articles/10.1186/s13007-019-0399-7 [Accessed August 7, 2019].

Linden, P. Van der and Mitchell, J. (2009) *ENSEMBLES: Climate Change and its Impacts: Summary of*

research and results from the ENSEMBLES project, Available at: https://www.eea.europa.eu/data-and-maps/indicators/global-and-european-temperature-1/ensembles-climate-change-and-its [Accessed July 2, 2019].

Liu, W., Cao, X., Fan, J., Wang, Z., Yan, Z., Luo, Y., West, J.S., Xu, X. and Zhou, Y. (2018) Detecting Wheat Powdery Mildew and Predicting Grain Yield Using Unmanned Aerial Photography. *Plant Dis.*, **102**, 1981–1988. Available at: https://apsjournals.apsnet.org/doi/10.1094/PDIS-12-17-1893-RE [Accessed August 6, 2019].

Lobell, D.B., Burke, M.B., Tebaldi, C., Mastrandrea, M.D., Falcon, W.P. and Naylor, R.L. (2008) Prioritizing climate change adaptation needs for food security in 2030. *Science*, **319**, 607–10. Available at: http://www.ncbi.nlm.nih.gov/pubmed/18239122 [Accessed July 2, 2019].

Lobell, D.B., Schlenker, W. and Costa-Roberts, J. (2011) Climate trends and global crop production since 1980. *Science*, **333**, 616–20. Available at: http://www.ncbi.nlm.nih.gov/pubmed/21551030 [Accessed July 2, 2019].

Lobos, G., Escobar-Opazo, A., Estrada, F., et al. (2019) Spectral Reflectance Modeling by Wavelength Selection: Studying the Scope for Blueberry Physiological Breeding under Contrasting Water Supply and Heat Conditions. *Remote Sens.*, **11**, 329. Available at: http://www.mdpi.com/2072-4292/11/3/329 [Accessed March 29, 2019].

Lou, L., Li, X., Chen, J., Li, Y., Tang, Y. and Lv, J. (2018) Photosynthetic and ascorbate-glutathione metabolism in the flag leaves as compared to spikes under drought stress of winter wheat (Triticum aestivum L.). *PLoS One*. Available at: http://journals.plos.org/plosone/article/file?id=10.1371/journal.pone.0194625&type=printable [Accessed June 11, 2018].

Lovell, J.T., Shakirov, E. V., Schwartz, S., et al. (2016) Promises and Challenges of Eco-Physiological Genomics in the Field: Tests of Drought Responses in Switchgrass. *Plant Physiol.*, **172**, 734–748. Available at: http://www.plantphysiol.org/content/172/2/734?ijkey=4cddda4b53d7b44c3efd349debfa1c586c4c6c28&keytype2=tf_ipsecsha [Accessed August 22, 2019].

Martinez-Moreno, F. and Solís, I. (2019) Wheat rust evolution in Spain: an historical review. *Phytopathol. Mediterr.*, **58**, 3–16.

Maruyama, K., Urano, K., Yoshiwara, K., et al. (2014) Integrated Analysis of the Effects of Cold and Dehydration on Rice Metabolites, Phytohormones, and Gene Transcripts. *Plant Physiol.*, **164**, 1759–1771. Available at: http://www.ncbi.nlm.nih.gov/pubmed/24515831 [Accessed September 2, 2019].

Masuka, B., Araus, J.L., Das, B., Sonder, K. and Cairns, J.E. (2012) Phenotyping for Abiotic Stress Tolerance in MaizeF. *J. Integr. Plant Biol.*, **54**, 238–249. Available at: http://www.ncbi.nlm.nih.gov/pubmed/22443263 [Accessed July 3, 2019].

Matsuoka, Y., Vigouroux, Y., Goodman, M.M., Sanchez G, J., Buckler, E. and Doebley, J. (2002) A single domestication for maize shown by multilocus microsatellite genotyping. *Proc. Natl. Acad. Sci. U. S. A.*, **99**, 6080–4. Available at: http://www.ncbi.nlm.nih.gov/pubmed/11983901 [Accessed July 29, 2019].

Merah, O., Evon, P. and Monneveux, P. (2017) Participation of Green Organs to Grain Filling in Triticum turgidum var durum Grown under Mediterranean Conditions. *Int. J. Mol. Sci.*, **19**. Available at: http://www.ncbi.nlm.nih.gov/pubmed/29295600 [Accessed June 20, 2018].

Mercado-Luna, A., Rico-García, E., Lara-Herrera, A., Soto-Zarazúa, G., Ocampo-Velázquez, R., Guevara-González, R., Herrera-Ruiz, G. and Torres-Pacheco, I. (2010) Nitrogen determination on tomato (Lycopersicon esculentum Mill.) seedlings by color image analysis (RGB). *African J. Biotechnol.*, **9**. Available at: https://www.ajol.info/index.php/ajb/article/view/92074/81517 [Accessed August 7, 2019].

Mohanty, S.P., Hughes, D.P. and Salathé, M. (2016) Using Deep Learning for Image-Based Plant Disease Detection. *Front. Plant Sci.*, **7**, 1419. Available at: http://journal.frontiersin.org/article/10.3389/fpls.2016.01419/full [Accessed August 6, 2019].

Muller, B., Pantin, F., Génard, M., Turc, O., Freixes, S., Piques, M. and Gibon, Y. (2011) Water deficits uncouple growth from photosynthesis, increase C content, and modify the relationships between C and growth in sink organs. *J. Exp. Bot.*, **62**, 1715–1729. Available at: https://academic.oup.com/jxb/article-lookup/doi/10.1093/jxb/erq438 [Accessed September 3, 2019].

Nakashima, K., Yamaguchi-Shinozaki, K. and Shinozaki, K. (2014) The transcriptional regulatory network in the drought response and its crosstalk in abiotic stress responses including drought, cold, and heat. *Front. Plant Sci.*, **5**, 170. Available at: http://www.ncbi.nlm.nih.gov/pubmed/24904597 [Accessed September 2, 2019].

Obata, T., Witt, S., Lisec, J., Palacios-Rojas, N., Florez-Sarasa, I., Yousfi, S., Araus, J.L., Cairns, J.E. and Fernie, A.R. (2015) Metabolite Profiles of Maize Leaves in Drought, Heat, and Combined Stress Field Trials Reveal the Relationship between Metabolism and Grain Yield. *Plant Physiol.*, **169**, 2665–83. Available at: http://www.ncbi.nlm.nih.gov/pubmed/26424159 [Accessed July 6, 2018].

Oerke, E.C. (2006) Crop losses to pests. *J. Agric. Sci.*, **144**, 31–43. Available at: http://www. [Accessed July 8, 2019].

Olesen, J.E., Trnka, M., Kersebaum, K.C., Skjelvåg, A.O., Seguin, B., Peltonen-Sainio, P., Rossi, F., Kozyra, J. and Micale, F. (2011) Impacts and adaptation of European crop production systems to climate change. *Eur. J. Agron.*, **34**, 96–112. Available at: https://www.sciencedirect.com/science/article/abs/pii/S1161030110001061 [Accessed July 2, 2019].

Olsoy, P.J., Mitchell, J.J., Levia, D.F., Clark, P.E. and Glenn, N.F. (2016) Estimation of big sagebrush leaf area index with terrestrial laser scanning. *Ecol. Indic.*, **61**, 815–821. Available at: https://www.sciencedirect.com/science/article/pii/S1470160X15005853 [Accessed January 21, 2019].

Oosterhuis, D.M. and Cartwright, P.M. (1983) Spike Differentiation and Floret Survival in Semidwarf Spring Wheat as Affected by Water Stress and Photoperiod. *Crop Sci.*, **23**, 711. Available at: https://www.crops.org/publications/cs/abstracts/23/4/CS0230040711 [Accessed August 23, 2019].

Orlandini, S., Bindi, M. and Howden, M. (2009) Plant Biometeorology and Adaptation. In *Biometeorology for Adaptation to Climate Variability and Change*. Dordrecht: Springer Netherlands, pp. 107–129. Available at: http://link.springer.com/10.1007/978-1-4020-8921-3_6 [Accessed July 2, 2019].

Pádua, L., Marques, P., Hruška, J., et al. (2018) Multi-Temporal Vineyard Monitoring through UAV-Based RGB Imagery. *Remote Sens.*, **10**, 1907. Available at: http://www.mdpi.com/2072-4292/10/12/1907 [Accessed August 8, 2019].

Pauli, D., Chapman, S.C., Bart, R., Topp, C.N., Lawrence-Dill, C.J., Poland, J. and Gore, M.A. (2016) The Quest for Understanding Phenotypic Variation via Integrated Approaches in the Field Environment. *Plant Physiol.*, **172**, 622–634. Available at: http://www.ncbi.nlm.nih.gov/pubmed/27482076 [Accessed August 22, 2019].

Peng, S., Huang, J., Sheehy, J.E., Laza, R.C., Visperas, R.M., Zhong, X., Centeno, G.S., Khush, G.S. and Cassman, K.G. (2004) Rice yields decline with higher night temperature from global warming. *Proc. Natl. Acad. Sci. U. S. A.*, **101**, 9971–5. Available at: http://www.ncbi.nlm.nih.gov/pubmed/15226500 [Accessed July 2, 2019].

Peñuelas, J. and Filella, L. (1998) Visible and near-infrared reflectance techniques for diagnosing plant physiological status. *Trends Plant Sci.*, **3**, 151–156.

Peñuelas, J., Gamon, J.A., Griffin, K.L. and Field, C.B. (1993) Assessing community type, plant biomass, pigment composition, and photosynthetic efficiency of aquatic vegetation from spectral reflectance. *Remote Sens. Environ.*, **46**, 110–118. Available at: https://www.sciencedirect.com/science/article/abs/pii/003442579390088F [Accessed July 3, 2019].

Peterson, C.M., Klepper, B., Pumphrey, F. V. and Rickman, R.W. (1984) Restricted Rooting Decreases Tillering and Growth of Winter Wheat. *Agron. J.*, **76**, 861. Available at: https://www.agronomy.org/publications/aj/abstracts/76/5/AJ0760050861 [Accessed August 23, 2019].

Pfeiffer, W., Trethowan, R., Ginkel, M., Ortiz-Monasterio, I. and Rajaram, S. (2005) Breeding for abiotic stress tolerance in wheat. Abiotic stresses plant resistance through breeding and molecular approaches. In No. CIS-4737. CIMMYT, pp. 401–489. Available at: http://www.sidalc.net/cgi-bin/wxis.exe/?IsisScript=CIMMYT.xis&method=post&formato=2&cantidad=1&expresion=mfn=040311 [Accessed August 7, 2018].

Poorter, H. and Evans, J.R. (1998) Photosynthetic nitrogen-use efficiency of species that differ inherently in specific leaf area. *Oecologia*, **116**, 26–37. Available at: http://link.springer.com/10.1007/s004420050560 [Accessed July 3, 2019].

Porter, J.R. and Gawith, M. (1999) Temperatures and the growth and development of wheat: a review. *Eur. J. Agron.*, **10**, 23–36. Available at: https://www.sciencedirect.com/science/article/abs/pii/S1161030198000471 [Accessed July 2, 2019].

Rahaman, M.M., Chen, D., Gillani, Z., Klukas, C. and Chen, M. (2015) Advanced phenotyping and phenotype data analysis for the study of plant growth and development. *Front. Plant Sci.*, **6**, 619. Available at: http://journal.frontiersin.org/Article/10.3389/fpls.2015.00619/abstract [Accessed August 1, 2019].

Rasheed, S., Bashir, K., Matsui, A., Tanaka, M. and Seki, M. (2016) Transcriptomic Analysis of Soil-Grown Arabidopsis thaliana Roots and Shoots in Response to a Drought Stress. *Front. Plant Sci.*, **7**, 180. Available at: http://www.ncbi.nlm.nih.gov/pubmed/26941754 [Accessed September 2, 2019].

Remigereau, M.-S., Lakis, G., Rekima, S., Leveugle, M., Fontaine, M.C., Langin, T., Sarr, A. and Robert, T. (2011) Cereal domestication and evolution of branching: evidence for soft selection in the Tb1 orthologue of pearl millet (Pennisetum glaucum [L.] R. Br.). *PLoS One*, **6**, e22404. Available at: http://www.ncbi.nlm.nih.gov/pubmed/21799845 [Accessed June 5, 2019].

Rickman, R.W., Klepper, B.L. and Peterson, C.M. (1983) Time Distributions for Describing Appearance of Specific Culms of Winter Wheat. *Agron. J.*, **75**, 551. Available at: https://www.agronomy.org/publications/aj/abstracts/75/3/AJ0750030551 [Accessed August 23, 2019].

Riedelsheimer, C., Lisec, J., Czedik-Eysenberg, A., et al. (2012) Genome-wide association mapping of leaf metabolic profiles for dissecting complex traits in maize. *Proc. Natl. Acad. Sci. U. S. A.*, **109**, 8872–7. Available at: http://www.ncbi.nlm.nih.gov/pubmed/22615396 [Accessed August 23, 2018].

Rosenzweig, C., Arnell, N.W., Ebi, K.L., et al. (2017) Assessing inter-sectoral climate change risks: the role of ISIMIP. *Environ. Res. Lett.*, **12**, 010301. Available at: http://stacks.iop.org/1748-9326/12/i=1/a=010301?key=crossref.8b61ee6c8aa6d3b1b3ec37505238fb98 [Accessed July 2, 2019].

Rosyara, U.R., Duveiller, E., Pant, K. and Sharma, R.C. (2007) Variation in chlorophyll content, anatomical traits and agronomic performance of wheat genotypes differing in spot blotch resistance under natural epiphytotic conditions. *Australas. Plant Pathol.*, **36**, 245. Available at: http://link.springer.com/10.1071/AP07014 [Accessed August 21, 2019].

Rounsevell, M.D.A., Reginster, I., Araújo, M.B., et al. (2006) A coherent set of future land use change

scenarios for Europe. *Agric. Ecosyst. Environ.*, **114**, 57–68. Available at: https://www.sciencedirect.com/science/article/pii/S0167880905005347 [Accessed July 2, 2019].

Sagaram, M., Lombardini, L. and Grauke, L.J. (2007) Variation in Leaf Anatomy of Pecan Cultivars from Three Ecogeographic Locations. *J. Am. Soc. Hortic. Sci.*, **132**, 592–596. Available at: https://journals.ashs.org/jashs/view/journals/jashs/132/5/article-p592.xml [Accessed August 21, 2019].

Saia, S., Fragasso, M., Vita, P. De and Beleggia, R. (2019) Metabolomics Provides Valuable Insight for the Study of Durum Wheat: A Review. *J. Agric. Food Chem.*, **67**, 3069–3085. Available at: https://pubs.acs.org/doi/10.1021/acs.jafc.8b07097 [Accessed September 3, 2019].

Sanchez-Bragado, R., Elazab, A., Zhou, B., Serret, M.D., Bort, J., Nieto-Taladriz, M.T. and Araus, J.L. (2014) Contribution of the ear and the flag leaf to grain filling in durum wheat inferred from the carbon isotope signature: Genotypic and growing conditions effects. *J. Integr. Plant Biol.*, **56**, 444–454. Available at: http://www.ncbi.nlm.nih.gov/pubmed/24028829 [Accessed July 9, 2018].

Sanchez-Bragado, R., Molero, G., Reynolds, M.P. and Araus, J.L. (2016) Photosynthetic contribution of the ear to grain filling in wheat: a comparison of different methodologies for evaluation. *J. Exp. Bot.*, **67**, 2787–2798. Available at: https://academic.oup.com/jxb/article-lookup/doi/10.1093/jxb/erw116 [Accessed March 19, 2019].

Sanchez-Bragado, R., Molero, G., Reynolds, M.P. and Araus, J.L. (2014) Relative contribution of shoot and ear photosynthesis to grain filling in wheat under good agronomical conditions assessed by differential organ δ13C. *J. Exp. Bot.*, **65**, 5401–13. Available at: http://www.ncbi.nlm.nih.gov/pubmed/25053645 [Accessed March 12, 2019].

Schlenker, W. and Roberts, M.J. (2009) Nonlinear temperature effects indicate severe damages to U.S. crop yields under climate change. *Proc. Natl. Acad. Sci. U. S. A.*, **106**, 15594–8. Available at: http://www.ncbi.nlm.nih.gov/pubmed/19717432 [Accessed July 2, 2019].

Serret, M.., Ortiz-Monasterio, I., Pardo, A. and Araus, J.. (2008) The effects of urea fertilisation and genotype on yield, nitrogen use efficiency, δ ^{15} N and δ ^{13} C in wheat. *Ann. Appl. Biol.*, **0**, 080617165316730-??? Available at: http://doi.wiley.com/10.1111/j.1744-7348.2008.00259.x [Accessed July 3, 2019].

Smith, P. and Olesen, J.E. (2010) Synergies between the mitigation of, and adaptation to, climate change in agriculture. *J. Agric. Sci.*, **148**, 543–552. Available at: https://www.cambridge.org/core/product/identifier/S0021859610000341/type/journal_article [Accessed July 2, 2019].

Smith, R.C.G., Heritage, A.D., Stapper, M. and Barrs, H.D. (1986) Effect of stripe rust (puccinia striiformis west.) and irrigation on the yield and foliage temperature of wheat. *F. Crop. Res.*, **14**, 39–51. Available at: https://www.sciencedirect.com/science/article/pii/0378429086900456 [Accessed August 15, 2019].

Stewart, W.M., Dibb, D.W., Johnston, A.E. and Smyth, T.J. (2005) The Contribution of Commercial Fertilizer Nutrients to Food Production. *Agron. J.*, **97**, 1. Available at: https://www.agronomy.org/publications/aj/abstracts/97/1/0001 [Accessed July 3, 2019].

Sun, Y., Tong, C., He, S., et al. (2018) Identification of Nitrogen, Phosphorus, and Potassium Deficiencies Based on Temporal Dynamics of Leaf Morphology and Color. *Sustainability*, **10**, 762. Available at: http://www.mdpi.com/2071-1050/10/3/762 [Accessed August 8, 2019].

Svensgaard, J., Roitsch, T., Christensen, S., Svensgaard, J., Roitsch, T. and Christensen, S. (2014) Development of a Mobile Multispectral Imaging Platform for Precise Field Phenotyping. *Agronomy*, **4**, 322–336. Available at: http://www.mdpi.com/2073-4395/4/3/322 [Accessed July 3, 2019].

Tambussi, E.A., Bort, J., Guiamet, J.J., Nogués, S. and Araus, J.L. (2007) The Photosynthetic Role of Ears in

C 3 Cereals: Metabolism, Water Use Efficiency and Contribution to Grain Yield. *CRC. Crit. Rev. Plant Sci.*, **26**, 1–16. Available at: http://www.tandfonline.com/doi/abs/10.1080/07352680601147901 [Accessed July 5, 2018].

Taylor, B.R., Parkinson, D. and Parsons, W.F.J. (1989) Nitrogen and Lignin Content as Predictors of Litter Decay Rates: A Microcosm Test. *Ecology*, **70**, 97–104. Available at: http://doi.wiley.com/10.2307/1938416 [Accessed July 3, 2019].

Teixeira, E.I., Fischer, G., Velthuizen, H. van, Walter, C. and Ewert, F. (2013) Global hot-spots of heat stress on agricultural crops due to climate change. *Agric. For. Meteorol.*, **170**, 206–215. Available at: https://www.sciencedirect.com/science/article/pii/S0168192311002784 [Accessed July 2, 2019].

Tezara, W., Mitchell, V.J., Driscoll, S.D. and Lawlor, D.W. (1999) Water stress inhibits plant photosynthesis by decreasing coupling factor and ATP. *Nature*, **401**, 914–917. Available at: http://www.nature.com/articles/44842 [Accessed August 27, 2018].

Tholen, D., Boom, C. and Zhu, X.-G. (2012) Opinion: Prospects for improving photosynthesis by altering leaf anatomy. *Plant Sci.*, **197**, 92–101. Available at: https://www.sciencedirect.com/science/article/pii/S0168945212001963 [Accessed August 21, 2019].

Trnka, M., Olesen, J.E., Kersebaum, K.C., et al. (2011) Agroclimatic conditions in Europe under climate change. *Glob. Chang. Biol.*, **17**, 2298–2318. Available at: http://doi.wiley.com/10.1111/j.1365-2486.2011.02396.x [Accessed July 2, 2019].

Turner, W., Spector, S., Gardiner, N., Fladeland, M., Sterling, E. and Steininger, M. (2003) Remote sensing for biodiversity science and conservation. *Trends Ecol. Evol.*, **18**, 306–314. Available at: https://www.sciencedirect.com/science/article/abs/pii/S0169534703000703 [Accessed August 29, 2019].

Ullah, N., Yüce, M., Neslihan Öztürk Gökçe, Z. and Budak, H. (2017) Comparative metabolite profiling of drought stress in roots and leaves of seven Triticeae species. *BMC Genomics*, **18**, 969. Available at: https://bmcgenomics.biomedcentral.com/articles/10.1186/s12864-017-4321-2 [Accessed July 2, 2018].

Ustin, S.L., Gitelson, A.A., Jacquemoud, S., Schaepman, M., Asner, G.P., Gamon, J.A. and Zarco-Tejada, P. (2009) Retrieval of foliar information about plant pigment systems from high resolution spectroscopy. *Remote Sens. Environ.*, **113**, S67–S77. Available at: http://dx.doi.org/10.1016/j.rse.2008.10.019.

Ventrella, D., Charfeddine, M., Moriondo, M., Rinaldi, M. and Bindi, M. (2012) Agronomic adaptation strategies under climate change for winter durum wheat and tomato in southern Italy: irrigation and nitrogen fertilization. *Reg. Environ. Chang.*, **12**, 407–419. Available at: http://link.springer.com/10.1007/s10113-011-0256-3 [Accessed July 2, 2019].

Vergara-Diaz, O., Kefauver, S.C., Elazab, A., Nieto-Taladriz, M.T. and Araus, J.L. (2015) Grain yield losses in yellow-rusted durum wheat estimated using digital and conventional parameters under field conditions. *Crop J.*, **3**, 200–210. Available at: https://www.sciencedirect.com/science/article/pii/S2214514115000355 [Accessed July 3, 2019].

Vergara-Díaz, O., Zaman-Allah, M.A., Masuka, B., Hornero, A., Zarco-Tejada, P., Prasanna, B.M., Cairns, J.E. and Araus, J.L. (2016) A Novel Remote Sensing Approach for Prediction of Maize Yield Under Different Conditions of Nitrogen Fertilization. *Front. Plant Sci.*, **7**, 666. Available at: http://journal.frontiersin.org/Article/10.3389/fpls.2016.00666/abstract [Accessed July 3, 2019].

Vergara-Díaz, O., Chairi, F., Vicente, R., Fernandez-Gallego, J.A., Nieto-Taladriz, M.T., Aparicio, N., Kefauver, S.C. and Araus, J.L. (2018) Leaf dorsoventrality as a paramount factor determining spectral performance in field-grown wheat under contrasting water regimes. *J. Exp. Bot.*, **69**, 3081–3094. Available at: https://academic.oup.com/jxb/article/69/12/3081/4957039 [Accessed April 25,

2019].

Vergara-Diaz, O., Vatter, T., Vicente, R., Obata, T., Nieto-Taladriz, T., Aparicio, N., Kefauver, S.C., Fernie, A.R., and Araus, JL. (2019a) Metabolome profiling supports the key role of the spike in wheat yield performance. Submitted.

Vergara-Diaz, O., Vatter, T., Kefauver, S.C., Obata, T., Fernie A.R. and Araus, J.L. (2019b) Assessing durum wheat ear and leaf metabolomes in the field through hyperspectral data . Submitted.

Vicente, R., Ver.gara-Díaz, O., Medina, S., Chairi, F., Kefauver, S.C., Bort, J., Serret, M.D., Aparicio, N. and Araus, J.L. (2018) Durum wheat ears perform better than the flag leaves under water stress: Gene expression and physiological evidence. *Environ. Exp. Bot.*, **153**, 271–285. Available at: https://linkinghub.elsevier.com/retrieve/pii/S0098847218301795 [Accessed June 19, 2018].

Wada, Y., Wisser, D., Eisner, S., et al. (2013) Multimodel projections and uncertainties of irrigation water demand under climate change. *Geophys. Res. Lett.*, **40**, 4626–4632. Available at: http://doi.wiley.com/10.1002/grl.50686 [Accessed July 2, 2019].

White, J.W., Andrade-Sanchez, P., Gore, M.A., et al. (2012) Field-based phenomics for plant genetics research. *F. Crop. Res.*, **133**, 101–112. Available at: https://www.sciencedirect.com/science/article/pii/S037842901200130X [Accessed July 3, 2019].

Xu, S., Xu, Y., Gong, L. and Zhang, Q. (2016) Metabolomic prediction of yield in hybrid rice. *Plant J.*, **88**, 219–227. Available at: http://www.ncbi.nlm.nih.gov/pubmed/27311694 [Accessed August 23, 2018].

Xu, Z.-Z. and Yu, Z.-W. (2006) Nitrogen metabolism in flag leaf and grain of wheat in response to irrigation regimes. *J. Plant Nutr. Soil Sci.*, **169**, 118–126. Available at: http://doi.wiley.com/10.1002/jpln.200420418 [Accessed August 27, 2018].

Yadav, A.K., Carroll, A.J., Estavillo, G.M., Rebetzke, G.J. and Pogson, B.J. (2019) Wheat drought tolerance in the field is predicted by amino acid responses to glasshouse-imposed drought. *J. Exp. Bot.* Available at: https://academic.oup.com/jxb/advance-article/doi/10.1093/jxb/erz224/5514325 [Accessed September 9, 2019].

Yang, X., Tang, J., Mustard, J.F., Wu, J., Zhao, K., Serbin, S. and Lee, J.E. (2016) Seasonal variability of multiple leaf traits captured by leaf spectroscopy at two temperate deciduous forests. *Remote Sens. Environ.*, **179**, 1–12. Available at: http://dx.doi.org/10.1016/j.rse.2016.03.026.

Yousfi, S., Márquez, A.J., Betti, M., Araus, J.L. and Serret, M.D. (2016) Gene expression and physiological responses to salinity and water stress of contrasting durum wheat genotypes. *J. Integr. Plant Biol.*, **58**, 48–66. Available at: http://www.ncbi.nlm.nih.gov/pubmed/25869057 [Accessed September 3, 2019].

Zadoks, J.C., Chang, T.T. and Konzak, C.F. (1974) A decimal code for the growth stages of cereals. *Weed Res.*, **14**, 415–421. Available at: http://doi.wiley.com/10.1111/j.1365-3180.1974.tb01084.x [Accessed October 1, 2018].

Zheng, B., Chapman, S., Christopher, J., Frederiks, T. and Chenu, K. (2015) Frost Trends and their Estimated Impact on Yield in the Australian Wheatbelt. *Procedia Environ. Sci.*, **29**, 171–172. Available at: https://www.sciencedirect.com/science/article/pii/S1878029615005216 [Accessed August 28, 2019].

Zheng, H., Cheng, T., Li, D., et al. (2018) Evaluation of RGB, Color-Infrared and Multispectral Images Acquired from Unmanned Aerial Systems for the Estimation of Nitrogen Accumulation in Rice. *Remote Sens.*, **10**, 824. Available at: http://www.mdpi.com/2072-4292/10/6/824 [Accessed August 8, 2019].

Zhu, L., Liang, Z.S., Xu, X., Li, S.H. and Monneveux, P. (2009) Evidences for the association between carbon

isotope discrimination and grain yield—Ash content and stem carbohydrate in spring wheat grown in Ningxia (Northwest China). *Plant Sci.*, **176**, 758–767. Available at: https://www.sciencedirect.com/science/article/pii/S0168945209000661 [Accessed August 14, 2019].

Ziska, L.H., Bunce, J.A., Shimono, H., et al. (2012) Food security and climate change: on the potential to adapt global crop production by active selection to rising atmospheric carbon dioxide. *Proc. R. Soc. B Biol. Sci.*, **279**, 4097–4105. Available at: http://www.ncbi.nlm.nih.gov/pubmed/22874755 [Accessed July 2, 2019].